Structural Damage Assessment under Uncertainty

by

Israel López Martínez
B.S. University of California, Davis 2002
M.S. University of California, Davis 2004

DISSERTATION

Submitted in partial satisfaction of the requirement for the degree
Doctor in Philosophy
in
Mechanical and Aerospace Engineering
in the
OFFICE OF GRADUATE STUDIES
of the
UNIVERSITY OF CALIFORNIA
DAVIS

Approved:

Prof. Nesrin Sarigul-Klijn (chair) _____

Prof. Dean C. Karnopp _____

Prof. Donald Margolis _____

Committee in Charge
2010

AUTHOR'S DECLARATION

I hereby declare that I am the sole author of this dissertation. This is a true copy of the dissertation, including any required final revisions, as accepted by my Ph.D. degree committee.

I understand that my dissertation may be made electronically available to the public.

Abstract

Structural damage assessment has applications in the majority of engineering structures and mechanical systems ranging from aerospace vehicles to manufacturing equipment. The primary goals of any structural damage assessment and health monitoring systems are to ascertain the condition of a structure and to provide an evaluation of changes as a function of time as well as providing an early-warning of an unsafe condition. There are many structural heath monitoring and assessment techniques developed for research using numerical simulations and scaled structural experiments. However, the transition from research to real-world structures has been rather slow. One major reason for this slow-progress is the existence of uncertainty in every step of the damage assessment process.

This dissertation research involved the experimental and numerical investigation of uncertainty in vibration-based structural health monitoring and development of robust detection and localization methods. The basic premise of vibration-based structural health monitoring is that changes in structural characteristics, such as stiffness, mass and damping, will affect the global vibration response of the structure. The diagnostic performance of vibration-based monitoring system is affected by uncertainty sources such as measurement errors, environmental disturbances and parametric modeling uncertainties. To address diagnostic errors due to irreducible uncertainty, a pattern recognition framework for damage detection has been developed to be used for continuous monitoring of structures. The robust damage detection approach developed is based on the ensemble of dimensional reduction algorithms for improved damage-sensitive feature extraction. For damage localization, the determination of an experimental structural model was performed based on output-only modal analysis. An experimental model correlation technique is developed in which the discrepancies between the undamaged and damaged modal

data are isolated based on the integration of sensitivity analysis and statistical sampling, which minimizes the occurrence of false-damage indication due to uncertainty. To perform diagnostic decision-making under uncertainty, an evidential reasoning approach for damage assessment is developed for addressing the possible imprecision in the damage localization results. The newly developed damage detection and localization techniques are applied and validated through both vibration test data from literature and in house laboratory experiments.

Acknowledgements

There are many people who assisted me in my completion of the doctoral program. I wish to acknowlege the support each has given me during my four-year journey at UC Davis.

I would like to express my sincere gratitude and appreciation to my advisor Prof. Nesrin Sarigul-Klijn for her enthusiastic guidance and encouragement throughout the course of my research. One of the things that I most appreciate is the freedom she gave me to do my work. I am very grateful to Nesrin as she has been a greatmentor since my undergraduate years; for teaching me all those skills, not written in any book, yet needed by any researcher; for listening to me and given me excellent advice in all matters. I want also to thank my dissertation committee: Prof. Dean C. Karnopp and Prof. Donald Margolis. I would like to thank my committee for their insightful and honest comments, teaching, and knowledge.

This research was in part funded by the Louis Stokes Alliances for Minority Participation Bridge to the Doctorate (LSAMP-BD) fellowship of the National Science Foundation (NSF). I express my sincere appreciation for the support provided by this funding organization.

My family deserve more than a simple "thank you." Specially my parents, Agripina and Manuel, who provided me with a great education, who supported me in all my endeavors and adventures, who sacrificed so much to make this possible, and fed me along the way. My brother Alvaro; and sisters Maria Luisa and Angela were fundamental in my education. Being the youngest, I always looked up to them as family and friends.

Last, but certainly not least, to my beautiful wife Mirella, who has being a continuous support for the last four years. Thank you for all the things we shared, for your patience, for your prayers, and for all the things that awaits us. All my love to her.

Para mi esposa Mirella y mis padres, Agripina y Manuel

Nomenclature

List of Operators

j	$j^2 = -1$
$*$	convolution operator
$\Re$	denotes a set of real numbers
$\{...\}$	set defined by elements
$\Rightarrow$	logical implication operator
$(\cdot)^T$	matrix transpose
$(\cdot)^{-1}$	matrix inverse
$(\cdot)^*$	complex conjugate
$(\cdot)^H$	Hermitian response
I	identity matrix
$\otimes$	Kronecker matrix product
$\oplus$	combination operator
$\|\cdot\|$	norm
$\forall$	universal quantification; for all; for any
$\neg$	logical negation
$\propto$	proportionality
$\in$	set membership
$\subseteq$	subset; $A \subseteq B$ where A is a subset of (or is included in) B
$\supseteq$	superset; $B \supseteq A$ where B is a superset of (or includes) A
$\cap$	set-theoretic intersection
$\cup$	set-theoretic union
$\sum(\cdot)$	summation operator
$\prod(\cdot)$	product operator
$\bigcup(\cdot)$	union operator
$\bigcap(\cdot)$	intersection operator
$L(\cdot)$	likelihood function

Λ	likelihood ratio test
$\overline{P}(\cdot);\underline{P}(\cdot)$	upper and lower boundary or probability
$P(\cdot)$	probability of propositional arguments
$p(\cdot)$	probability of numerical value arguments
$P(A \mid B)$	probability of A given B
$E[\cdot]$	expected value
$\mathrm{var}[\cdot]$	variance
$\mathrm{cov}[\cdot]$	covariance
$Pos(\cdot)$	possibility measure
$Nec(\cdot)$	necessity measure
$Con(\cdot)$	conflict measure
$BetP(\cdot)$	pignistic (bet) probability measure
$\sup(\cdot)$	supremum - upper bound of set
$\inf(\cdot)$	infinum - lower bound of set
$m(\cdot);m_i$	basic belief mass or assignment
$Bel(\cdot)$	belief measure
$Pl(\cdot)$	plausibility measure
Δ	change operator

List of Symbols

k, m, c	stiffness, mass, damping values
K, M, C	stiffness, mass, damping matrices
$\omega = 2\pi f$	angular frequency at frequency f
$s = j\omega$	Laplace transform variable
$\omega_n; f_n$	natural frequency
λ	eigenvalue; singular value
φ	eigenvector
ϕ	mode shape
ζ	damping ratio
R_i	residue for mode i
$G(\cdot)$	cross-spectra function
$T(\cdot)$	transmissibility function
$H(j\omega)$	frequency response function
H_i	i^{th} hypothesis
H_D	hypothesis of damage state
H_U	hypothesis of undamaged (healthy) state
θ	random variable; model parameter
c_i	pattern recognition true class i
L_i	pattern recognition output (label) class i
Ω_i	region i in measurement space
$\tau(\cdot)$	threshold value
α	fuzzy set membership value
μ_A	characteristic function of set A
Θ	universal set; frame of discernment
Ψ	set of all subsets of universal set
$\varnothing$	empty set
$\mu(\cdot)$	mean
$\sigma(\cdot)$	standard deviation

t	time step; time variable
$d; D$	reduced feature size; original feature size
N_t	number of training vectors or values
$n; N$	number of samples, responses or variables
N_e	number of elements
N_{DI}	number of damage indices
N_{dof}	number of degrees of freedom
N_{gr}	number of groups
N_m	number of modes
$\hat{x}$	estimate of parameter x

List of Abbreviations

AI	artificial intelligence
ANN	artificial neural networks
BBA	basic belief assignment
BBN	Bayesian belief network
BNs	Bayesian networks
CDF	cumulative distribution function
COMAC	coordinate modal assurance criterion
DAGs	directed acyclic graphs
DM	diffusion mappings
DOF	degree of freedom
D-R	dimensional reduction
D-S	Dempster-Shafer evidence theory
EM	expectation maximization
EMA	experimental modal analysis
ENs	evidential networks
FDAC	frequency domain assurance criterion
FDD	frequency domain decomposition
FDI	fault detection and isolation
FEA	finite element analysis
FEM	finite element method
FoD	frame of discernment
FP	false positive
FN	false negative
FRAC	frequency response assurance criterion
FRF	frequency response function
FT	Fourier transform
IVHM	integrated vehicle health monitoring
kNN	k-nearest neighbor
KPCA	kernel principal component analysis

LLE	local linear embedding
LRT	likelihood ratio test
LTSA	local tangent space analysis
MAC	modal assurance criterion
MDLAC	multiple damage local assurance criterion
MDOF	multi-degree of freedom
MDS	multi-dimensional scaling
MSC	mode shape curvature
NN	neural network
NP	non-deterministic polynomial-time (computational complexity)
ODS	operating deflection shapes
OMA	operational (output-only) modal analysis
PCA	principal component analysis
PDF	probability density function
PSD	power spectra density
RLS	recursive least squares
RMS	root mean square
RPCA	recursive principal component analysis
RPM	revolutions per minute
SDI	sensitivity analysis damage index
SDOF	single degree of freedom
SEDI	strain energy damage index
SHM	structural health monitoring
SNR	signal to noise ratio
SVD	singular value decomposition
SVM	support vector machine
TFRAC	transmissibility frequency response assurance criterion
TN	true negative
TP	true positive
UAV	unmanned aerial vehicle

Table of Contents

List of Figures

List of Tables

Chapter 1

Introduction

1.1 Motivation

In today's modern society, the availability, reliability and high-performance of flight vehicles is increasingly more demanding. The flight transportation systems are major source of network support for every-day life and economic stability. The impact that aircraft and aerospace industry has had on our lives and world economy is very pronounced. As such, the aerospace industry continues at the forefront of engineering research and development technologies. An ever constant objective in all technological innovations is the maintenance of highly reliable and safe transportation systems, but as complexity of components and systems increases, and continuous deterioration of current aircraft exists due to aging, the risk of system faults and failures increases. Technologies addressing these safety and performance issues rapidly evolving. Recent developments in sensing technology, signal processing, controllers, and their systematic integration, have attractive potential for resolving numerous issues related to aircraft diagnostics and prognostics, such as maintenance optimization, improved performance, extended life of structures and overall safety improvement.

Figure 1.1 presents a general architecture representing the flight vehicle structural damage assessment. Automated structural health monitoring and diagnostics based on advanced technologies will alleviate service and in-flight damage problems.

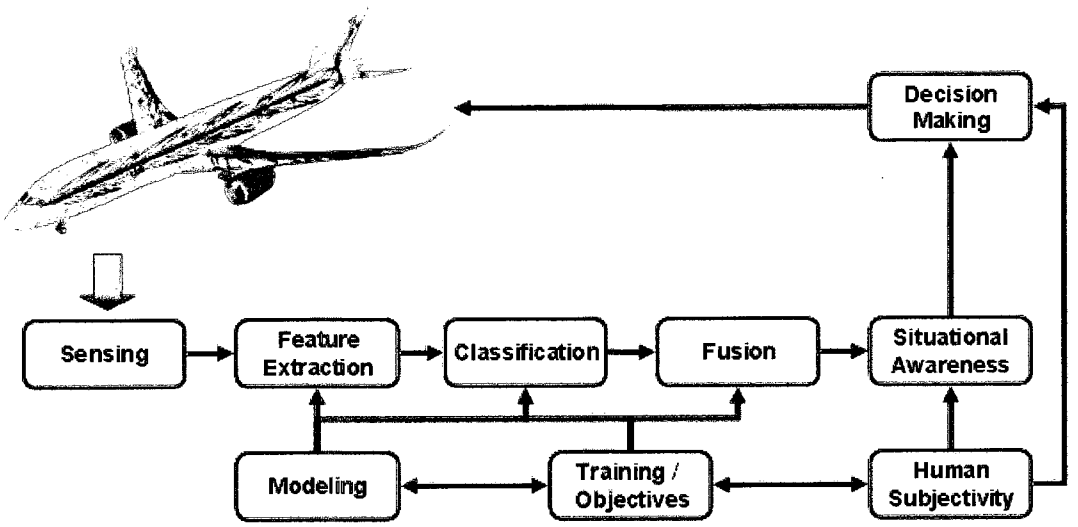

Figure 1.1. Structural damage assessment process of flight vehicles.

The primary goals of any structural damage monitoring and assessment system are to ensure reliability, safety and to minimize life-cycle cost of the structure in question. Damage assessment has applications in the majority of engineering structures and mechanical systems ranging from aerospace systems to manufacturing equipment. As a result, a multitude of different approaches appear in the literature to address the problem of damage assessment, some recent reviews provide valuable categorization of existing structural heath management methods [21,37,52,56,72,101,122,163,167,169-171,177]. Multiple structural health monitoring (SHM) and diagnostic technologies have been developed and applied to numerical simulations and scaled structural experiments. However, the transition from research to practice has been rather slow with exception of the rotating machinery industry. Successful applications of rotating machinery damage diagnosis and prognosis exist because extensive training data is available, and more importantly, the damage location and damage types as well as operational and environmental conditions are often well known a priori and do not vary significantly [76].

One major reason for the slow-progress in applying diagnostic technologies to real-world structures is the existence of uncertainty in every step of the damage assessment process. Early works in the area of damage estimation focused in direct application of physics-based system identification techniques, such as estimation of system stiffness matrix and/or modal parameters [21]. These conventional damage estimation approaches deal with deterministic models where all the parameters are considered identifiable and uncertainties are not directly accounted for, which makes it rather difficult to evaluate how reliable the estimated damage index is. Along with the studies in deterministic damage assessment, consideration of uncertainties has received more attention in recent years particularly in data-based damage assessment methods. Data-driven methods rely on previous system measurements for training and assessment of the current system health state. Although, data-driven methods are great for indicating the presence of damage, damage assessment results obtained from data-driven methods are generally more simplistic and lack information in regards to the nature of the damage. More recent works [107,108,134,148,175,177] have attempted at finding a balance between physics-based and data-driven methods to maximize the information and confidence levels of the damage diagnosis. Increasing confidence in damage diagnosis is directly proportional to the uncertainty level considered.

In applications of structural diagnostic systems, uncertainty may take the form of component and/or system variability, environmental and operational conditions, data acquisition errors, and data interrogation errors, to name a few. Uncertainty in plain words is lack of certainty. In more detail, uncertainty is a sate of limited knowledge where it is impossible to exactly describe existing state or future outcome(s) [38]. In cases where uncertainty cannot be fully described via deterministic or random approaches, also known as aleatory uncertainty, then uncertainty is categorized as epistemic, which deals with lack-of-knowledge of quantities or processes of the

system or the environment. Many applications of uncertainty analysis in damage assessment have assumed an aleatory model when the uncertainty is of epistemic nature. Legitimate reasons can be leveled for reducing epistemic uncertainties to aleatory uncertainties. Consequently, selecting and developing an uncertainty model can sometimes be more of an art than a science. The systematic consideration of uncertainties is as important as having the appropriate structural system model, especially during model validation where the total error between physical observation and model prediction must be characterized.

1.2 Objectives

This study is to develop a vibration-based damage assessment framework for effective and robust detection and localization of small scale damage under uncertainty. The research of structural assessment has been going on for a few decades now, but the transition from laboratory experiments to industry practice has been rather slow. One of the main reasons is the existence of uncertainty throughout the damage assessment process. Structural health monitoring has been identified as a pattern recognition problem, and in order to effectively detect and localize damage using experimental models, the issue of uncertainty must be properly dealt with. While most previous studies focused solely on the use of modal parameters, such as natural frequencies and mode shapes, this study introduces techniques based on pattern recognition and uncertainty analysis for effectively detecting and localizing structural damage.

The main objectives of this dissertation are:

1. To develop vibration-based SHM techniques which recognize and mitigate the associated uncertainties. Damage detection and localization is to be performed considering (i) uncertainties in the measurement noise and the analytical modeling and (ii) the cases when

only a small number of degrees of freedom are available for measurement and a few modes are estimated.

2. To study the proper representation, analysis and management of context uncertainties. The motivating question behind this work is how information should be managed to support diagnostic decision-making under uncertainty. By addressing the uncertainty issue in structural diagnostics, the goal of reduced false-diagnosis in structural damage assessment may be achieved.

3. To develop an effective and robust damage detection technique based on pattern recognition. Damage in structures needs to be detected at an early stage in order to reduce the cost of maintenance and possibility of an unsafe scenario, but the change of dynamic characteristics of structures is relatively insensitive to small scale damage. The goal therefore is to enhance damage detection by incorporating pattern recognition in a robust framework. In addition, the question as to whether vibration-based methods are sensitive enough to detect and localize small scale damage will be addressed.

4. To develop a damage localization approach based on the modal parameter sensitivity to local structural changes, such as stiffness reduction and mass modifications.

5. In order to perform model-based damage localization under limited sensor outputs, an output-only modal analysis technique is to be developed in order to obtain un-scaled mode shapes. Given the experimental model obtained using output-only modal analysis approach, damage localization can then be performed on modal parameters correlation analysis of damaged and undamaged conditions.

6. To address the environmental effects on the modal parameters of engineering structures and to validate the developed damage assessment approach with benchmark vibration data.

Figure 1.2 shows the schematic diagram of the proposed framework for damage detection and localization. First, perform an evaluation of uncertainty levels or noise content due to experimental measurement and environmental conditions. Based on vibration experimental data accumulated through repeated measurements, the objective is to develop a damage detection approach, which minimizes false indications due to the relatively small sensitivity of modal parameters to structural changes. Given a true-positive damage detection indication, modal parameters, such as mode shapes, are estimated based on a sensor merging technique with output-only structural response. A sensitivity-based modal parameter correlation technique is proposed, which is based upon the correlation interpretation of changes in modal parameters between an undamaged reference condition and a damaged one. It should be noted that inclusion of modal-sensitivity into the damage correlation analysis does not guarantee damage localization results to be free of false-positives. To minimize false-positives (damage indication in damage-free areas), a statistical sampling method is introduced into the damage localization process. The proposed damage assessment techniques are applied and validated using both in-house experiments on simple structures in laboratory conditions and real engineering structures.

1.3 Organization of Dissertation

The content and structure of this dissertation is arranged as follows:

Chapter 2 presents a literature review of the state-of-the-art vibration-based structural health monitoring, and uncertainty issues associated with the damage assessment process.

Chapter 3 presents established methods for addressing and analyzing the two types of data uncertainty, which are known as aleatory and epistemic uncertainties. Well known techniques such as probability theory, fuzzy sets, and evidence theory are described in terms of diagnostic reasoning support systems.

Chapter 4 presents a proposed damage detection approach which minimizes false-diagnosis due to aleatory uncertainty. To address the problem of noise content in damage detection, an ensemble of dimensional reduction method is given to facilitate the damage detection classification process.

Chapter 5 presents a computational study of structural damage assessment under varying conditions and uncertainty. Quantitative comparison of dimensional reduction and classification techniques is given via vibration analysis of a cantilever beam finite element model.

Chapter 6 describes a proposed output-only modal analysis technique based on sensor-merging for experimentally estimating structural mode shapes. The proposed approach is needed when limited number of sensor outputs are available and input excitation is not known.

Chapter 7 presents two vibration-based damage localization studies with a proposed sensitivity-based damage localization method. An in-house experimental structure is analyzed under mass modifications and their locations are approximated using the proposed damage localization approach. To validate the proposed damage localization method, the benchmark I-40 bridge data is also analyzed and comparison is made with baseline damage localization methods.

Chapter 8 presents an evidential reasoning approach for diagnostic decision-making under uncertainty. The proposed approach is applied to the vibration-based damage localization results obtained in Chapter 7. The evidential reasoning approach is based on the Dempster-Shafer (D-S) theory. This approach is found particularly useful for damage assessment of structures in the presence of uncertainties and imprecision.

Chapter 9 summarizes and concludes the dissertation. Future work recommendations are also provided.

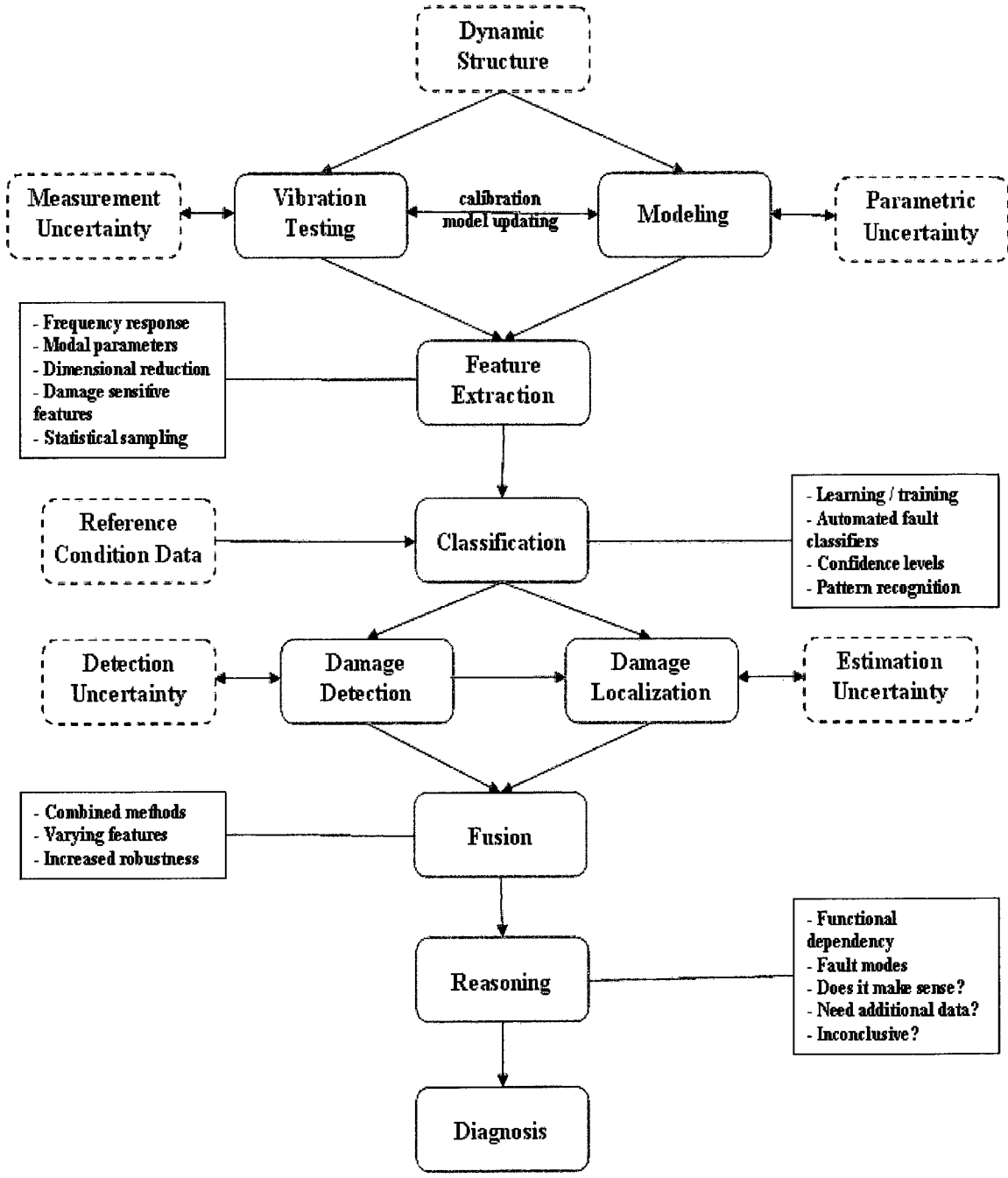

Figure 1.2. Damage assessment framework under uncertainty.

Chapter 2

Literature Review

This chapter reviews the definitions and state-of-the-art structural health monitoring under uncertainty with a particular focus on vibration-based techniques. We state the need for developing structural health monitoring technologies for diagnosing aircraft systems particularly as well as others, such as aerospace, automotive, and civil structural systems. In order to put this research in the appropriate context, a review of uncertainty sources in damage assessment is provided.

2.1 Vibration-Based Structural Health Monitoring

Over the last three decades, significant research work has been performed in the area of vibration-based structural health monitoring (SHM). In parallel, development in related and required fields, such as modal analysis, system identification and signal processing, have been evolving to support increase of damage identification performance in its accuracy and reliability.

Multiple research review papers have been written on the theoretical development and experimental application of damage assessment using structural dynamic properties. Doebling et al. [37] presented an extensive review of vibration-based SHM up to 1996. Sohn et al. [156] presented an extension of the vibration-based damage detection methods up to 2001. Carden and Fanning [21] presented a literature survey with particular emphasis on the research conducted and published between 1996 and 2003. Humar et al. [72] presented a performance comparison among the predominant vibration-based SHM methods. In addition, numerous conferences and field-specific journals have been established to further advance the development and practical

application of SHM. Although tremendous amount of literature exists on this topic at hand, significant issues remain to be studied, which have limited the transition from laboratory experiments to wide industry practice. The work presented in this dissertation aims at addressing the particular issue of diagnostic uncertainty in SHM. To facilitate the discussion, a brief review of the relevant literature to the current research is presented.

The basic premise of vibration-based SHM is that changes in structural properties, such as mass, stiffness, and damping, affect the structural dynamic response of the structure being observed. By studying the changes in vibration response behavior and performing system identification, the current health state of the structure can be obtained. For vibration tests, when available, the excitations and structural responses are measured via sensors and recorder in form of time history. Time-domain data can then be transformed into the frequency domain, and from which, the modal properties can be extracted. Although damage identification techniques exist which can be applied directly to time-domain data, the current review will focus on frequency- and modal domain data. The modal domain methods have generally attracted more attention and played a dominant role in state-of-the-art structural damage identification. In addition, the modal domain analysis has evolved in parallel with the experimental and operational modal analysis research areas. The physical meanings of the modal properties are more desirable and easier to interpret than the abstract time-domain mathematical features. Vibration-based SHM techniques can be grouped in multiple ways, such as physics model-based, inverse models, data-driven, among others. SHM can be classified based on the level of identification attempted:

Level 1. Detection - determination that damage is present in the structure.

Level 2. Localization - determination of the geometric location of the damage.

Level 3. Quantification - assessment of the severity of the damage.

Level 4. Prognosis - prediction of the remaining useful life or reliability of the structure.

The predominant approach for achieving Level 1 is data-driven techniques, such as statistical pattern recognition. For Levels 2 and 3, no dominant approach exists since in order to locate and assess the damage, structural domain-specific knowledge is required and that can only be obtained with the integration of either some form of system identification or reference finite element model. It is the author's opinion that data-driven techniques are still required to obtain reliable results. Therefore, a combination of model-based and data-driven techniques must be utilized to improve localization and quantification. Level 4 requires all of the above, pattern recognition and reference models, but also knowledge of failure modes, future usage and loading, and reliability models in order to estimate the remaining useful life. The damage identification methods based on vibration features can be grouped into: frequency-based methods, mode shape-based methods, mode shape curvature-based methods, and vibration-based other approaches.

2.1.1 Frequency-based Methods

Initial research in vibration-based SHM techniques focused primarily in damage detection using shifts in natural frequency [22,37, 145, 174]. The observation that changes in structural properties can be correlated to changes in natural frequencies was the impetus for using modal methods for damage identification. Although its simplicity makes it an attractive means for achieving damage detection, frequency shifts have proven to be relatively insensitive to damage, and even worse, these are sensitive to changes in environment and operations.

Early research by Whittome and Dodds in 1983 [174] used changes in resonant frequencies and response spectra to identify damage in offshore oil platforms. Changes in resonant frequencies of 3% over time were observed and attributed to changes to the mass of the decks and to changes in

the tide level (excitation). Frequency changes of 10-15% were observed when a structural modification was implemented that resembled a structural failure near the waterline. Cawley and Adams [22] studied how damage changes the dynamic stiffness of structures and used frequency measurements to detect damage using finite element model of structures. Salawu [145] presented an extensive review of publications prior to 1997 dealing with the detection of structural damage through frequency changes. Salawu concluded that natural frequency changes along are not sufficient for a unique damage localization because cracks associated with similar crack lengths but at two different locations may cause the same amount of frequency change. The latter issue if a major problem in damage localization. The same modal parameter changes can be obtained via multiple damage scenarios. Heylen and Lammens [71] developed the frequency response assurance criterion (FRAC) to correlate any two frequency response functions representing the same input-output relationship. The FRAC method was initially developed to correlate synthesize data with experimental data. A similar variation in the FRAC is the frequency domain assurance criterion (FDAC) developed by Pascual et al. [131], which is a FRAC-type method evaluated with different frequency shifts. Since the difference in frequency response function (FRF) model updating is often an FRF that is in question due to frequencies or resonances and antiresonances, the FDAC is formulated to identify this problem. Messina et al. [113] proposed a correlation coefficient termed the multiple damage location assurance criterion (MDLAC) by introducing two methods of estimating the size of defects in a structure. MDLAC is defined as a statistical correlation between the analytical and experimental predictions of the frequency changes.

A major drawback of the frequency-based techniques is that unrealistic damage patterns are often found. These methods cannot distinguish between damage at symmetrical locations in a symmetric structure. In addition, the number of measured eigenfrequencies is generally lower than the number of unknown model parameters, resulting in a non-unique solution. Due to its

inherent drawbacks, the frequency-based damage assessment applications for real complex structures or multiple damage detection are limited. Therefore, additional modal parameters, such as mode shapes are utilized in damage assessment analysis.

2.1.2 Mode Shape-based Methods

Compared to frequency-based methods, the advantage of using mode shapes for damage assessment is that mode shapes provide local information, which makes them more sensitive to local damages and enables them to be used directly in multiple damage detection. Given that resonant frequencies are properly identified, the mode shapes are less sensitive to environmental effects than natural frequencies.

The most common technique used for simple mode shape correlation between two states is known as the modal assurance criterion (MAC) developed by Allemang and Brown [4]. The MAC is a measure of similarity of two or more mode shapes. A MAC value of 1 indicates perfect correlation, and a value of 0 indicates no correlation or orthogonal modes. The MAC value only provides correlation among mode shapes, but not by each degree of freedom (DOF), which prevents damage localization. Lieven and Ewins [91] developed the coordinate modal assurance criterion (COMAC) to identify which measurement DOF contribute negatively to low value of MAC. The COMAC method compares a set of mode pairs, analytical versus experimental or experimental versus experimental. The two modal vectors in each mode pair represent the same modal vector, but each mode pairs represents all modes of interest in a given frequency range.

Shi et al. [151] extended the damage localization method based on MDLAC by using incomplete mode shape instead of modal frequency. The proposed two-step damage localization procedure is to preliminary localize damage sites by using incomplete measured modes and its extent again by using natural frequencies. Multiple other variations of mode shape correlation

approaches have been proposed in the literature, but additional issues exist on top of the correlation process. Given simulated or well-controlled experimental data, the mode shape correlation methods are well verified, but there are significant difficulties with full scale structures. The predominant issues with mode shape-based methods is the noise and estimation errors in the modal analysis techniques, which are highly dependent on excitation levels and type, and available inputs and outputs measurements.

2.1.3 Curvature-based Methods

Seeking further sensitive to damage, researchers have sought additional features based on modal parameters to deal with the shortcomings of frequency and mode shape-based methods. Among the features studied, the mode shape curvature (MSC) has been shown to have high sensitivity to localized damage. Pandey et al. [129] suggested that the MSC, that is, the second derivatives of mode shape, are highly sensitive to damage and can be used to localize it. Because MSC method is highly sensitive to mode shape changes, then it has been shown [50,72] that it is also highly sensitive to errors. In order to reduce the possibility of a false-positives, only the first few low curvature mode shapes can be used in for damage identification.

The development of high-sensitivity methods for increasing damage assessment accuracy demonstrates one of the main problems, which is that in all methods the same features that are sensitive to damage are also sensitive to errors or noise. The use of strain energy method or strain energy damage index (SEDI) to detect structural damage has been employed in several studies. Because the SEDI approach is also based on the second derivative of mode shapes, this particular can be categorized as a curvature-based method. The SEDI method was originally developed by Stubbs et al. [165] and applied it to beam like structures and is based on the comparison of modal strain energy before and after damage. When a particular vibration mode stores a large amount of

strain energy in particular structural load path, the frequency and shape of that mode are highly sensitive to changes in that load path. A particular advantage of this method is that it also quantifies damage by estimating the percent reduction in the localized stiffness.

Kim and Stubbs [84] applied the SEDI method to locate damage in finite element computational simulations and experimental plate girder. The method was demonstrated to find multiple damage sites. In addition, it was found that false-negative and false-positive outcomes were strongly influenced by the quality and amount of modal information. Humar et al. [72] conducted a damage localization comparison study which included frequency-based, mode-shape based, curvature-based methods, among others. Results demonstrated that the SEDI method appeared to be the most successful in predicting the location of damage. However, it was pointed out that method may not be successful when a damaged member contributes little to the energy in the measured modes. Farrar et al. [49] were successful using the SEDI method in locating damage in a bridge. They found that using this method outperformed the direct comparison of mode shape curvature before and after the damage.

Cornwell et al. [27] extended the SEDI method to 2D strain method for use in plate-like structures. Both the 1D and 2D SEDI methods were applied to experimental aluminum plate with two saw cuts induced damage. At low levels of damage, the SEDI approaches exhibited a tendency to produce false-positives.

Although damage localization methods based on curvature analysis have been shown to have higher sensitivity to damage, they also have an increasing sensitivity to measurement and parametric estimates noise, which creates significant false-positives. More robust damage identification methods are required that maintain the damage sensitivity, but at the same time, can minimize the negative effects caused by uncertainty in the measured and estimated data.

2.1.4 Other Vibration-Based Methods

Another category of damage identification methods makes use of the dynamically measured flexibility matrix to estimate structural changes. The flexibility matrix is defined as the inverse of the stiffness matrix. In the flexibility matrix, each column represents a set of nodal displacements of the structure due to a unit force applied at one of the DOF. Pandey and Biswas [128] suggested using changes in modal flexibility for damage identification. The method was applied to numerical models and an actual spliced beam. The numerical studies suggested that method worked best when damage was located at a section with high bending moments.

Based on the modification of structural model parameters in a numerical model, the model updating general approach is another class of damage identification. The model updating technique requires a finite element model (FEM) in combination with an optimization algorithm in which differences between experimental and numerical modal data are minimized by adjusting uncertain model parameters. The FEM has to approximate very well or as closely as possible the real structure in order to be efficient in the damage identification process. Yuen et al. [190] presented a method for detecting significant stiffness changes through continual updating of a structural model using vibration measurements. A Bayesian probabilistic formulation was used to treat uncertainties which arose from the measurement noise, modeling errors, and an inherent non-uniqueness common to this type of inverse problem. Zimmerman and Kaouk [195] presented the minimum rank perturbation technique, which was motivated by the observation that damage will tend to be concentrated in a few structural members, rather than distributed throughout the structure. The method was successfully applied on a eight-bay truss where damage was induced by removing specified members.

The main advantage of model updating techniques is that once a FEM has been found with good and consistent correlation to experimental results, one can then use the model to estimate

the severity of damage, such as stiffness reduction. Numerous published results of this class of methods have been published; however limited success has been demonstrated to date.

2.2 Sources of Uncertainty in Structural Health Monitoring

Flight vehicle structures are different than any other engineering systems in terms of primarily their dynamic environment, see Figure 2.1. The literature review presented in this section is based on a review paper by Lopez and Sarigul-Klijn [101] in which a comprehensive review of uncertainties involved in flight vehicle structural damage monitoring, diagnosis, prognosis and control was presented.

In flight vehicle structural terms, diagnostics is the detection and quantification of damage; prognostics occur when given damage assessment estimation of useful life remaining and/or performance life remaining until full failure is determined. In order to conduct diagnosis and prognosis several steps are required. Diagnostics is to investigate or analyze the cause or nature of a condition, situation, or problem, whereas prognosis is to know before, to calculate or predict the future as a result of rational study and analysis of available pertinent data [51].

In general, a diagnostic system consists of data acquisition system, signal processing, feature extraction and selection, physical models, and knowledge base of damage when possible, which may be derived from expert knowledge, such as historical data. Decision making is made by comparing the extracted feature information with the knowledge base, essentially becoming a pattern recognition method. For degradation analysis and prognosis, performance and degradation predictive models, which could be derived from time-series analysis methods, probability theory and/or artificial intelligence approaches, are required to forecast when the structural performance will decrease to an unacceptable level. In the areas of damage assessment and prognosis, information gathering and decision making processes are plagued by imperfect communication

channels, in other words noise and ignorance, which have been improved via enhanced signal and sensing capabilities, additional data mining techniques, and adding diagnostic system redundancy.

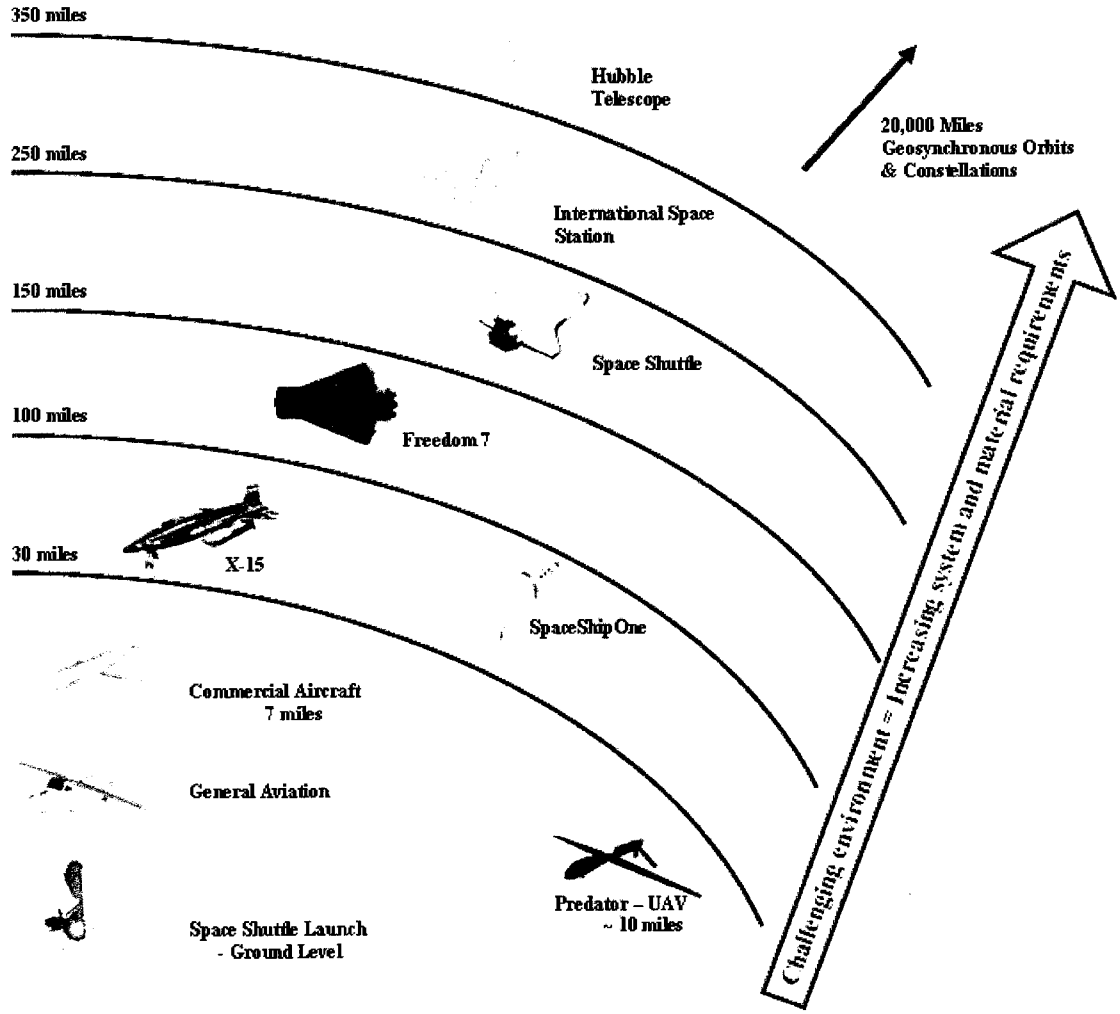

Figure 2.1 Aeronautical and aerospace vehicles shown along with their design environment within the atmosphere and beyond [100].

2.2.1 Model Uncertainties

The demand for expansion of the performance envelope of structures, such as ever increasing speeds, has generated significant advances in the development of lighter, more flexible, and consequently, more complex and nonlinear structural systems. At the same time, higher-fidelity models with faster solution methods and algorithms have been developed for many applications resulting in reduced simulation and cycle times. However, for complex structural systems, the computational advances still fall short for many reasons. Furthermore, the potential of modeling and simulation to understand the innate system behavior under unforeseen damage scenarios becomes highly inefficient. Recently, Worden et al. [176] presented a review of nonlinear dynamics applications to structural health monitoring. The uncertainties of models of complex systems are much greater than for simple systems. Reduced order models are simplifications of system descriptions which allow one to use incomplete information about the system, and as such, if high definition of information is not necessary, one is allowed to suppress or reduced the order of the mode without loss of model accuracy. The concept of uncertainty is therefore connected with complexity and information. This review classifies nonlinear techniques for SHM into three main categories: (i) nonlinear indicator functions; (ii) nonlinear dynamical systems theory; (iii) and nonlinear system identification. Research developments in nonlinear dynamical systems have resulted in increasing applications that take advantage of nonlinear phenomena to design damage detection algorithms.

Nonlinear instabilities experienced by many engineering systems and the resulting aperiodic motions have been studied. Numerous works [83,123] using damaged and buckled beams have been made chaotic motions are studied to understand the fractal characteristics of strange attractors via Poincare maps. In related work, the changes in the geometrical features of an attractor associated with the structural response have been studied in the considered system.

Epureanu et al. [43] presented the application of probability distribution function of sampled attractor dynamics and proper orthogonal decomposition to damage detection of an aeroelastic system under stretching and bending coupling. Although this study addresses nonlinear dynamics and complex fluid-structure interaction, the study only presented a numerical study without accommodation of signal noise and measurement variability.

Recently, progress has been made by using chaotic excitation and attractor analysis to detect damage in structures [83]. The approach is validated through experiments of a cantilever beam. By tailoring the chaotic excitation, these studies have shown that differences in response attractors can be used to identify structural damage. To accommodate for uncertainty, a baseline of healthy attractors, the damage attractors are identified. In addition, statistical process control is used to create and track the nonlinear cross-prediction error (NCPE) as structure changes from healthy to increasingly damage. Harrison et al. [68] presented a comparative study among NCPE, chaotic amplification of attractor distortion (CAAD), Holder exponent, attractor continuity map, and the simple root mean square (RMS) statistic. This study was performed on a composite unmanned aerial vehicle (UAV) wing using fibre-bragg grating sensors. Due to the timescale of experiments, environment effects and measurement errors are part of the presented analysis. Results of this work demonstrate that CAAD and Holder exponent identify damage in all test cases, while the NCPE and continuity measures based on attractor analysis and RMS features fail at detecting the damage. Adams et al. [2] presented a nonlinear dynamical systems framework for structural diagnosis and prognosis based on lower dimensional damage manifolds and normal form simplifications. However, the experimental results demonstrated were rather limited and no clear identification and assessment of damage was made based on the proposed nonlinear approach. Many other nonlinear dynamical systems approaches, such as Lyapunov exponents, local and global bifurcation, for SHM have been studied [176]. Kerschen et al. [83] presented a

review of nonlinear system identification methods. The authors concluded that due to the highly individualistic nature of nonlinear systems, no general analysis method is applicable to all systems in all instances. For nonlinear systems, analytical description is rarely possible. Hence, there is a great need to develop a robust and less model dependent approach of damage diagnosis in a complex nonlinear dynamic system.

Structural damage management systems based on system identification approaches can be broadly classified into the following three categories: (a) nonparametric identification approaches; and (b) parametric identification approaches. Nonparametric techniques attempt to identify the functional representation of the structure without any priori assumptions of the model's structure. Nonparametric models are described by curves, functional relationships, such as neural networks, and tables. Nonparametric analysis methods applied to the area of damage assessment are transient analysis, frequency response, correlation analysis, time-frequency analysis, spectral analysis, and black box modeling. Frequency domain methods have been widely studied for SHM applications and they suffer from the fact that they are limited to linear systems. Worden et al. [176] presented a survey containing multiple applications of correlation and spectral analysis in the area of nonlinear dynamics in structural health monitoring. Correlation and spectral analysis can detect presence of nonlinear response, and cannot handle non-monotonic nature of many nonlinear systems. Fassois et al. [52] presented a paper on timer-series methods for fault detection and identification. Uncertainties are naturally taken into account using time-series methods since they are data based rather physics based. Time-series nonparametric nonlinear system identification for damage assessment include spectral models, Hilbert transform, Huang-Hilbert transform, and stochastic subspace identification, among others [83, 176,185].

Frequency-domain nonlinear system identification methods include Volterra-Wiener series, nonlinear normal mode (NNMs), and higher order spectra [82]. In the last decade, time-frequency analysis has been shown to be an effective tool in studying nonlinear phenomena, especially damage characteristics. As its name states, time-frequency analysis blends the frequency and time-domain methods to offer "continuous" snapshots of nonlinear and nonstationary system dynamics [122, 160,161,163,167]. Analytical approaches for time-frequency analysis include, but are not limiter to, Gabor transform, Wigner-Ville distribution, Haar wavelet, short time Fourier transform (STFT), Choi-Williams distribution, and multiple wavelet analysis methods [160,167]. The nonparametric approach can have general applicability without restriction on the system input excitation and can effectively model structural nonlinearity.

Neural network (NNs) approaches for SHM relies on estimating the outputs and residuals of the system response. Given the lack of comparative studies of NNs, Markou and Singh [108] presented a guide to enable proper selection of neural network approach for its desired application. Several studies have considered uncertainty in application of artificial neural networks (ANNs) [8,55,132,139,142,179,194]. The noise rejection learning method proposed by Matsouka [110] has been a popular method of considering uncertainties in ANN applications. In the noise rejection method, certain amounts of noise are applied to the training data to consider either modeling or measurement error. Bakhary et al. [8] studied the uncertainty generated from errors in the finite element model and noises in the measurement data. The statistical approach applied to the ANN assumes normal distribution and generated a probability of damage existence by comparing model probabilities generated using Monte Carlo simulation. ANN do not quantify the uncertainty involved in a process event, instead, they are used to filter out uncertainty.

Patton et al. [132] developed a neural network approach for multi-input and multi-output nonlinear dynamic system where residual analysis is used to detect and localize faults. Work by

Patton demonstrate that NNs are excellent for nonlinear systems, but with moderate noise tolerance, extensive training sessions during design, complex implementation, and requires a large amount of computation. Recently, Yang et al. [187] presented a neural network approach for diagnosis of complex dynamic systems based on multi-sensor and multi-domain knowledge fusion (MSMDK). By using the MSMDK model, fault decision uncertainty was reduced by making full use of the sensor information and system knowledge. Yang proposed the use of Dempster-Shafer evidence theory to reduce the conflict of different evidences by defining the preference weight. The proposed approach was demonstrated via an experiment of the diagnosis of a helicopter autopilot.

Primary strengths of ANNs are its application to problems with robustness, complex nonlinear systems and on-line identification. However, the non-uniqueness of the neural network models of the dynamics of systems is a major impediment in matching physical behavior with a change in neural network parameters. Although NNs are very effective in identifying nonlinear relationships, the reliability of the damage assessment remains questionable due to the errors in the input modal parameters. Model updating would improve the modeling accuracy, but the applicability of this process is rather limited due to complexity of real structures.

The problem of parametric model identification using dynamic data is a promising area in various engineering applications due to its applications when structures are time-varying. In practice, it is not possible to fully capture the dynamic characteristics of a structure via high fidelity simulation models due to incompleteness in parameter and model uncertainty. Much attention has been devoted to the identification of mass-stiffness and modal parameters of linear systems under stationary input excitation. The linearity and stationary assumption is valid only in small-amplitude (relative) and when Gaussian noise analysis is applicable. Methods based on least-squares and Kalman filter [26,96,154,186] have been proposed to estimate dynamics

properties such as stiffness, mass, natural frequencies, modal damping, and mode shapes of multi-degree-of-freedom (MDOF) systems.

In practice, stationarity is not always applicable, and nonstationarity analysis is required. For the identification of time-varying structures and their variations due to damage, time domain analyses have been used extensively, in particular, the methods of least-square estimation, extended and regular Kalman filters, adaptive recursive least squares (RLS) with constant or varying forgetting factor and/or matrix [186]. The commonly used technique is the application of a forgetting factor. The drawback of a constant forgetting factor is that if the forgetting factor is small, it has a better capability of tracking parametric variation, but it is very sensitive to measurement noises. But if the forgetting factor is too big, its tracking capability is compromised. The application of forget matrix, in other words an individual factor per varying parameter, attempts to isolate each parameter and its variation from the rest of the system, which allows for detection and localization of damage. Furthermore, Smyth et al. [154] and Yang et al. [186] show that the direct and simultaneous identification of stiffness and mass parameters requires the acceleration, velocity and displacement measurements, which are rarely all obtainable or available. Likewise, if displacement and velocity responses are derived through integration of acceleration response, significant errors will result. These approaches can identify and track time-varying system parameters; however, they are not very efficient when non-Gaussian uncertainties are involved and require the availability of all DOF and state responses. Additional nonlinear system identification approaches discussed in literature include the nonlinear auto-regressive moving average with exogenous input (NARMAX) which is a generalization of the ARMA time-series models [83].

In order to properly describe the uncertainties arising from measurement noise, modeling error, data incompleteness, statistical methodologies based on Bayesian probabilistic inference have

been developed. The advantage of Bayesian approach is that it follows directly from the probability axioms and there are no ad-hoc assumptions that lead to loss of information. Multiple works have been presented in the use of Bayesian inference to identify and update the uncertainties in model parameters and model selection [12,26,79,119,189-191]. Model identification and selection for both linear and nonlinear dynamic models have been studied in the case of measured input and outputs and for the case of output only measurements. Katafygiotis and Yuen [79] present a statistical model updating methodology based on modal identification method. This study was limited with training data since it was based on benchmark study. When noise was included, the results showed multiple false-positive damage locations. Yuen et al. [189-191] presented a Bayesian approach for damage detection using output measurements only. The method presented does not make any assumptions about stationarity of input excitation and signal noise content, but it was limited to a numerical example.

Muto et al. [79] and Kerschen et al. [83] applied Bayesian inference and Markov Chain Monte Carlo (MCMC) to identify the unknown probability distribution, which captures the uncertainty of a parametric model and as a goodness-of-fit model comparison. These works have been based on the quantitative expression of model parsimony, also known as Ockham's razor, which states that effective simpler models are to be preferred over unnecessarily complicated models. The reason for such is that complicated models will tend to over-fit data and result in poor future prediction performance. In addition, most of these studies have only been demonstrated with numerical and experimental models that have limited degrees of freedom.

State estimation and system identification of nonlinear structures with non-Gaussian uncertainties can be applied. However, this technique is computationally expensive and to reduce this expense, significant experience is required to develop a simplified model that captures the necessary system dynamics. Through comparative analysis, Ching et al. [26] demonstrate that

Gaussian-based estimation and identification algorithms, such as Kalman filter, are only reliable for models that are almost linear on the time scale of the updating intervals, and when applied to real structural data, their applicability and reliability is questionable.

The uncertainties associated with structural model predictions have a significant impact on the decision-making process in structural health monitoring. System identification based on updating finite-element models using system response data is challenging and computationally expensive, however the large number of uncertain parameters associated with these models makes the inverse problem extremely ill-conditioned. In addition, non-Gaussian estimation capability is required in order to properly capture the uncertainty probability distribution. Direct calculation of the probability density function of the model parameters allows for quantification of the uncertainties of the parameter estimates. As stated by Ockhams' razor, simplified models are required, but with appropriate model selection. In real world applications, complicated models would require a large number of sensors and its data processing would be computationally expensive.

While significant work has been done to understand the structural damage under external excitations, little work has been done to understand damage characteristics under coupled loading conditions, such as aeroelastic phenomena. Wang et al. [173] studied the aeroelastic characteristics of a cantilevered composite panel. This paper investigated the effects edge crack growth and location has on flutter and divergence speeds. The crack damage was assumed to remain open; thus negating the nonlinear phenomena. This qualitative analysis demonstrates the multiple difficulties involved when considering complex structural and loading conditions.

Furthermore, as pointed out by Worden et al. [176] nonlinear response contains nonuniqueness ability, meaning that system responses will not vary monotonically. Therefore, the monotonicity

of the structure in question needs to be well understood if required for damage assessment. As a result, complex system dynamics often generates significant epistemic uncertainty in damage assessment since understanding and predicting response of nonlinear systems - even when undamaged – is a very challenging task. The stronger the nonlinear response is, the bigger the lack-of-knowledge becomes. As stated in Worden et al, with the exception of the Holder exponent example, all applications of nonlinear dynamics to SHM have been made at the numerical and laboratory scaled experiments where system variability and system complexity uncertainties are well controlled and limited. Furthermore, Kerschen et al. [83] points out most nonlinear approaches assume a deterministic nature, and the degree of uncertainty is rarely quantified, and the following fundamental questions need to be properly addressed: (1) Are the experiments and simulations consistent statistically speaking?; (2) What is the degree of confidence associated with the first answer?; and (3) If additional data sets are available, by how much does the confidence increase? Nonlinearity and system complexity is a type of uncertainty where there is not enough information, in other words it is an epistemic uncertainty.

2.2.2 Environmental Uncertainties

In practice, engineering structures are exposed to varying operational or forced and environmental or natural conditions. In the structural health monitoring area, it has been widely recognized that changes in structural response and/or behavior attributed to damage is difficult to discriminate from those due to environmental and operational effects.

Considerable research efforts have been made to investigate the separability and/or filtering of environmental variability from structural changes due to damage. Sohn [155] published a review of the effects of environmental and operational variability on structural health monitoring. In this survey, data normalization is determined as the primary path for filtering the unwanted effects of

operational and environmental conditions. In civil engineering structures, numerous studies [3,34,48,85,92,155,158] have been performed to determine the variability of modal properties of the civil transportation and structural systems in consideration of different environmental factors. The natural variability of the eigenfrequencies of bridges have been approximately determined to vary 5-10% over a 24-hour period. Sohn et al. [158] proposed a linear adaptive model to discriminate the changes of modal parameters due to temperature changes from those caused by structural damage. Peeters et al. [138] proposed a methodology to detect damage in the presence of varying environmental conditions using ARX models and confidence intervals.

Most of the work in accounting for environmental and operational effects during damage assessment has been done via a data normalization scheme. Data normalization requires a knowledge basis or training at all the normal conditions of the structure in question. Data normalization methods include neural networks, dimensional reduction, novelty detection, principal component application, and regression modeling, among others [97,155]. Balmes et al. [9] proposed a nonparametric based on residual associated with a subspace identification algorithm. In this study, temperature effects are accounted for by merging reference data sets recorded at unknown temperatures. To deal with the uncertainties associated with varying environmental conditions, Sohn et al. [158] proposed an outlier analysis approach based a neural network trained with results of a nonlinear principal component analysis (NPCA) that determines the distribution of certain identified structural parameters over an undetermined number of environmental factors. Koo et al. [86] proposed an impedance-based SHM technique combining a temperature compensation technique and outlier analysis. The compensation technique is based on cross-correlation coefficient with an effective frequency shift, which is defined as the frequency shift causing the concurrent impedance data to have the maximum correlation with the reference-impedance data.

Lopez et al. [95,97] presented a comparative study of linear and nonlinear dimensional reduction techniques to normalize modal data of a deteriorating cantilever beam model under temperature variations and artificial noise. The study demonstrates the importance of dimensionality reduction techniques prior to proper classification of damage or undamaged data. Manson et al. [106] studied the damage detection of composite panel under changing conditions of humidity and temperature. In this study, the analysis was based on Lambs waves, PCA pre-processing and outlier analysis. Piezoelectric (PZT) sensors used to generate Lamb waves can be used as both exciter and sensory receiver, which provides the very important benefit of having the capability of controlling the input excitation. Results of this study demonstrate that damage-sensitive features are more sensitive to temperature in comparison to humidity, and emphasize the need for normalization data which covers all normal operations of 'damage-free' structure. Raghavan et al. [141] presented the use of the pulse-echo approach of guided-waves to study damage detection at elevated temperature for space applications. Indentation damage detection was possible at temperatures up to 80°C, and thru-hole damage was achievable at all temperatures, 20°C to 150°C. In this study, a search for temperature insensitive material properties and simple signal similarity difference approach was used to perform outlier analysis.

Environmental factors can also have a significant effect on the boundary conditions of the structure. Lew et al. [89] presented the use of feedback control to enhance the sensitivity of natural frequencies to structural damage, while minimizing the sensitivity due to uncertain boundary conditions. This study, however, assumes primary structure has or allows for a secondary structure (up to 20% of primary mass) to act as passive controller, disregards any effects the vibration control would have on the structural performance, and does not take noise content into account. Moyo et al. [118] presented the use of Box-Jenkins modeling to assess and separate the effects of operational anomalies, such as traffic, accidents and maintenance, from

permanent effects originating from damage on a bridge. In this study, temporary structural response anomalies, i.e. operational changes, were identified and separate from permanent changes, i.e. damage.

2.2.3 Sensor Uncertainties

In the process of damage assessment, a very critical communication component is the sensor unit and network chosen and designed for the monitored structure. The information provided by the sensory system must be assessed under a complete understanding of the principles governing the operation of the sensor and its physical and spatial limitations. Sensors imprecision and uncertainty is an inherent property because they are subject to noise, which is a generic term encompassing imprecise and/or unwanted behavior. The occurrence of sensor noise are poor understanding of the principles governing the sensor behavior, a lack of understanding of the environment, changing environmental and/or operational conditions, and tolerances within the sensor, among others. Note to the reader, this section does not deal with the typical filtering, such as windowing and sampling rate, of signal in order to remove noise. Due to its uncertain nature, sensor data must be validated for damage assessment since high fidelity is required. Sensing uncertainty may arise from non-permitted deviations due to sensing device, transducer, signal processor, and communication interface, which may appear mainly as bias, drift, complete failure and precision degradation.

Sensor or instrument fault detection and identification (IFDI) has been studied by numerous researchers in multiple areas. Mehranboud [111] offers a detail review on the application of Kalman filters, parity relation, PCA, artificial neural networks (ANN) and Bayesian belief networks (BBN) to detect and identify faults in sensors. Mehranboud's work is based on BBNs for dealing with uncertain knowledge on the reliability of sensors. In this context, the sensor

becomes the structure under question for health monitoring. Furthermore, it is recognized that simultaneous IFDI and structural damage assessment should be performed; thus, quantifying and incorporating sensor uncertainty into the overall SHM process.

Often times, redundancy is included in sensor network design to make sure that sensor data is available even when discrete sensor failures occur. Friswell and Inman [57] presented sensor validation methods based on modal filtering as well as PCA residual analysis given the case of data redundancy. For modal filtering, the analysis assumes low uncertainty in the modal parameters. In a follow up work, Abdelghani and Friswell [1] presented a residual analysis method for the localization of faulty sensors for additive and multiplicative faults in sensors. The damage localization is based on a correlation index; however, the correlation index fails at providing sensor fault magnitude. Thus; the deciding if sensor is faulty depends on user's threshold or experience. Kerschen et al. [81] makes use of PCA for sensor fault detection, isolation and correction. The procedure was experimentally evaluated using a beam under linear and nonlinear behavior. Kerschen identifies that work needs to be done in separating sensor faults from structural damage.

Ibarguengoytia et al. [74] presents an algorithm for sensor validation in real-time environments. The algorithm is based on Bayesian networks and was applied to temperature sensors from a combined cycle gas turbine for sensor fault diagnosis. A hierarchical process is applied where one Bayesian network is applied for detection and a separate one for faulty sensor isolation. Mengshoel et al. [112] applied Bayesian networks for sensor validation and diagnosis to an electrical power system of aerospace vehicles. Dai et al. [29] proposed an adaptive distributed coordination framework for handling sensor uncertainty. This approach is based on multi-agent systems and rough set theory, an extension of set theory and similar to fuzzy theory. The

framework offers a hierarchical approach to handle multiple types of sensor uncertainties via data fusion techniques; however, demonstration of such framework was not provided.

Goebel [61] studied fuzzy logic to achieve sensor validation by expressing a confidence for a given measurement based upon an expected value, the system state, the environmental conditions, sensor reliability, and physical limitations of the system. In this work, uncertainty management is achieved via validation of sensor readings, sensor fusion, and sensor diagnosis. Sensor validation and fusion are addressed by probabilistic, fuzzy and neural networks, while sensor diagnosis was addressed via fuzzy theory. Guo et al. [62] proposed a framework for sensor validation in classification problems based on evidence theory. The proposed evaluation framework is applied to a target classification of moving vehicles using acoustic, seismic, and infrared sensors.

Significant progress has been done in addressing sensor placement in the area of SHM. Because sensor placement is essentially an optimization problem and not uncertainty problem, only a few sensor placement papers address the issue of sensor related uncertainty for structural damage applications. Guratzch [66] proposes a methodology for sensor placement optimization for SHM under uncertainty. This methodology was numerically evaluated using stochastic finite element models to generate random uncertainty levels. Optimal sensor placement was derived from probabilistic and reliability-optimization analysis of model responses. Guratzch points out that proposed approach is computationally expensive due to the optimization of stochastic finite element models. In addition, the study provides optimal sensor placement but no validation with experiments. For further information, Staszweski and Worden [164] present an overview of optimal sensor placement methods for damage detection applications.

When dense sensor networks are utilized, wireless communication becomes attractive since electrical wiring is practically eliminated or centralized. Promising research area is that of 'smart'

sensors. Nagayama [120] studied the application of smart sensors in SHM. Smart sensors are designed with the following capabilities: signal pre-processing, such as measurement of multiple physical quantities and data compression; low- or self-power feature; and self-organizing collaborative capability. Giurgiutiu et al. [60] present a brief review and application of embedded PZT in which sensors act as a receiver and actuator. The sensor-actuator approach enhances the control over the damage-sensitive feature being extracted from acquired signal. In this study, it is identified that work is still required to account for operational and environmental variations in order to reduce uncertainty affecting the damage diagnosis. For practical implementation of smart sensors, several challenges, such as data loss, time synchronization errors, scalability, sensitivity, communication range, and power limitations, must be overcome.

2.3 Essential Concepts in Information Processing and Pattern Recognition

Damage detection and assessment is fundamentally a correlation problem between known healthy structural response data and unhealthy structural response data. Because of the uncertainties that exist in the damage assessment process, which causes noise content to be at the same or greater level than the change or anomaly caused by damage, the damage assessment problem has been identified essentially as a pattern recognition problem [51]. As such, the discussion and work presented in this dissertation will contain multiple terms normally used in signal processing and computer science algorithms research.

The following terms are defined below:

- *features*: individual measurable or identified properties of the phenomena being observed. For structures, features can be natural frequencies, damping properties, stiffness, etc.

- *datasets*: matrices in which the columns represent the measurement sample and the rows represent the features, class memberships, or other fixed sets of properties.
- *mappings*: transformations operating on datasets. For example a projection from 3D to 2D.
- *dimensionality reduction*: process of reducing the number of random variables under consideration, which is divided into feature selection and feature extraction.
- *feature selection*: process of finding a subset of the original dataset, which provide relevant information for the a desired task.
- *feature extraction*: transformation of initial data into a reduced representation set of features, which are expected to contain the relevant information from the initial data in order to perform a desired task.
- *class* or *pattern*: groups of measurement or observations defined by on *a priori* knowledge or on statistical information extracted from the patterns.
- *classification*: task of generalizing known patterns or classes to apply to new data. For example, in damage detection, a classification algorithms attempts to properly allocate new measurement data to undamaged or damaged classes.
- *data fusion*: use of techniques that combine data from multiple sources and gather information in order to achieve inferences, which will be more efficient and potentially more accurate than if they were achieved by means of a single source.

For recognizing the classes of objects or structural response data, the structure is first measured by sensors. The raw measurement data is then represented in a feature space, and after some possible feature reduction steps, the measurement samples are finally mapped by a classifier on the set of class labels, i.e. damaged or undamaged. From the initial raw-data representation in the

feature space, and this final mapping on the set of class labels, the representation of measurement samples may be modified and transformed multiple times, such as: data transformations (time to frequency domain), simplified feature spaces (feature selection), normalization of features (scaling), linear or nonlinear mappings (feature extraction), classification by a possible set of classifiers, and final damage diagnostics decision.

2.4 Information Processing for Diagnostic Decision-Making

Different preprocessing techniques for handling measurement error, noisy data, and data transformation and compression exist. Multiple reviews concerning the application of advancements in signal processing to damaged structural response have been published, as reported in [52,122,163]. Most signal processing techniques for damage detection rely on Fourier analysis for time-invariant stationary problems, and time-variant methods, such as wavelets, time-frequency and time-series analyses.

Staszewski [162,163] has written multiple review papers discussing the usage of time-variant analysis in damage assessment. Time-frequency methods include, but are not limited, short time Fourier transform (STFT), Wigner-Ville distribution (WVD), Choi-Williams distribution (CWD), among others. Staszewski states that the major difference between each time-frequency method is the way that it handles the problem of uncertainty. Staszewski [162] and Taha [167] present a review of wavelet analysis for damage assessment. Wavelets serve as time-varying analysis tools suitable for decomposition, compression and feature selection. Well known wavelet methods include continuous, discrete, and multi-resolution wavelets. Wavelets are also subject to the uncertainty principle. In the case of wavelets, Staszewski marks the difference between time-frequency representations and time-scale representations, i.e. wavelets. An important usage of time-variant methods is its application to nonlinear and non-stationary signal response analysis.

In general, time history response from sensors can be analyzed as is or can be transformed to frequency or time-frequency domain. Fassois et al. [52] presented a review of time-series methods for fault detection. Fassois argument that for linear systems there is little information loss between time and frequency domains. Further feature extraction, such as modal properties from frequency response data, inevitably results in loss of information since the tails of data range are usually discarded and it's contaminated by error propagation. Time-series analysis uses statistical tools for developing mathematical models describing one or more measured stochastic signals and analyzing their observed and future behavior. Furthermore, Fassois states that time-series methods account for uncertainty since they are data-driven based rather than physics based. But it must be also recognized that uncertainties are present and need be quantified even for data-driven methods, and that statistical methods are not always sufficient to account for and quantify the related uncertainties.

2.4.1 Feature Extraction and Selection

Subsequent to data pre-processing is the data mining process, whose main purpose is to discover the hidden knowledge and patterns within data, which may be applied for information management, optimization purposes, decision support, and process control. Critical to the objectives of data mining is the generation of quality data, which facilitates the decision-making in the assessment of structural health. Given large sets of data with multiple features, there exists significant amount of redundancy or unnecessary features which reduces the effectiveness, accuracy, and understandability of the data mining results. As such, data compression and dimensional reduction techniques may be utilized to reduce the size of datasets. One must understand that uncertainties will arise from the way data is truncated and compressed during the removal of unnecessary data features, feature extraction, feature selection and noise cleansing.

Uncertainties are inevitable, but they can and should be systematically addressed and accounted for.

In general, data mining must performed in order to facilitate the decision-making process of classification. The performance of the classifier depends on the interrelationship between datasets, number of features, and classifier complexity. Increasing number of data and dimensions results in what is known as "curse of dimensionality," which leads to the "peaking phenomenon" in classifier design [87]. In other words, more data does not necessarily mean more information due to the dependency and correlation of many multidimensional dataset. Jain et al. [75] states that increasing number of features may in fact degrade the performance of a classifier if the number of training samples that are used to design the classifier is small relative to the number of features.

Due to the complexity and high dimensionality of dynamic response data, the simple binary classification (detection case) of structural health into damaged or undamaged categories is not always clear. To perform binary classification, a pattern needs to be identified among signal features. In real-world data, these patterns are scattered in high-dimensional and very often nonlinear subspaces.

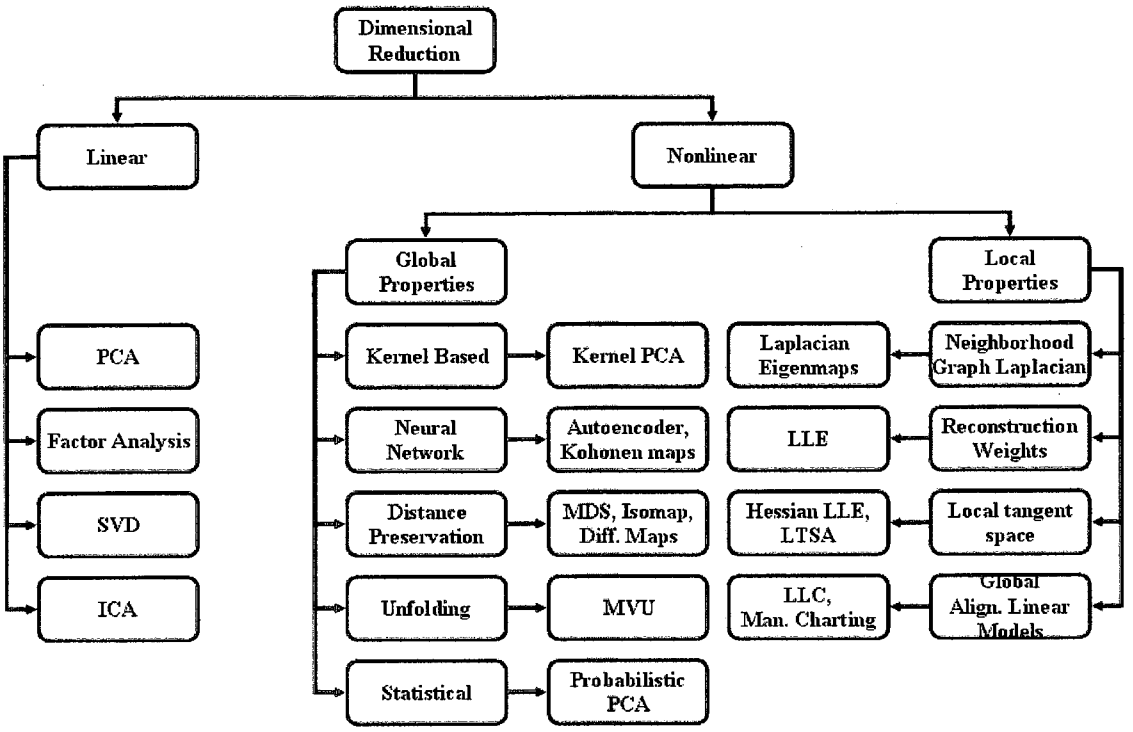

Figure 2.2. Taxonomy of dimensional reduction techniques [100].

Dimensional reduction simplifies the pattern representation and reduces the computational effort required from classifiers [94,98]. Dimensionality reduction can be defined as follows. Given a measurement matrix $\mathbf{X} \in \Re^{M \times D}$ consisting of M data vectors and D features, dimensional reduction techniques transform dataset $\mathbf{X}$ into a new dataset $\mathbf{Y} \in \Re^{M \times d}$, where $d < D$, with minimal loss of data geometry. Figure 2.2 shows taxonomy of techniques for dimensional reduction, where the main distinction is made between linear and nonlinear methods [75,98,101,107,115].

The best known feature extractor is the principal component analysis (PCA) or Karhunen-Loeve expansion that computes the m largest eigenvectors of the d x d covariance matrix of the n d-dimensional patterns. PCA has been used as feature extractor, selector, data compressor and

data clustering technique. Other methods, like nonlinear-PCA, KPCA, factor analysis (FA), projection pursuit, neural network based mappings, among other nonlinear mapping techniques have been used for feature extraction and clustering in damage assessment studies [76, 95,98,107,175,177,182,183]. Lopez et al. [95,98] presented a comparative study of dimensional reduction methods for damage detection applied to an aeroacoustic experiment. Results of this study demonstrate that nonlinear dimensional reduction techniques can be more effective than PCA in cluster analysis for damage detection, but not consistently and PCA tends to be more robust to lack of excitation. In the reviewed literature, limited studies have been published in using nonlinear dimensional reduction methods for SHM research.

Feature reduction can also be achieved via selection of features based on theoretical and/or practical engineering knowledge. The problem of feature selection is defined as follows: given a set of d features, select a subset of size m that leads to the smallest classification error. Feature selection methods that have been applied in SHM include branch-and-bound search, sequential forward selection (SFS), and sequential backward selection (SBS), [75]. Other works include similarity based feature selection methods. Mitra et al. [115] present an unsupervised feature selection using feature similarity and a brief review of feature selection methods. A more detailed explanation and review of these methods can be found in [75,101].

In general, different dimensional reduction and selection approaches will generate different feature spaces, and consequently result in different concept spaces and discovering different knowledge spaces. Feature extraction and selection is critical in the area of damage assessment. In general, these data mining techniques are based on methodologies of machine learning, pattern recognition, and statistical analysis. Given that the user is not clear on the properties of the damage knowledge that is of interest, the adoption of mining algorithms will be uncertain. The aim of applying data mining techniques in diagnostics is to provide the user with novel, useful

knowledge, which can be easily understood and evaluated in order to make decisions quickly and precisely.

In system diagnostics, it is desired and necessary to properly induce and reduce the acquired knowledge, and describe it in a way that can be easily understood and classified. Given that data mining has been performed, the next step is that of evaluation and explanation of discovered knowledge, in our case damage assessment. One major problem in knowledge explanation is to account and describe the uncertainties in qualitative concepts and how to implement the uncertainty transformation from quantitative data to qualitative concepts. Therefore, there are uncertainties not only in the process of data mining, but also in the discovered structural health state knowledge.

2.4.2 Classification Techniques

Classification is the most fundamental and most significant activities in SHM research activities. Classification is applied to describe the known data classes or models of concepts, so as to classify the objects with unknown class index by the known models/classes. As a supervised or unsupervised learning method, classification contains uncertainties. Complex classifiers are needed when the object to be classified is adjacent to two classes, or lies in the overlap region of multiple classes. In addition, if insufficient training is performed, the learning result will probably not be reflective of the overall structure of the data set, and therefore, will not categorize the damage state correctly, which for new data, there will be a lot of uncertain problems in its classification. Many classification approaches have been used and proposed for classification of SHM data, such as similarity metrics, decision tree induction, Bayesian-based classification, neural networks, genetic algorithms, fuzzy set classifiers, and so on [101]. The most general and well known of performing classification in damage assessment process is via direct statistical

analysis. Most of the initial work in diagnostics focused in applying statistical analyses, as reported and/or reviewed in [70,101,155,158,168,169-171,177].

Given a set of vectors $\mathbf{X}=(\mathbf{x}_1,\mathbf{x}_2,...,\mathbf{x}_n)$ with d extracted features, the decision-making process in pattern recognition is based on assigning these vectors to one of the possible classes $C=(c_1,c_2,...,c_{N_c})$. A decision rule partitions the measurement space into N_c regions Ω_i, $i=1,2,...,N_c$. Each region may be made up of multiple overlapping regions. The boundaries between the regions are the decision boundaries or decision surfaces. In terms of damage diagnosis, the overlap of these regions, in other words health states, are the highest proportions of misclassifications or false-diagnosis. In general, two decision-boundary methods exist in classification. The first assumes knowledge of the underlying class-conditional probability density function, which in many situations this will be unknown and must be approximated. The second approach develops decision rules that use the data to estimate decision boundaries directly, without explicit calculation of the probability density functions. Consider the binary hypothesis testing problem where a sequence of independent identically distributed damage index vectors are observed, then the likelihood ratio test (LRT) function is denoted as

$$\prod_{k=1}^{m} L(\mathbf{x}_k) \underset{H_U}{\overset{H_D}{\gtrless}} \tau(m) \tag{1}$$

where H_D denotes the damage state, H_U the undamaged state, and $\tau(m)$ is a predefined (if prior information exists) damage threshold.

A major issue in damage classification is that many classification algorithms assume that for training, class labels, i.e. information on each class, are available, but in practical damage assessment applications, labels of damaged data is not available unless destructive testing is

performed. As a result, direct application of supervised classification approaches is not always possible. Figure 2.3 shows the taxonomy of classification methods [101]. Clustering methods aims at finding groups in data via feature similarity. Although clusters are important in pattern recognition, because in SHM we are interested in classes with labels, clustering will not be covered in this paper. Structural classifiers are used for building classifier ensembles. Structural classifiers are usually described in graph, network, or membership terminology. Structural classifiers are becoming important and continuously growing as the demand for more robust and more accurate classification decisions are required.

In particular, classifier combination is highly justified as the next logical step in increasing decision knowledge. Comparing classifier combination to feature extraction, prior to extracting the most informative features, data is integrated as a single set, and then transformed to a lower dimension. Given that we can combine multiple classifiers, the next logical step will be to select the most effective classifier set. In the following paragraphs, we explore the multiple applications of classification methods in SHM.

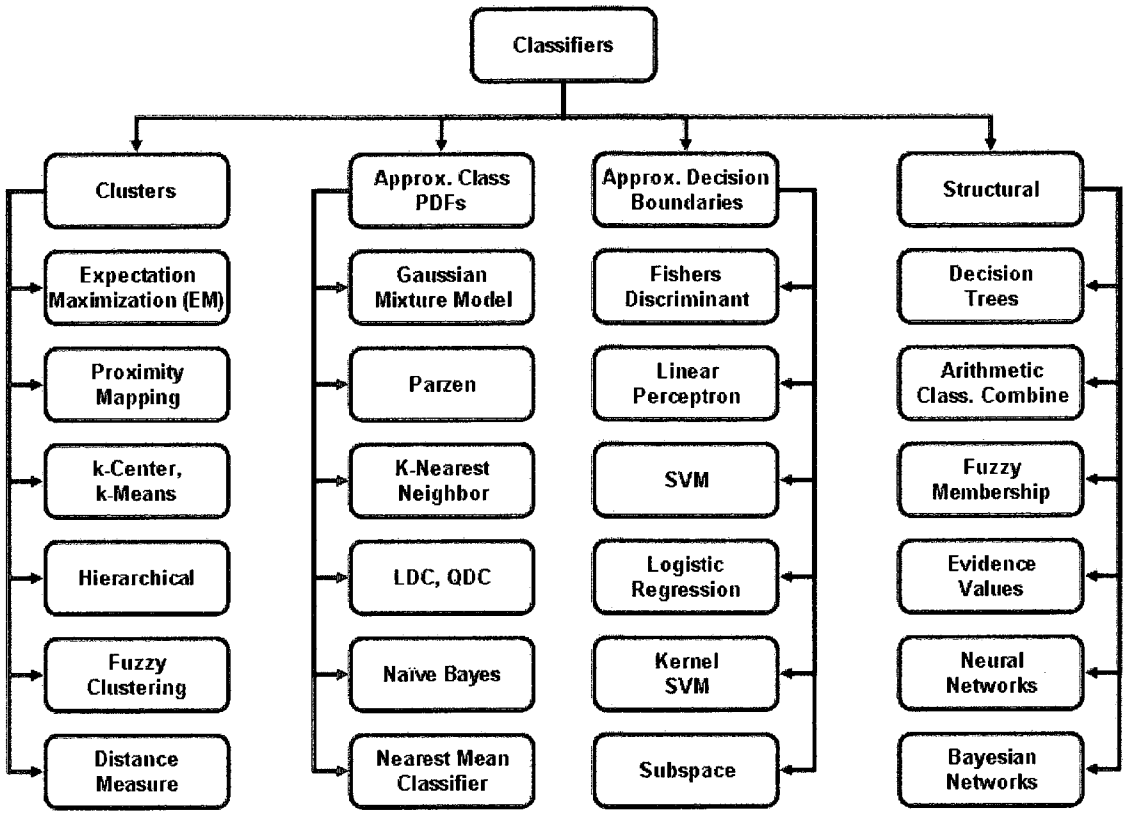

Figure 2.3. Taxonomy of classifier techniques [100].

Neural networks (NNs) have been extensively applied for feature extraction and classification of structural health data. Zang et al. [194] performed structural damage detection via artificial neural networks (ANNs) compressed by PCA. The integration of ANNs with PCA allowed for reduction in FRF data, i.e. reduction of computational expense, without loss of accuracy. The author states that pattern recognition and system identification are complementary; thus, indicating that methodologies should be fused for maximization of damage knowledge. Niu et al. [125] presented a comparison study of classifiers for fault diagnosis of a motor using multi-type signals. The study used the following classifiers for comparison: support vector machines (SVMs), linear discriminant analysis (LDA), k-Nearest Neighbors (kNN), random forests (RF), and adaptive resonance theory-Kohonen neural network (ART-KNN). The study demonstrates

that individual classifier performance is highly dependent on the damage scenario (binary to m-ary classification). Critiques of NNs point out that this approach conceals important information, such as data statistics, from the user and tend to be computationally expensive. Jain [75] states that despite these issues, NNs do offer several advantages, such as unified approaches for feature extraction and classification, and flexible procedures for finding good, moderately nonlinear solutions.

One of the most interesting developments in classifier design is the introduction of the support vector machine (SVM). Cao [20] used SVMs to develop a framework of probabilistic uncertainty modeling and reliability analysis and compared to Monte Carlo simulation method, first and second order reliability methods. In this work, uncertainties due to system lack-of-knowledge and human induced factors were studied as random variables with normal distributions. Using SVMS, accurate results relative to Monte Carlo simulation method were obtained with much less training data. Das et al. [30] used one-class SVMs based on time-frequency information for damage assessment of composite panels. One-class SVMs are useful for outlier detection when data is not available on damaged states. Das points out that further research is necessary in order to increase robustness of classifier in the presence of material and experimental uncertainties.

In diagnostic systems, knowledge from domain specific experts is usually inexact and reasoning on knowledge is therefore imprecise. Thus, measures of uncertainties in knowledge and reasoning are required for classification and decision-making to provide more robust damage assessment results. As stated previously, commonly used uncertainty measures are probability, fuzzy member functions and belief functions. The performances of statistical pattern recognition methods depend on the prior knowledge, which is often imperfect and incomplete. Probability theory can handle the uncertainty contained in the data, but it cannot treat the imprecision. The imperfect knowledge can be addressed by the use of belief- and/or evidence-based methods. The

problem of uncertainty in classification for damage assessment can be addressed by a continuous learning in order to add information carried by each new classified pattern to the database or prior knowledge.

Fuzzy-sets classifiers assigns degrees of membership in several classes to each input pattern. Fuzzy-sets theory was introduced by Zadeh to solve the problem of data imperfection. Ramu and Johnson [142] integrated ANNs and fuzzy logic to treat uncertainties related to damage assessment of composites. They point out that appropriate network construction is extremely heuristic and laborious. Altunok et al. [5] presented a damage pattern recognition approach based on fuzzy set theory. The proposed method does not assume any special statistical assumptions and does not require finite element modeling and was tested on an experimental model steel bridge. One drawback to this method is that damage quantification is as accurate as the number of sets chosen, which can be insufficient or rough.

Lei et al. [88] presented a clustering technique based on fuzzy c-means (FCM), PCA and compensation distance technique for rotating machinery. The features selected for clustering analysis are based on the characteristics of statistical-moments. Pierce et al. [140] applied MLP neural network classifiers to a damage detection problem within a framework of an interval arithmetic-based information-gap technique. The inclusion of interval analysis allowed the assessment of robustness of trained classifiers to uncertainty. DeSimio et al. [35] studied the effects of uncertainty via statistical classification in decision-making for SHM systems. Loose bolt damage assessment was performed on a composite thermal protection panel. Feature selection via sequential forward greedy approach is discussed and applied. Uncertainty analysis was limited to defining rejection criteria for classification of anomalous data, so when uncertainty is high and labeling is not clear, data is discarded. The latter approach relies on significant training data being available. Altunok et al. [5] presented the use of possibility distributions to

quantify healthy and unknown events, in other words outlier detection, to an ASCE benchmark problem. By applying possibility theory, the authors observe intervals without assuming any particular probability distribution.

Chandrashekhar et al. [24] proposed a fuzzy logic system for damage detection and isolation in beam structures with uncertainty. Taha and Lucero [166] applied fuzzy-sets to develop a damage metric combined with Bayesian updating scheme. Da Silva et al. [28] demonstrated an approach to vibration-based damage classification via fuzzy-sets. Pawar and Ganguli [135] developed a genetic fuzzy system and applied it for damage detection in beams and helicopter rotor blades. The genetic algorithm facilitated the selection time and optimality of fuzzy-sets. Application of fuzzy-sets and possibility has also been applied to fault diagnostic systems, such as satellite fault diagnosis [23], and rotating machinery fault diagnosis [78].

Structural design problems have been investigated via fuzzy-logic and evidence theory by multiple researchers, such as Nikolaidis et al. [124], Mourelatos et al. [117], Bae et al. [6,7], Yang et al. [184], to handle imprecise data situations arising from structural complexity. In particular, evidence theory has been used by multiple researchers for data-fusion applications. Bao et al. [10] employed D-S theory to combine evidence individual damage basic probability assessments from multi-sensory data. Such combination improved the damage assessment results in comparison to individual sensor damage assessment results. Guo and Zhang [63] used the D-S theory to identify multiple damage locations of a structure. They made use of Yager's weighted D-S theory approach to address the fact that different sources have different levels of importance and/or reliability. Li et al. [90] used the Shannon entropy to measure the uncertainty of the evidence and presented a weighted and selective fusion method by using an artificial neural network combined with D-S evidence theory and Shannon entropy. Basir and Yuan [11] performed engine fault

diagnosis based on multi-sensor information fusion using D-S theory. In particular, they focused on the combining schemes for evidence sources to address conflictive information.

Denoeux [32,33] developed an adaptive neural network classifier and a k-nearest neighbor classifier based on D-S theory. Denoeux points out that D-S theory is suitable for classifier combination, since it yields robust decisions procedures to changes in environment and possible sensor failures. Parikh et al. [130] made use of D-S theory and predictive rates for combining classifiers in a case study of thermostatic valve faults in a diesel engine cooling system. By using D-S theory base approach, the authors were able to properly classify multiple engine conditions. Results from the multiple classification comparison studies demonstrate the need for classifier combination or fusion schemes since it can be unpredictable which classifier will be the most effective on a case-by-case basis. Classifier combination aims at integrating the benefits of individual classifiers to maximize performance robustness; thus, reducing uncertainty in the classification outputs.

2.4.3 Data Fusion and Decision-Making

Due to uncertainty and imprecise nature of data acquisition and processing, individual informational data sources must be appropriately integrated and validated. To maximize diagnostic performance, data must be processed and contextually filtered to extract valuable relevant information. In terms of diagnostics, data fusion can be used at the feature and decision levels. Data fusion can be used to combine information from a multi-sensor arrangement to validate signals and extract damage sensitive features. System sensory data is generally processed to extract damage signature features, which can then be mapped to different health condition states. In the multisensory approach, individual sensory data may be classified and contribute a unique set of classifications represented by measured of belief or probability, which can be

numerical or of symbolic nature. The representation as numerical classification degrees lead to a quantification of its uncertainty content or incompleteness. Due to the less than unity classification, classified features when combined, provide a better estimate of the true diagnostic state. In terms of decision-level data fusion, the main task of data fusion is to combine information from several sources to make a better decision compared to decisions based on a single data source. The goal of data fusion is to reduce imprecision and uncertainty by increasing information completeness [67].

Various techniques exist for performing data fusion. To discriminate between feature-level and decision-level data fusion, we will focus on ensemble classifiers as the main feature-level data fusion approach, and inference engines as the decision-level data fusion approaches. Figure 2.4 shows a sample architecture for data fusion based on the distinction between feature-level and decision-level fusion. The final goal of condition monitoring and diagnostics is to make diagnostic decision under uncertainty and impreciseness. To distinguish between inference and decisions, we use the following definitions. Inference is the process of drawing conclusions from premises or evidence, and decision is the process of choosing an action. As stated in Walley [172], inference is more theoretical and impersonal, while decision is a more practical and specialized activity since it has practical consequences and it requires consideration of these consequences and their values. Inference engines include Bayesian networks, Dempster-Shafer's evidence theory, fuzzy sets, amongst others. Inference systems combine evidence to assess probabilities or possibilities of relevant events, in our case damage states.

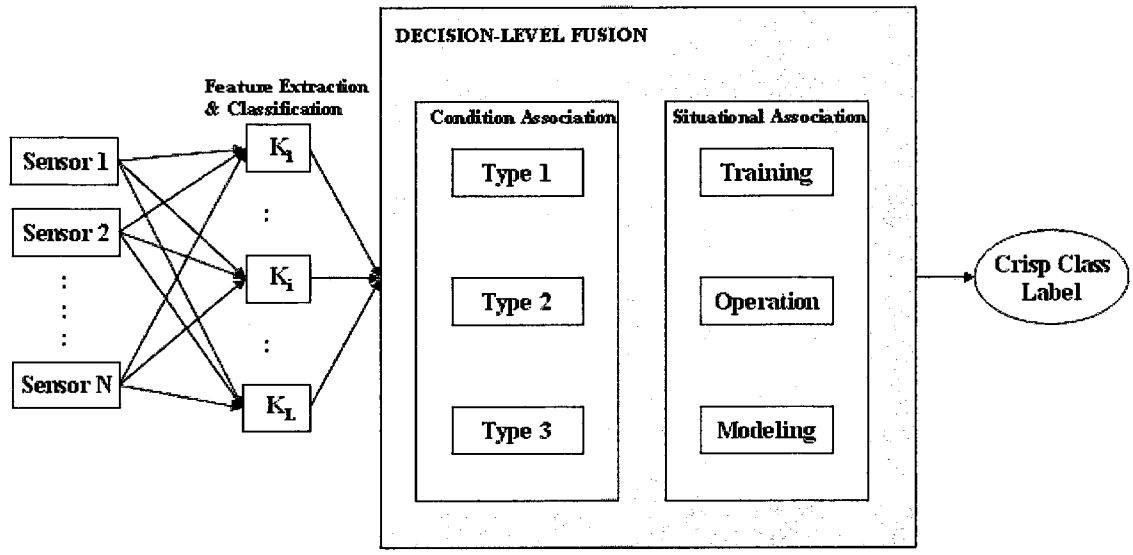

Figure 2.4. Architecture of multi-source and multi-classifier information fusion.

Kuncheva [87] defines these outputs in four categories:

Type 1 - Abstract Level: Each classifier K_i produces a class label L_j. At this level, there is no information about the certainty of the obtained labels (condition), nor are any alternative labels suggested.

Type 2 - Rank Level: Each classifier K_i produces alternative class labels L_j ranked in order of plausibility of being the correct label.

Type 3 - Measurement Level: Each classifier K_i produces a d-dimensional vector, $[\kappa_{i,1},...,\kappa_{i,d}]$ consisting of values $\kappa_{i,j}$ representing the support for the hypothesis that the given measurement comes from class c_j.

Type 4 - Oracle Level: The output of classifier K_i for a given measurement is only known to be either correct (value = 1) or wrong (value = -1). The oracle output is artificial since it can only

be applied to a labeled data set. So, for a given labeled dataset, the classification of correct or wrong pertains to having the correct label on the data vector.

To this we add an intermediate classifier output:

Type 3.5: Imprecise Level: Each classifier K_i produces a d-dimensional vector, $[\{\underline{\kappa}_{i,1}, \overline{\kappa}_{i,1}\},...,\{\underline{\kappa}_{i,d}, \overline{\kappa}_{i,d}\}]$ consisting of values $\underline{\kappa}_{i,j}$ and $\overline{\kappa}_{i,j}$ representing the lower and upper probabilistic support, respectively, for the hypothesis that the given measurement comes from class c_j. The inclusion of this level is to acknowledge the existence of imprecise probabilities as outputs from inference engines, such as Dempster-Shafer approach.

The possible ways of combining the outputs of multiple classifiers or information sources in data fusion depends on what type of information is extracted from the individual classifiers. Some of the well know classifier combinations are product rule, sum rule, majority vote, Naive Bayes combination, Singular Value Decomposition (SVD), neural networks, adaptive weighting, bagging and boosting. Jain [75] provides a review of classifier combination schemes and their selection process. Bloch [15] presented a classification of numerical fusion operators with respect to their behavior in terms of severity or indulgence. A number of researchers have reviewed the multisensor fusion algorithms, architectures and application to diagnostic systems. Kuncheva's book [87] on combined classifiers offers a great review of multiple classifier fusion approaches. Hall and Llinas [67] have edited an informative handbook of multisensor data fusion. Luo [102] reviewed the multisensor fusion and integration focusing in sensor technology development and varying applications, such as robotics, biomedical and equipment monitoring.

Byington [18] addressed false alarms originating from faulty sensor performance, transient operating conditions, improper damage indicator selection and logic by performing feature-level and decision-level data fusion. Vachtsevanos et al. [168] provides an overview of data fusion

applications in fault diagnostics and prognostics. To date, the great majority of data fusion works in diagnostics have focused on the Bayesian approach. Basir [11] performed engine diagnostics based on the D-S evidence theory with decision-making rules. Fan [45,46] conducted a two part study using fuzzy membership functions and conflict factor in conjunction with D-S evidence theory to perform gearbox fault diagnosis. The proposed method was used to resolve conflicting information from multisource information by embodying uncertainty and expert's subjective knowledge in decision-making. Li [90] developed a weighted and selective diagnostic fusion approach by combining artificial neural networks, D-S evidence theory and entropy information.

Data fusion studies comparing D-S evidence theory, Bayesian probability fuzzy sets, etc. have been performed [15,16,78,124,127,144,150,159]. Nikolaidis [124] compared Bayesian theory and possibility theory in terms of fuzzy sets to study reliability assessment for designing against catastrophic failure. The main conclusion was that both methods are useful when used in parallel since big discrepancies between their results might be an indication that design analysis problems exist. Osegueda [127] enhanced probabilistic data fusion with D-S evidence theory in testing structural integrity of aerospace structural components. One problem that needs considerable attention is that of performing multisensor data fusion under imprecise information. Multisensor fusion often requires exact information about the sensed environment, but in real situations, information about the sensed environment is often imprecise and scarce. Soundpappan [159] compared evidence theory and Bayesian theory to model uncertainty and assess the safety of a system when information is of interval type. Because the study was performed for interval probability bounds, the performance was biased for the evidence theory since it focuses in dealing with imprecise probabilities. Given that interval gap are relatively small, then Bayesian theory, as it's well known, will provide a better decision result.

Given that diagnostic decision problems relate to uncertain events, it is generally acceptable that quantification of expert opinions about the occurrence of these events should be in terms of probabilities or related concepts. An expert system consists of two parts, as given by the following equation [172]

$$Expert\ System = Knowledge\ Base + Inference\ Engine \tag{2}$$

The knowledge base consists of the domain specific knowledge of the problem, and the inference engine, as previously described, processes the acquired data and encodes it according to the knowledge base. An inference engine also improves the knowledge in light of new information, and thus, facilitates learning. Expert systems are designed to act as consultants by replacing or enhancing domain-specific human knowledge. Types of expert systems can be classified into diagnostic trees, rule-based systems, fuzzy logic, certainty factors (CF), rough sets, Bayesian networks, and probabilistic logic [136,172]. Procedures for dealing with uncertainty and imprecision are essential requirements for expert systems. In situations where uncertainty, imprecision, and contradictory information exists, the usage of opinions elicited from domain specific expert systems is a way of complementing such lack or imprecision of information.

Generation of expert opinions can be done qualitatively or quantitatively. In the quantitative form, the expert may provide opinions as numeric according to the uncertainty theory that will be used to represent available information. In the qualitative form, experts expresses opinions in a natural way deferring the use of numeric representation. For example, an expert diagnostic system might require the faulty features or symptoms, operational information, and other relevant context information, and would utilize this information to search the knowledge base to determine the corresponding diagnostic condition. An expert system does not only manage large quantities of data and sources, but it also manipulates the information, such that the result is intelligent and

has significance in order to respond to questions that are not completely specified. For further details on expert systems please refer to [67,136,172].

The end goal for aggregating information is to generate diagnostic decisions by assessing the uncertainty levels an utility information. The decision problem can be decomposed by specifying a set of possible actions or outcomes, and assessment of the available information supporting each outcome. The decision process determines preferences between actions, reduces the set of actions from which you must choose, or may result in the requirement of acquiring additional information. Multiple works related to decision-making under uncertainty have been made recently with some application to machinery and aircraft diagnostics [41,42,70,76,121,180]. The overall trend in aircraft structure and overall system diagnostics is the emulation of natural intelligence by incorporating declarative actions involving expert decision-making, incorporation of system modeling, and completeness in contextual information identification.

2.5 Discussion

Structures in non-laboratory conditions or highly controlled manufacturing environments exhibit higher and different levels of uncertainty that are hard to manage. Damage assessment methods rely on model-based system identification approaches, which assume linearity, stationarity, and observability. The epistemic and aleatory uncertainty sources violate these fundamental assumptions of system identification techniques. Data-driven methods have been developed to mitigate these shortcomings of model-based methods. However, data-driven methods face a major challenge in performing damage localization and assessment due to the limit on model-knowledge. While several examples of influential studies focused on damage assessment under aleatory uncertainties, such as random varying conditions, and nonlinearities of structural systems exist, the reliable implementation is still plagued by epistemic uncertainties. Structural damage

assessment is required to improve knowledge of structural reliability, but partial answers can only be provided under partial information. The task of properly addressing and quantifying accurate estimates of the structural system reliability remains to date a major task given aleatory and epistemic uncertainties.

Multiple methods based on "robust" approaches have been developed and published for dealing with damage assessment uncertainty. The great majority are developed by combining diverse technical knowledge from structural dynamic models, controlled experiment assumptions, data-driven (pattern recognition, data-mining, machine learning, neural networks, etc.) algorithms, and domain specific knowledge. The level of information regarding method's limitations and challenges remains, to this date, somewhat limited. There are no guidelines in the current literature as to when vibration-based damage assessment methods are applicable and desirable. Guidelines in deciding this and which specific damage assessment method could be used with confidence would be very useful. It is important to recognize that not all applications are in need of such, but numerous applications, such as those requiring high levels of precision and under increasing structural complexity, do require more specific information on method's applicability.

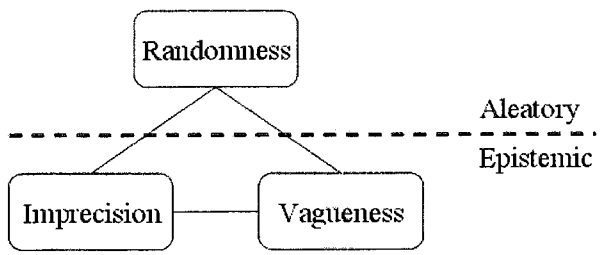

Figure 2.5. Uncertainty types.

Table 2.1. Uncertainty sources in structural condition assessment.

Parametric	Inaccuracy in finite element model discretization. Difficulty in obtaining a representative structural model is highly dependent on minimizing the unknown parameters, which are described below. Parametric uncertainty is perhaps the most widely studied type of uncertainty.
Boundaries	Numerous structures have unknown and unobservable boundary interfaces that are often non-stationary. Structures exposed to varying environment tend to change boundary conditions due to pressure, temperature, and moisture.
Non-isotropic	Variations in materials properties. Structures composed of non-metallic materials, such as composites and ceramics, can vary significantly from member to member. In addition, failure prognosis of non-metallic materials are not always well understood.
Nonlinearities	Structural systems exhibit nonlinear behavior under changes in operating conditions. Examples of nonlinear behavior are material yielding, hysteresis, local instability, interface friction, hardening and softening material behaviors. Numerous damage assessment methods depend on the assumption of linearity, especially those based on modal analysis.
Uniqueness	Numerous structural systems, such as bridges and satellites, are custom-designed for specific applications and their mechanical behavior are strongly affected by events during and immediately following their construction. Training data for understanding structural response under varying conditions might be limited due to uniqueness.
Environment	Structural systems are often exposed to extreme environmental conditions, and unknown or unforeseen operational conditions. Structures, such as satellites during vehicle launch, are exposed to non-stationary excitations. For example, the simple interaction of temperature and humidity effects with rate changes is highly complex, which may lead to structural intrinsic forces inducing changes in boundary and continuity conditions.
Measurement	Arises during the actual measurement process, which may be due to noise factors, such as thermal instability, faulty sensors or equipment, and signal processing errors. Measurement errors can becomes the major problem when measurement data is taken as the indisputable truth.
Excitation	Numerous approaches rely on persistency and consistency of excitation.
Equipment	Limited measurement points and access to critical structural components can result in immeasurable critical modes.

2.6 Summary

In this section, we reviewed issues and challenges facing the diagnostics research area in terms of the associated uncertainties. Statistical pattern recognition techniques can be very useful and extremely effective for well defined types of problems, but their effectiveness is very much limited by the quality and representation of the data from which it is trained. Emerging developments in data mining techniques have extended the capabilities of statistical pattern recognition and machine learning approaches. With the developments in sensing and data collection hardware, also comes increases in databases volume; therefore, in order to separate the 'bad' data from the 'good' data, data mining techniques are necessary and very important tools in the area of structural health monitoring and management. Data-driven techniques are also dependent on the quality and representation of the training data. Model selection, feature extraction, feature selection, and classification remain critical components that need to be addressed and optimized under imprecise information and uncertainties. To reduce uncertainty in the diagnosis process knowledge must be maximized via integration of various information sources.

The world we live is not deterministic. Physics-based models can only be used up to certain accuracy. Even if we had all the time to collect and re-collect data on a given system, it would be impossible to collect all the information needed to predict all possible phenomena. As such, data-driven techniques have clear limitations as well. No single method is capable of being the best solution in all situations; therefore, the strengths of multiple methods must be integrated intelligently to the appropriate flight vehicle damage management systems. In order to address the issue of uncertainty, contextual information, knowledge, and experience must be well incorporated into the flight vehicle structural health management.

Chapter 3

Diagnostic Reasoning under Uncertainty

This chapter introduces some techniques which may be used to model uncertainty in diagnostic reasoning. For humans, reasoning about the physical world appears to be qualitative and heavily dependent on causality. In the artificial intelligence (AI) research area, specifically mathematical logic, reasoning can break down when trying to come in grips with causality. Human reasoning methods break down when trying to come in grips with numerical aspects of uncertainty. Thus, a computational method incorporating numerical uncertainty and causality is desired when making critical decisions under uncertainty. The second half of this chapter is devoted to the principles of Bayesian Networks (BNs) and Dempster-Shafer evidence theory, which in this dissertation, has been selected to develop a diagnostic reasoning approach under uncertainty.

3.1 Coping with Uncertainty

Uncertainty is intrinsically joined to diagnosis. When a medical doctor asserts which was the cause of the symptoms in a patient, the physician is never completely sure about the diagnosis - sad but true. Uncertainty is ever present in all terms that consist of reality. In our daily lives, take language for example, we make vague statements, such as "probably," "maybe," "more or less," as well as others, and leave the decision-making to the intelligent agent - person receiving vague statement - to perform reasoning under such uncertain terms. In structural diagnostics, there are different sources of uncertainty. Aside from the random nature of measurements and observations, uncertainty can take the form of imprecision, vagueness, and incompleteness. The sensory system may be defective; thus making data unreliable. The sensory system might be

incomplete; thus making data partial and imprecise. Therefore, structural diagnosis requires a means for reasoning with uncertainty.

Different approaches have been developed to quantify uncertainty. Probability is the standard tool for dealing with uncertainty, more specifically randomness. Although it is well understood and mathematically sound, the direct application of probabilistic analysis is not always practical or possible due to limitations in defining and assigning probability values and densities. This approach has the restrictive assumption of probability model and the preciseness of the probability distributions. During the last few decades, significant effort towards generalizing uncertainty quantification has been made, which includes concepts such as fuzzy sets, Dempster-Shafer (D-S) belief functions, certainty factors, amongst others [67,172].

In time-constrained situations, such as aircraft forced landing, there may be few statistical data available and decisions must be made utilizing subjective expert knowledge. Human decision making is well known to deviate from classical probability theory and instead is made based on causal and heuristic methods based on personal experience. In the next sections, we will examine the probability method with alternate choices - fuzzy reasoning and imprecise probabilities - as diagnostic reasoning support systems.

3.2 Probabilistic Approach

In the probabilistic approach, uncertainties are characterized by the probabilities associated with the events. The probability can be represented by the frequency of occurrence, if sufficient data is available, from which a probability distribution is generated for statistical analysis. Probabilistic analysis is the most widely used method for characterizing uncertainty, which could be due to stochastic disturbances, such as noise, variability conditions, and risk considerations.

Uncertainty can be modeled using either discrete or continuous probability distributions. In general, there are three approaches to calculate the probability of event A. Classical probability: $P(A) = k / n$, where k is the number of elementary events involved in A, and n is the total number of elementary events. Frequency approach: $P(A) = m / n$, here n is the number of repeated times of the experiment, and m is the total number of times A happens. Subjective determination (Bayesian) approach: $P(A) =$ the value given by priors or experts [172]. It is usually used for random events that cannot be repeated in large quantity. Any probability measure, $P(\cdot)$ on a finite set Θ can be uniquely determined by a probability distribution function

$$p: \Theta \rightarrow [0,1] \tag{3}$$

from the formula

$$P(A) = \sum_{\Theta \in A} p(\theta) \tag{4}$$

If A represents a certain event, then $P(A) = 1$. Given two mutually exclusive events, A and B, then $P(A \cup B) = P(A) + P(B)$. Based on the latter probability definitions or rules, the Bayes' rule of additivity is defined as $P(A) = 1 - P(\neg A)$.

In probability theory, Bayes theorem serves as the basis for the Bayesian inference technique to aggregate uncertain information. The Bayesian approach combines existing information with prior information to compute a posteriori probability of a particular outcome as follows

$$\begin{aligned} &P(A \mid E_i) \propto P(E_i \mid A) P(A) \\ &Posterior \ \propto \ Likelihood \text{ x } \Pr ior \end{aligned} \tag{5}$$

When multiple information sources are available, the probability of event A is given by

$$P(A \mid E_1, ..., E_n) \propto P(E_1, ..., E_n \mid A) P(A) = P(A) \prod_{i=1}^{n} P(E_i \mid A) \tag{6}$$

The latter equation is shown with the assumption of independent information sources E_i. The main requirements of Bayesian approach is a prior distribution that can be updated to obtain a posteriori distribution and independent evidence sources. In diagnostic analysis, we are interested in making 'correct' decisions. Therefore, comparison of decision options in Bayesian formulation can be formulated as a likelihood ratio test

$$\Lambda = \frac{L(A \mid E_1,...,E_n)}{L(B \mid E_1,...,E_n)} = \frac{P(A \mid E_1,...,E_n)}{P(B \mid E_1,...,E_n)} \tag{7}$$

where $L(\cdot)$ is the likelihood function. In the formulated likelihood ratio test, if $\Lambda > 1$, then event A is preferable over B, if $\Lambda < 1$, then event A is not preferable over event B, thus selection for event B is made. Given that more than two event outcomes are available, then a composite hypothesis test is used where essentially all events are compared to select the choice with the highest probability support.

An issue with Bayesian approach is that it require precise probabilistic distribution, and when data are incomplete, exact Bayesian inference is typically computationally infeasible [172]. In this case, approximations are required, which has a significant impact of the inference performance. When data is not complete or available, expert knowledge may be used. Furthermore, if no expert information is available, then prior probabilities can be set equal by using

$$P(A) = P(B) = \frac{1}{2} \quad \text{or} \quad P(O_k) = \frac{1}{N}, \text{ where } k = 1,...,N \tag{8}$$

The a priori probabilities can then be updated recursively as new information becomes available.

3.3 Bayesian Belief Networks

A Bayesian Network (BN) is a graphical framework to model a probabilistic problem of interests, which is defined by a pair of a graph and probabilities, and are a promising solution for assessment reasoning under uncertainty. BNs efficiently represent a joint probability distribution over a set of random variables. BNs a graphically depicted as directed acyclic graphs (DAGs). A DAG consists of a set of nodes representing uncertain variables and a set of directed links, edges, or arcs, between variables. An arc indicates a probabilistic dependency from one node (a parent) to the other (a child). The child node is associated with a conditional probability distribution (CPD) dependent on the parent's state. A node without a parent node is called a root node. A probability distribution associated with a root node is called a prior distribution.

Consider a BN consisting of n variables, $\mathbf{X}$, then the joint probability distribution (JPD) of the variables is a product of the CPDs and is defined as

$$p(\mathbf{X}) = \prod_{i=1}^{n} p_i(X_i \mid X_1, ..., X_{i-1}) \tag{9}$$

The JPD can be simplified as follows

$$p(\mathbf{X}) = \prod_{i=1}^{n} p(X_i \mid \pi_i) \tag{10}$$

where π_i is the set of parents of node X_i.

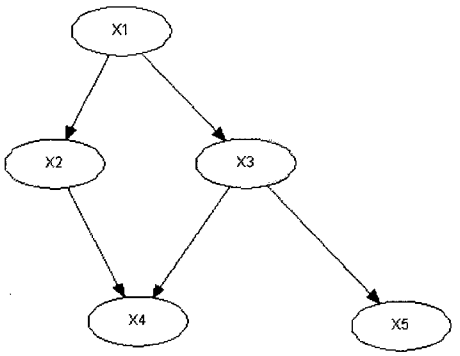

Figure 3.1. An example of BN

Variable may be continuous or discrete. If the variables are continuous, the quantitative part of the BN is composed of conditional probability density functions (PDFs). On the other hand, if the variables are discrete, the quantitative part of the BN is composed of probability tables. BNs may be used to obtain the probability of certain variable X_i given the available evidence, i.e. $P(X_i = x_i \mid Evidence)$. This process is commonly known as inference or model updating. The problem of computing the posterior probability on a BN is NP-difficult [136].

Bayesian networks have been recognized as one of the most promising methodologies for prediction under uncertainty [136]. However, a problematic area in Bayesian approach is that of handling complete ignorance or scarce information about the prior. Under complete ignorance of the prior, the uniform distribution is assigned to the different choices available. In addition, BNs are difficult to build with missing data, which can be overcome by providing input from subjective human domain experts. In numerous real-world applications, information is scarce and incomplete, and for these situations, BNs are not reliably implemented. Therefore, multiple techniques have been developed to address problems like these, such as imprecise probabilities.

3.4 Fuzzy Sets

Fuzzy sets theory allows uncertainty modeling when training or historical data are not available for analysis. Fuzzy theory facilitates uncertainty analysis where the uncertainty arises from lack-of-knowledge or "fuzziness" rather than randomness alone. Fuzzy sets theory was introduced by Zadeh [192] as a means to model the uncertainty of natural language, which developed the notion of partial-truths or fuzzy form of determining if an element is a member of a set or not. Classical set theory allows for "crisp" membership, while on the other hand, fuzzy theory allows for gradual degree membership. This approach has been used to analyze uncertainty associated with incomplete and subjective information in engineering design and analysis. It is important to note that in this work, the possibility theory is assumed to be part of the fuzzy theory. Zadeh used fuzzy sets as a basis for possibility since a proposition that associates an uncertain parameter to a fuzzy set induces a possibility distribution for this quantity, which provides information about the values that this quantity can assume [193].

Given the universal set Θ, the possibility is defined on S and it is a set function with values in $[0,1]$. A possibility measure, Pos, is characterized by the property

$$Pos\left(\bigcup_{i\in I} A_i\right) = \sup_{i\in I} Pos\left(A_i\right) \tag{11}$$

for any value of subsets of Θ defined by an arbitrary index set I; it is semi-continuous from below. A necessity measure, Nec, is characterized by the following property

$$Nec\left(\bigcap_{i\in I} A_i\right) = \inf_{i\in I} Nec\left(A_i\right) \tag{12}$$

for any family of subsets of Θ; it is semi-continuous from above. Possibility theory satisfies the following conditions

$$Pos(\varnothing) = 0,\ Pos(\Theta) = 1 \tag{13}$$

$$Pos(V \cup W) = \max\left(Pos(V), Pos(W)\right) \tag{14}$$

where V and W are two non-intersecting sets involved in Θ.

The essential difference between possibility theory and probability theory is that the probability sum of all non-intersecting events in probability theory is 1, while it may not be 1 in possibility theory. Furthermore, possibility theory may be viewed as a special branch of imprecise probabilities, in which focal elements are always nested [136,172]. This makes possibility theory naturally suited for representing evidence in fuzzy sets, since α-cuts of fuzzy sets are also nested. The imprecision in probabilities and utilities is modeled in fuzzy sets through membership functions defined on the sets of possible probabilities and utilities [172]. The theory of fuzzy sets aims to model ambiguity by assigning a degree of membership $\mu(x)$, between zero and 1, see Figure 3.2. The parameter x is represented as a triangular fuzzy number with support A_0. The wider the support of the membership function, the higher the uncertainty. The fuzzy set that contains all elements with a membership of $\alpha \in [0,1]$ and above is called the $\alpha - cut$ of the membership function. At a resolution level of α, it will have support of A_α. The higher the value of α, the higher the confidence in the parameter. The membership function is cut horizontally at a finite number of α-levels between 0 and 1. For each α-level of the parameter, the model is run to determine the minimum and maximum possible values of the output. This information is then directly used to construct the corresponding fuzziness (membership function) of the output which is used as a measure of uncertainty.

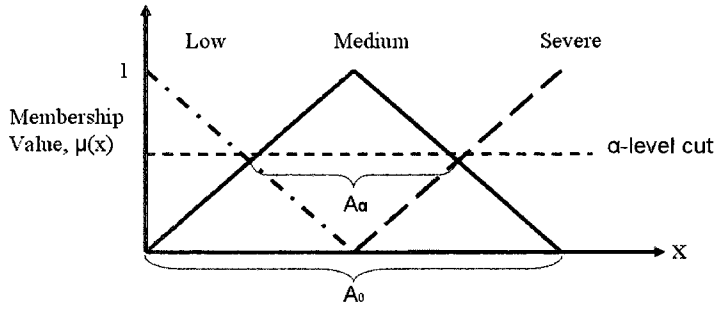

Figure 3.2. Example membership function, μ in fuzzy-sets theory.

Operations on fuzzy sets are defined in a similar manner as operations on ordinary sets, where operators such as complement, union and intersection are applied to characteristic functions [192]. The complement of the fuzzy set is defined as $\mu_{\neg A}(x) = 1 - \mu_A(x)$. The union operation takes the maximum (possibility) of the characteristic functions of two sets, $\mu_{A \cup B}(x) = \mu_A(x) \cup \mu_B(x)$, whereas the intersection takes the minimum (necessity), $\mu_{A \cap B}(x) = \mu_A(x) \cap \mu_B(x)$. A fuzzy rule relates two or more fuzzy propositions, which are statements that assert a value for a fuzzy variable. Fuzzy inference determines a belief in a rule's conclusion given evidence on the rule's premise. After the rule's have been applied, the output is a fuzzy set. Typically, such as in control systems, this fuzzy set has to be converted to a crisp value. This process is called defuzzification, which produces a quantifiable result in fuzzy logic.

Fuzzy memberships are not probabilistic measures. Fuzzy logic has been successfully applied industrially in areas such as character recognition, speech recognition, control systems, medical diagnosis, amongst others. In practice, fuzzy systems usually undergo extensive tuning. Fuzzy methods do play vital roles in process control applications and low-level processing on sensory data. In terms of complex reasoning, fuzzy methods probably won't play a significant role. For further details on fuzzy sets, see [192,193].

3.5 Imprecise Probabilities

Imprecise probabilities, also known as interval probabilities, have gained particular interest in multiple research areas. Imprecise probabilities generalizes probability theory by bounding an uncertain event A via interval probabilities $[\underline{P}(A), \overline{P}(A)]$, where $\underline{P}(A)$ is the lower probability, also known as certainty or belief, and $\overline{P}(A)$ is the upper probability, also known as plausibility or possibility [172]. In terms of generalizing probability, the notion behind interval probabilities is that if the situation allows for precise or complete information regarding the uncertainty of A, then the determined upper and lower probabilities would be close to each other and approach a single probability distribution. On the other hand, if the information collected is very imprecise or incomplete, then the separation between lower and upper probabilities would be significant and thus would need to be considered. Imprecise probability approach avoids having to make precise statements, and allows for representation of knowledge according to the data quality without introducing any extra unsubstantiated information. The resulting indeterminacy in the belief about the unknown state can be viewed as a shortcoming for any subsequent decision analysis, but it is also a strength since it reflects the reality of the situation faced by a decision maker. In addition, say information for determining $P(A)$ is obtained from two conflicting expert sources, in the sense that one expert's probability is less than or greater than the second expert's probability estimate, then it would be useful to know that their information or knowledge comes from different types of evidence.

The concept of imprecise probabilities has been proposed by many statisticians [136] as a way of representing weak information. Representative imprecise probability approaches are Bayesian Robustness, interval probability, Walley's imprecise probability, and Dempster-Shafer evidence theory. Comparison of different probability approaches can be found in [136, 172, 181].

3.5.1 Dempster-Shafer Evidence Theory

The Dempster-Shafer (D-S) evidence theory is derived from Dempster's original work [181] which was aimed at relaxing certain Bayesian restrictions when dealing with the inference of unknown parameters. Shafer [149] expanded Dempster's original works and produced what is now known as the D-S theory.

Dempster-Shafer's evidence theory is an imprecise probability method, relies on the concept that information of a given problem can be inherently imprecise. Hence, the bound result which consists of both belief values, the lower bound of probability; and, plausibility, upper bound of probability, is presented. Unlike possibility or fuzzy set and probability theory, in evidence theory there is no need to make an assumption or approximation for the imprecise information. Epistemic plausibility can be represented in evidence theory via belief functions, where the degrees of belief may or may not have mathematical properties of probabilities. In comparison to probability theory, instead of using probability distributions to capture system uncertainties, a belief function is used to represent a degree of belief. Probability values are assigned to sets of possibilities rather than single event. The basic entity in the D-S theory is a set of exclusive and exhaustive hypotheses about some problem domain. It is called the frame of discernment (*FoD*), denoted as Θ. Given a universal set or frame of discernment Θ, then a basic belief assignment (BBA) is a function $m: \Psi \rightarrow [0,1]$, where Ψ is the set of all subsets of Θ; and the power set of Θ is $\Psi = 2^{\Theta}$. The function m can be interpreted as distributing belief to each of element in Ψ, with the following criteria satisfied:

$$\sum_{A \in \Psi} m(A) = 1, \; m(\varnothing) = 0 \tag{15}$$

In evidence theory, we do not assign any degree of belief to the empty proposition $\varnothing$ and we ignore the possibility for an uncertain parameter to be allocated outside of the frame of

discernment. Thus, the element A is assigned a basic belief assignment (BBA) $m(A)$ describing the degree of belief that is committed exclusively to A. Note that a situation of total ignorance is characterized by $m(\Theta)=1$. The total evidence that is attributed to A is the sum of all probability numbers assigned to A and its subsets

$$Bel(A)=\sum_{\forall B:B\subseteq A} m(B) \tag{16}$$

Given that we have q number of information sources affecting decision-making, then each information source S_i will contribute by assigning its beliefs over Θ. The information sources can distribute masses on every subset of the FoD

$$A_i \in 2^{\Theta}:\left\{\varnothing, A_1=\{H_1\},...,A_q=\{H_q\}, A_{q+1}=\{H_1,H_2\},...,A_{2^q-1}=\{H_1,...,H_q\}\right\} \tag{17}$$

A source of information assigns a BBA between 0 and 1 on hypothesis A_i on which it has direct knowledge. The assignment function of each source is denoted by m_i.

The lower bound of the evidence interval is the belief function, which amounts for all the evidence B that supports the selection of A_i

$$Bel(A_i)=\sum_{B\subseteq A_i} m(B) \tag{18}$$

The upper bound of the evidence interval is the plausibility function, which accounts for all the observations that do not rule out the selection A_i

$$Pl(A_i)=1-Bel(\overline{A}_i)=1-\sum_{\varnothing\neq B\cap A_i} m(B) \tag{19}$$

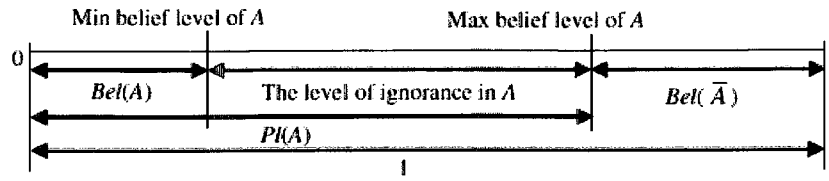

Figure 3.3. Plausibility and belief measures and their complement.

Thus, according to the observations of information source, the uncertainty concerning hypothesis A_i the interval, see Figure 3.3,

$$\left[Bel(A_i), Pl(A_i)\right] \tag{20}$$

The above interval reduces to a single point in the case of Bayesian analysis.

From plausibility and belief measures, we obtain the basic belief assignment by the möbius transform [153]

$$m(A_i) = \sum_{B \subseteq A_i} (-1)^{|A_i|-|B|} Bel(B) \tag{21}$$

where $|A_i|$ is the cardinal set of A_i.

If the imprecision on a probability measure is described by an interval, the relation with a BBA is directly obtained by

$$\left[\underline{P}_{H_i}, \overline{P}_{H_i}\right] = \left[Bel(H_i), Pl(H_i)\right] \tag{22}$$

where $\underline{P}_{H_i}$ and $\overline{P}_{H_i}$ are the lower and upper probability bounds of hypothesis H_i, respectively, with $i = 1,2,...,q$ being the number of hypothesis. The transformation of a probability interval vector or interval set $\mathbf{P_X}$ of a random variable $\mathbf{X}$ to a BBA $\mathbf{M_X}$ is obtained as follows

$$\mathbf{P}_{\mathbf{X}} = \left[\left[\underline{P}_{H_1}, \overline{P}_{H_1} \right], ..., \left[\underline{P}_{H_q}, \overline{P}_{H_q} \right] \right] \tag{23}$$

then

$$\begin{aligned} \mathbf{M}_{\mathbf{X}} &= \left[m(\varnothing), m(A_1), ..., m\left(A_{2^q-1}\right) \right] \\ &= \left[\underline{P}_{\varnothing}, \underline{P}_{A_1}, ..., \sum_{B \subseteq A_i} (-1)^{|A_i|-|B|} \underline{P}_B, ... \right] \end{aligned} \tag{24}$$

with $A_i \in 2^{\Theta}$. As argued by Smets [153], the knowledge of $[Bel(A_i), Pl(A_i)]$ is equal to the knowledge of the BBA on the FoD.

3.5.2 Belief Function Combination

Given two independent belief functions over the same frame of discernment, Dempster's rule gives a way for combining BBA structures

$$m(C) = m_1(A) \oplus m_2(B) = \frac{\sum_{A \cap B = C} m_1(A) m_2(B)}{1 - \sum_{A \cap B = \varnothing} m_1(A) m_2(B)} \tag{25}$$

The denominator of Eq. (25) is a conflict of information given by independent information sources. Dempster's rule disregards every contradiction by normalizing with the complementary degree of contradiction because it is designed to use consistent opinions from multiple sources as much as possible. For n mass functions $m_1, m_2, ..., m_n$, the combined mass function and measure of contradiction are given by

$$m(A) = (m_1 \oplus m_2 \oplus ... \oplus m_n)(A) = \frac{1}{1-K} \sum_{\cap_{i=1}^{N} B_i = A} m_1(B_1) \cdot m_2(B_2) \cdots m_n(B_n) \tag{26}$$

$$K = \sum_{\cap_{i=1}^{N} B_i = \varnothing} m_1(B_1) \cdot m_2(B_2) \cdots m_n(B_n) > 0 \tag{27}$$

D-S theory has become an important tool for dealing with uncertainty. Recent advancements in the D-S theory are best covered in [181]. Dempster's rule of combination has some important features, such as being commutative and associative. When a BBA is combined with an ignorance BBA, the resultant BBA is always identical to the original BBA, which suggests the idea that the complete ignorance does represent zero informational input. Dempster's rule of combination, which is central to combining evidence and updating probabilities, has limitations when dealing with highly conflictive data sources, which render the rule unreliable [136]. While Dempster's rule of combination has a credible basis for data fusion and it has been widely applied to multiple works [172,181], numerous discrepancies exist due theoretical weaknesses, which are beyond the current work being presented. For more discussion on Dempster's rule of combination, see [136,149,181].

In addition, greater generality is needed because the class of belief functions in D-S theory is not large enough to model all reasonable types of uncertainty. While the D-S approach can exhibit desirable properties in terms of imprecision and ignorance analysis, the utility or practicality of this approach depends on how well they account for the origin of imprecision or ignorance, and how well they can integrate new evidence or information. Given the interval belief between belief and plausibility measures, how can hard (clear and definite) decisions be made?

3.6 Evidential Networks

In the modeling of structural systems for the analysis of their structural safety and reliability, the variables which represent the system, its components, its function or the events are related to each other. These relations are represented by conditional dependencies. In this section, we propose the application of Evidential Networks (ENs) to represent the conditional dependencies among the system variables in a description space integrating uncertainty as belief masses of the Dempster-

Shafer theory. The proposed ENs are directed acyclic graphs which represent uncertain knowledge as aleatory and epistemic ways. ENs with conditional dependencies were originally proposed by Smets [153] for propagation of beliefs. Variations and advances of these networks have been studied by [73, 152,188].

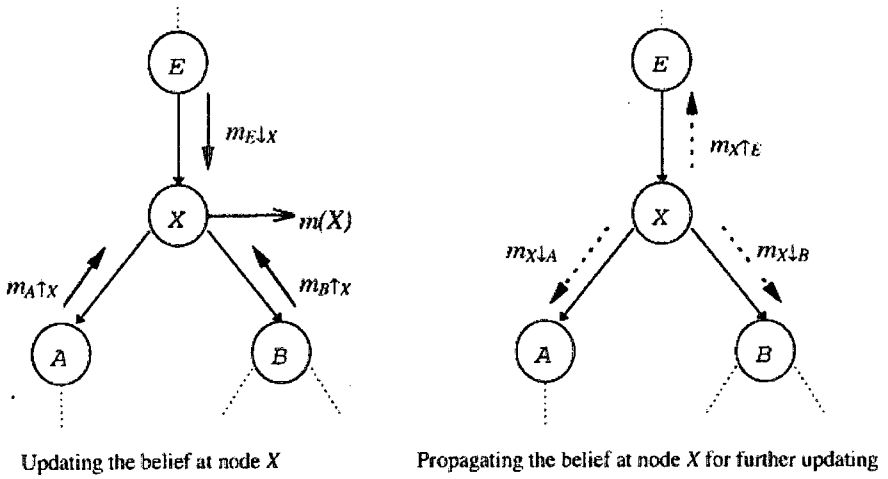

Figure 3.4. Evidential network with updating and propagation of node X.

Graphically, ENs has similar aspects to Bayesian networks (BNs); however, in the networks using belief functions, the relations among the variables are represented by conditional belief functions. Each variable X in the EN has a set of possible values, called frame of discernment, FoD, that consists of q mutually exclusive and exhaustive values of the variable. For each root node X (variable without parents), uncertainty is represented by *a priori* belief function $Bel_0(X)$. For the other nodes (variables with parents), uncertainty is represented by a conditional belief function $Bel(X \mid Parents)$ given the value taken by its parents. Similar definitions apply to BBA and plausibility functions. When evidence from distinct sources is observed for certain nodes, it is combined by the Dempster-Shafer theory. Thus, beliefs for the corresponding nodes are updated and propagated to the neighboring nodes through the network.

The vector $\mathbf{M_X}$ is the belief mass distribution over the 2^q focal sets A_i^X and is defined by

$$\mathbf{M_X} = \left[m(X \subseteq \varnothing), m\left(X \subseteq A_1^X\right), ..., m\left(X \subseteq A_i^X\right), ..., m\left(X \subseteq A_{2^q-1}^X\right) \right] \quad (28)$$

with $m\left(X \subseteq A_i^X\right) \geq 0$ and $\sum_{A_i^X \in 2^\Theta} m\left(X \subseteq A_i^X\right) = 1$, where $m\left(X \subseteq A_i^X\right)$ is the belief that variable X verify the hypothesis of focal element A_i^X.

To compute the marginal belief mass of each node, we use inference algorithms. The exact inference is carried out by the algorithm proposed by Jensen [77] based on the construction of junction tree. This algorithm updates the marginal belief mass distributions on each node according to the evidence representing the knowledge introduced into the evidential network. Due to node connectivity, in ENs, the updated belief can be propagated throughout the network. Belief updating and propagation starts from each observed node and propagates belief to its neighboring nodes. For singly-connected networks, the fundamental algorithm for exact probabilistic inference was proposed by Pearl [136]. The main principle underlying Pearl's polytree algorithm is the use of probabilistic independence properties implicit in the structure of these networks. By exploiting these independence properties, the probability computation can be factored into a number of local computations which communicate by message-passing between neighboring variables. In this research, we make use of an efficient propagation algorithm for evidential networks with conditional belief functions, which extends Bayesian networks to the representation of uncertain information according to the framework of Dempster-Shafer theory.

3.7 Case Study: Illustrative Example in Car Diagnostics

We illustrate the use of D-S and Bayesian theory with a representative example based on sensor fault diagnosis as a basis for comparison. Suppose your car has problems starting and you have

narrowed down the possible reasons to 4 possible component malfunctions. To verify that car starts without problems, each component is required to work adequately. For this situation, we assume that a single component is faulty, which negates the possibility for two or more components being bad simultaneously. This simplification greatly simplifies the analysis. The diagnostic problem consists of finding which sensor is broken. The causal and belief networks for this example are shown in Figure 3.5.

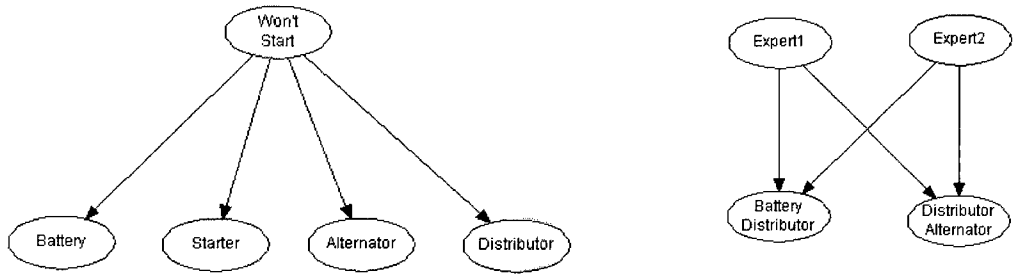

Figure 3.5. Car diagnostics network. (a) Causal network; (b) Expert aggregation network for experts 1 and 2.

Suppose there are four possible sensor network fault conditions, which are given by $S = \{f_1, f_2, f_3, f_4\} = \{battery, starter, distributor, alternator\}$, where f_i indicates that component-i is faulty. Assume we have three sequential informational reports from three "experts" sources. Since you are a novice at car repair, you decide to get help as follows: initially you ask your neighbor, second you look for information on the internet, and finally you decide to call a mechanic. Table 3.1 shows the expert knowledge sources for their reports on the car diagnosis and the interpretation by each of the uncertainty analysis methods. The "certain" statements are interpreted in the D-S approach as belief values for the particular set. The first two experts coincide with partial knowledge in that fault might be associated with f_3, but different partial evidence for f_1 and f_4. The third expert is used here to add conflict and inconsistency. In contrast to the first two experts, the third expert evidence has the inconsistency in that he extends

the possible fault selection to an unknown one, $\{Other = fuse\}$, which questions the accuracy of the probability space S.

Table 3.1. Expert knowledge base for car diagnosis.

	Expert 1	Expert 2	Expert 3
Report	60% certain choice is "battery" or "distributor"	60% certain fault is "distributor" or "alternator"	75% certain one of the four components is faulty, and: "starter" is 2X likely as "battery", "distributor" is 3X as likely as "battery", and "alternator" is 2X likely as "battery"
Set Attribution	$\{f_1, f_3\}$	$\{f_3, f_4\}$	see below
Probability Interpretation	$P(\{f_1, f_3\} \mid Expert1) = 0.6$ $P(\{f_2, f_4\} \mid Expert1) = 0.4$ $0 \le p_1 \le 0.6,\ 0 \le p_2 \le 0.4$ $p_3 = 0.6 - p_1,\ p_4 = 0.4 - p_2$	$P(\{f_3, f_4\} \mid Expert2) = 0.6$ $P(\{f_1, f_2\} \mid Expert2) = 0.4$	$P(\{f_1\} \mid Expert3) = 0.05$ $P(\{f_2\} \mid Expert3) = 0.1$ $P(\{f_3\} \mid Expert3) = 0.4$ $P(\{f_4\} \mid Expert3) = 0.2$ $P(\{Other\} \mid Expert3) = 0.25$
Dempster-Shafer Interpretation	$m_1(\{f_1, f_3\}) = 0.6$ $m_1(S) = 0.4$ $[Bel, Pl]_{\{f1,f3\}} = [0.6, 1.0]$ $[Bel, Pl]_S = [1.0, 1.0]$	$m_2(\{f_3, f_4\}) = 0.6$ $m_2(S) = 0.4$ $[Bel, Pl]_{\{f3,f4\}} = [0.6, 1.0]$ $[Bel, Pl]_S = [1.0, 1.0]$	$m_3(\{f_1\}) = 0.1$ $m_3(\{f_2\}) = 0.1$ $m_3(\{f_3\}) = 0.4$ $m_3(\{f_4\}) = 0.2$ $m(S) = 0.2$

The expert reports are sequential and we will aggregate the information from experts 1 and 2 first. Table 3.2 and Figure 3.6 show the aggregation of experts 1 and 2 for both Bayesian and D-S approaches. At this point, using the information provided by first two experts, the probability method offers a partial decision for a particular decision, in this case choosing fault f_3. On the other hand, D-S approach does not provide any direct or clear decision information on fault isolation. For example, Table 3.3 shows a $Bel(\{f_3\}) = 0.649$, but this is not enough to make a decision since $Bel(\{f_1, f_3\}) = 0.6$, $Bel(\{f_3, f_4\}) = 0.7$ which means that there is the possibility that f_1 and f_4 could potentially have high beliefs, but the current information is not sufficient.

Advocates of D-S theory would indicate that this no-decision result indicates that additional information is needed. Critics of D-S theory would indicate the decision-making weakness of the approach [136].

Aggregating the information from the third expert offers some difficulty in the probability approach. The probability space must be modified to accommodate for the selection $\{Other\}$, which necessitates that the early aggregation results of experts 1 and 2 be updated to include this option. Recalculation of results will be omitted here. On the other hand, the information inconsistency of expert 3 can be handled using D-S theory.

Table 3.3 and Figure 3.6(b) show the results obtained using from aggregating information given by expert 3. Since expert 3 offers beliefs on individual paths, the aggregation results do show a partial decision for f_3 as the probability method showed previously, but now with inconsistent evidence. Due to the additional evidence from expert 3, the probability intervals from D-S approach are smaller.

Table 3.2. Aggregation of expert 1 and expert 2.

	Probability: Expert1 + Expert2	**D-S: Expert1 + Expert 2**
Available Information	$P(\{f_1,f_2\})=0.4,\ P(\{f_1,f_3\})=0.6$ $P(\{f_1,f_4\})=1-x,\ P(\{f_2,f_3\})=x$ $P(\{f_2,f_4\})=0.4,\ P(\{f_3,f_4\})=0.6$ $P[\{f_1\}]+P[\{f_2\}]=0.4$ $P[\{f_1\}]+P[\{f_3\}]=0.6$ $P[\{f_2\}]+P[\{f_3\}]=x$	Dempster's rule: $m_{1,2}(\{f_3\})=m_1(\{f_1,f_3\})\oplus m_2(\{f_3,f_4\})=0.36$ $m_{1,2}(\{f_1,f_3\})=m_1(\{f_1,f_3\})\oplus m_2(\{S\})=0.24$ $m_{1,2}(\{f_3,f_4\})=m_1(\{S\})\oplus m_2(\{f_3,f_4\})=0.24$ $m_{1,2}(\{S\})=m_1(\{S\})\oplus m_2(\{S\})=0.16$
Aggregation Results	$P[\{f_1\}]=0.55-x/2$ $P[\{f_2\}]=x/2-0.15$ $P[\{f_3\}]=0.15+x/2$ $P[\{f_4\}]=0.45-x/2;\ (p_4=0.3-p_2)$ where $0.2\le x\le 1.0$	$[Bel,Pl]_{\{f3\}}=[0.36,1.0]$ $[Bel,Pl]_{\{f1,f3\}}=[0.6,1.0]$ $[Bel,Pl]_{\{f3,f4\}}=[0.6,1.0]$ $[Bel,Pl]_S=[1.0,1.0]$

Table 3.3. Dempster-Shafer aggregation of experts 1 through 3.

	$m_{1,2}(\{f_3\}) = 0.36$	$m_{1,2}(\{f_1, f_3\}) = 0.24$	$m_{1,2}(\{f_3, f_4\}) = 0.24$	$m_{1,2}(\{S\}) = 0.16$
$m_3(\{f_1\}) = 0.05$	$\varnothing 0.018$	$m(\{f_1\}) = 0.012$	$\varnothing 0.012$	$m(\{f_1\}) = 0.008$
$m_3(\{f_2\}) = 0.1$	$\varnothing 0.036$	$\varnothing 0.024$	$\varnothing 0.024$	$m(\{f_2\}) = 0.016$
$m_3(\{f_3\}) = 0.4$	$m(\{f_3\}) = 0.144$	$m(\{f_3\}) = 0.096$	$m(\{f_3\}) = 0.096$	$m(\{f_3\}) = 0.064$
$m_3(\{f_4\}) = 0.2$	$\varnothing 0.072$	$\varnothing 0.048$	$m(\{f_4\}) = 0.048$	$m(\{f_4\}) = 0.032$
$m_3(\{S\}) = 0.25$	$m(\{f_3\}) = 0.09$	$m(\{f_1, f_3\}) = 0.06$	$m(\{f_3, f_4\}) = 0.06$	$m(\{S\}) = 0.04$

$k = 0.018 + 2x0.012 + 0.036 + 2x0.024 + 0.072 + 0.048 = 0.246,\ 1 - k = 0.754$

$Bel(\{f_1\}) = (0.012 + 0.008) / 0.754 = 0.026$

$Bel(\{f_2\}) = 0.016 / 0.754 = 0.021$

$Bel(\{f_3\}) = (0.144 + 2x0.096 + 0.064 + 0.09) / 0.754 = 0.649$

$Bel(\{f_4\}) = (0.096 + 0.032) / 0.754 = 0.169$

$Pl(\{f_1\}) = 1 - Bel(\{\neg f_1\}) = 0.159$

$Pl(\{f_2\}) = 1 - Bel(\{\neg f_2\}) = 0.153$

$Pl(\{f_3\}) = 1 - Bel(\{\neg f_3\}) = 0.782$

$Pl(\{f_4\}) = 1 - Bel(\{\neg f_4\}) = 0.302$

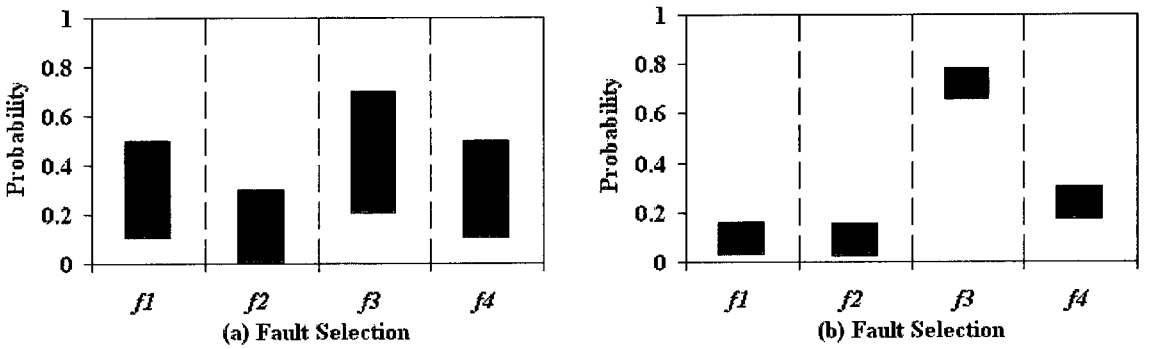

Figure 3.6. (a) Probability aggregation interval results for experts 1-2. (b) Dempster-Shafer aggregation interval results for experts 1-3.

3.8 Discussion

The diagram shown in Figure 3.7 illustrates the relationship among the main classes of uncertainty theories. The structural analysis uncertainty sources and uncertainty quantification strategies is depicted in Figure 3.8 based on the characteristics of the source information. Given a random nature, structure damage uncertainties are aleatory uncertainties, and when insufficient

data and/or lack of knowledge exist to construct probability distribution, uncertainties are treated as epistemic uncertainties. Due to the broad concept of uncertainty, this research area and its engineering applications are still in its infancy.

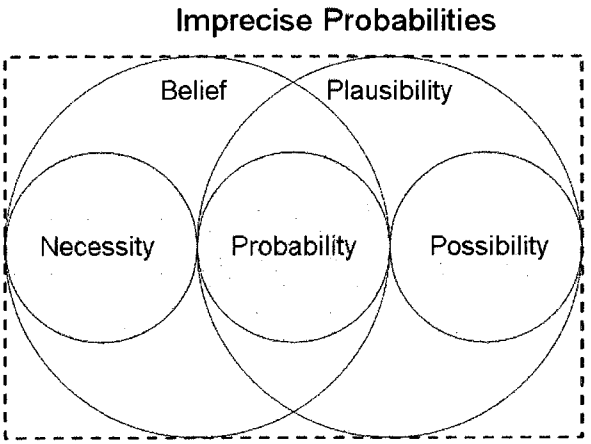

Figure 3.7. Relationship among main classes of uncertainty measures.

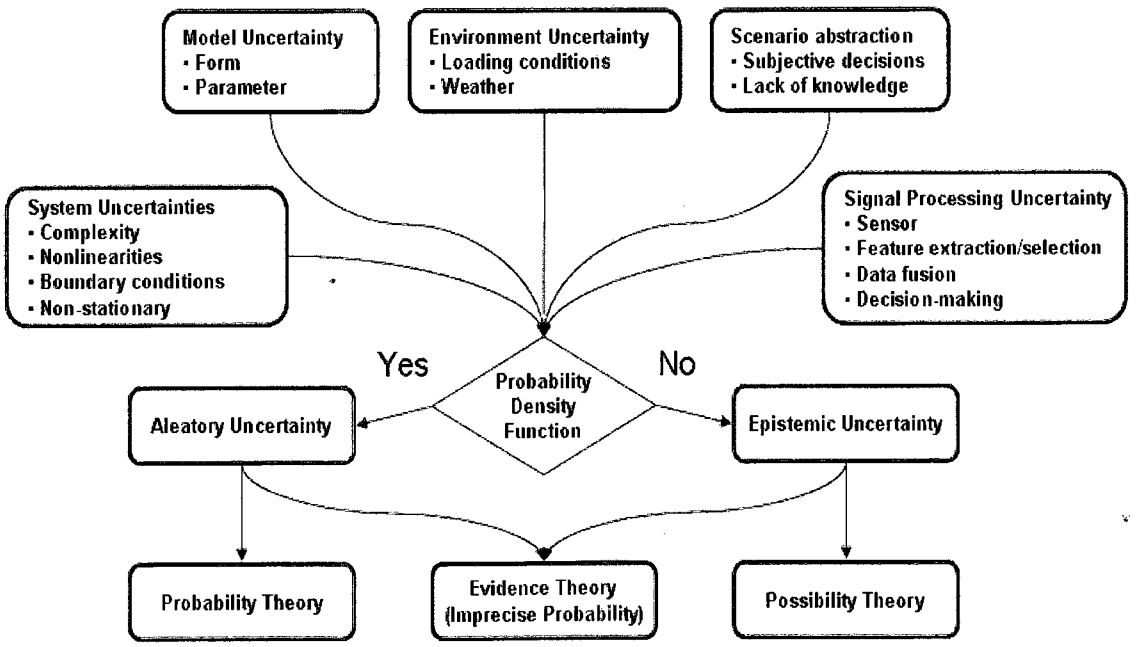

Figure 3.8. Uncertainty sources and analysis approaches.

A central assumption of the Bayesian theory is that uncertainty should always be measured by a single probability measure, and values should always be measured by a precise utility function, which is called the Bayesian dogma of precision [172]. Alternative formalisms in uncertainty analysis have been motivated by the fact that the dogma of precision is mistaken in addressing non-random uncertainties. Imprecision, indeterminacy, vagueness and indecision are incompatible with individual probabilistic expressions. The Bayesian approach assesses precise prior probabilities of parameters and combines these to output precise posterior probabilities, even when there is very little prior information, which may render unreliable and irrational results. Alternative formalisms, such as D-S theory, give explicit notation to confidence measures, also known as imprecise probabilities, where lower and upper probabilities are generated. In general, lower probability is taken as the minimum certainty at which you are willing to make a specific decision, and upper probability is the maximum certainty at which you are willing to make a specific decision. From the standpoint of D-S theory

$$p(\theta) = m(\{\theta\}) \tag{29}$$

for all $\theta \in \Theta$. Probability measures are the point where belief and plausibility measures coincide.

Admission of imprecision in probabilities is needed to reflect the amount of information on which they are based. In terms of time-constraint situations, assessment of precise probabilities might be impractical due to lack of time or computational ability, or because of the level of system complexity. In other words, for partial data, partial answers should be given. The D-S theory handles both the uncertainty and imprecision contained in data due to the belief and plausibility functions which can be seen as an interval enclosing imprecise probability. The D-S theory does not pretend to provide full answers to probabilistic data, but rather provides partial answers by estimating how much does the evidence supports the truth of a hypothesis, instead of

estimating how close the hypothesis is to being true. But, greater generality is needed because the class of belief functions in D-S theory is not large enough to model all reasonable types of uncertainty. Furthermore, Dempster's rule of combination, which is central to combining evidence and updating probabilities, has limitations when dealing with highly conflictive data sources, which render the rule unreliable [136]. While imprecise probability approaches can construct mathematical theories that exhibit desirable properties in terms of imprecision and ignorance analysis, the utility or practicality of such approaches depends on how well they account for the origin of imprecision or ignorance, and how well they can integrate new evidence or information. Given that interval probabilities are generated as outputs, how do these intervals convey information for inference and decision-making processes?

In terms of damage assessment, the fuzzy-sets theory can also have problems when dealing with pattern recognition. For example, assume we have a normal and a faulty operating condition. If a given pattern is far away from the normal operating class, it will have a small membership value according to this class, and consequently, it will have a bigger membership to faulty class. But if in addition, this pattern is far from both classes, it will be wrongly assigned to second class instead of being rejected, which could be a rejection class. In other words, fuzzy sets can only deal with vagueness and not necessarily imprecision. Ambiguity is only one potential source of imprecision in probabilities and, unlike other sources of imprecision, it can be eliminated through careful elicitation [172]. Critics of fuzzy sets argue that the membership functions that are chosen to model ambiguous probability judgments seem both arbitrary and inappropriately precise and that no clear interpretation of the membership function has been established [136, 172]. The assessment of fuzzy sets requires substantial input from a user, which might render its usage closer to that of expert systems.

Table 3.4. Axioms of Probability, Fuzzy-Set (Possibility), and Evidence theories.

Probability Theory	Fuzzy-Sets (Possibility) Theory	D-S Evidence Theory
$P(\Theta)=1$	$Pos(\varnothing)=0,\ Pos(\Theta)=1$	$m(\varnothing)=0,\ \mathrm{m}(\Theta)=1$
$P(A)\geq 0\ \forall A\in S$	$\forall A,B\in S$ if $A\subseteq B$, *then* $Pos(A)\leq Pos(B)$	$\forall A,B\in m(\Theta)$ if $A\subseteq B$, *then* $\mathrm{m}(A)\leq m(B)$
$\forall A_i,\ i\in I,\ A_i$ disjoint $P\left(\bigcup_{i=1}^{I}A_i\right)=\sum_{i\in I}P(A_i)$	$\forall A_i,\ i\in I,\ A_i$ disjoint $\Pi\left(\bigcup_{i=1}^{I}A_i\right)=\max_{i\in I}\left(Pos(A_i)\right)$	$\forall A_i,\ i\in I,\ \mathrm{g}(\cdot)$ of subsets of Θ if sequence is monotonic, then $\lim_{i\to\infty} g(A_i)=g\lim_{i\to\infty}(A_i)$
		$Bel(A)+Bel(\overline{A})\leq 1$ $Pl(A)+Pl(\overline{A})\geq 1$

Table 3.4 compares the uncertainty theories in terms of their axioms. Probability theory can handle uncertainty contained in data, but it cannot treat the imprecision. Fuzzy-sets theory can handle the vagueness type imprecision by replacing the additive axiom in probability theory with the weaker monotonicity axiom. In the case of insufficient information and no-conflicting evidence, the possibility theory is a suitable method to quantify uncertainty. If conflicting information exists, the evidence theory should be used instead. Evidence theory is the general theory to represent uncertainty and includes the possibility and probability theories.

3.9 Summary

The multiple uncertainty management paradigms produce different numerical responses and with different limitations, which makes the choice clearly not arbitrary. Thus, the choice of uncertainty analysis approach depends on the nature of the problem and the expertise of the user. There have been relatively few reports of experiments to directly compare methods to combine probabilistic information under imprecision with D-S, fuzzy-sets and Bayesian theory. Several comparison papers based on simulation data or assumed situations have concluded that differences in performance for the latter evidence combination approaches, but no definite advantage exists

among the algorithms aside from the well known, such as that Bayesian is better fitted for precise prior probabilities and that it's sensitive to parameter errors and imprecision. Bayesian theory is best suited for applications where there is no ignorance and conditioning is easily obtainable through probabilistic representation and prior odds are available. D-S theory, and other similar imprecise probability approaches, are more appropriate where uncertainty cannot be assigned precise probability to a proposition, and conditioning effects are difficult or impossible to measure separately, and prior odds are not pertinent.

Chapter 4

Novel Dimensional Reduction Approach for Damage Detection with Increased Robustness

Problems of structural design and analysis always involve an element of aleatory uncertainty due to randomness. No matter how much is known about the phenomenon, the behavior of the structure is incapable of precise prediction. To address the problem of randomness in damage detection, we propose the implementation of diversified ensemble diagnostic algorithms. In this section, instead of choosing the best diagnostic method on a case-by-case basis, we combine the outputs of multiple dimensional reduction techniques for robust damage detection classification.

In this section, we present a damage detection and monitoring method based on a distance similarity matrix of dimensionally reduced data wherein redundancy therein is removed. The matrix similarity approach is generic in nature and has the capability of multiscale representation of datasets. To extract damage-sensitive features, dimensional reduction techniques are applied and compared. An ensemble method of dimensional reduction feature outputs is presented and applied to two case studies. The results supports why ensembles can often perform better than any single-feature extraction method. For the first case study, aeroacoustic datasets are collected from controlled scaled experimental tests of controlled known damaged subscale wing structure. For the second case study, a vibration experiment study is used for abrupt change detection and tracking. The results of the two case studies demonstrate that the proposed method is very effective in detecting abrupt changes and the ensemble method developed here can be used for deterioration tracking.

4.1 Introduction

Important to the field of structural health monitoring (SHM) is finding a clear structural damage indicator. Sequential hierarchical levels of damage diagnosis, such as localization, quantification, and prognosis, rely on how well of a damage indicator is being used. Real-world data usually has high dimensionality, which under low-variability from undamaged to damage states can make it difficult to separate outliers in the one-class classification problem of damage detection. To aid in the classification process, dimensionality reduction, a data-driven technique class, reduces the representation to a transformed subset of features necessary for the intrinsic data properties. Dimensionality reduction can be used to facilitate classification, visualization, and compression of high-dimensional data. Dimensionality reduction deals with the transformation of a high-dimensional data set into a low dimensional space, while retaining most of the useful structure in the original data. Dimensionality reduction has become increasingly important in system diagnostics due to diverse and increasing number of data sets with a large of number of features, such as the frequency response of complex and continuous structural system. The underlying assumption for dimensionality reduction is that the data points do not lie randomly in the high-dimensional space; rather, there is a certain structure in the relationship among the points that can be exploited, and the useful information in the high dimensional data can be summarized by a small number of attributes.

In damage detection, the modeling required should be as minimal as possible in order to deploy a real-time monitoring system. Therefore, dimensionality reduction techniques are suitable for the initial step of damage detection. Dimensionality reduction techniques do not assume any form of model information and rely only on the training data available. The detection and tracking of structural damage can only be observed via extracted features from the available system response measurements. Feasibility and accuracy in performing feature extraction and selection is a very

critical step in the diagnostic decision process since it determines how relative information is presented to a human or computational classifier.

Finding features that allow us to identify and track structural damage can be a challenging task. For this reason there exist several approaches that have been shown to perform well on various types of engineering systems. Markou [107,108] summarizes the necessary principles for novelty detection approaches in terms of robustness, uniform data scaling, minimization of parameters used, capability of generalization, feature independent, adaptive (re-trainable), and minimal computational complexity. Common feature extraction methods that have been used in damage assessment studies include neural network-based techniques [108], fuzzy methods [40,133], multivariate statistical techniques, such as principal component analysis (PCA) [59,80,94,95,156,182,183], and nonlinear dimensional reduction techniques [98,101,158].

Dimensionality reduction is a key step in feature extraction and selection since it simplifies the classification level. For example, 2D or 3D projection of the multivariate data vector might be required if visual classification of output data will be performed. In addition, it alleviates the 'curse of dimensionality,' which means that the number of training samples per feature increase exponentially with increasing number of features in order to maintain a good level of accuracy. Lei et al. [88] presented a weighted clustering algorithm using a compensation distance evaluation technique (CDET) where extracted features are weighted and selected according to damage sensitivity. Using this approach, Lei was able to demonstrate damage assessment at different levels of severity and emphasized the importance of feature extraction prior to classification. Data-driven techniques are limited to simplistic information levels in terms of damage characteristics, e.g. detection and location. When increasing diagnosis levels of damage information, such as type and detailed location, model-based and machine learning algorithms

can be applied in a supervised learning context where data from both damage and undamaged states can be gathered for proper damage assessment.

4.2 Dimensionality Reduction Methods

Due to the complexity and high dimensionality of dynamic response data, the simple binary classification (detection case) of structural health into damaged or undamaged categories is not always clear. To perform binary classification, a pattern needs to be identified among signal features. In real-world data, these patterns are scattered in high-dimensional and very often in nonlinear subspaces. Dimensional reduction simplifies the pattern representation and reduces the computational effort required from classifiers. However, reducing the number of features could lead to loss of valuable information. The goal of this study is to obtain two- and three-dimensional projection of multivariate acoustic and vibration data to permit visual and computational classification of data. The dimensional reduction techniques evaluated and applied to vibration and acoustics experiments in this work are: (1) principal component analysis (PCA), (2) kernel PCA (KPCA), (3) local linear embedding (LLE), (4) local tangent space analysis (LTSA), (5) diffusion maps (DM), and (6) multidimensional scaling (MDS). The dimensional reduction methods presented here are based on a review paper presented by Matten [104].

Dimensional reduction methods reduce the original data dimensionality D to a subspace dimensionality d ($d \leq D$). The most well known linear feature extractor is principal component analysis (PCA). This method computes the d largest eigenvectors of the $D \times D$ covariance matrix of the $n \times D$ data matrix. Given the pattern matrix $\mathbf{X}$

$$\mathbf{X} \in \Re^{n \times D} \tag{30}$$

consisting of n data vectors and D features, PCA transforms this dataset to the derived pattern matrix Y as

$$\mathbf{Y} \in \Re^{n \times d} \tag{31}$$

This linear transformation is defined as

$$\mathbf{Y} = \mathbf{XH} \tag{32}$$

where

$$\mathbf{H} \in \Re^{D \times d} \tag{33}$$

is the linear transformation matrix whose columns are the eigenvectors. The main drawback to PCA is the computation of the covariance matrix, which becomes quite demanding with increasing number of features. PCA is a linear technique since it embeds the data into a linear subspace.

Numerous nonlinear dimensional reduction techniques are available. Kernel PCA (KPCA) follows directly from PCA. The difference is that before PCA is performed the dataset is mapped into a new feature space via a nonlinear function called kernel. Therefore, PCA is applied to the kernel matrix K on the datapoints $\mathbf{x}_i$, with the following dot product decomposition property

$$k_{ij} = k\left(\mathbf{x}_i, \mathbf{x}_j\right) \tag{34}$$

where k is typically a nonlinear function, in other words kernel, by which the input data is mapped into a new feature space. This kernel based method relies on the choice of the kernel function k. Common kernels include p^{th}-order polynomial, Gaussian, and linear kernel, which is equivalent to regular PCA.

Multidimensional scaling (MDS) is another nonlinear feature extraction technique which creates low-dimensional projection while retaining pairwise distances between datapoints as much as possible. The degree of correspondence between the distances among points implied by

MDS map and the matrix input by the user is measured by the so called "stress function". The general form of this function is as follows

$$\underset{function}{stress} = \sqrt{\frac{\sum_{i,j=1}^{N}\left(f\left(x_{ij}\right)-d_{ij}\right)^2}{scale}} \tag{35}$$

where d_{ij} refers to the Euclidean distance, across all dimensions, between points i and j on the map, $f\left(x_{ij}\right)$ is some function of the input data, and *scale* refers to a constant scaling factor, used to keep stress values between 0 and 1. When the MDS map perfectly reproduces the input data, $f\left(x_{ij}\right)-d_{ij}$ is for all i and j, so stress is zero. Thus, the smaller the "stress function" value is, the better the representation becomes. Several stress functions are used to express the quality of the mapping, the most well known are the Sammon and Niemann stress functions [104]. In this work, the Sammon stress function is used for the MDS algorithm.

Diffusion maps (DM) are based on defining a Markov random walk on the graph of the data [104]. By performing the random walk for a number of time steps, a measure of the proximity of the data points is obtained. The end result is the diffusion distance. Given the graph of the data, the spectral properties of the graph matrix are used to embed the data points into a lower dimensional space. The DM approach has been shown to perform rather well with 'clean' data, however it is sensitive to the presence of signal noise. In the diffusion maps framework, a graph of the data is constructed first. The weights of the edges in the graph are computed using Gaussian kernel function, leading to a matrix $\mathbf{W}$ with entries

$$w_{ij} = e^{\frac{-\left\|\mathbf{x}_i-\mathbf{x}_j\right\|^2}{2\sigma^2}} \tag{36}$$

where σ indicates the variance of the Gaussian. Normalization of the matrix $\mathbf{W}$ is performed in such a way that its rows add up to 1, which forms a matrix $\mathbf{P}^{(1)}$ with entries

$$p_{ij}^{(1)} = \frac{w_{ij}}{\sum_k w_{ik}} \tag{37}$$

Because diffusion maps originate from dynamical systems theory, the resulting matrix $\mathbf{P}^{(1)}$ is considered a Markov matrix that defines the forward transition probability matrix of a dynamical process. Hence, the matrix $\mathbb{P}^{(1)}$ represents the probability of a transition from one datapoint to another datapoint in a single timestep. The forward probability matrix for t timesteps $\mathbf{P}^{(t)}$ is thus given by $\left(\mathbf{P}^{(1)}\right)^t$. Using the random walk forward probabilities p_{ij}^t, the diffusion distance is defined by

$$D^{(t)}\left(\mathbf{x}_i, \mathbf{x}_j\right) = \sqrt{\sum_k \frac{\left(p_{ik}^{(t)} - p_{jk}^{(t)}\right)^2}{\psi\left(\mathbf{x}_k\right)^{(0)}}} \tag{38}$$

where $\psi\left(\mathbf{x}_i\right)^{(0)} = m_i / \sum_j m_j$ is a term that attributes more weight to parts of the graph with high density and m_i is the degree of node $\mathbf{x}_i$ defined by $m_i = \sum_j p_{ij}$. The diffusion distance is small if there are many high probability paths of length t between two points. As the diffusion process runs forward, revealing the geometric structure of the data, the main contributors to the diffusion distance are paths along that structure. In the low-dimensional space representation $\mathbf{Y}$, diffusion maps attempt to retain diffusion distances. Using spectral theory on the random walk, the low-dimensional representation $\mathbf{Y}$ retains the diffusion distances $D^{(t)}\left(x_i, x_j\right)$ as good as possible by the d non-trivial principal eigenvectors of the eigenproblem

$$\mathbf{P}^{(t)}\mathbf{v} = \lambda\mathbf{v} \tag{39}$$

Because the graph is fully connected, the largest eigenvalue is trivial, $\lambda = 1$, and its eigenvector, $\mathbf{v}_1$, is thus discarded. The low-dimensional representation $\mathbf{Y}$ is given the next d principal eigenvectors, which are normalized by their corresponding eigenvalues.

Local linear embedding (LLE) is a technique that preserves local properties of the data by writing the high-dimensional datapoint $\mathbf{x}_i$ as a linear combination $\mathbf{w}_i$ of their k nearest neighbors $\mathbf{x}_{ij}$. LLE fits a hyperplane through the datapoint $\mathbf{x}_i$ and its nearest neighbors. The local linearity assumption of LLE implies the construction weights $\mathbf{w}_i$ are invariant to translation, rotation, and rescaling; thus, any linear mapping of the hyperplane to a lower dimensionality preserves the local geometry of the manifold. In other words, the reconstruction weights $\mathbf{w}_i$ that reconstruct datapoint $\mathbf{x}_i$ from its neighbors in the high-dimensional space also reconstruct datapoint $\mathbf{y}_i$ from its neighbors in the low dimensional space. Finding the d-dimensional data representation $\mathbf{Y}$ amounts to minimizing the cost function

$$\phi(\mathbf{Y}) = \sum_i \left\| \mathbf{y}_i - \sum_{j=1}^{k} \omega_{ij} \mathbf{y}_{ij} \right\|^2 \quad \text{subject to } \left\| \mathbf{y}^{(k)} \right\|^2 = 1 \text{ for } \forall k, \tag{40}$$

where $\mathbf{y}^{(k)}$ represents the k-th column of the solution matrix $\mathbf{Y}$. The coordinates of the low-dimensional representations $\mathbf{y}_i$ that minimize this cost function are found by computing the eigenvectors corresponding to the smallest d nonzero eigenvalues of the product $(\mathbf{I} - \mathbf{W})^T (\mathbf{I} - \mathbf{W})$, where $\mathbf{I}$ is the identity matrix and $\mathbf{W}$ is a sparse $n \times n$ matrix whose entries are set to 0 if i and j are not connected in the neighborhood graph, and equal to the corresponding reconstruction weight otherwise.

LLE has become very popular in numerous applications, such as sound source localization and image classification. However, LLE can become unstable (fail) with even simple datasets [104]. In addition, LLE tends to collapse large portions of the data very close together in the low-dimensional space, which is useful for classification, but not if cluster distribution analysis is desired.

Similar to LLE, Local Tangent Space Analysis (LTSA) is a technique that describes properties of the high-dimensional space using local tangent space of each point. LTSA is based on the observation that there exists a linear mapping $\mathbf{L}_i$ from high-dimensional datapoint $\mathbf{x}_i$ to its local tangent space exists and that there exists a linear mapping from the corresponding low-dimensional datapoint $\mathbf{y}_i$ to the same local tangent space, hence the similarity to LLE. LTSA computes bases for the local tangent spaces at the datapoints $\mathbf{x}_i$ by applying PCA on the k datapoints that are neighbors of the datapoint $\mathbf{x}_i$, which results in a mapping $\mathbf{M}_i$ from the neighborhood of $\mathbf{x}_i$ to the local tangent space of Θ_i. LTSA performs the following minimization

$$\min_{\mathbf{Y}_i,\mathbf{L}_i} \sum_i \left\| \mathbf{Y}_i \mathbf{J}_k - \mathbf{L}_i \Theta_i \right\|^2 \tag{41}$$

where $\mathbf{J}_k$ is the "centering" matrix, which performs the modification of subtracting mean of the features in the feature space defined by the kernel function κ. The solution $\mathbf{Y}$ is formed by the eigenvectors of an alignment matrix $\mathbf{B}$, that correspond to the smallest nonzero eigenvalues of $\mathbf{B}$. The entries of the matrix $\mathbf{B}$ are obtained via iterative summation

$$\mathbf{B}_{N_i N_j} = \mathbf{B}_{N_{i-1} N_{j-1}} + \mathbf{J}_k \left(\mathbf{I} - \mathbf{V}_i \mathbf{V}_i^T \right) \mathbf{J}_k \tag{42}$$

where N_i represents the set of indices of the nearest neighbors of datapoint $\mathbf{x}_i$. Subsequently, the low-dimensional representation $\mathbf{Y}$ is obtained by computation of the eigenvectors corresponding to the d smallest nonzero eigenvectors of the symmetric matrix $(\mathbf{B}+\mathbf{B}^T)/2$.

In this section, we have presented the dimensional reduction techniques which can be utilized for feature extraction via data compression. The effectiveness of dimensionality reduction techniques in extracting features will be utilized for performing damage detection. In the next

section, we present a novel robust approach for utilizing dimensionality reduction in damage detection applications.

4.3 Proposed Dimensional Reduction Ensemble Approach for Damage Detection

Structural systems are exposed to varying operating and environmental conditions during their lifetime, which causes gradual deterioration of structural health overtime, i.e. aging. Therefore, it is necessary to take aging into account when performing structural damage assessment. Most methods in SHM focus on looking for damage using one set of data or damage index vector from the undamaged and damaged states. Treating the problem in this fashion leaves out the real-time and long-duration of continuous monitoring of a structure so that gradual degradation and damage from severe events, such as impacts, can be detected.

In many damage detection studies [21,37], the Mahalanobis distance is used to evaluate distance among multivariate feature vectors, which can be written as

$$d_{i,j} = \sqrt{\left(\mathbf{f}^i - \mathbf{f}^j\right)^T \boldsymbol{\Sigma}^{-1} \left(\mathbf{f}^i - \mathbf{f}^j\right)} \tag{43}$$

where $\mathbf{f}^i$ is the extracted feature vector obtained from the dimensional reduction techniques, and $\boldsymbol{\Sigma}$ is the covariance matrix of the training data. Given that training data is available to describe the natural variation of the response signal, then, when new data vectors become available a comparison can be made using the Mahalanobis distance measure. The similarity between multiple feature vectors can be expressed by using a Mahalanobis distance matrix as depicted in Figure 4.1, where 'Old' refers to training data, and 'New' to test data.

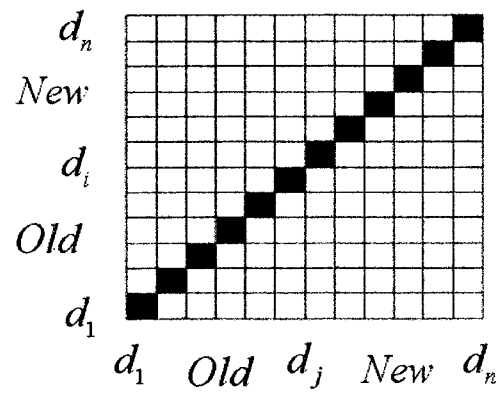

Figure 4.1. Mahalanobis distance similarity matrix.

To obtain a damage index value, the mean distance value of rows 1-to-*nt*, where *nt* is the number of training vectors, is obtained for all matrix columns. Once the mean values, D_j, are obtained, the resulting feature mean vector, I_j, is normalized by dividing each damage index value by the mean of the first N_t values. This process is captured by the following equations

$$D_j = \left(\frac{1}{N_t} \sum_{i=1}^{N_t} d_{i,j} \right) \tag{44}$$

$$I_j = \frac{D_j}{(1/N_t)\sum_{j=1}^{N_t} D_j} \tag{45}$$

It's worth noting that feature vectors, both training and testing, used in the distance similarity approach must be normalized so as to take into account the normal variations of training data. Real-life measurements contain considerable levels of noise, causing the feature vectors vary from sample to sample. Therefore, the training data must be comprehensive of all known operational conditions in order to cancel out normal variability from the abrupt change or damage detection goal. In the work presented in this paper, the distance similarity matrix approach is validated for identifying system variability by incorporating system modifications to the vibration experimental setup.

In normal dimensional reduction (D-R) problems, one method hardly ever captures all characteristics of the data. To improve performance, the results of different D-R techniques, with varying complexity, are combined, as depicted in Figure 4.2. This can not only improve the performance, but it can also increase the robustness of the damage detection. By combining D-R techniques we are aiming at a more accurate and clear decision-boundaries at the expense of increased complexity. The proposed approach is based on combined classifiers [36]. The combined-classifier pattern recognition approach has been rapidly growing in recent years in the machine learning communities.

Dietterich [36] provides three reasons as to why combined-classifiers are better than a single classifier. These will be presented here and applied to in the context of combining D-R techniques. The first reason is based on simple statistics. Suppose we have a number of D-R techniques to choose from, but since each technique has different properties, we run the risk of choosing the wrong D-R technique for the particular application. Based on statistics, a safer option would be to use all available techniques and "average" their outputs, which might not be the best single result, but will minimize the risk of selecting an inadequate D-R technique. Second, certain D-R techniques, in particular nonlinear, perform some type of random search or optimization approach, which results in varying local minima. Given appropriate combination technique, an approximation to the optimal manifold unfolding, in other words extracting effective differentiating features, might be achieved. Last, it is possible that our D-R techniques under consideration does not contain the optimal approach. For example, the data manifold might be nonlinear, and all we have in our basket are individual linear D-R techniques. However, a set of linear D-R techniques can approximate the nonlinearity more accurately than a single linear technique. In addition, the ensemble of simple D-R techniques is better than using a complex nonlinear technique, which might contain several tuning parameters. This latter reason can be

thought of as a linearization of a nonlinear problem in system dynamics. The goal of building combined-classifiers aims at building accurate decision boundaries. In our proposed approach, the goal of using combined D-R techniques aims at providing extracted features that can be used to build clear decision boundaries, which would facilitate the classification work.

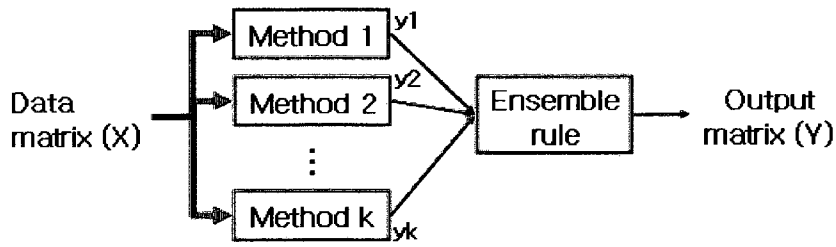

Figure 4.2. Combination of dimensional reduction techniques.

In this work, we will make use of the simple product combination rule. The simplicity of this combination rule will demonstrate the efficacy of combining D-R techniques. To suppress the errors unique to each dimensional reduction technique, the outputs of each technique, I_j, may be combined using the product combination rule

$$f_j = \prod_{k=1}^{K_d} I_j^k \tag{46}$$

where K_d is the number of dimensional reduction techniques being combined.

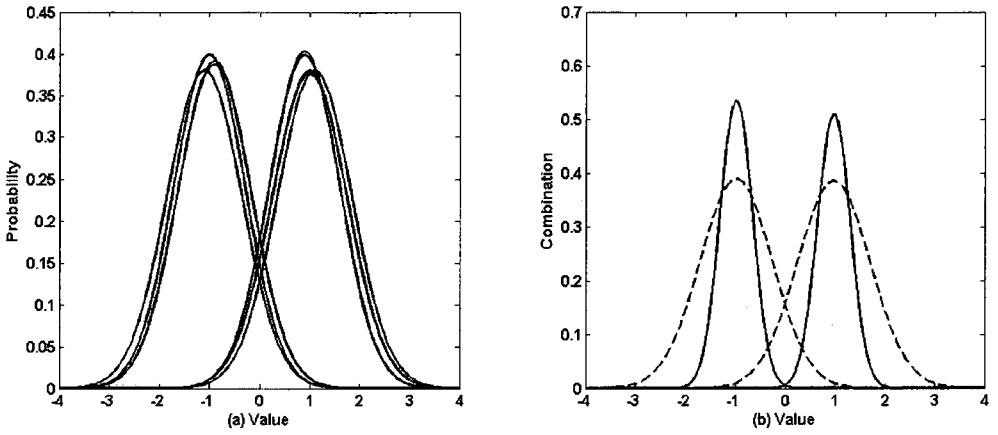

Figure 4.3. Binary class probability distributions for damage and undamaged data. (a) Five target probability density estimates per class. (b) Combination of the five target probability density estimates, (mean rule - dashed, product rule - solid).

The next logical step in applying combined D-R techniques is the selection of individual approaches for the best combination. Assuming that the data characteristics are not well known, the ensemble of combined D-R techniques must be varied and should be capable of dealing with both linear and nonlinear manifolds. D-R techniques can be categorized into two main areas: linear and nonlinear. Nonlinear D-R techniques can be further separated into local and global approaches. Taking this into consideration, in our work, we base our D-R technique selection on categorical diversity. By choosing diverse D-R techniques, the performance of the combined D-R technique will be improved. In addition, by not combining highly similar D-R techniques we reduce the risk of simply combining equal extracted features, which would only result in increased complexity but without any gains. For our work, we chose to combine PCA (linear technique), LLE (local nonlinear technique), and MDS (global nonlinear technique). The proposed combined D-R technique is applied to two case studies, the acoustic and vibration experimental data.

4.4 Case Study I: Cantilever Beam Experiment

The proposed distance similarity matrix and combined D-R technique was applied to vibration data obtained from a base-excited cantilever beam. The in-house vibration experiment was designed to evaluate and validate the proposed damage detection approach. Figure 4.4 shows a picture of the cantilever beam experimental setup. The experimental aluminum cantilever beam is of uniform rectangular cross-section. The dimensions of the beam were $50\text{cm}\times3.81\text{cm}\times0.635\text{cm}$.

The beam was instrumented with 5-accelerometers at evenly-spaced with a 7.62cm separation distance. A Bruel&Kjaer signal analyzer was used to collect the raw vibration data and transform it to the frequency domain. An electromagnetic shaker manufactured by Ling Electronics, and Endevco Type 2215 accelerometers were utilized.

Four different conditions were tested: (a) base experiment setup; (b) Mass-1 (17g) between accelerometer 4 and 5; (c) Mass-2 (27g) between accelerometer 4 and 5; and (d) Mass-3 (54g) between accelerometer 4 and 5. The latter setup conditions were made so as to simulate increasing structural damage. In this case, the increase of mass has similar effects as the decrease in stiffness, which can be easily observed in the undamped natural frequency, ω_n, equation of a single-degree-of-freedom (SDOF) equation $\omega_n = (k/m)^{1/2}$, where k is the system stiffness and m is the system mass.

Each condition was tested 15 times; thus, making 60 feature vectors. The frequency span was of 1.6 kHz with a sampling frequency of 1 Hz. The base of the cantilever beam was randomly excited using the same frequency band of 1.6 kHz at an approximate 1.3 m/s^2 RMS level.

Figure 4.4. Cantilever beam experimental setup.

Acceleration transmissibility, ratio of input acceleration to output acceleration, data vectors were obtained for each accelerometer. Feature selection was applied to each transmissibility response data vector by applying peak-picking in the frequency range of interest and to the well-separated frequency peaks in the transmissibility plots. A simple algorithm was written which located the peaks based on a criteria standard deviation of transmissibility magnitude at frequency f_i over surrounding frequency range $(f_i - \Delta f < f_i < f_i + \Delta f)$, and a threshold of minimum peak-to-peak separation distance. The resulting peak data vector was a feature vector of length 7 for each experimental test.

4.4.1 Data Analysis and Results

The vibration data was dimensionally reduced first via peak-picking feature selection and then via application of D-R techniques to 5 features. The cluster results are shown in Figure 4.5 for the four experimental setups. Visual analysis demonstrates that all methods, with exception of KPCA, were able to form well separated clusters. The KPCA method formed string like clusters, which seem to share the same origin point. The undamaged dataset is represented with blue cross markers and the damaged datasets are represented with red dot markers. Although clear

separation exists among the clusters, because in this case study we are analyzing more than two class labels, via simple visual classification, it is not very clear to assign labels (identify) to the three different damaged datasets. Assuming that training data is only available on the undamaged state, applying a trained binary classifier would only be able to separate damaged from undamaged datasets, but not the within the damaged datasets.

Figure 4.6 shows the combined D-R technique results for the distance similarity matrix of the vibration data. The upper and lower 3σ standard deviation limits were also plotted. Similar to the aeroacoustic mean index similarity results, a very clear step exists between damaged and undamaged datasets. The mean index results indicate a range of approximately $1\sim10^{17}$. In contrast to cluster analysis, Figure 4.6 clearly shows a difference among the three damaged datasets. As the setup is changed from undamaged to Mass-1 (17g) setup, the mean index jumps significantly. As the mass is incrementally increased to Mass-2 (27g) and Mass-3 (54g), the mean index value also increases proportionally. The results of the distance similarity mean index in combination with the combined D-R technique demonstrate that not only can abrupt change detection can be achieved, but tracking of change progression can be performed, which would be very applicable to damage assessment of time-varying structures, such as structural deterioration.

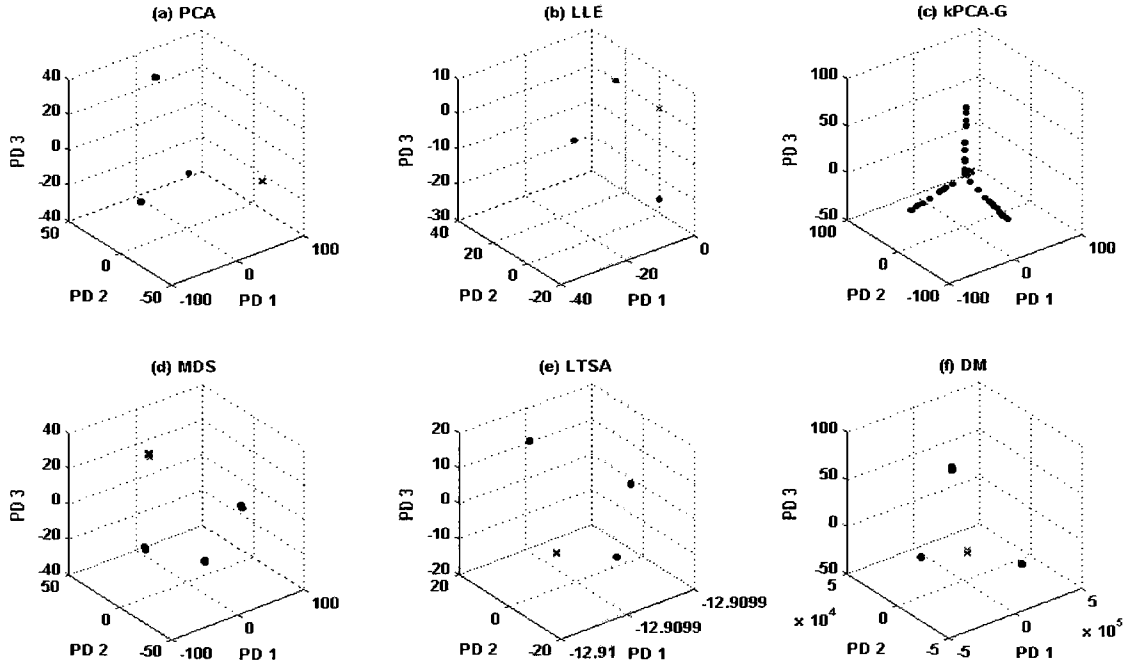

Figure 4.5. Principal directions plot for dimensional reduction methods of undamaged (blue cross) and damaged (red dots) data where each cluster represents an experimental setup.

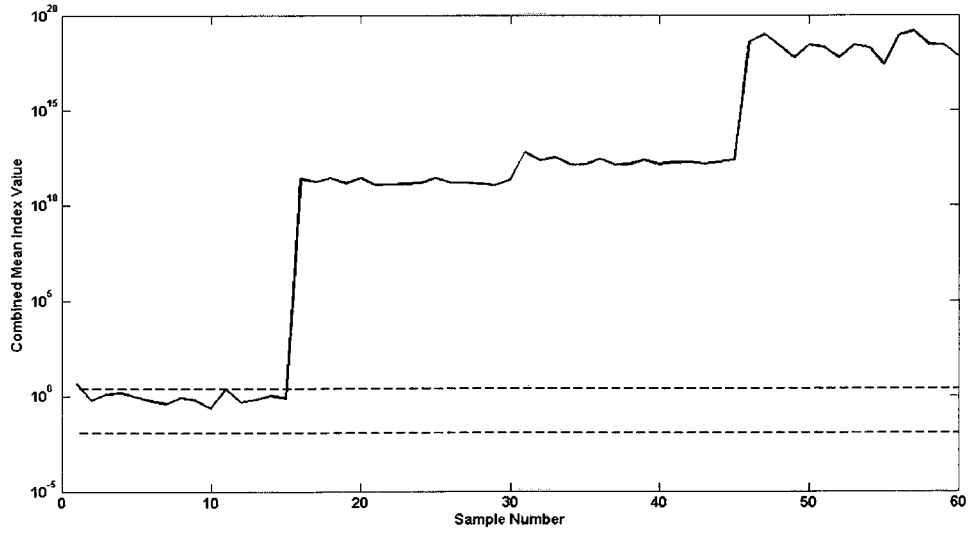

Figure 4.6. Combined dimensional reduction methods. NoMass: sample 1-15, Mass-1: sample 16-30, Mass-2: sample 31-45, Mass-3: sample 46-60.

4.5 Case Study II: Aeroacoustic Scaled Wing

In this study, an in-house subscale wing structure model of a Boeing-767 using the Scaled Anechoic Wind Tunnel (SAWT), see Figure 4.7, is used and tested in the anechoic chamber at the Transportation Noise Control Center (TNCC) at UC Davis. Acoustic tests were performed at multiple 60 RPM intervals ranging from 80-280 RPM. The armature has a radius of 102 cm, which transforms to equivalent test speeds to a range of approximately 9-30 m/s. The acoustic tests were recorded for two structural conditions: (1) undamaged wing; and (2) wing with single cavity. The transducer was positioned 1cm away from the cavity at location number 11, see sketch shown in Figure 4.8(a). In all tests, the signals were recorded in the time domain and transformed to the frequency domain using the Fourier transform. In all acoustic experiments, the number of undamaged samples was 200, and the number of samples corresponding to each damage scenario was 100. The frequency span was 12.8 kHz with a center frequency at 7.5 kHz, and a frequency step of 16Hz.

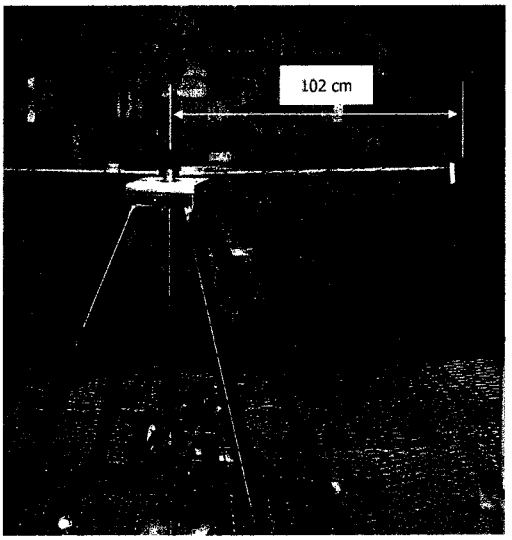

Figure 4.7. Scaled Anechoic Wind Tunnel (SAWT) for noise experiments [146].

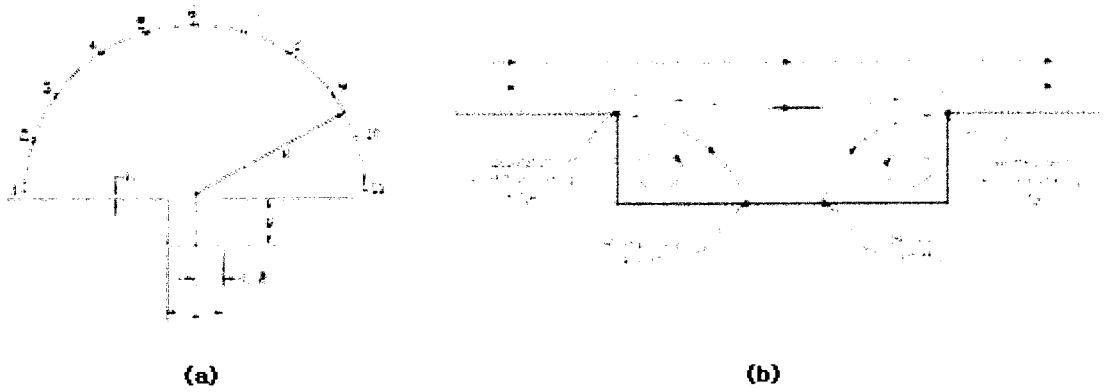

Figure 4.8. (a) Cavity geometry and near-field microphone location, and (b) cavity flow field, 2D representation.

Two sample experiments were conducted with cavity present. First, the acoustic transducer was mounted one centimeter away from the cavity. Second, the cavity was modified to a thru hole on the wing, and the transducer was used to cover the hole and be the base of the cavity. Figure 4.9 shows a comparison of the latter sample experiments. Although, the acoustic transducer was placed only a short distance away from the cavity, no clear visual indication of resonant peaks can be observed from acoustic measurements. For the case when the transducer was placed directly behind the cavity, the resonant peaks are clearly visible. Therefore, feature extraction techniques must be applied to measured data in order to determine the presence or absence of structural cavities.

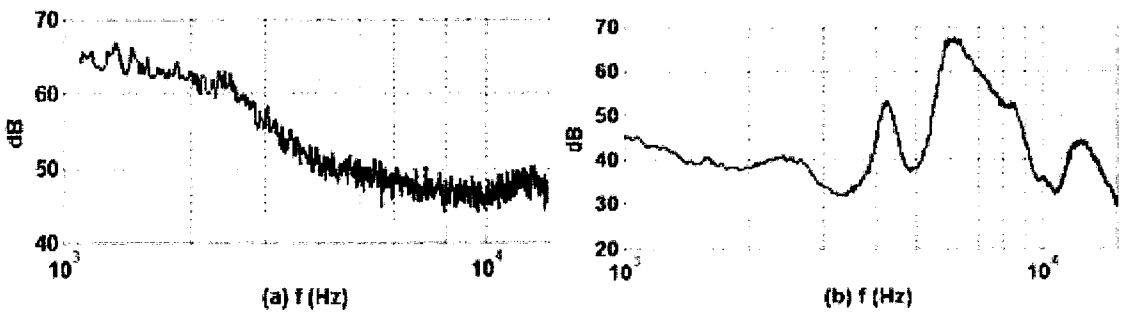

Figure 4.9. Frequency response (a) transducer 2.54 cm from cavity; (b) transducer as base of cavity, 250 RPM.

4.5.1 Data Analysis and Results

The newly proposed approach is applied to the test results of the aeroacoustic experiment. The high-dimensional frequency response data for the 200 and 100 datasets of the undamaged and damaged cases, respectively, were dimensionally reduced to 5 features. The original dimensional space was 801 features, a number corresponding to the number of 16Hz divisions in the available 12.5 kHz span. The extracted feature subspace was chosen to be considerably smaller, because in our case, we are not concerned with the loss of information from the dimensional reduction since data reconstruction is not one of our goals.

The mapping results for the 80-140 RPM and experiments are shown in Figure 4.10 and Figure 4.11, respectively. The results in Figure 4.10 and Figure 4.11 exhibit 'string' line clusters within the damaged and undamaged datasets. This clustering phenomenon is due to the fact that individual measurements were taken to reproduce approximately 35 feature vectors, or, in other words frequency response. These measurements were concatenated to produce the 200 and 100 data vectors for the dimensional reduction analysis. Therefore, each string corresponds to an individual measurement. The mapping results demonstrate that the dimensional reduction techniques are sensitive enough to show the test-to-test variability. The mappings show the first three principal directions obtained from the corresponding dimensional reduction technique.

Visual inspection of Figure 4.10 shows all D-R techniques failed at creating a clear cluster separation between damaged and undamaged data. In Figure 4.11, mapping results for a rotational speed of 200-260 RPM for the wing with and without cavity. In contrast to Figure 4.10, some techniques demonstrate cluster separation between the damage and undamaged datasets. Visual analysis shows that PCA, LLE, KPCA (with Gaussian kernel), and LTSA methods demonstrate possible 3-D hyperplane separation between damaged and undamaged data points. The MDS and DM methods obtain partial cluster separation, but the separation is nonlinear, for which it would

be more difficult for a classifier to generate such a hyperplane. From this experiment, LLE outperforms the other methods, because the distance created between damaged and undamaged data is larger, thus minimizing the potential for false-positive and false-negatives results. In addition, the cluster spread for damaged and undamaged states is minimal, which would minimize false-classification. Using visual analysis of the D-R results as a classifier demonstrates the difficulty in creating decision boundaries, which would allow proper classification of all data points. Therefore, blind application of D-R techniques for feature extraction does not guarantee the facilitation of dataset classification.

The distance similarity matrix approach was applied to the individual D-R feature vector outputs. Figure 4.12 and Figure 4.13 shows the similarity results at the 200-260 RPM range for LLE and PCA approaches. Figure 4.12(a) and Figure 4.13(a) show the similarity matrix in pseudocolor or "checkerboard" plot format. The values of the elements in the similarity matrix specify the color in each cell of the plot. As was previously shown, the diagonal of the matrix is expected to be of value 1. The results obtained using the LLE technique show that similarity matrix exhibits two very distinct color ranges, blue and red. The shift in color from blue to red is due to the strong shift in similarity element value range. Using the mean index value of the similarity matrix, the linear plot of Figure 4.12(b) was obtained. Upper and lower 3σ standard deviation limits of the training data were also plotted as dashed lines to capture the 99.7% assumed normal distribution of the data. The linear plot shows a very clear jump after sample number 200, which indicates the beginning of the damaged feature vectors. As can be seen from the plots, the mean index value ranges from 1 to a scale of 10^{24}, which indicates an immense dissimilarity. After sample number 270, the linear plot drops below 4, but remains above the upper standard deviation line, which can be used as a simple outlier detection metric or classifier.

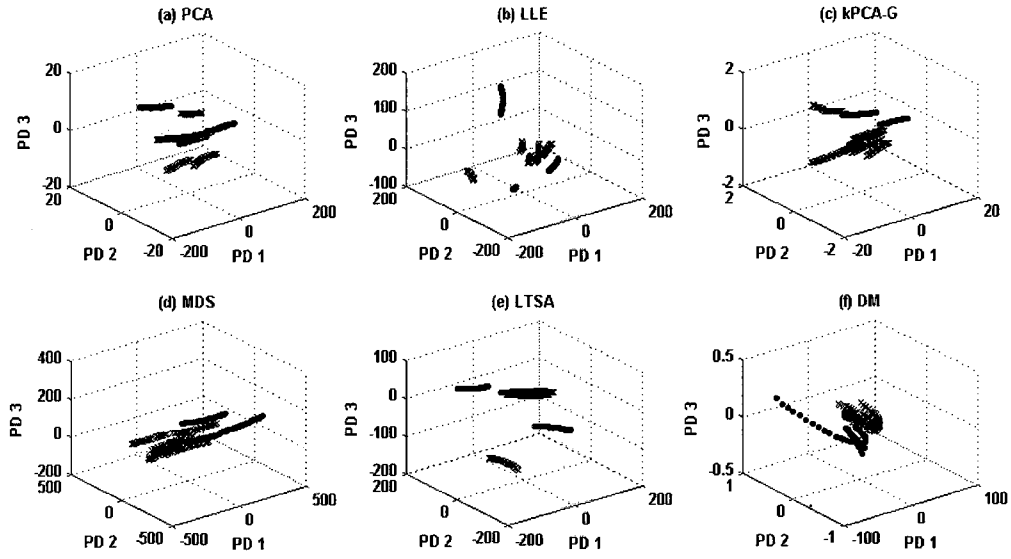

Figure 4.10. Principal directions plot for dimensional reduction methods of undamaged (blue cross) and damaged (red dots) data with feature selection applied at 80-140 RPM.

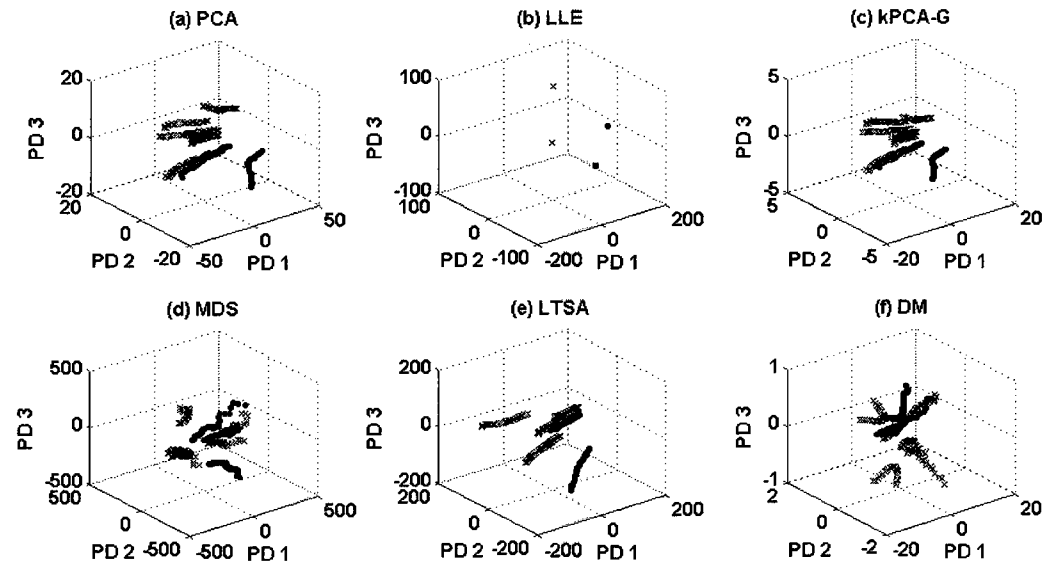

Figure 4.11. Principal directions plot for dimensional reduction methods of undamaged (blue cross) and damaged (red dots) data with feature selection applied at 200-260 RPM.

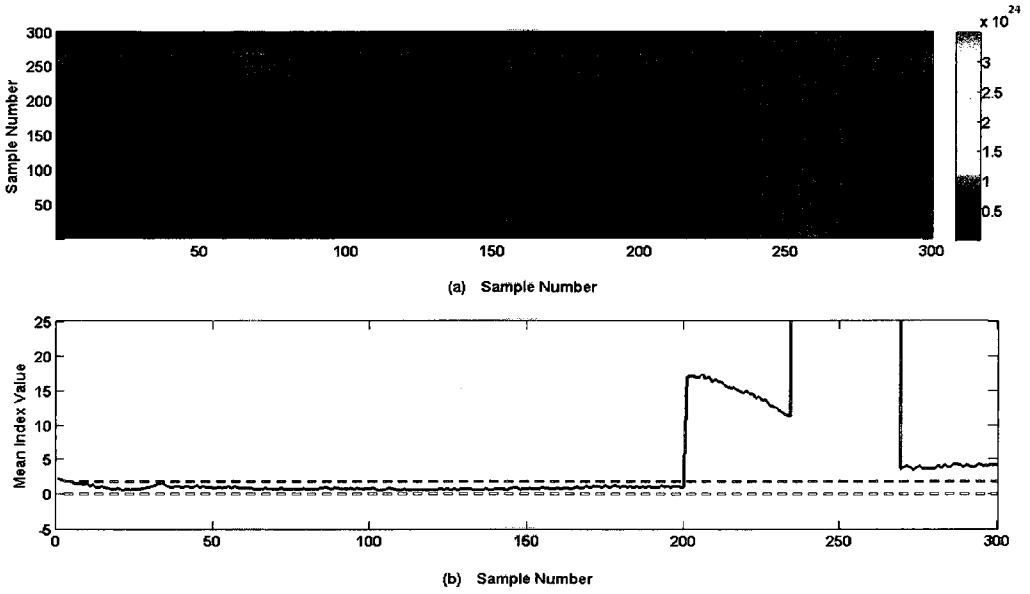

Figure 4.12. Similarity results of dimensionally reduced data - undamaged (sample 1-200) and damaged (201-300), using LLE approach and feature selection. (a) Mahalanobis distance matrix; (b) Mean index value results. RPM=200-260.

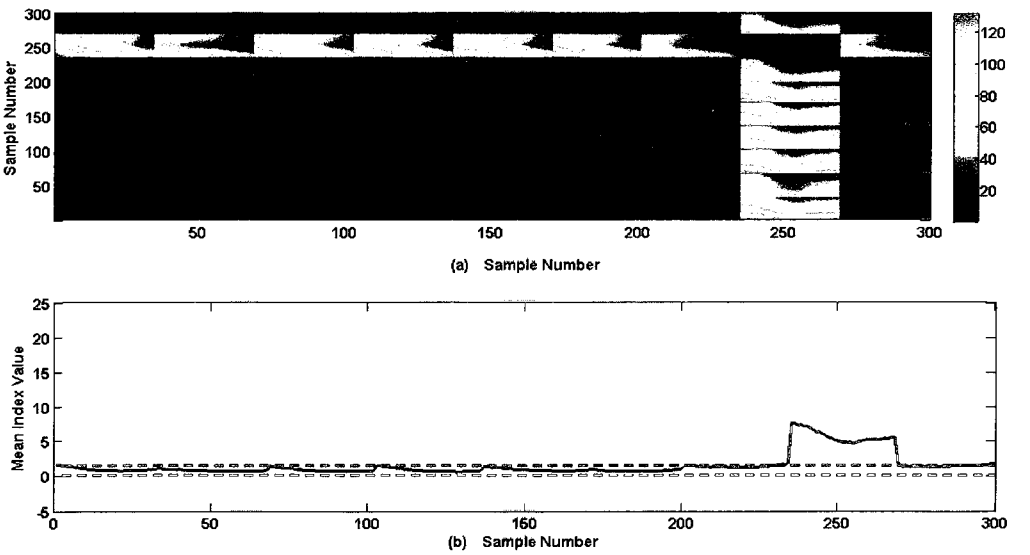

Figure 4.13. Similarity results of dimensionally reduced data - undamaged (sample 1-200) and damaged (201-300), using PCA approach and feature selection. (a) Mahalanobis distance Correlation matrix; (b) Mean index value results. RPM=200-260.

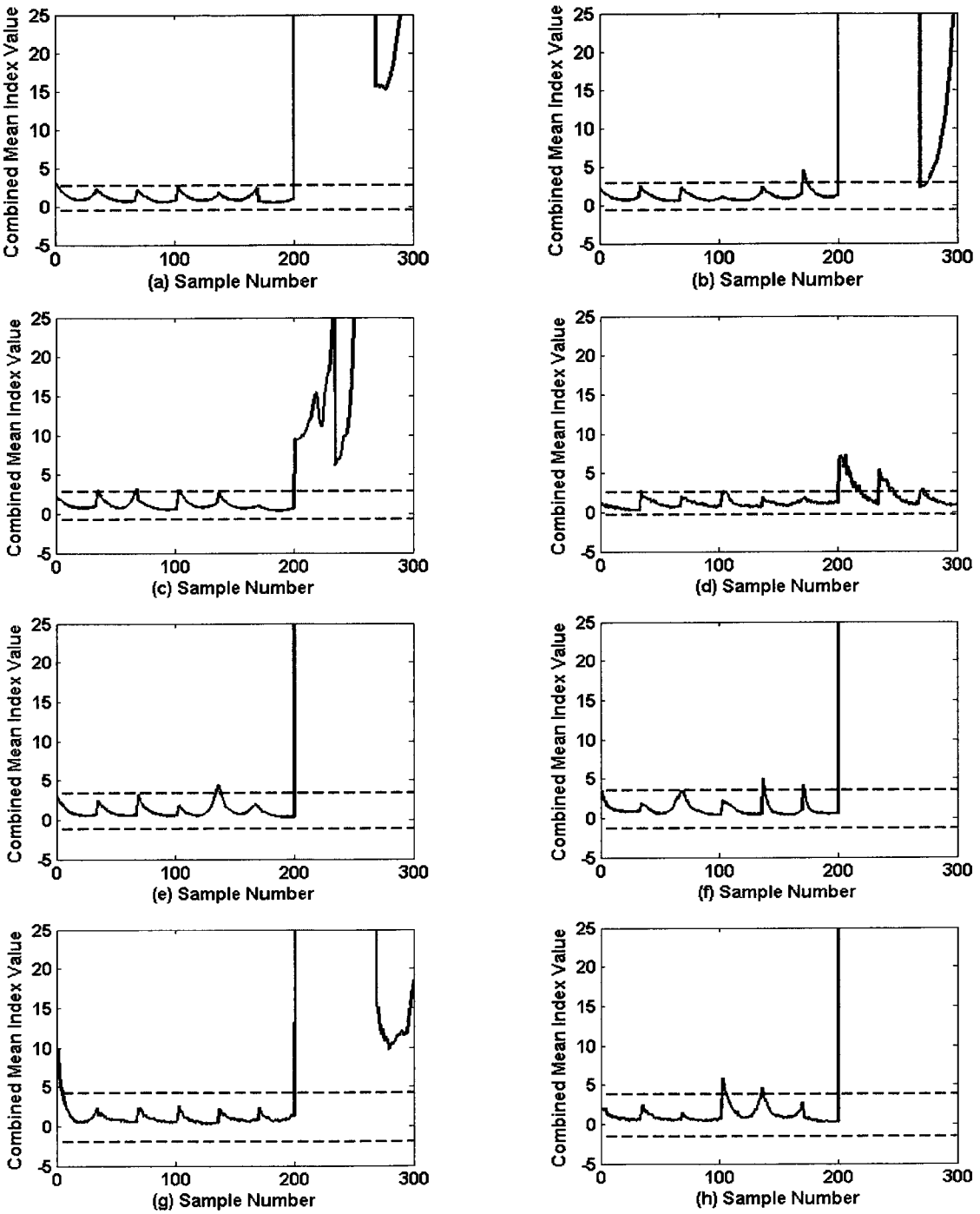

Figure 4.14. Combined mean index value results for PCA, LLE, MDS, at each speed: (a)80-140, (b)100-160, (c)120-180, (d)140-200, (e)160-220, (f)180-240, (g)200-260, and (h) 220-280 RPM.

Figure 4.13 shows the results obtained using PCA for the distance similarity matrix calculations. In contrast to LLE results, the range of the similarity element values ranges from 1~130. Again, upper and lower one standard deviation lines were plotted for the training data. In this case, PCA fails to provide a clear jump in mean index similarity value after sample number 200. Only samples 235-270 demonstrate a jump in dissimilarity, but again after sample 270, the mean index value drops very close to 1.

Evaluation of the results shown in Figure 4.12 and Figure 4.13 demonstrate that the similarity matrix approach indeed provide clearer separation between damaged and undamaged datasets. Comparison of LLE and PCA similarity results show that a blind selection of D-R technique can be inefficient due to the variability from experiment to experiment. In these results, the nonlinear D-R method, LLE, performed much better than the standard PCA method in differentiating damaged and undamaged datasets. This result is critical since PCA is the predominant D-R choice for feature extraction in the area of structural damage assessment. Therefore, unless the user has significant experience in feature extraction, the damage detection monitoring system is at risk of providing multiple false-diagnosis.

Figure 4.14 shows the results of the combined D-R technique at multiple speed ranges. Comparing the results in Figure 4.14(g) to the LLE results of Figure 4.12(b) demonstrate similar characteristics but the combined D-R technique has a minimum value after sample number 270 of 10, while the LLE method had a minimum number of 4. With exception to Figure 4.14(d), the combined D-R technique was able to differentiate between damaged and undamaged datasets very clearly. In Figure 4.14(d), at the sample number 200, the jump in mean index magnitude occurs, but drops down to levels inside the upper standard deviation line, which is not a desirable property. Although indication of an abrupt change is shown in Figure 4.14(d), the mean index value in this instance would not provide reliable information for classification. Analysis of the

raw decibel, dB, acoustic data was performed to investigate as to why differentiation was not clearly achieved for speed range 140-200 RPM.

Table 4.1 shows the mean dB levels for the undamaged (U) and damaged (D) datasets at all the specified speed intervals. The difference of the mean values is also given, which shows that with exception to the 140-200 RPM interval, all other speed intervals result in an increase of mean dB value when going from undamaged to damaged. In addition, the magnitude of the dB difference value is the second smallest. The smallest difference magnitude is obtained in the 100-160 RPM interval, which is an interval that also demonstrates low mean index values after sample number 270, as shown in Figure 4.14(b). Therefore, the lack of similarity separation between damaged and undamaged datasets at the 140-200 RPM interval is possibly due to the significant overlap that exists between both classes, and to test-to-test variability.

Table 4.1. Mean standard deviation of acoustic frequency response for each speed range.

RPM	80-140	100-160	120-180	140-200	160-220	180-240	200-260	220-280
Mean σ - U (dB)	6.4640	5.8199	5.4062	5.1459	4.5606	4.2459	4.2459	3.8482
Mean σ – D (dB)	6.6654	5.8865	5.5499	5.0752	4.7154	4.4801	4.4801	4.1547
Difference (dB)	-0.2014	-0.0666	-0.1437	0.0706	-0.1548	-0.2342	-0.2342	-0.3065

4.6 Summary

The results of two case studies presented in this paper support that damage assessment based on the proposed ensemble of dimensional reduction techniques can be used to effectively detect and track spontaneous damage in structures. The proposed approach is based on a Mahalanobis distance similarity matrix of training and test feature vectors. Notable importance is given to obtaining feature vectors via diverse dimensional reduction methods, and their ensemble. Two case studies were conducted. The aeroacoustic experimental studied impact damage detection in a

sub-scale wing structure via pattern recognition of acoustic measurements under varying excitation levels. The detection of structural cavities was achieved via dimensional reduction of multiple time measurements of frequency response datasets. From the results obtained, we may conclude that under test-to-test variability and with no clear visible changes of the frequency response, the distance similarity matrix method with dimensional reduction techniques can serve as a means to detect the presence of a cavity in the near-field of an acoustic transducer. The vibration experiment studied the detection of abrupt structural changes and their variation. The structural changes simulating damage were induced by localized mass modifications. By applying the proposed damage detection approach, clear indication of damage was obtained with zero false-positive or false-negative.

The idea of integrating decisions of several diverse diagnostic systems into an ensemble, which improves upon the performance and robustness of the individual members, is novel. This chapter addressed the issue of aleatory uncertainty in damage diagnostics. Continuing chapters will address the examination of epistemic uncertainty in damage diagnostics of vibration experiments.

Chapter 5

Classification of Dimensional Reduction Results in Damage Assessment

In this chapter, we present a classification study of dimensional reduction techniques for structural damage assessment of time-varying structures under uncertainty. Discrete tracking of the modal parameters and the strain energy damage index (SEDI) method is employed to perform damage localization and assessment. Assessment of spontaneous damage in deteriorating structures is important as it can have potential benefits in improving their safety and performance. Most of the available damage assessment techniques incorporate the usage of system identification and classification techniques for detecting damage, location and/or severity; however, much needed work is needed in the area of dimensional reduction in order to compress the ever-increasing data and facilitate decision-making in damage assessment classification. Comparison of dimensional reduction and classification techniques is presented and evaluated in terms of separating damaged from undamaged data sets under two types of uncertainty, structural deterioration and environmental uncertainties, via finite element model simulations. The use of recursive principal component analysis for detecting and tracking structural deterioration and spontaneous damage is evaluated via computational simulations. The results of this study reveals that dimensional reduction techniques can greatly enhance structural damage classification under uncertainties.

5.1 Introduction

In the past two decades, significant effort has been made towards the development of smart damage diagnosis and prognosis systems in order to increase safety and performance of dynamic structures as well as minimizing their maintenance cost [37]. Spontaneous damage events on

flight vehicles represent a threat to for example wing structure. Sources of discrete damage include hail impact, lightning strike, transport and handling, and foreign objects. In addition, aircraft are exposed to severe operating environments during flight. The high number of flight-cycles causes permanent deteriorating damage, i.e. aging [101]. Therefore, it is necessary to take deterioration into account when performing structural damage assessment of in-flight vehicles. Most methods focus on looking for damage using one set of data from the undamaged and damaged states. Treating the problem in this fashion ignores the real-time and long-duration of continuous monitoring a structure so that gradual degradation and damage from severe events, such as impacts, can be detected.

In real-world applications of structural health monitoring (SHM) systems, uncertainty may take the form of component and/or system variability, environmental and operational conditions, data acquisition errors, and data interrogation errors, to name a few. In order to account for the uncertainties involved in damage assessment approaches, pattern recognition techniques have been studied to statistically distinguish structural conditions [101,157]. Numerous SHM works are available on the use of statistical analysis to categorize damage in structures, such as statistical process control, defining confidence intervals for damage indices, and statistical pattern analysis. In most pattern recognition approaches the raw data is pre-processed to extract damage discriminant features, for example using principal component analysis (PCA) [59,80,94,95,156,182,183].

Given large sets of data with multiple features, there exists significant amount of redundancy or unnecessary features which reduces the effectiveness, accuracy and understandability of the data mining results. As such, data compression and dimensional reduction techniques may be utilized to reduce the size of datasets. One must understand that uncertainties will arise from the way data is truncated and compressed during the removal of unnecessary data features, feature

extraction, feature selection and noise cleansing. Uncertainties are inevitable, but they can and should be systematically addressed and accounted for. In general, data mining must performed in order to facilitate the decision-making process of classification. The performance of the classifier depends on the interrelationship between data sets, number of features, and classifier complexity. Increasing number of data and dimensions results in what is known as "curse of dimensionality," which leads to the "peaking phenomenon" in classifier design. In other words, more data does not necessarily mean more information due to the dependency and correlation of many multidimensional dataset. Jain et al. [75] states that increasing number of features may in fact degrade the performance of a classifier if the number of training samples that are used to design the classifier is small relative to the number of features.

This section presents a classification study of features extracted via dimensional reduction techniques for spontaneous damage diagnosis that yields reliable results under multiple uncertainties, including the aging effects under nominal operating conditions. The dimensional reduction techniques of principal component analysis (PCA), local linear embedding (LLE), local tangent space analysis (LTSA), kernel PCA (KPCA), and diffusion mappings (DM) will be utilized in this simulation work. The latter dimensional reduction methods have already been described in Chapter 4. In contrast to the analysis presented in Chapter 4, the damage assessment results presented in this chapter will include quantitative damage detection and localization based on the machine learning process known as classification. Due to the uncertainties involved in obtaining robust and reliable damage estimates, modal analysis and pattern recognition techniques will be used to properly categorize spontaneous damage events in deteriorating structures.

5.2 Dimensionality Reduction

The problem of dimensionality reduction in SHM appears when the system response data are in fact of a higher dimension than tolerated or desired. Structural damage assessment is based on identifying and extracting damage feature indicators that are robust to system uncertainties, such as high signal-to-noise (SNR) ratios, system and operational variability. Furthermore, it is desired that such extracted features are of minimal size to aid classification and reduce computational complexity. Therefore, in general, it can be useful or even necessary to first reduce the dimensionality of the data to a manageable size, and then feed the reduced-dimension data to the damage classification system.

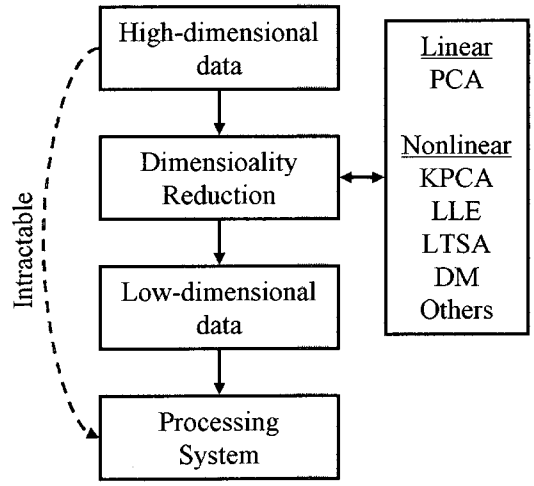

Figure 5.1. Dimensionality reduction.

Dimensional reduction is important in damage assessment since it facilitates classification, visualization, and compression of high dimensional data. The process of dimensional reduction is depicted as a flow chart in Figure 5.1. The application of dimensional reduction techniques in feature extraction has already been introduced and reviewed in section 4.2 with information regarding each particular method shown in Figure 5.1. In this section, an extension of

dimensional reduction methods, in particular the PCA approach, to noise reduction is presented. Because we are interested in the integration of these techniques with a continuous structural monitoring system, we present a recursive dimensional reduction approach for adaptive structural health monitoring.

5.2.1 Noise Reduction

As described in section 4.2, PCA transforms the original $\mathbf{X}$ dataset of size $D \times n$ to a reduced data matrix $\mathbf{Y}$ of size $d \times n$, which is a linear transformation defined by $\mathbf{Y} = \mathbf{HX}$, where H is a $d \times D$ linear transformation matrix whose rows are the eigenvectors, i.e. principal components, of $\mathbf{X}$. Matrix $\mathbf{H}$ is a linear mapping formed by the first d principal eigenvectors of the sample covariance matrix by solving the following eigenproblem

$$\mathrm{cov}(\mathbf{X})\mathbf{H} = \lambda\mathbf{H} \tag{47}$$

Alternatively, the covariance matrix eigenvectors can be calculated via singular value decomposition (SVD) of the covariance matrix of the features as follows

$$\mathbf{X}\mathbf{X}^T = \mathbf{U}\boldsymbol{\Sigma}^2\mathbf{U}^T \tag{48}$$

where $\mathbf{U}$ is an orthonormal matrix, $\boldsymbol{\Sigma} = diag(\lambda_1, \lambda_2, ..., \lambda_D)$ is a diagonal matrix whose elements are the singular values. By definition, the singular values are written in decreasing order $\lambda_1 > \lambda_2 > ... > \lambda_D$. Generally, the first $k < d$ principal components contain the largest variances, and one can conclude that the most data information occurs only in the first k dimensions.

The data compression capability of PCA can be extended to noise suppression. The basic idea is that the variance captured by the least important principal components is noise which should be rejected. To original data $\mathbf{X}$ can be reconstructed with reduced noise as follows

$$\hat{\mathbf{X}} = \mathbf{X}\left(\mathbf{H}\mathbf{H}^T\right) \tag{49}$$

The degree of noise reduction is controlled by the number of principal components retained.

The main drawback to PCA is the computation of the covariance matrix, which becomes quite demanding with increasing number of features. PCA is a linear technique since it embeds the data into a linear subspace. The objective of PCA is to find a linear transform for each class using the training patterns for that class in the feature space.

5.2.2 Recursive Dimensional Reduction Approach

Major limitation of static-dimensionality reduction is that it is time-invariant, while most engineering structures contain time-varying characteristics due to aging, maintenance, and sensor drifting. The time-varying characteristics of structural properties include: (i) changes in the mean; (ii) changes in the variance; and (iii) changes in the correlation among system variables.

When a time-invariant PCA model is used to monitor impact damage events, false alarms and misses would often result due to the accumulation go structural deterioration. In this paper we present the use of recursive PCA (RPCA) to model the non-stationary statistics of our structural model. Given a random process

$$\mathbf{x}_n \in \Re^{1xD} \tag{50}$$

its recursive mean can be estimated by

$$\hat{\mathbf{m}}_n = \alpha\hat{\mathbf{m}}_{n-1} + (1-\alpha)\mathbf{x}_n \tag{51}$$

where α is an adaptive (forgetting) factor, which puts more weight on recent samples than on older samples. The forgetting factor is a tuning parameter that be varied according to how fast the observed process is changing. The covariance matrix can be estimated as

$$\hat{\mathbf{C}}_n = \alpha\hat{\mathbf{C}}_{n-1} + (1-\alpha)(\mathbf{x}_n - \hat{\mathbf{m}}_n)(\mathbf{x}_n - \hat{\mathbf{m}}_n)^T \tag{52}$$

Given $\widehat{\mathbf{C}}_n$, we can perform PCA and obtain corresponding eigenvectors, where we keep N largest eigenvalues. To ease the computational burden of recursive eigen-decomposition, the following algorithm based on the inner-product matrix [93] has been adopted. Given an initialized set of eigenvectors, $\varphi_{n-1}^{(i)}$, and eigenvalues, $\lambda_{n-1}^{(i)}$, we can write the covariance matrix as

$$\widehat{\mathbf{C}}_n \approx \mathbf{B}_n \mathbf{B}_n^T \tag{53}$$

where $\mathbf{B}_n$ is

$$\mathbf{B}_n = \begin{bmatrix} \sqrt{\alpha\lambda_{n-1}^{(1)}\varphi_{n-1}^{(1)}} \\ \sqrt{\alpha\lambda_{n-1}^{(2)}\varphi_{n-1}^{(2)}} \\ \vdots \\ \sqrt{\alpha\lambda_{n-1}^{(N)}\varphi_{n-1}^{(N)}} \\ \sqrt{1-\alpha}\left(\mathbf{x}_n - \widehat{\mathbf{m}}_n\right) \end{bmatrix} \tag{54}$$

Based on the $\mathbf{B}_n$ matrix, the inner product-matrix can be formulated to obtain

$$\mathbf{A}_n = \mathbf{B}_n^T \mathbf{B}_n \tag{55}$$

and obtain its eigenvectors, $\psi_n^{(i)}$ and eigenvalues $\lambda_n^{(i)}$. As in regular PCA, the eigenvalues are sorted and corresponding N eigenvectors are kept. The eigenvectors of covariance matrix are then obtained as

$$\varphi_n^{(i)} = \lambda_n^{(i)-1/2} \mathbf{B}_n \psi_n^{(i)} \tag{56}$$

The proposed RPCA approach is useful in that it adapts to a time-varying monitored structure. Given this recursive approach, the PCA dimensional reduction technique can be used in time-varying structures in order to perform damage detection by tracking extracted features over time and finding outliers. Once outliers have been detected during the monitoring process, further analysis, such as system identification via modal analysis, can be performed to localize and assess

the source of the outlier or damage. The performance of RPCA is evaluated in the results section using a time-varying simulation.

5.3 Classification (Pattern Recognition) of Extracted Features

In this section, we formalize the process of conducting damage classification based on pattern recognition. In the previous chapter, classification of damage detection was performed visually. Once the extracted parameter that was used to detect if damage is present or not falls outside statistical variance control lines, then we can indicate that damage could be present. This simple classification approach relies on a single feature and human input for classification. In more complex classification problems, there are multiple features are used to classify a dataset or object, which can become problematic for a human when the number of features are numerous. For such situations when clear and quantitative results are necessary, the human input can be replaced by classification algorithms based on statistical pattern recognition.

The goal of classification algorithms is to assign a class label to a new object or observation from a set of predefined classes, such as color class - red, blue or green. The classifier which should perform this operation is based on a set of example objects. This type of classification is known as supervised classification with all known class labels known. In our work, we will not focus on this classification problem, but instead we will focus on what is known as the one-class classification. In damage detection, the class label of normal operation or response is the known class. When damage occurs, the particular label or type of the damage can be difficult to identify since the particular signature of each damage type can vary significantly. For example, the structural response due to cracks, changing boundary conditions, loose components, etc, are not exactly the same. In damage detection classification, the goal is to simply find a clear

discriminant boundary between healthy structural response and unhealthy, regardless of what is causing the unhealthy response.

In one-class classification, it is assumed that only information of one of the classes, the target or healthy class, is available. Only training data on healthy structural response can be used for classification and that no other information about the other class of outlier objects is present or available. The task is then to define a boundary around the target class, such that it accepts as much of the target objects as possible, in other words minimize false-positive, and minimize the chance of accepting outlier objects, in other words minimize false-negative.

A major issue in damage classification is that many classification algorithms assume that for training, class labels, i.e. information on each class, are available, but in practical damage assessment applications, labels of damaged data is not available unless destructive testing is performed. As a result, direct application of supervised classification approaches is not always possible.

Table 5.1. Confusion matrix.

	Predicted	
	H_U	H_D
Undamaged (U)	True Negative (TN)	False Positive (FP)
Damaged (D)	False Negative (FN)	True Positive (TP)

Consider the binary hypothesis testing problem where a sequence of independent identically distributed (*iid*) damage index vectors, $\mathbf{x}_k$, are observed, then the likelihood ratio test (LRT) function is denoted as

$$\prod_{k=1}^{m} L(\mathbf{x}_k) \underset{H_U}{\overset{H_D}{\gtrless}} \tau(m) \tag{57}$$

where H_D denotes the damage state, H_U the undamaged state, and $\tau(m)$ is a predefined (if prior information exists) damage threshold.

For all classifiers, two types of errors have be minimized, mainly the false-positives and the false-negatives. Table 5.1 shows the possible classifications for a one-class classification problem. In most applications, the minimization of false-diagnosis will not reach 0. Therefore, an acceptable error threshold must be selected to reject outliers. By varying this threshold, and measuring the error on the outlier objects, a receiver operating characteristic (ROC) curve can be obtained, see Figure 5.2. This curve shows how the fraction of false-positives varies with true-positive. For one-class classifiers, the goal is to obtain perfect true-positive, y-axis value of 1 in ROC curve, and zero false-positive, x-axis value of 0 in ROC curve. As mentioned earlier, this operating point is not always possible, and classifier designer must choose an acceptable ration between accepted outliers and accepter targets, see Figure 5.2.

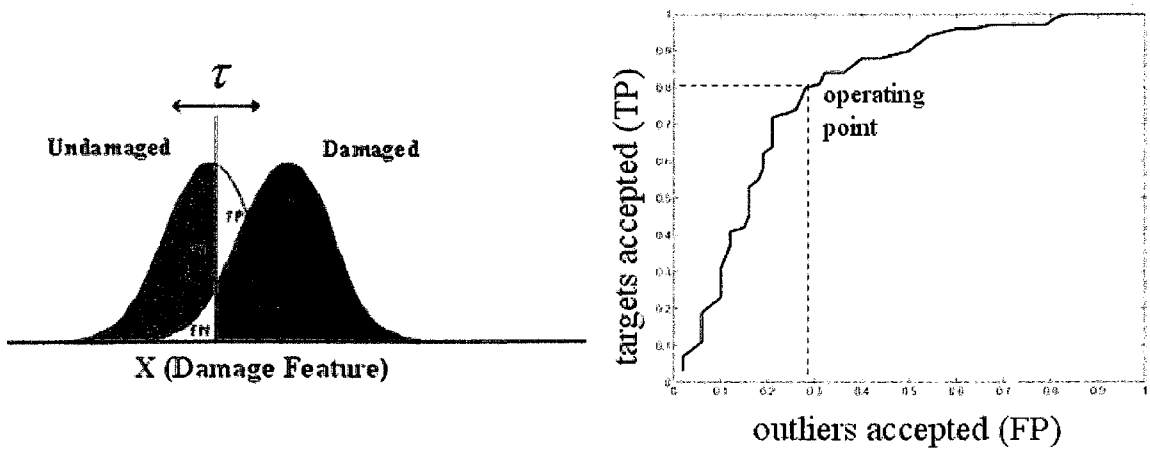

Figure 5.2. Example of binary classification with ROC curve.

Performance of classification schemes is governed by the amount of information about the classes involved, i.e. damaged and undamaged. In this work, m samples for each signal feature

were taken. To train the classifier, $m/2$ samples were used to train unsupervised classifier parameters, and the rest of the data were used for classification test and evaluation. The performances measures for binary classification are shown in Table 5.1, and they are defined as follows:

$$\text{Damage Detection Rate (DDR)} = \frac{TP}{FN+TP} \tag{58}$$

$$\text{False Alarm Rate (FAR)} = \frac{FP}{TN+FP} \tag{59}$$

$$\text{Overall Accuracy (OA)} = \frac{TP+TN}{TP+TN+FP+FN} \tag{60}$$

$$\text{Overall Miss (OM)} = \frac{FP+FN}{TP+TN+FP+FN} \tag{61}$$

5.3.1 Individual Classifiers

In this work, the following classifiers on the damaged class are evaluated: (1) k-Nearest Neighbor (kNN), (2) Parzen density, (3) Expectation-Maximization (EM), and (4) k-Mean, (5) combined mean of (1)-(4), and (6) combined product (1)-(4) classifiers. For classifiers not estimating a density, its output is mapped to a probability before used in the combined classifiers. All of the methods analyzed in this work are well known in traditional pattern recognition, so they will only be discussed briefly. Of the multiple classification approaches, we have chosen to use the selected subset of methods because they cover a broad range of possible methods. For further information on classifiers please refer to [69,87].

The most straightforward method to obtain a one-class classifier is to estimate the variance or density of the training data. When a probability model is assumed and the training data is sufficient, this approach is very advantageous and reliable. The most common distribution used is the Gaussian distribution, as shown in Figure 5.3. The method is very simple and it imposes a

strict unimodal and convex distribution model on the data. The rejection region or outlier class area is typically determined according to a variance value, such as $n\sigma$, where σ is the standard deviation value.

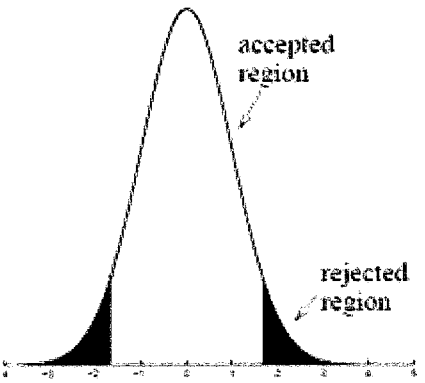

Figure 5.3. One-dimensional Gaussian distribution classification.

Because in most cases, we cannot assumed normally distributed data, the Gaussian distribution one-class classification approach is not always reliable.

The Parzen density estimation method (Parzen, 1962) estimates the density of a mixture of Gaussians kernels centered on the individual training objects, with diagonal covariance matrices Σ_i

$$p(x)=\frac{1}{N}\sum_i p_N(x;x_i,\Sigma_i) \tag{62}$$

where N is the number of samples, $p(x)$ is the estimated probability density of classified variable x. The Parzen density estimation approach is a refinement of the histogram approach which partitions the training data, i.e. known healthy condition data, into sub-regions, and counts the number of samples that fall in each of these partitions or bins. The estimated probability density within a bin is proportional to that count. This technique works fine if the number of

samples within each bin is sufficiently large. Hence, with a small training set, or a large dimension of the measurement space, the resolution of the estimation will be very poor.

In Parzen estimation, each sample in the training set contributes in a like manner to the estimate. The estimation process is space-invariant. Therefore, a there is always a trade-off between resolution and variance. The k-Nearest Neighbor (kNN) classifier (Duda and Hart, 1973) is an estimator with high resolution in regions where the training set is dense, and with low resolution in other regions. The kNN classifier is based on a majority vote by using the distance to its neighbors, with the object or sample being assigned a class most common amongst its k nearest neighbors. Let $R(x)$ be a hypersphere (region around x) with volume $V(x)$ and centered at x. Suppose that the radius of the sphere around x is selected such that it contains exactly k samples. The estimate of the density is given by

$$p(x) = \frac{k}{N_k V(x)} \tag{63}$$

where N_k is the number of samples in the training set taken from a total number of samples N_s. Combination with a uniform cost function produces the following suboptimal classification

$$L_{\max} = \underset{i=1,\ldots,L}{\operatorname{argmax}} \left\{ \frac{k_i}{N_i V(x)} \frac{N_i}{N_s} \right\} \tag{64}$$

where $L_{\max}$ is the chosen class. The class assigned to a sample x is the class with the maximum number of votes coming from k samples nearest to x.

The last method used for classification is a clustering method known as c-means (Bishop, 1995). This clustering technique basically determines the distances between objects. C-means clustering assigns each object randomly to one of the available clusters. Next, the mean of each cluster is computed as follows

$$\mu_c = \frac{1}{N_c} \sum_{x_i \in L_c} x_i \tag{65}$$

where L_c is the c^{th} cluster. Given the new means of each cluster, each object x_i is reassigned to the cluster with the closest mean μ_c. This process is repeated until the means of the clusters do not change anymore.

The c-means method is dependent on the distance measure between the objects x_i and cluster's mean μ_c. The main advantage of k-means is that it is very easy to implement. On the other hand, it is an unstable approach. Depending on the random initialization, the algorithm will converge to different local minima. This problem generally occurs more when high number of clusters are requested. In our particular application of binary classification, there are only two clusters - damaged and undamaged.

The last classification method used in our analysis is known as the expectation-maximization (EM) algorithm. The EM classifier is a based on finding the maximum likelihood estimates of parameters in statistical models, where the model depends on unobserved (latent) variables. The EM method contains two iterative steps. The expectation step computes the expectation of the log-likelihood evaluated using the current estimate for the latent variables, and the maximization step computes parameters maximizing the expected log-likelihood on the expectation step.

The log-likelihood is defined as

$$L(\theta) = \ln p(x|\theta) = \ln \sum_z p(x|z,\theta) p(z|\theta) \tag{66}$$

where θ is the parameter vector, z represents the hidden variables, and x is the observed data. The objective is to choose θ such that $p(x|\theta)$ is a maximum, which is known as the Maximum

Likelihood Estimate (MLE). The EM is an iterative procedure for maximizing $L(\theta)$, so after the n^{th} iteration, the current estimate for θ is given by θ_n. The update value is given by

$$\theta_{n+1} = \arg\max_{\theta} \left\{ E_{z|x,\theta_n} \left\{ \ln p(x, z|\theta) \right\} \right\} \tag{67}$$

The EM algorithm thus consists of the following iterations:

1. *E-Step*: Determine the conditional expectation $E_{z|x,\theta_n} \left\{ \ln p(x, z|\theta) \right\}$.

2. *M-Step*: Maximize this expression with respect to θ.

5.3.2 Combined Classifiers

A drawback to single classifiers is that hardly do they ever fit the data distribution optimally. In addition, using the best classifier and discarding the rest of the lower performing classifiers might waste valuable information. To improve classification performance, multiple researchers [36,58, 75,87] have shown that individual classifiers may be combined, which may also increase robustness and generalization.

The possible ways of combining the outputs of multiple classifiers or information sources in data fusion depends on what type of information is extracted from the individual classifiers. Jain [75] provides a review of classifier combination schemes and their selection process. Some of the well know classifier combinations are product rule, sum rule, majority vote, Naive Bayes combination, Singular Value Decomposition (SVD), neural networks, adaptive weighting, bagging and boosting. Commonly a combined decision is obtained by just averaging the estimated posterior probabilities (output distribution) of different classifiers, which has been shown to give very good results. When the Bayes theorem is adopted for the combination of

different classifiers, under the assumption of independence, also known as naive-Bayes, a product combination rule automatically is obtained.

In this work, the product rule is adopted to combine the individual classifiers. To suppress the errors unique to each classifier K_i, the outputs of each technique may be combined using the product combination rule

$$\prod_{i=1}^{N_\mathrm{K}} \mathrm{K}_i = p\left(L_1, L_2, ..., L_{N_\mathrm{K}} \middle| c_i\right) = \prod_{i=1}^{N_\mathrm{K}} p\left(L_i \middle| c_i\right) \tag{68}$$

where N_K is the number of individual classifiers being combined, L_i is the class-label produced by classifier, and c_i is the true class.

The product combination rule is apt for different, class-conditional independent feature spaces where classifiers make small estimation errors. The Bayes product rule classifier has been found surprisingly accurate and efficient in many experimental studies. The surprise comes from the fact that the objects being combined are seldom independent, which violates the independence assumption. However, it turns out that the classifier performance is quite robust, even in the case of dependence.

5.4 Damage Assessment Based on Strain Energy Damage Index (SEDI)

Vibration-based methods are based on the fact that damage alters the dynamic properties of structures, such as natural frequencies, damping, mode shapes, and operational deflections shapes (ODS). Measurement and tracking of such modal properties can provide information regarding structural health condition.

Damage detection based on vibration extracted features can be performed using varying technique. In this study, we focus on using the frequency response and mode shapes as the

features used in the dimensional reduction analysis. First set of features is based purely on the frequency response vector $\mathbf{f} = [f_1, f_2, ..., f_n]$ with a frequency span of f_n Hz, dimension $n \times NE$ (NE is total number of elements) and a sampling frequency of $(f_i - f_{i-1})$ Hz. Complete usage of the whole frequency response vector as the input to each dimensional reduction method is made under the assumption of complete ignorance of system informative modal features, such as resonant frequencies. The presence of damage in a structure would be indicated by changes in the frequency response.

The second set of features is based on extracted structural mode shapes. Compared to frequency-based damage detection, extraction of structural mode shapes requires knowledge of resonant frequencies and is a system identification method. Mode shape extraction process is in itself a dimensional reduction process. The advantage of using mode shapes for damage detection is that features with greatest system information are pre-selected. On the other hand, damage detection based on mode shapes runs the risk of valuable information being lost due to the data reduction and system identification process. In contrast, direct application of the frequency response for damage detection avoids initial risk of lost information since all acquired frequencies are used in the damage detection process. Comparison of these two feature sets based on damage detection performance is conducted in this study.

Damage detection and localization of continuous structures based on the strain energy damage index (SEDI) method developed by Stubbs and improved by Kim et al. [84] utilized the modal strain energy distribution in a structure due to damage. In this work, the damage index method is utilized for the analysis of mode shapes. This method requires that mode shapes before and after damage are known, and only a few modes are required; thus applying a reduced-order model approach.

For beam elements, N_{nm} measured modes and N_e number of elements, the damage index, β_j, is written as

$$\beta_j = \frac{E_j}{E_j^*} = \frac{\sum_{i=1}^{N_{nm}} \left(\gamma_{ij}^* U_i + \sum_{k=1}^{N_e} \gamma_{ik}^* U_i \right)}{\sum_{i=1}^{N_{nm}} \left(\gamma_{ij} U_i^* + \sum_{k=1}^{N_e} \gamma_{ik} U_i^* \right)} \tag{69}$$

where E_j represents the Young's modulus, "*" indicates the damaged structure, U_i is the i^{th} modal strain energy, and $\gamma_{ij} = \mathbf{\Phi}_i \mathbf{C}_{j0} \mathbf{\Phi}_i$ where $\mathbf{\Phi}_i$ is the i^{th} mode shape and $\mathbf{C}_{j0}$ is a matrix involving only geometric properties obtained from $\mathbf{K}_j = E_j \mathbf{C}_{j0}$, which is the j^{th} contribution to the system stiffness matrix.

If the structure being considered is an linear elastic beam of length L and with the assumption of negligible shear strain, then it can be shown that the modal strain energy representation of Eq. (69) becomes

$$\beta_j = \frac{E_j}{E_j^*} = \frac{\sum_{i=1}^{N_{nm}} \left(\int_{x_j}^{x_j + \Delta x_j} \left(\Phi_{i(x)}^{*"} \right)^2 dx + \int_0^L \left(\Phi_{i(x)}^{*"} \right)^2 dx \right) / \int_0^L \left(\Phi_{i(x)}^{*"} \right)^2 dx}{\sum_{i=1}^{N_{nm}} \left(\int_{x_j}^{x_j + \Delta x_j} \left(\Phi_{i(x)}^{"} \right)^2 dx + \int_0^L \left(\Phi_{i(x)}^{"} \right)^2 dx \right) / \int_0^L \left(\Phi_{i(x)}^{"} \right)^2 dx} \tag{70}$$

Once damage is located at the j^{th} member, damage severity of the j^{th} element is estimated using the following equation

$$\alpha_j = 1/\beta_j - 1 \tag{71}$$

where damage severity is indicated as the reduction in the j^{th} member if $\alpha_j < 0$.

Based on this damage index, information is obtained on the location and severity of the damage from changes in the mode shapes of the structure under analysis. As a correlation function, an α_j

value close to 0 indicates full correlation between damaged and undamaged j^{th} structural member, and a value close to -1 indicates no correlation.

5.5 Case Study: Cantilever Beam Simulation

Structural damage is represented by reduction in the elemental stiffness. Uncertainty is inherent between modeling predictions and test results. Uncertainties are modeled as random measurement noise, time-varying structural parameters, and environmental, i.e. temperature, variations. The motivation of this investigation stems from the impact damage potential of in-flight vehicles in civilian and military applications. The relative large wing span and high aspect ratio of many in-flight vehicles, such as Unmanned Air-Vehicles (UAVs), makes wings highly susceptible to impact damages. To demonstrate the proposed damage assessment approach, the wing is modeled as an isotropic aluminum cantilever beam with an aspect ratio of 9.84 and constant rectangular cross-section, as shown in Figure 5.4. The structural system consists of 50 elements, and only vertical motion is measured at each nodal point. Frequency responses are generated using the software packages MSC.NASTRAN with a frequency span of 3 kHz and a sampling frequency of 1 Hz. To simulate unavoidable data acquisition noise, a bandwidth limited white noise signal will be added to all measuring points. For the parameters shown in Figure 5.4, values for the geometric properties of the scaled wing model were assigned as follows: $L = 0.5\text{m}$, $h_0 = 3.2\text{x}10^{-3}\text{m}$, and $c_0 = 2.032\text{x}10^{-1}\text{m}$.

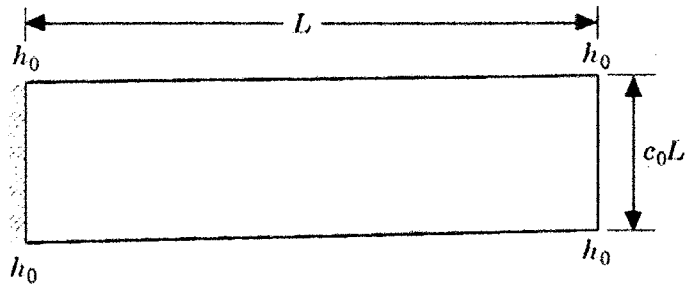

Figure 5.4. Schematic of cantilever beam model.

The damage diagnosis will be evaluated in two stages. Via numerical simulation, the pre- and post-damage transient and modal responses of the test structure are measured. The first 10 mode shapes (feature set 1) and natural frequencies (feature set 2) are considered as the vibration features. To account for the presence of random effects, noise is added. Table 5.2 shows the damage scenarios studied in this work. To train the unsupervised classifiers on the natural variation due to noise content of the undamaged features, 100 samples were taken using undamaged structure with noise content. To test the classifiers, 100 samples of damage feature vectors were generated. The reduced stiffness damage scenario is representative of impact damage without penetration and/or loss of structural mass. The change is stiffness due to damage will be modeled by a reduction in the modulus of elasticity of the section. The degree of damage is then related to the extent of reduction in the modulus of elasticity. This method requires only a simple modification in the finite element model. A study will be conducted with 5% to 20% reduction of the modulus of elasticity, imposed in turn on discrete number of elements for the analytical model. Finally, to study the effects of structural deterioration, the modulus of elasticity is modeled as a non-increasing function of time. The deterioration rate is assumed to be much slower than the impact damage period.

For the second stage of damage estimation, the strain energy damage index (SEDI) method will be applied when signal noise is present. Because the damage index feature is sensitive to changes in mode shapes, which allows it to estimate damage, it is also highly susceptible to noise content. Kim and Stubbs [84] utilized a Z-test criteria to eliminate relatively small false-positives due to noise content. The Z values are obtained by calculating $Z_j = (\beta_j - \bar{\beta}_i)/\sigma_i$ where $\bar{\beta}_i$ and σ_i are the mean and standard deviation of the collection of damage indicators β_j values, respectively. The decision criteria is given as follows: if $Z_j < 2$ then $\beta_j = 0$, else if $Z_j \geq 2$ then $\beta_j = \beta_j$. The main drawback with this simple statistical criteria to eliminate false-positives is that it assumes that damage severity values of true-positive damage locations will always be significantly bigger (in magnitude), which is not always the case due to noise content. In our approach, prior to performing the statistical Z-test criteria, we make the assumption that a small number N_{DI} of damage index vectors can be obtained following the spontaneous damage event. For each damage index extraction, the modal data was randomized separately; thus achieving varying noise content. By doing so, dimensional reduction can be applied as a noise reduction technique at each element value α_j of the damage index method. The assumption of having the capability to calculate multiple damage index vectors is required to increase the classification robustness based on higher number of observations.

Table 5.2. Damage scenarios investigated.

Case	Damaged Element (s) Location	Corresponding Severity (%)	Noise (%)
1	-	-	1, 2, 2.5, 3.5
2	4	-10	1, 2, 2.5, 3.5
3	9, 34	-10, -5	1, 2, 2.5, 3.5
4	25	-10	1, 2, 2.5, 3.5
5	4, 14, 19, 39	-20, -10, -5, -20	1, 2, 2.5, 3.5

To study the effects of structural deterioration and temperature effects, the modulus of elasticity is modeled as temperature-dependent with a constant rate of deterioration. To simulate varying temperature conditions, temperature changes are assumed to be a random variable uniformly distributed between -21 to 50 °C. In addition, a deterioration rate of 1% over the span of the simulation is applied to simulate the slow deterioration experienced by structures. Given this setup, RPCA is then applied to the first 10 natural frequencies of the cantilever beam model. For this simulation, damage is induced after 700 data vectors. For the second stage, having detected the presence of damage, the damage index vector is utilized to evaluate the location and magnitude of damage. As in the first stage, to train the unsupervised classifiers on the natural variation of the measured features prior to damage, 100 samples will be evaluated.

In the numerical examples, noise is simulated by adding pseudorandom numbers on the simulated frequencies and mode shapes. To simulate unavoidable data acquisition noise, a bandwidth limited white noise signal will be added to all measuring points. The amplitude of this noise is denoted as the noise-to-signal ratio, $NSR = 1/SNR$, which is a ratio of the induced random noise series to the amplitude of the mode shapes or frequencies.

5.6 Results and Discussion

5.6.1 Damage Detection

The variation of the principal component (D1), extracted feature for which the data varies the most, for each dimensional reduction technique is illustrated in Figure 5.5 and Figure 5.6 for the natural frequencies and mode shapes, respectively, using only 70-undamaged and 30-damaged samples. The principle direction data was normalized by removing the mean of the reference

undamaged data set. Finally, upper and lower control limits (dashed lines) corresponding to one standard deviation, which provides a quick look at data outliers, were also plotted.

Figure 5.5 shows how the principal direction of each dimension reduction technique is affected when damage corresponding to Case 2 of Table 5.2 is introduced after 70 samples. Comparison of the separation between undamaged and damaged samples created by each dimensional reduction technique does not render clear superior mapping technique. By using the natural frequencies as damage indicators, the damage classification would yield significant number of false-diagnosis due to the uncertainty in the reported results. Figure 5.6 shows the results obtained using the mode shape features as damage indicators. The principal feature obtained from each dimensional reduction technique remains outside the upper and lower control limits of normal operation with given noise levels.

Table 5.3 provides the false-negative count of the damaged data samples that fall within the one standard deviation control limits for each dimensional reduction method and vibration feature set, in other words the mode shape and frequency response features. Visual classification based on the standard deviation control limits of the damage detection results demonstrate that the results obtained from the mode shape data outperforms those obtained from the frequency response data. With exception of the LLE dimensional reduction method, which resulted in one false-negative method, at the 2% noise level, the mode shape based dimensional reduction results in zero false negatives For the given simulation, comparison of the results obtained in Figure 5.5 and Figure 5.6 shows that extracted feature obtained from mode shapes is a better damage indicator in comparison to the extracted feature obtained from natural frequencies.

The advantage of mode shapes over natural frequencies can be explained as a result of the extra feature extraction step taken in order to obtain mode shapes from frequency response data. By

extracting mode shapes via a system identification process, prior to performing dimensional reduction, intelligent data compression is performed based on prior knowledge of structural properties and aids in the physically interpretation in terms of established mathematical modeling of vibrating characteristics. Direct application of dimensional reduction techniques to minimally transformed data, such as frequency response, attempts at extracting the most informative features via raw computational power. The intelligent pre-selection of known informative features, such as natural frequencies, is found to be the main advantage of using mode shape based method over the frequency response based method. In addition, assignment of equal signal-to-noise levels for the mode shape and frequency set data has major effect on the results. In practice, noise content levels found in the frequency response function can be magnified when extracting the structural mode shapes due to the additional data manipulation and transformation steps. It is recognized that simulations cannot reproduce all of the critical steps and challenges involved in the application of vibration-based damage detection. In practice, frequency response and experimental modal analysis faces numerous challenges, particularly regarding signal processing and compounding errors during system identification process.

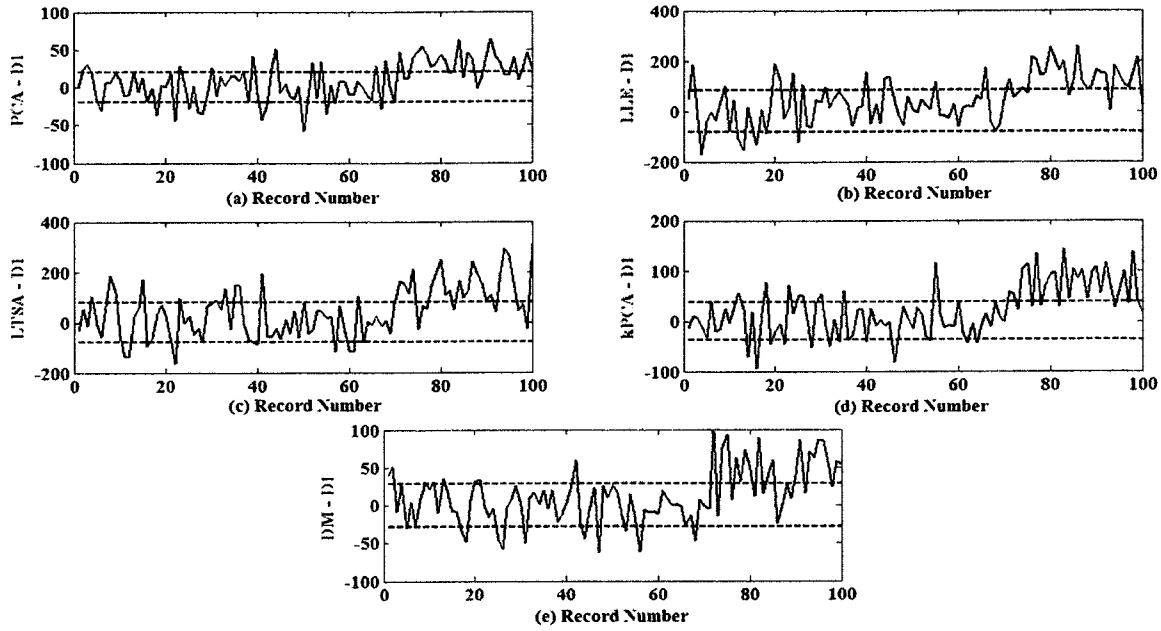

Figure 5.5. Principal component of natural frequency feature set for each dimensional reduction method with 2% noise.

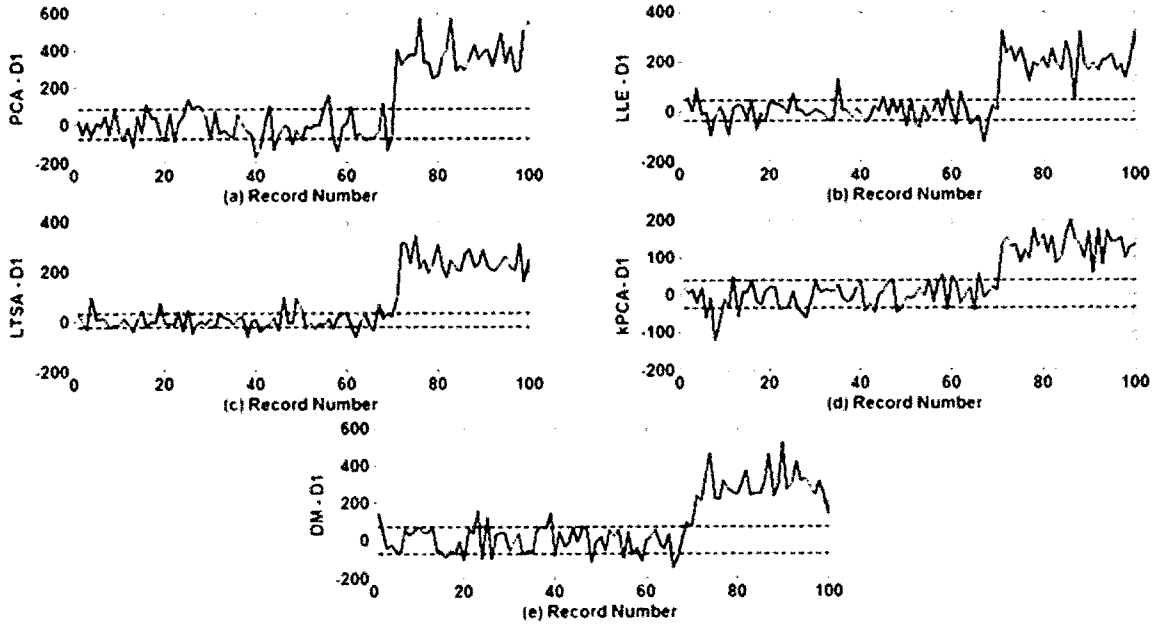

Figure 5.6. Principal component of mode shape feature set for each dimensional reduction method with 2% noise.

Table 5.3. False-negative count in damage detection.

	Mode Shape Data	Frequency Response Data
PCA	0	9
LLE	1	7
LTSA	0	8
kPCA	0	7
DM	0	11

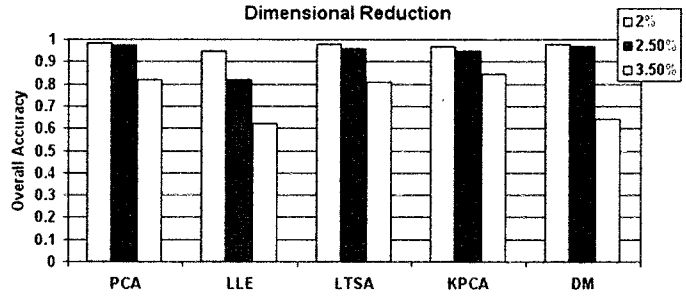

Figure 5.7. Comparison of dimensional reduction overall accuracy results under varying noise levels.

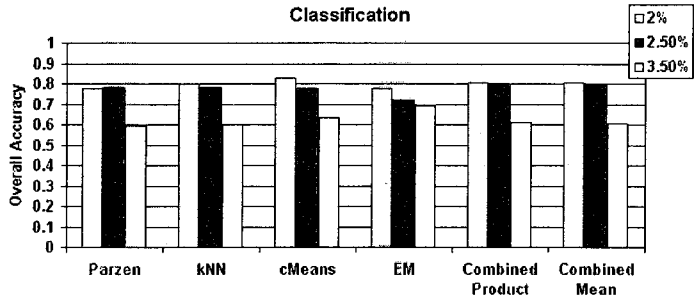

Figure 5.8. Comparison of classification overall accuracy results under varying noise levels.

Figure 5.7 and Figure 5.8 provide the dimensional reduction and classification performance comparison, respectively, in terms of overall accuracy (OA), for damage Case 2 for the mode shapes feature set at 2, 2.5 and 3.5% noise levels. For each test case, 100-damaged and 100-undamaged samples were used. Individual dimensionality reduction results shown in Figure 5.7 were obtained by averaging all classification results for the corresponding dimensional reduction technique. In similar fashion, the individual classification results shown in Figure 5.8 were obtained by averaging the dimensional reduction results.

Overall, LTSA and PCA provided the highest OA for the dimensional reduction methods, and EM provided the highest OA for the classifiers. From the dimensionality reduction and classification results, we conclude that PCA was not outperformed in most cases by the nonlinear and more complex dimensional reduction techniques, LLE, LTSA, KPSA and DM. Second, class separation was consistently applied when using PCA. In contrast, LLE and DM methods failed in some cases for Case 2 dataset at 3.5% noise level, see [97] for non-averaged individual results. For this reason, LLE and DM have the poorest OA values at 3.5% as shown in Figure 5.7. These failures might be a result of the inability of the eigensolver to identify the smallest eigenvalues. Also, nonlinear methods require the selection of proper kernel function and k-neighbors, which might improve class separation results, but at the cost of computational costs. Third, no clear performance superiority was observed on any of the classifiers, including the combined product-rule classifiers as shown in Figure 5.8. Results demonstrate that classifier performance is highly dependent on the performance of the dimensionality reduction method in maximizing between-class variance. Fourth, in none of the test cases the combined classifiers achieved clear improvement over the individual performances of the individual classifiers, and the product and mean classifiers provided very similar results. From this observation, we may infer that combined classifiers are as good as its best individual classifier.

The deterioration study was performed on Case 4 of Table 5.2 at 1% noise. Figure 5.9(a) shows the effect of deterioration has on the principal eigenvalue obtained from applying RPCA to 1000 sample vectors of the model frequencies with damage induced after 700 samples. Using RPCA, the eigenspace of the model is updated to account for the time-varying characteristics caused by the deterioration rate induced on the modulus of elasticity. The forgetting factor of the RPCA was set at 0.9 to accommodate the slow deterioration rate. From Figure 5.9(a) and Figure 5.9(b), we can see that the impact damage event, starting with record number 700, can be separated from the undamaged data sets. By using RPCA, the simulation uncertainties relating to signal-to-noise ration (SNR), structural deterioration and environmental variability were addressed. The results demonstrate that the usage of dimensional reduction and recursive methods can be very useful in extracting and analyzing features under different uncertainties for damage detection.

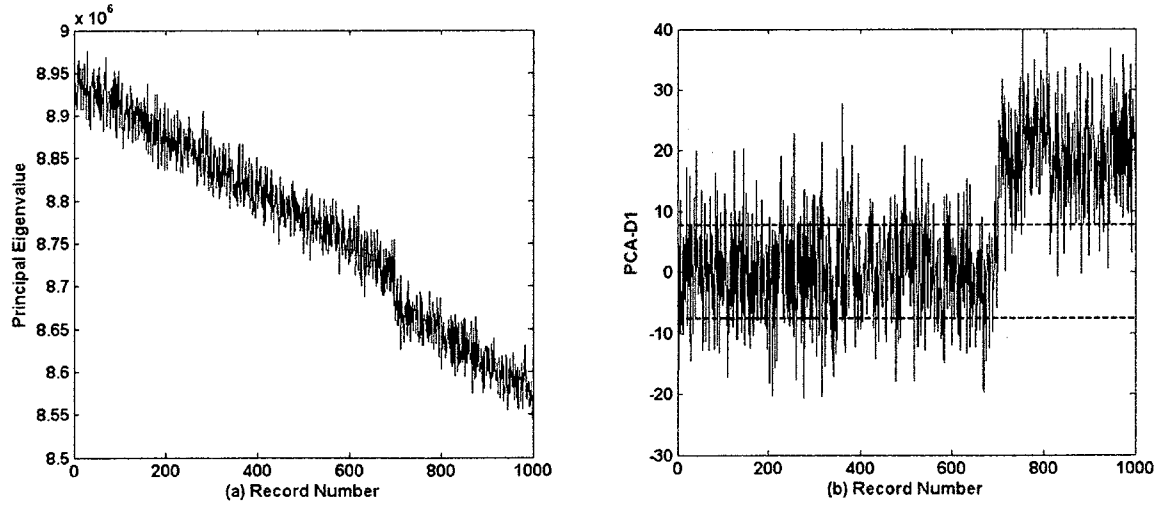

Figure 5.9. Application of RPCA, (a) principal eigenvalue, and (b) principal component.

5.6.2 Damage Quantification

Given that a damage case has been detected, the next step is to evaluate the location and magnitude of the impact damage. Damage assessment will be based on the modal curvature damage index method. Using the first 10 mode shapes generated from the cantilever finite element model, the damage index vectors were obtained using the damage cases shown in Table 5.2. To highlight deterioration effects, dimensional reduction was not applied to this sample simulation.

Comparison of Figure 5.10(a)-(b) shows that if system identification approach assumes that no structural deterioration has occurred, then spontaneous damages location and magnitude could be lost along the rest of the damage indicators caused by aging. This simple evaluation shows the need for continuous monitoring and model updating of a structure, which can become beneficial in separating deterioration effects from discrete damage events.

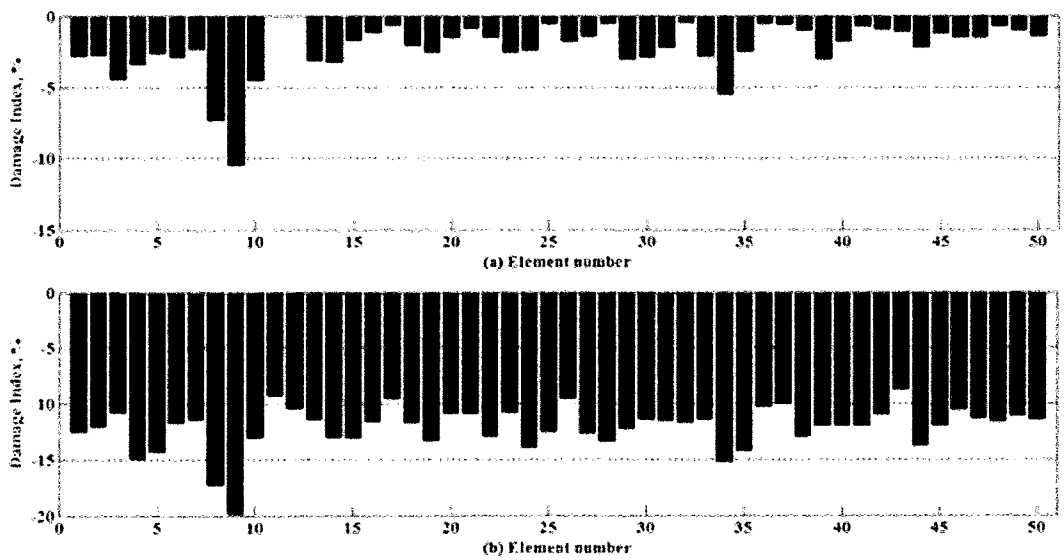

Figure 5.10. Case 3 damage index (a) with deterioration, and (b) without deterioration.

Next, the noise effects in extracting clear damage index values were analyzed. Prior to performing the statistical Z-test criteria, we generate a number damage index vectors, N_{DI}, using the same damage test case. For each damage index extraction, the modal data was randomized separately. By doing so, dimensional reduction was then applied as a noise reduction technique, see Eq. (49), at each element value α_j of the damage index method.

To demonstrate the problem of relying only on the Z-test to make damage decisions, Case 3 results at 1% noise level were obtained. Figure 5.11(a) shows a damage case where the true-positive damage locations are located at Elements 9 and 34, but due to the noise content, false-positives were also found at other elements. In addition, the worst damage is indicated in Element 3, which had no damage induced. This significant error can only be attributed to the random accumulation of noise at this particular element.

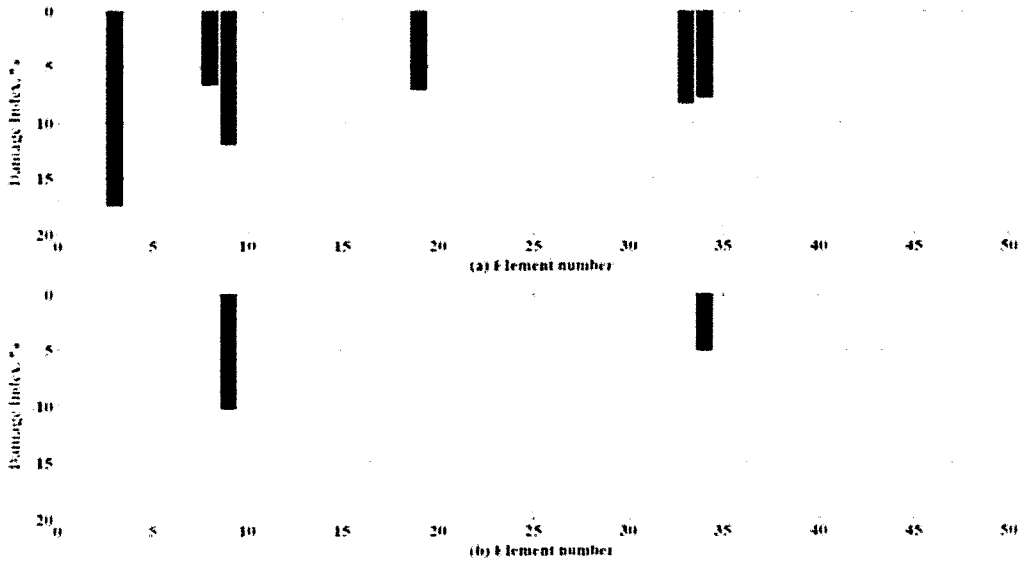

Figure 5.11. Case 3 damage index at 1% noise results. (a) without PCA and Z-test, (b) with PCA and Z-test.

Next, the results for damage Case 3 at 1% noise was enhanced by applying PCA training prior to applying the Z-test statistical criteria. For this analysis, the assumption is made that multiple damage index vectors can be extracted. More specifically, we assume that the procedure for extracting mode shapes and generating a single damage index vector can be repeated N_{DI} times. By doing so, dimensional reduction can be applied as a noise reduction technique at each element value α_j of the damage index method.

Using Eq. (49) and the 3-principal directions obtained from PCA, the original damage index data was reconstructed with reduced noise content. The damage index vector was extracted a total of $N_{DI} = 5$ times. Figure 5.11(b) shows the improved results obtained by PCA training and Z-test statistical criteria. The corresponding damage estimated at Elements 9 and 34 are well captured. Because noise is assumed to be random and un-biased, the probability of getting multiple indicators of damage for a particular element is rather low even for a small number of samples. The latter results demonstrate the importance of supervised classification in damage diagnostics. Damage assessment decisions based on training of data greatly enhances diagnostic performance in comparison to those based on single-set of measurements.

Based on PCA training and Z-test criteria, performance evaluation measures are given in Table 4 for N=100 samples. The performance measures of missed detection rate (MDR), false alarm rate (FAR), and mean severity error (MSE) are defined as follows:

$$MDR = \frac{1}{NT}\sum_{i=1}^{N}(MD)_i \tag{72}$$

$$\text{FAR} = \frac{1}{NP}\sum_{i=1}^{N}(FA)_i \tag{73}$$

$$MSE = \frac{1}{NP}\sum_{i=1}^{N}\frac{\left|\beta_i^t - \beta_i^p\right|}{\beta_i^p} \tag{74}$$

where NT is the number of true damage locations, MD is the number of missed detections, NP is the number of predicted damage locations, FA is the number of false damage locations, and the true damage severity and predicted severity for i^{th} location are, respectively, β_i^t and β_i^p.

Table 5.4. SEDI estimation performance.

Noise	Case #	1	2	3	4	5
1%	MSE %	0.00	4.43	1.68	0.91	8.25
	FAR	0.00	0.68	0.96	0.00	38.90
	MDR	0.00	0.38	0.00	0.00	0.36
2%	MSE %	0.08	6.66	3.02	1.86	8.39
	FAR	0.02	1.44	2.58	0.52	39.10
	MDR	0.00	0.62	0.06	0.00	0.68
2.5%	MSE %	0.99	5.50	3.67	3.05	8.40
	FAR	0.22	1.56	4.18	1.54	38.60
	MDR	0.00	0.50	0.12	0.00	0.54
3.5%	MSE %	3.75	5.88	4.82	4.08	8.67
	FAR	1.30	3.98	7.60	3.42	38.70
	MDR	0.00	0.56	0.36	0.02	0.58

From Table 5.4, the following observations can be made. For the undamaged Case 1, the noise levels of 2, 2.5 and 3.5% caused nonzero FAR values, which means that false damage alarms will be generated past the 2% noise level. Case 2 and 4 had single damage locations of equal magnitude. For Case 2, the MDR values ranged from 0.38 to 0.56. The reason for the nonzero MDR values is because as noise levels are increased, the probability of detecting the smaller damage is lower. The FAR values for this case range from 0.68 to 3.98 indicating that false alarms are almost unavoidable given any level of noise. Case 4 provided better performance values than Case 2. For Case 4, MDR and FAR values ranged, respectively, from 0 to 0.02 and 0 to 3.42. The improved performance of Case 4 over Case 2 is attributed to the location of damage. Damage in Case 2 is located at Element 4 near the base of the cantilever, while damage in Case 4 is located at midspan, Element 25. For the cantilever beam, the magnitude of deflections due to excitations is much higher compared to near base elements; thus, making Element 25 more

sensitive to structural changes. The lower sensitivity of Element 4 to structural changes caused the increased levels of MDR and FAR. For example, many of the sample runs for Case 2 estimated the damage location to be at Element 3 or 5 instead of Element 4, which would simultaneously result in a missed detection and false alarm. The performance measures were less accurate when it came to Cases 3 and 5, which consisted of multiple damage locations of different magnitudes. For Case 3, the MDR and FAR values ranged, respectively, from 0 to 0.36 and 0.96 to 7.60. In terms of the MSE, Case 4 provided the lowest levels of error, which ranged from 0.91% to 4%. Comparison of MDR values for Case 3 and Case 2 again shows that damage estimation is location sensitive. The lower MDR values obtained for Case 3 in comparison to Case 2 can be attributed to the damage locations, which were further away from the base (Element 1). Finally, the estimation performance results obtained for Case 5 indicate that the damage index method fails to isolate the damage location once multiple (> 2) damage locations exist.

With increasing levels of noise, in other words uncertainty, and damage scenario complexity, the performance of the damage diagnosis deteriorates. Extracting modal parameters, such as mode shapes, and using them to discriminate between normal and abnormal structural conditions is very susceptible to uncertainty in operational and environmental conditions. In experimental and real world applications, very often the changes resulting from normal variations in the structural system are greater than the changes caused by low levels of damage. During the modal and system identification process, fundamental assumptions, such as linearity, stationarity, and observability, are made. While in general, the system identification process does take into account measurement uncertainty, such as random noise, increasing structural complexities, such as nonlinearity and changing boundary conditions due to temperature variations, cannot be taken into account and be well isolated from the structural identification process. This demonstrates the

need for uncertainty analysis in SHM. Although significant research has been done in developing approaches and tools for data mining and knowledge discovery there is still a large gap between the performance of the existing methodologies and the expectation and requirements desired for SHM. In SHM, it is desired and necessary to properly induce and reduce the acquired knowledge, and describe it in a way that can be easily understood and classified. One major problem in knowledge explanation is to account and describe the uncertainties in qualitative concepts and how to implement the uncertainty transformation from quantitative data to qualitative concepts. Therefore, there are uncertainties not only in the process of data mining, but also in the discovered structural health state knowledge.

5.7 Summary

The results presented in this chapter have shown that damage assessment based on computational dimensional reduction of vibration data can be used to effectively detect and estimate spontaneous damage under different types of uncertainty. One major reason for the slow-progress in applying SHM technologies to real-world structures is the existence of uncertainty in every step of the damage assessment process. Adaptive pattern recognition techniques have been applied to a cantilever model and demonstrated that damage assessment can be performed at considerable levels of noise. Dimensionality reduction and feature classification methods were employed to discriminate between damaged and undamaged data. A comparative study is presented of dimensionality reduction and classification techniques.

From the results obtained, we may conclude that statistical discrimination of damage from undamaged data is more dependent on the efficiency of the dimensionality reduction method, than the classification method. Furthermore, a balance between physics-based and data-driven methods must be achieved to maximize the information and confidence levels of the damage

diagnosis. Increasing confidence in damage diagnosis is directly proportional to the uncertainty level considered. The systematic consideration of uncertainties is as important as having the appropriate structural system model, especially during model validation where the total error between physical observation and model prediction must be characterized.

Chapter 6

Proposed Sensor-Merging Technique for Output-Only Modal Analysis

In order to perform damage localization based on modal parameters, an experimental structural model must be obtained via modal analysis. Experimental modal analysis can be performed in a traditional way namely in a laboratory environment. In standard experimental modal analysis (EMA) externally applied input forces are measured together with dynamic responses of the system at different locations. Artificial external excitation is not always possible or measurable. In operational condition, it is often impossible to apply standard EMA since in one hand applying excitations in a controlled way might be intricate and dangerous and, on the other hand, the presence of immeasurable external and ambient forces jeopardizes the application of system identification techniques. When the vibration response of a structure is due to natural or ambient conditions, output-only or operational modal analysis (OMA) is required.

In this chapter, we present a roving sensor operational modal analysis technique based on transmissibility measurements. Measurement of dynamic properties, such as modal parameters, are an important step in vibration-based structural health monitoring. A brief review of output-only (operational) modal analysis is provided. A new technique is proposed based on a sensor-merging approach when limited output-only sensors are available.

6.1 Output-Only (Operational) Modal Analysis

Modal analysis has been widely used for the task of extracting structural modal parameters from the response of structural components and systems. In traditional EMA, the structure is often removed or isolated from its operating environment and tested in controlled laboratory

conditions, which may vary significantly from the operating conditions. Numerous modal identification algorithms for single-input-single-output (SISO), single-input-multiple-output (SIMO), and multiple-input-multiple-output (MIMO) have been developed both in the time and frequency domain. EMA is a relatively well understood technique and is well described in a number of texts [44,71,105]. EMA requires structure excitation by means of known forces and measuring the output responses over the structure. The structure's modal parameters are then characterized or estimated on the basis of both the known input forces and output responses.

In many engineering applications, direct measurement of mode shapes is not always possible. Structural mode shape extraction requires input (e.g. force) and output (e.g. acceleration) measurement. When control of input excitations is not possible, approximating methods must be utilized. System identification techniques, referred as operational modal analysis (OMA) have been developed to identify modal parameters from structural systems under their operating conditions using output-only data [105]. OMA allows for a more realistic modal models for in-operation structures, such as bridges and aircraft. In addition, very often it is not possible to provide sufficient artificial forced excitation to complex structures, such as bridges and high-speed ships. Also, the cost associated with performing modal testing can be too high to be justified. Thus, difficulties involved in providing sufficient excitation and simulating the realistic operating conditions proves to be a major support for OMA in place of EMA, which require the structure to be excited by a known artificial force.

Table 6.1 provides an overview an comparison of OMA and EMA modal analysis methods. The main advantage of OMA over EMA is that during modal testing, the structure remains in its real operation conditions, which can vary significantly from results obtained during a forced-excitation laboratory experiment. Moreover, performing modal testing while in operation includes the effects of unknown and/or uncontrollable ambient sources, such as temperature. The

contribution of these ambient sources can have a significant effect on the dynamic response of structures. A drawback to using OMA is that the obtained operational deflection shapes (ODS) are approximations on the true mode shapes of the structure, and can be heavily dependent on the force or loads being applied. Theoretical mode shapes do not depend on either the amplitude or location of the applied loads, they are natural properties that do not change unless the properties of the structure change, hence their use in damage detection problems. Furthermore, if the excitation level is quite low, then the OMA will provide poor results.

Table 6.1. Overview and summary of EMA and OMA approaches.

	Input(s) Available	All Outputs Available	Limited Outputs Available	Time Domain	Frequency Domain	Consistent Persistent Excitation	Scaled Mode Shapes
Experimental Modal Analysis (EMA)*	X	X	X	X	X	X	X
Operational Modal Analysis (OMA)**		X		X	X	X	

***Existing methods require artificial known excitation, but provides scaled mode shapes and can be used with roving sensor approach.**

****Existing methods do not require known excitation, but do not provide scaled mode shapes and cannot be used with roving sensor approach.**

6.2 Output-Only Identification Algorithms

The simplest method to estimate modal parameters from operation data in the frequency domain is the so-called Peak Picking (PP) technique applied to the auto and cross-spectrum of the response signal [44]. The PP method is based on a single-degree-of-freedom (SDOF) approach, which involves selecting peaks in the spectra corresponding to resonance frequencies. This method yields reliable estimates when the structure exhibits low damping and structural modes

are well separated. An advanced version of the PP method is known as the Complex Mode Indicator Function (CMIF) [71] or Frequency Domain Decomposition (FDD), which is based on singular value decomposition (SVD) of the matrix of power spectra. The common steps in the peak picking family methods are:

- Individual peak regions are visually chosen and marked from the cross-spectra between responses and a reference signal. In the vicinity of each peak, the maximum is found and associated to the eigenfrequency of the mode.
- Two points are identified on the cross-spectra curves, one below the eigenfrequency ω and one above, both having an amplitude $C(\omega)/\sqrt{2}$, where $C(\omega)$ is the amplitude at the eigenfrequency. These two points are called half-power points.
- The damping ratio ζ of the associated mode is then computed by

$$\zeta = \frac{\omega_2^2 - \omega_1^2}{4\omega_n^2} \tag{75}$$

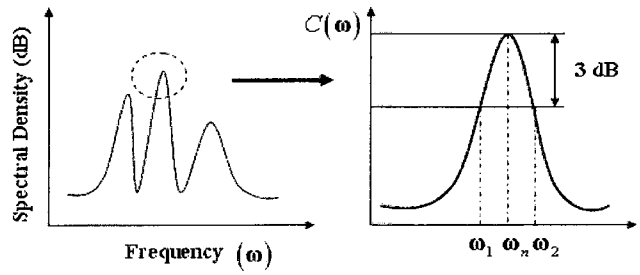

Figure 6.1. Half-power bandwidth method.

Aside from SDOF techniques, more advanced model-based algorithms, for the identification of output-only data, are available in the frequency and time domains. The time domain methods include the Least Squares Complex Exponential (LSCE) estimator [71], and a wide range of Stochastic Subspace Identification (SSI) techniques [25,34,39,114,137]. The Maximum

Likelihood Estimation (MLE) technique is a frequency domain method [25,31]. Describing these methods is beyond the scope of the present manuscript. A detailed overview of output-only system identification methods can be found in [25,71].

If all N-responses of a structure under test are measured simultaneously, each of the structural responses can be used in output-modal analysis to extract operating deflection shapes. This approach results in a $N \times N$ power spectrum matrix $\mathbf{G}(\omega)$. In our work, simultaneous measurements of all points of interest was not possible due to insufficient sensory and data acquisition equipment. For some structural engineering applications, not all outputs are measured at once. Therefore, direct application of output-only modal analysis based on cross-power spectrum matrix, which is the basis for frequency domain OMA, could not be performed. Usually, a limited number of sensors is available for measuring a large number of experimental DOFs of the structure. The standard allocation of sensors for ambient vibration testing uses a group of roving sensors and a group of fixed reference response sensors that simultaneously measure the structural response. Since ambient excitation has a non-stationary nature, the reference responses are required for creating a composite measurement from the roving measurements. When non-stationary signal are encountered, the scaling of the ODS from test to test can vary significantly. In addition, performing vibration measurements on a structure via roving sensor groups increases the possibility of mass loading non-stationary effects due to imprecise mass properties variations induced by the roving sensors. Since this type of non-stationarity depends on the variability experimental setting, attention must be paid to maintaining mass variability to a minimum.

In order to extract scaled modal parameters from multiple locations, we made use of a re-scaling of the auto- and cross-spectra approach to compensate for variation in excitation and

modal participation. Throughout the work presented in this thesis, use was made of this re-scaling approach for output-only modal analysis, which will be presented next.

6.3 Sensor Merging Output-Only Modal Analysis Re-Scaling Technique

The idea to re-scale and merge data from different groups of roving accelerometers before performing mode shape extraction is based on the work of Mevel et al. [114]. Consider a linear time invariant structural system with a total of N_{dof} experimental DOFs, N_{gr} measurement groups containing N_{rov} measurements, and for all measuring groups, N_{ref} fixed reference measurement points are simultaneously measured. For each group of roving output measurements, the time response is transformed to the frequency domain by estimating the auto and cross power spectra among the response signals and their reference responses. The auto and cross spectra for group i and frequencies ω, are contained in matrix $\mathbf{G}_i(\omega)$ with size $((N_{gr}+N_{ref})\times N_{ref})$, which can be organized into sub-matrices as follows

$$\mathbf{G}_i(\omega)=\begin{bmatrix}\mathbf{G}_i^{gr}(\omega)\\ \mathbf{G}_i^{ref}(\omega)\end{bmatrix} \tag{76}$$

with $\mathbf{G}_i^{ref}$ being a $(N_{ref}\times N_{ref})$ sub-matrix that contains the auto and cross power spectrum estimates of the reference responses, and $\mathbf{G}_i^{gr}$ a $(N_{gr}\times N_{ref})$ sub-matrix containing the auto and cross spectra of the non-reference with the reference responses.

The $\mathbf{G}_j^{gr}$ matrix, containing the cross-spectra of group j, can be re-scaled for all frequencies to a common level dictated by the matrix $\mathbf{G}_k^{ref}$, containing the cross-spectra of the reference responses from group k, as follows

$$\mathbf{G}_{j\to k}^{gr}(\omega)=\mathbf{G}_{j}^{gr}(\omega)\cdot\left(\mathbf{G}_{j}^{ref}\right)^{-1}\cdot\mathbf{G}_{k}^{ref}(\omega)=\mathbf{T}_{j}(\omega)\cdot\mathbf{G}_{k}^{ref}(\omega) \tag{77}$$

where $\mathbf{T}_j$ is the transmissibility matrix of group j with respect to reference measurements j. Note that peak resonant locations of transmissibility functions in general do not correspond to system poles. The transmissibilities are multiplied by the same power spectrum matrix of reference group k to bring the pole locations back into the re-scaled data. The complete data set of re-scaled cross-spectra is given by

$$\mathbf{G}^{tot}(\omega)=\begin{bmatrix}\mathbf{G}_{1\to k}^{gr}(\omega)\\ \mathbf{G}_{1\to k}^{gr}(\omega)\\ \vdots\\ \mathbf{G}_{N_{gr}\to k}^{gr}(\omega)\\ \mathbf{G}_{k}^{ref}(\omega)\end{bmatrix} \tag{78}$$

Given the complete set of re-scaled cross-spectra matrix, re-scaled operational deflection shapes can be obtained via well known OMA methods, see next section. The re-scaled mode shape vectors are organized in the $(N_{dof}\times N_m)$

$$\mathbf{\Phi}=\begin{Bmatrix}\left\{\phi_{1\to k}^{gr}(\omega)\right\}_r\\ \left\{\phi_{2\to k}^{gr}(\omega)\right\}_r\\ \\ \left\{\phi_{N_{gr}\to k}^{gr}(\omega)\right\}_r\\ \left\{\phi_{k}^{gr}(\omega)\right\}_r\end{Bmatrix} \tag{79}$$

Figure 6.2 shows a schematic of the re-scaling approach using the PSD matrix. In this research, the frequency domain decomposition technique is utilized to extract operational deflection shapes.

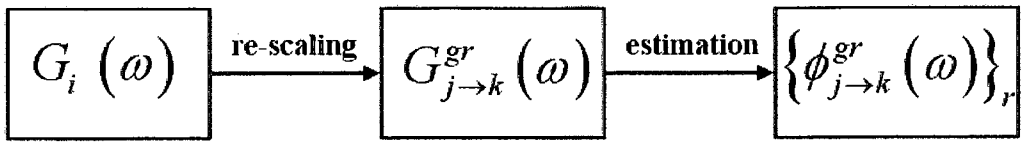

Figure 6.2. Schematic of re-scaling technique.

6.4 Frequency Domain Decomposition

The following section will deal with the modal decomposition of output-only data in the frequency domain. It will be shown that modal parameters can be identified from cross power spectra of output-only data. The frequency domain decomposition (FDD) (Brincker et al. [17]) is an extension of the well known peak picking technique. The approach uses the fact that modes can be estimated from the spectral densities calculated with the assumption of white noise input and a lightly damped structure.

6.4.1 Modal Decomposition of Cross Power Spectra

Prior to applying the frequency domain decomposition approach for obtaining mode shapes, the estimates of the auto and cross power spectra are to be obtained from finite sequences of measured time samples. For this work, the classical periodogram method [13] was utilized.

The FDD technique is based on the formula of input and output power spectrum relationship for a stochastic process defined as

$$\mathbf{G}_{yy}(\omega) = \bar{\mathbf{H}}(\omega)\mathbf{G}_{xx}(\omega)\mathbf{H}^{T}(\omega) \tag{80}$$

where $\mathbf{G}_{xx}$ and $\mathbf{G}_{yy}$ are the $(n_{in} \times n_{in})$ input and $(n_{out} \times n_{out})$ output power spectral density (PSD) matrices, respectively, top '$-$' indicates complex conjugate, $\mathbf{H}$ is the $(n_{in} \times n_{out})$ frequency

response function (FRF) matrix, which can be expressed as a partial fraction form via poles λ_k and residues R_k

$$\mathbf{H}(j\omega)=\sum_{k=1}^{N_m}\frac{\mathbf{R}_k}{j\omega-\lambda_k}+\frac{\bar{\mathbf{R}}_k}{j\omega-\bar{\lambda}_k} \tag{81}$$

with N_m being the number of modes, $\mathbf{R}_k=\phi_k\gamma_k^T$, where ϕ_k and γ_k are the mode shape vector and modal participation vector, respectively.

Using Eq. (80) and the Heaviside partial fraction theorem for polynomial expansions, we obtain the output PSD matrix as

$$\mathbf{G}_{yy}(j\omega)=\sum_{k=1}^{N_m}\frac{\mathbf{A}_k}{j\omega-\lambda_k}+\frac{\bar{\mathbf{A}}_k}{j\omega-\bar{\lambda}_k}+\frac{\mathbf{B}_k}{-j\omega-\lambda_k}+\frac{\bar{\mathbf{B}}_k}{-j\omega-\bar{\lambda}_k} \tag{82}$$

where $\mathbf{A}_k$ is the k^{th} residue matrix of the output PSD. The matrix $\mathbf{G}_{yy}$ is assumed to be a constant value $\mathbf{C}$, since the excitation signals are assumed to be uncorrelated zero mean white noise in all measured DOFs. Matrix $\mathbf{A}_k$ is Hermitian and is given by

$$\mathbf{A}_k=\mathbf{R}_k\mathbf{C}\sum_{s=1}^{N_m}\frac{\bar{R}_s^T}{-\lambda_k-\bar{\lambda}_s}+\frac{R_s^T}{-\lambda_k-\bar{\lambda}_s} \tag{83}$$

The contribution to the residue from the k^{th} mode is given by

$$\mathbf{A}_k=\frac{\mathbf{R}_k\mathbf{C}\bar{\mathbf{R}}_k^T}{2\alpha_k} \tag{84}$$

Considering a lightly damped model, we have the following relationship

$$\lim_{damping\to light}\mathbf{A}_k=\mathbf{R}_k\mathbf{C}\mathbf{R}_k^T=\phi_k\gamma_k^T\mathbf{C}\gamma_k\phi_k^T=d_k\phi_k\phi_k^T \tag{85}$$

where d_k is a scalar constant. The contribution of the modes at a particular frequency is limited to a finite number. The response spectral density matrix can then be written as follows

$$\mathbf{G}_{yy}(j\omega) = \sum_{k \in Sub(\omega)} \frac{d_k \phi_k \phi_k^T}{j\omega - \lambda_k} + \frac{\bar{d}_k \bar{\phi}_k \bar{\phi}_k^T}{j\omega - \lambda_k} \tag{86}$$

where $Sub(\omega)$ is the set of modes that contribute at the particular frequency.

The spectral density matrix is then decomposed by using singular value decomposition (SVD), which is performed to identify the SDOF models of the structure. The decomposed spectral density matrix after applying SVD is given by

$$\mathbf{G}_{yy}(\omega) = \mathbf{\Phi \Sigma \Phi}^H \tag{87}$$

where the matrix $\mathbf{\Phi}$ is a unitary matrix holding the singular vectors ϕ_i, $\mathbf{\Sigma}$ is a diagonal matrix holding the scalar singular values s_i:

$$\mathbf{\Sigma} = diag\left(s_1, ..., s_{N_m}\right) = \begin{bmatrix} s_1 & 0 & \cdots & 0 \\ 0 & s_2 & & 0 \\ \vdots & & \ddots & \vdots \\ 0 & 0 & \cdots & s_{N_m} \end{bmatrix} \tag{88}$$

$$\mathbf{\Phi} = \begin{bmatrix} \{\phi_1\} & \{\phi_2\} & \cdots & \{\phi_{N_m}\} \end{bmatrix} \tag{89}$$

SVD is performed for each of the matrices at each frequency and for each measurement. The singular vectors correspond to an estimation of the mode shapes. Each of the SDOF systems obtained by the SVD allows us to identify the natural frequency and unscaled mode shape at a particular peak. Peak-picking technique can then be performed on each resonant peak on the average of the normalized singular values for all data sets.

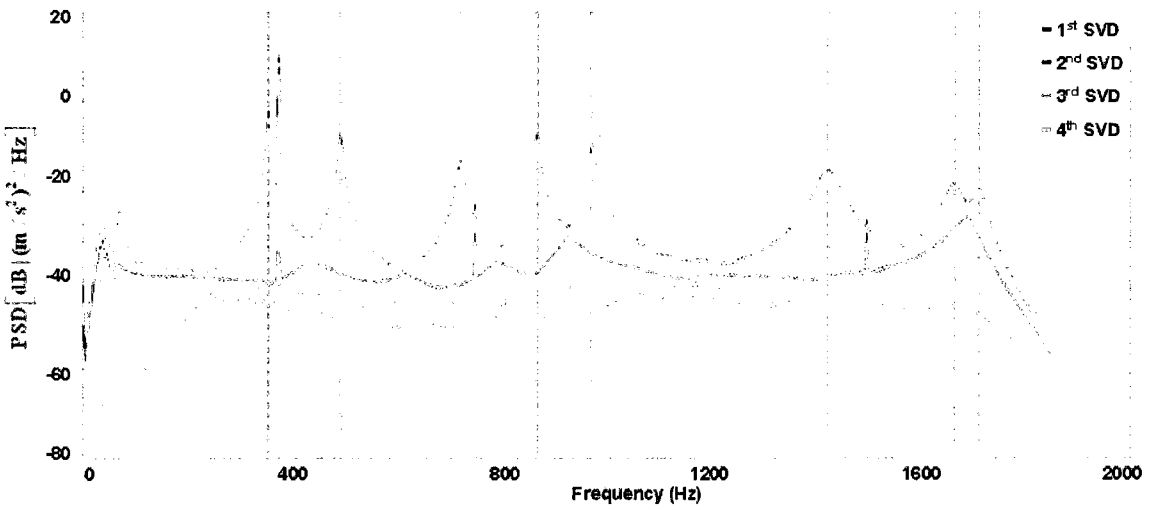

Figure 6.3. Singular values of the PSD matrix of the response.

Figure 6.3 shows the result of the SVD of a spectral density matrix. The example presented here is the response of a rectangular steel plate coupled with engine oscillations. The test is described in detail in Møller et al. [116]. The red vertical lines indicate structural mode frequency locations. The singular vectors are ranked in singular value descending order. Compared to regular peak picking method, this techniques allows us to identify possible coupled modes that are usually hard to identify via regular PSD functions.

6.5 Case Study: Application to Plate Experiment

This section illustrates the evidential reasoning damage assessment approach using an in-house designed experiment. An aluminum plate structure was hanged using fishing strings to simulate free-free boundary conditions (Figure 6.4). Dimensions of the plate are 45.72cm x 45.72cm x 0.3175cm. Impact excitation was applied on the structure to provide impulse response excitation. Sampling was done at 1024Hz. The signals are lowpass filtered for the frequency band of interest, $(0Hz, 400Hz]$. We utilized 35-locations, as shown in Figure 6.4, where response signals were

taken. Due to the limited number of acquisition channels (four), two sets of measurements have been done for each test described hereafter.

Each accelerometer with hardware has a mass of 33-grams. In order to avoid varying mass loading effects while roaming the accelerometers on the plate, additional masses 33-grams each were placed at all measuring points where no accelerometer was used. Accelerometer one has been kept at the same location in each measurement set and is used as a referenced signal. The reference accelerometer is located at one of the corners of the plate, it is assumed that this location is free of damage. Since consistency in impact testing is hard to maintain, correlation functions in the tests presented here have been computed with reference to the response of the first accelerometer. The modal identification will work on the principle of the sensor merging technique for output-only modal analysis (OMA).

Figure 6.4. A free-free aluminum plate structure.

6.5.1 Modal Analysis - Undamaged Structure

Eigenfrequencies and damping values were identified with the OMA analysis version of the frequency domain decomposition (FDD) described in section 6.4. Figure 6.5 shows all the autospectrum responses of the output accelerometers. The first peaks around the 8Hz correspond

to rigid body modes. A total of 13 resonant peaks are captured in the 400Hz range. Figure 6.6 shows the isolated autospectrum of a corner accelerometer with mode indicators corresponding to peaks. Strong mode coupling exists between close modes in three frequency regions - at 115Hz, 202Hz, and 353Hz. Due to difficulty in extracting stable mode shapes from closed-coupled modes, these peak regions were not utilized in the damage assessment analysis. In Table 6.2 we report the natural frequencies and associated damping values.

The first 5 identified mode shapes of the undamaged structure are shown in Figure 6.7. Modes 4 (113 Hz), 6 (199 Hz) and 7 (201 Hz) were not well identified due to mode coupling and closeness to other resonant frequencies, and noisy character of the re-scaled cross-power spectra data. As such, these closely spaced modes will not be utilized in the damage assessment analysis based on mode shapes. Poorly identified modes would only increase the noise content of the data analyzed using the mode shape-based damage indicators. The poor quality mode shapes (4,6,7,11,12) and the additional identified modes (9,10,13) are shown in Appendix A. After the re-scaling procedure, the extracted mode shape estimates are of relative good quality, which will be beneficial in performing correlation analysis with modes extracted from damaged structure.

Using the method of frequency domain decomposition (FDD), mode coupling and closely spaced poles make modal parameter extraction difficult, especially in output-only modal analysis. More advanced techniques based on fitting models, such as least square complex exponential method (LSCE) and stochastic subspace identification (SSI), along with mode stability diagrams, can aid in extracting mode shapes from closely spaced modes. Application of these techniques is beyond the current research effort. For additional information on these modal parameter estimation methods refer to [25,71,105].

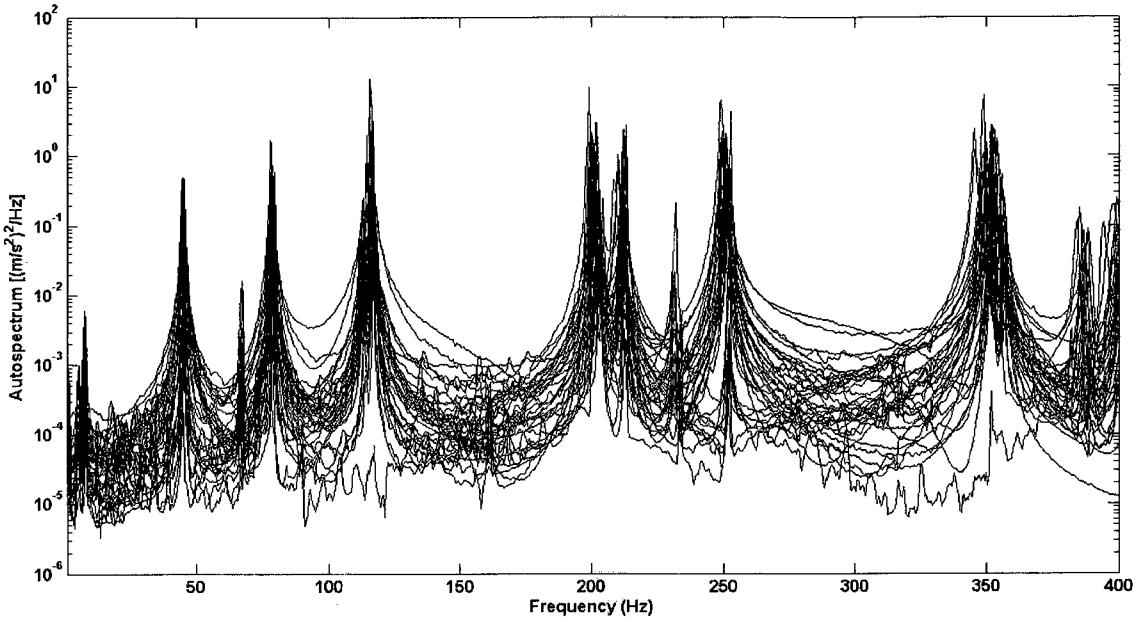

Figure 6.5. Autospectrum response for impact excitation of all output responses.

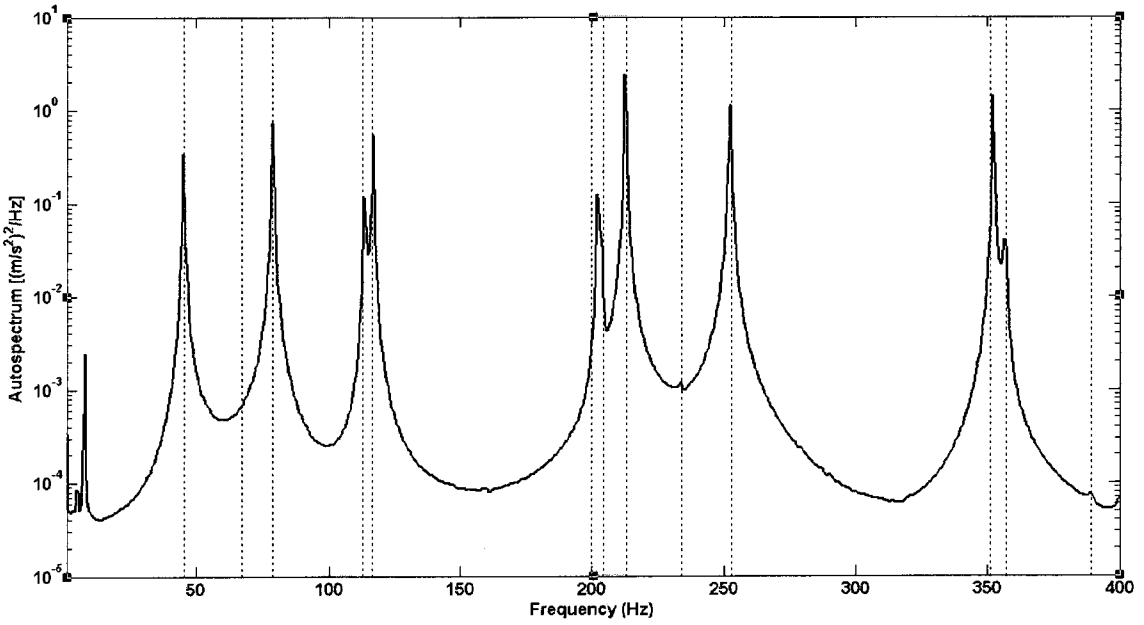

Figure 6.6. Autospectrum response for impact excitation of a corner measurement point.

Table 6.2. Frequencies and associated damping values for undamaged test case.

Mode	f (Hz)	σ_f (Hz)	$3\sigma_f$ (Hz)	ζ (%)
1	45.17	0.02	0.07	1.11
2	67.37	0.07	0.20	0.74
3	78.86	0.03	0.08	0.63
4	113.60	0.06	0.18	0.44
5	116.87	0.05	0.14	0.43
6	200.80	0.07	0.22	0.37
7	204.13	0.05	0.14	0.37
8	212.53	0.01	0.03	0.24
9	234.36	0.95	2.86	0.22
10	252.51	0.01	0.02	0.20
11	351.29	0.09	0.26	0.14
12	356.63	0.03	0.08	0.28
13	389.49	0.07	0.22	0.19

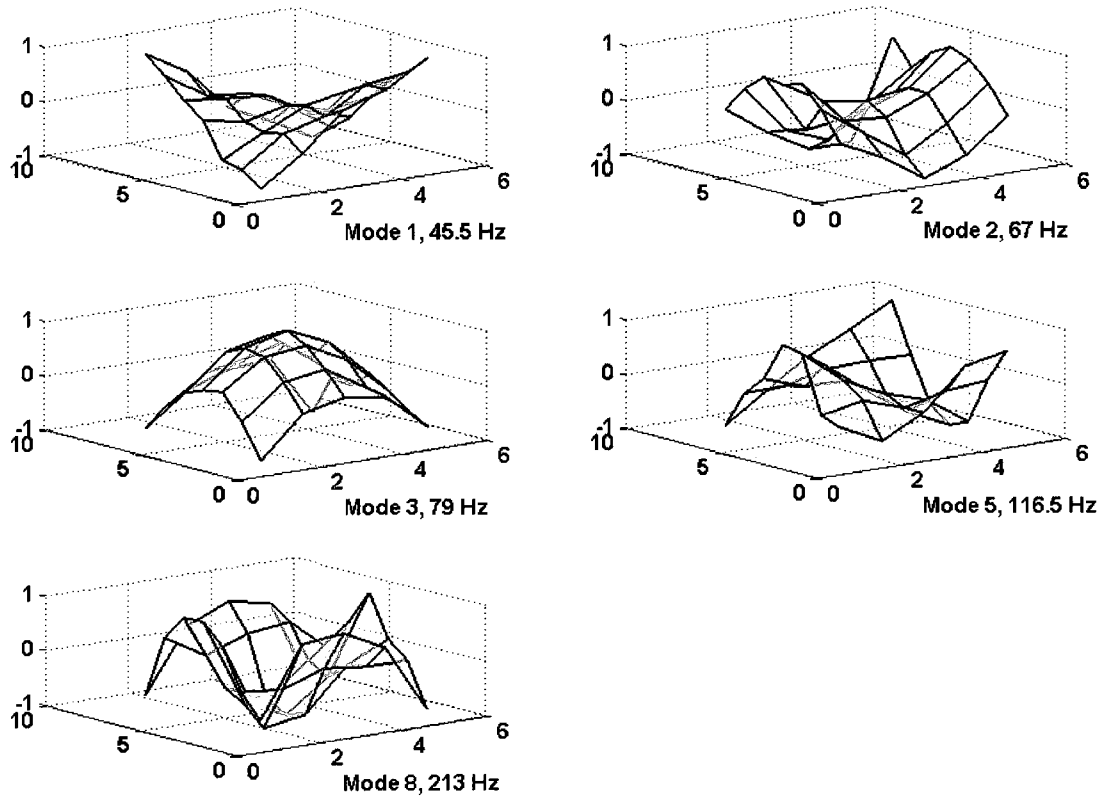

Figure 6.7. Mode shapes identified in the presence of impact excitation.

6.5.2 Modal Analysis - Damaged Structure

Now dummy masses will be added to structure to simulate damage. Three dummy masses, 12-grams, 27-grams, 54-grams, are chosen for structural modifications. By varying the additional mass, the uncertainty and sensitivity in the damage assessment method can be analyzed. Figure 6.8 and Table 6.3 show the locations where the dummy masses were placed and the test cases being analyzed. Table 6.4 gives an overview and comparison of the 13 natural frequencies f, together with the 99.8% confidence intervals $3\sigma_f$, and the corresponding changes in natural frequencies Δf from the undamaged to the damaged condition using the 54-grams mass. The presence of the attached mass can be detected since the changes in the natural frequencies Δf are clearly statistically significant. This conclusion is on a basis of the uncertainty on the experimentally measured shifts $3\sigma_f$.

In Figure 6.9, we report the first five identified mode shapes for experiments with a 54-grams dummy mass placed damage location $D1$. To maintain consistent mode shape orientation, all generated modes at each particular resonance were flipped-over (if required) about the plate's plane of symmetry to match the orientation obtained in the reference undamaged modes. Visual comparison of Figure 6.7 and Figure 6.9 demonstrate no clear indication, such as localized spikes, of dummy-mass location. As previously stated, due to difficulty in extracting stable mode shapes from closed-coupled modes, these peak regions were not utilized in the mode extraction process and damage assessment analysis.

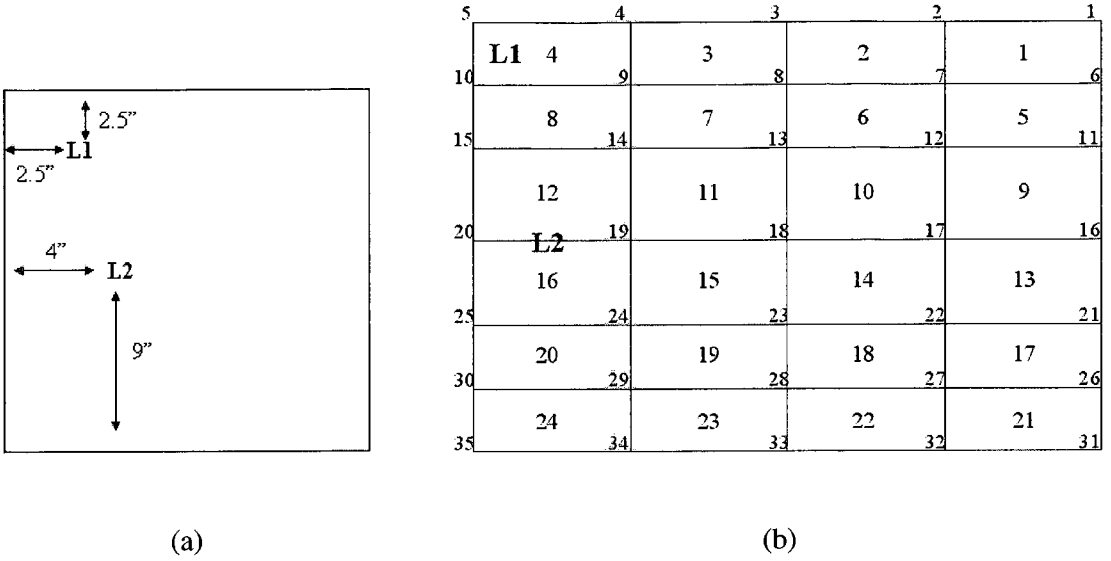

Figure 6.8. (a) Induced damage locations on a 18" X 18" plate; (b) Sensor locations (nodes 1 through 35), and finite element shells (1 through 24).

Table 6.3. Damage assessment test cases.

Test Case	Mass Location	Mass (g)
Undamaged	-	-
D1	L1	12
D2	L1	27
D3	L1	54
D4	L2	12
D5	L2	27
D6	L1, L2	27, 27

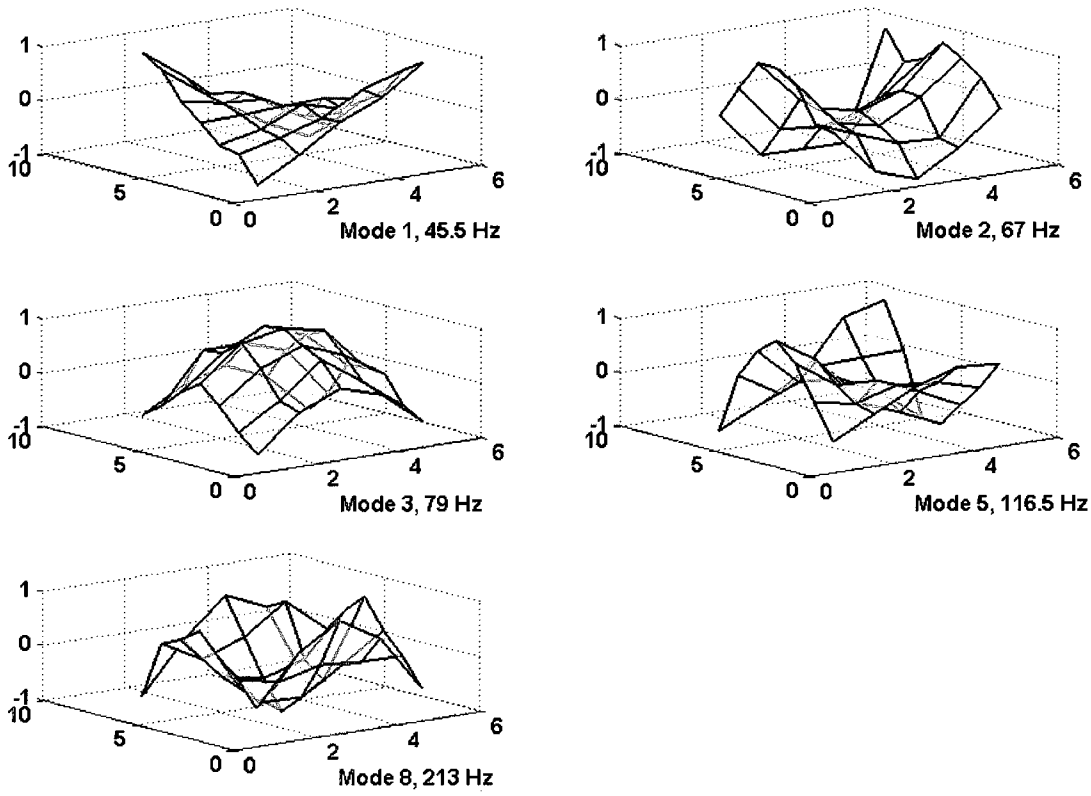

Figure 6.9. Mode shapes identified in the presence of impact excitation for damage case D3.

Table 6.4. Overview and comparison of the experimental results obtained on plate structure for case D3.

Mode	Undamaged f (Hz)	Undamaged $3\sigma_f$ (Hz)	Case D3 Δf (Hz)	Case D3 $3\sigma_{\Delta f}$ (Hz)	Case D3 $\Delta\zeta$ (%)
1	45.17	0.07	-0.31	0.08	-0.01
2	67.37	0.20	0.00	0.31	0.01
3	78.86	0.08	-0.22	0.11	0.00
4	113.60	0.18	-0.20	0.29	-0.01
5	116.87	0.14	-0.25	0.14	0.00
6	200.80	0.22	-0.01	0.31	-0.13
7	204.13	0.14	-0.05	0.25	-0.12
8	212.53	0.03	-0.12	0.09	0.12
9	234.36	0.28	-0.02	0.38	0.00
10	252.51	0.02	-0.08	0.08	0.10
11	351.29	0.26	-0.01	0.36	0.07
12	356.63	0.08	-0.01	0.14	0.00
13	389.49	0.22	-0.05	0.31	-0.06

Table 6.5 shows an overview of the natural frequencies shifts due to the additional mass for the identifiable modes only, together with the undamaged frequencies 99.8% confidence intervals. The changes incurred by case D1 were not statistically significant since the change in natural frequencies were smaller than the 99.8% confidence intervals. The reason for this is that case D1 used the smallest dummy mass of 12g. Using statistical significance as the damage detection indicator would result in a false-negative for case D1. In all the other damage cases, the presence of the attached mass can clearly be detected since the changes in the natural frequencies Δf are clearly statistically significant. As expected, case D3 and D6 had the biggest shifts in frequency due to their maximum mass addition of 54g.

Table 6.5. Overview of frequency changes due to additional mass for identifiable modes.

Mode	Undamaged f (Hz)	Undamaged $3\sigma_f$ (Hz)	Case D1 Δf (Hz)	Case D2 Δf (Hz)	Case D3 Δf (Hz)	Case D4 Δf (Hz)	Case D5 Δf (Hz)	Case D6 Δf (Hz)
1	45.17	0.07	-0.05	-0.14	-0.31	0.00	0.00	-0.14
2	67.37	0.20	0.00	0.00	0.00	-0.05	-0.13	-0.13
3	78.86	0.08	-0.04	-0.10	-0.22	-0.02	-0.05	-0.15
8	212.53	0.03	-0.02	-0.06	-0.12	-0.07	-0.20	-0.26
9	234.36	0.28	0.00	-0.01	-0.02	0.00	-0.01	-0.01
10	252.51	0.02	-0.01	-0.04	-0.08	-0.01	-0.02	-0.05
13	389.49	0.22	-0.01	-0.02	-0.05	-0.74	-2.13	-2.15

The output-only modal analysis base using roving accelerometers assume that the re-scaling approach based on the reference accelerometer yield consistent information on the same system with similar excitation. A violation of this assumption creates significant data inconsistency, which will lead to identification problems. If significant excitation inconsistencies, say impact versus random excitation, are made in between roving accelerometer measurements will show up in the mode shape estimation process.

6.6 Summary

The extension of experimental modal analysis (EMA) to operational modal analysis (OMA) has opened new innovative perspectives and possibilities that involve in-use dynamic characterization of engineering structures, such as aircraft and bridges, in their operating conditions. Aside from not requiring additional force excitation hardware, the main advantage of OMA is that structures is tested and modeled under realistic or actual working conditions. Moreover, freely available natural excitation sources can be used as an alternative to controlled artificial excitation.

In this chapter, we presented a proposed OMA method for estimating structural mode shapes by using a transmissibility-based sensor-merging technique. The proposed procedure for obtaining mode shape estimates can become lengthy and tiresome if a large number of patches are required. Using standard EMA techniques, problems can arise when extracting close-coupled or repeated modes. Now, this difficulty is more evident in the proposed approach due to additional estimation errors that can occur due to the multiple vibration tests required to perform sensor merging.

The proposed approach is quite useful when the number of required sensor outputs is much greater than the available measurement channels. The method was tested with an in-house aluminum plate experiment. Measurements were performed under 4xFree (FFFF) boundary conditions. The experimental results show that the proposed approach was able to extract well separated mode shapes.

Chapter 7

Improved Vibration-Based Damage Localization Technique

This chapter discusses the principles of damage localization based on vibration-based analysis. Baseline damage indicator approaches based on modal parameters are presented. To enhance the damage localization performance of these damage indicators, we propose a technique based on the localized structural sensitivity to mass or stiffness changes integrated with statistical sampling. The proposed approach is compared to results obtained using the baseline damage localization methods by means of in-house experiments conducted on a free-free plate structure and experimental data from the I-40 bridge damage assessment benchmark [48].

7.1 Baseline Damage Localization Methods

In this section, multiple vibration-based damage indicator functions are discussed, which are widely accepted as baseline techniques for performing damage detection and localization. Vibration-based methods are based on the fact that damage alters the dynamic properties of structures, such as natural frequencies, damping, mode shapes, and operational deflections shapes (ODS). Measurement and tracking of such modal properties can provide information regarding structural health condition.

The most widely used mode shape quality indicator is the single-number measure known as Modal Assurance Criterion (MAC) [4]. The MAC value indicates the degree of correlation between the undamaged, ϕ, and damaged, ϕ^*, mode shapes and defined as

$$MAC = \frac{\left|\sum_{j=1}^{N_{dof}} \phi_j \phi_j^*\right|^2}{\sum_{j=1}^{N_{dof}} \phi_j^2 \sum_{j=1}^{N_{dof}} \phi_j^{*2}} \tag{90}$$

where N_{dof} equals the degrees of freedom or measurement points defining the mode shape. The MAC value ranges from 0 to 1, with 0 representing null correlation and 1 representing perfect correlation. Abnormal deviation from unity is interpreted as possible structural damage. The MAC value only provides damage detection capability. To obtain damage localization and combine multiple mode shapes, the Coordinate Modal Assurance Criterion (COMAC) [91] is utilized and is defined as

$$COMAC_j = \frac{\left|\sum_{i=1}^{N_m} \phi_{ji} \phi_{ji}^*\right|^2}{\sum_{i=1}^{N_m} \phi_{ji}^2 \sum_{i=1}^{N_m} \phi_{ji}^{*2}} \tag{91}$$

where j represents the modal coordinate and N_m is the total number of modes. Similar to MAC values, COMAC value of 0 indicates low correlation and a value of 1 indicates high correlation.

An alternative to using direct mode shape changes to obtain information about damage is the use of mode shape derivatives, such as curvature, which is the second derivative of the mode shape with respect to position. The use of mode shape curvature (MSC) for damage detection was introduced by Pandey et al. [129]. The curvature is calculated from the measured mode shapes using a central difference approximation

$$\phi_j'' = \sum_{i=1}^{N_m} \frac{\phi_{j+1,i} - 2\phi_{ji} + \phi_{j-1,i}}{d_{j+1,j}^2} \tag{92}$$

where i is the mode shape number, j is the node or measurement point, and d is the distance between measurement points. The damage index using the curvature method is given as

$$MSC_j = \Delta\phi_j'' = \left|\phi_j''\right| - \left|\phi_j^{*''}\right| \tag{93}$$

where subscript '*' indicates damage condition. In this work, we normalize the curvature damage index so that values of 0 indicate zero correlation and value of 1 indicates perfect correlation, i.e. no difference in change of curvature.

Damage detection and localization of continuous structures based on the strain energy damage index (SEDI) method developed by Stubbs et al. [165] utilizes the modal strain energy distribution in a structure due to damage. In this work, the SEDI method is applied to the analysis of operational deflection shapes (ODS) based on the work of Cornwell et al. [27] which extended the SEDI method to 2D structures. This method requires that ODS before and after damage are known, and only a few modes are required; thus applying a reduced-order model approach.

For a particular mode shape, $\phi_i(x,y)$, of an undamaged structure, the energy associated with a mode shape is given as

$$U_i = \frac{D}{2}\int_0^b\int_0^a\left[\left(\frac{\partial^2\phi_i}{\partial x^2}\right)^2 + \left(\frac{\partial^2\phi_i}{\partial y^2}\right)^2 + 2\nu\left(\frac{\partial^2\phi_i}{\partial x^2}\right)\left(\frac{\partial^2\phi_i}{\partial y^2}\right) + 2(1-\nu)\left(\frac{\partial^2\phi_i}{\partial x\partial y}\right)^2\right]dxdy \tag{94}$$

where (x,y) are the particular coordinates of the 2D structure, D is the bending stiffness, and ν is the Poisson's ratio. Because ODS cannot be used to measure the true modal parameters of the structure, material and geometric properties variables are not utilized. The material-reference free pseudo-energy is now given by

$$U_i = \int_0^b\int_0^a\left[\left(\frac{\partial^2\phi_i}{\partial x^2}\right)^2 + \left(\frac{\partial^2\phi_i}{\partial y^2}\right)^2 + \left(\frac{\partial^2\phi_i}{\partial x^2}\right)\left(\frac{\partial^2\phi_i}{\partial y^2}\right) + \left(\frac{\partial^2\phi_i}{\partial x\partial y}\right)^2\right]dxdy \tag{95}$$

If the 2D structure is subdivided into N_x and N_y elements in the x and y directions, respectively, then the energy associated with sub-region jk for the i^{th} ODS is given by

$$U_{ijk} = \int_{b_k}^{b_{k+1}} \int_{a_k}^{a_{j+1}} \left[\left(\frac{\partial^2 \phi_i}{\partial x^2} \right)^2 + \left(\frac{\partial^2 \phi_i}{\partial y^2} \right)^2 + \left(\frac{\partial^2 \phi_i}{\partial x^2} \right) \left(\frac{\partial^2 \phi_i}{\partial y^2} \right) + \left(\frac{\partial^2 \phi_i}{\partial x \partial y} \right)^2 \right] dxdy \tag{96}$$

$$U_i = \sum_{k=1}^{N_y} \sum_{j=1}^{N_x} U_{ijk} \tag{97}$$

and the fractional energy at location jk is defined to be

$$f_{ijk} = \frac{U_{ijk}}{U_i} \tag{98}$$

$$\sum_{k=1}^{N_y} \sum_{j=1}^{N_x} f_{ijk} = 1 \tag{99}$$

Similarly, expressions can be written using the ODS of the damage structure, ϕ_i^*, where * indicates the damaged condition. The ratio of the parameters can be determined to indicate the relative ODS changes in the structure as follows

$$\beta_{ijk} = \frac{f_{ijk}}{f_{ijk}^*} \propto \frac{D_{jk}}{D_{jk}^*} \tag{100}$$

Eq. (100) becomes singular if the denominator goes to zero, which will occur when simultaneously the element size approaches zero and the element location coincides with a nodal point of a ODS. To overcome this limitation of dividing by zero, an approximation is made such that the axis of reference for the ODS sensitivities is shifted by a value of 1. Adding unity to both the numerator and denominator of Eq. (100) yields

$$\beta_{ijk} = \frac{f_{ijk} + 1}{f_{ijk}^* + 1} \tag{101}$$

In order to account for all measured modes, the following formulation for the damage index for sub-region jk is used

$$\beta_{jk} = \frac{\sum_{i=1}^{N_m}\left(f_{ijk}+1\right)}{\sum_{i=1}^{N_m}\left(f_{ijk}^{*}+1\right)} \tag{102}$$

where damage is indicated at the jk^{th} location if $\beta_{jk} > 1$. Once damage is localized, its severity can be estimated as follows

$$\alpha_{jk} = \frac{1}{\beta_{jk}} - 1 = \frac{\sum_{i=1}^{N_m}\left(f_{ijk}^{*}+1\right)}{\sum_{i=1}^{N_m}\left(f_{ijk}+1\right)} - 1, \quad \alpha_{jk} > -1 \tag{103}$$

where damage severity is indicated as the reduction in the jk^{th} member if $\alpha_{jk} < 0$. Kim and Stubbs [84] used this to indicate damage severity in terms of reduced stiffness.

A particular difficulty that exists with using mode shapes in damage assessment problems is that noise content can make mode shape extraction difficult and might create significant errors thereby generating false-positives or false-negatives. Correlation measures based on the frequency response function between damaged and undamaged structures can be useful since the error due to modal parameter extraction is eliminated, in particular when the modes are closely spaced or high damping exists in the structure.

Two frequency response functions (FRF) representing the same input-output relationship can be compared using the Frequency Response Assurance Criterion (FRAC) [71], which is defined as

$$FRAC_j = \frac{\left|\left\{\mathbf{H}^{*}(\omega_i)\right\}_j^T \left\{\mathbf{H}(\omega_i)\right\}_j\right|^2}{\left[\left\{\mathbf{H}^{*}(\omega_i)\right\}_j^T \left\{\mathbf{H}^{*}(\omega_i)\right\}_j\right]\left[\left\{\mathbf{H}(\omega_i)\right\}_j^T \left\{\mathbf{H}(\omega_i)\right\}_j\right]} \tag{104}$$

where $\{\mathbf{H}(\omega_i)\}_j$ is the FRF of the undamaged structure, superscript '*' indicates the damaged structure and j is the damage location or coordinate. This correlation measure returns a value between 0 and 1 for zero or perfect correlation.

In output-only modal analysis, the input force is not available for measurement; therefore, the FRF cannot be applied. For our work, we have modified the FRAC measure and replace the FRF with the transmissibility function, which is the frequency response between a motion response and a motion input, and are measured without the knowledge of the excitation forces. The modified FRAC function is called the Transmissibility Frequency Response Assurance Criterion (TFRAC) and defined as

$$TFRAC_j = \frac{\left|\{\mathbf{T}^*(\omega_i)\}_j^T \{\mathbf{T}(\omega_i)\}_j\right|^2}{\left[\{\mathbf{T}^*(\omega_i)\}_j^T \{\mathbf{T}^*(\omega_i)\}_j\right]\left[\{\mathbf{T}(\omega_i)\}_j^T \{\mathbf{T}(\omega_i)\}_j\right]} \tag{105}$$

where $\{\mathbf{T}(\omega_i)\}_j$ is the transmissibility function between the j^{th} measurement point and the pre-defined fixed reference measurement point.

For consistency in comparing all methods, we re-adjust all damage indicator outputs, such that a value of 1 indicates no correlation (damage) and a value of -1 indicates perfect correlation (no damage).

The aforementioned techniques were chosen because of their similar input requirements (natural frequencies, mode shapes) and their ability to identify damage without the use of a finite element model (FEM) of the structure.

7.2 Proposed Sensitivity-Based Damage Localization with Statistical Sampling

In this section, a method based on localized sensitivity of structure to changes in mass and stiffness is discussed in terms of its applicability to damage assessment. Theoretical background

for the formulation of the sensitivity approach is first given. Incorporation of sensitivity to localized changes in mass and stiffness is required to minimize stochastic errors introduced in the estimation of the modal parameters. Since the presence of measurement and modal estimation noise is unavoidable, confidence intervals are necessary to show the statistical significance of the changes caused by damage. For this reason, a statistical sampling technique, known as Monte Carlo, is employed to improve performance and to extract statistical measures of the results from the proposed damage localization technique.

7.2.1 Modal Parameter Sensitivity

The modal parameter sensitivity data is based on the undamaged state of the structure. For damage identification based on modal analysis, it is required to know how a change in the structural parameters, such as mass and stiffness, will affect the modal parameters. An important tool for the prediction of modal parameters changes is the knowledge of the derivatives of the modal parameters to the structural parameters. Many methods have been reported for the calculation of eigenvalues and eigenvector derivatives. An approach for real symmetric eigensystems was first presented by Fox and Kapoor [53]. Rogers [143] further extended the eigensystem derivative calculation to more general system matrices. With these methods the calculation of eigenvalue derivatives only requires the eigenvalue itself and the left and right eigenvectors. In contrast, the eigenvector derivative requires knowledge of all eigenvectors of the system. Without the requirement of full knowledge of the system matrices, Heylen et al. [71] derived for a linear mechanical system with general viscous damping the sensitivity modal parameters to changes in mass and stiffness can be calculated by means of the estimated poles and normalized mode shapes. In contrast to model updating methods, this approach does not require a continuously updated finite element model of the structure since the modal parameter

sensitivities are obtained from experimental measurements. The theoretical formulation and derivation hereafter is based on the derivative formulation by Heylen.

Consider the eigenvalue problem in Laplace form

$$(s\mathbf{A}+\mathbf{B})\mathbf{Y}=0 \tag{106}$$

$$\mathbf{A}=\begin{bmatrix}0 & \mathbf{M}\\ \mathbf{M} & \mathbf{C}\end{bmatrix},\mathbf{B}=\begin{bmatrix}-\mathbf{M} & 0\\ 0 & \mathbf{K}\end{bmatrix},\mathbf{Y}=\begin{bmatrix}s\mathbf{X}\\ \mathbf{X}\end{bmatrix} \tag{107}$$

where s is the Laplacian variable, $\mathbf{M}$ is the mass matrix, $\mathbf{C}$ is damping matrix, $\mathbf{K}$ is the stiffness matrix and $\mathbf{X}$ is the response vector. Eq. (106) yields N eigenvalues λ_k $(k=1,...,N)$ and eigenvectors Φ_k. The eigenvectors are orthogonal when weighted by the A and B matrices as follows

$$\mathbf{\Phi}^T\mathbf{A}\mathbf{\Phi}=a,\ \mathbf{\Phi}^T\mathbf{B}\mathbf{\Phi}=b,\ b=-a\mathbf{\Lambda} \tag{108}$$

$$a=diag\left\{a_1,...,a_N,a_1^*...,a_N^*\right\},\ \mathrm{b}=diag\left\{b_1,...,b_N,b_1^*...,b_N^*\right\} \tag{109}$$

where $\mathbf{\Lambda}$ is a diagonal matrix assembled by the eigenvalues and their complex conjugates denoted by '*', and the diagonal matrices a and b define the normalization of the eigenvectors.

Pre-multiplying the eigenvalue problem for mode k with Φ_k^T gives

$$\Phi_k^T(\lambda_k\mathbf{A}+\mathbf{B})\Phi_k=0 \tag{110}$$

Taking the derivative of Eq. (110) with respect to model parameter θ gives

$$\frac{\partial\Phi_k^T}{\partial\theta}(\lambda_k\mathbf{A}+\mathbf{B})\Phi_k+\Phi_k^T\frac{\partial(\lambda_k\mathbf{A}+\mathbf{B})}{\partial\theta}\Phi_k+\Phi_k^T(\lambda_k\mathbf{A}+\mathbf{B})\frac{\partial\Phi_k}{\partial\theta}=0 \tag{111}$$

Eq. (111) reduces to

$$\Phi_k^T\left(\frac{\partial\lambda_k}{\partial\theta}\mathbf{A}+\lambda_k\frac{\partial\mathbf{A}}{\partial\theta}+\frac{\partial\mathbf{B}}{\partial\theta}\right)\Phi_k=0 \tag{112}$$

The sensitivity of an eigenvalue to a change of parameter θ is given by Heylen as

$$\frac{\partial \lambda_k}{\partial \theta} = -\frac{1}{a_k} \Phi_k^T \left(\lambda_k \frac{\partial \mathbf{A}}{\partial \theta} + \frac{\partial \mathbf{B}}{\partial \theta} \right) \Phi_k \tag{113}$$

Since the eigenvectors define a base for the $2N \times 2N$ vectorspace (2x due to complex conjugate), the partial derivative for an eigenvector can be written as follows

$$\frac{\partial \Phi_k}{\partial \theta} = \sum_{i=1}^{2N} \rho_{ki} \Phi_k \tag{114}$$

where ρ_{ki} is a coefficient that enables the calculation of the mode shape sensitivities. Taking the derivative of Eq. (110), pre-multiplying by Φ_k^T and combining with Eq. (114) yields

$$\Phi_k^T \left(\lambda_k \mathbf{A} + \mathbf{B} \right) \frac{\partial \Phi_k}{\partial \theta} + \Phi_k^T \frac{\partial \left(\lambda_k \mathbf{A} + \mathbf{B} \right)}{\partial \theta} \Phi_k = 0 \tag{115}$$

Applying the orthogonality relationship defined in Eqn. (108), the ρ_{ki} coefficients can be obtained. In [71], the expressions for the coefficients ρ_{ki} are derived as

$$\rho_{ki} = \begin{cases} \dfrac{1}{a_i (\lambda_i - \lambda_k)} \Phi_i^T \left(\lambda_k \dfrac{\partial \mathbf{A}}{\partial \theta} + \dfrac{\partial \mathbf{B}}{\partial \theta} \right) \Phi_k & , \text{for } k \neq i \\ -\dfrac{1}{2a_k} \Phi_k^T \dfrac{\partial \mathbf{A}}{\partial \theta} \Phi_k & , \text{for } k = i \end{cases} \tag{116}$$

Combining Eqs. (114) and (116) yields the eigenvector derivative as

$$\frac{\partial \Phi_k}{\partial \theta} = -\frac{1}{2a_k} \Phi_k^T \frac{\partial \mathbf{A}}{\partial \theta} \Phi_k + \sum_{i=1, i \neq k}^{2N} \frac{1}{a_i (\lambda_i - \lambda_k)} \Phi_i^T \left(\lambda_k \frac{\partial \mathbf{A}}{\partial \theta} + \frac{\partial \mathbf{B}}{\partial \theta} \right) \Phi_k \Phi_i \tag{117}$$

In terms of mode shape vectors ϕ_k, mass, damping and stiffness matrices, the modal sensitivities are given by

$$\frac{\partial \lambda_k}{\partial \theta} = -\frac{1}{a_k} \phi_k^T \left(\lambda_k^2 \frac{\partial \mathbf{M}}{\partial \theta} + \lambda_k \frac{\partial \mathbf{C}}{\partial \theta} + \frac{\partial \mathbf{K}}{\partial \theta} \right) \phi_k \tag{118}$$

$$\frac{\partial \phi_k}{\partial \theta} = -\frac{1}{2a_k}\phi_k^T\left(2\lambda_k\frac{\partial \mathbf{M}}{\partial \theta}+\frac{\partial \mathbf{C}}{\partial \theta}\right)\phi_k\phi_k + \sum_{i=1,i\neq k}^{2N}\frac{1}{a_i(\lambda_i-\lambda_k)}\phi_i^T\left(\lambda_k^2\frac{\partial \mathbf{M}}{\partial \theta}+\lambda_k\frac{\partial \mathbf{C}}{\partial \theta}+\frac{\partial \mathbf{K}}{\partial \theta}\right)\phi_k\phi_i$$

(119)

The modal scaling factor a_k of mode k depends on the chosen normalization scheme [71]. For the general viscous damped system, Eqs. (118)-(119) are only exact if all modes with corresponding complex conjugates of the structure are available and taken into account. Therefore, a truncation error was introduced by Heylen in the calculated sensitivities of the identified mode shape estimates due to the lack of the remaining modes. However, the expressions for the sensitivity of the modal parameters is a good approximation even if only a limited number of modes are experimentally available, which in general is the case.

For an undamped system, a unit modal normalization scheme can be used for the normalization of the mode shapes. In this case, the modal scaling factor is then given by

$$a_k = 2i\omega_k \tag{120}$$

Provided that the modal model can be written as

$$\mathbf{H}(\omega) = \sum_{k=1}^{N_m}\left(\frac{\mathbf{R}_k}{i\omega - i\omega_k}+\frac{\mathbf{R}_k^*}{i\omega + i\omega_k}\right) = \sum_{k=1}^{N_m}\left(\frac{\phi_r\phi_r^T}{(i\omega - i\omega_k)a_k}+\frac{\phi_r^*\phi_r^H}{(i\omega + i\omega_k)a_k^*}\right) \tag{121}$$

The elements of the mass normalized mode shapes can be obtained from

$$\phi_{jk} = a_k\frac{\mathbf{R}_{[j,o],r}}{\sqrt{a_k\mathbf{R}_{[o,o],r}}} \tag{122}$$

where $\mathbf{R}_k$ is the residue matrix for mode k.

For an undamped system, Eqs. (118)-(119) become

$$\frac{\partial \omega_k}{\partial \theta} = \frac{1}{2}\phi_k^T\left(-\omega_k\frac{\partial \mathbf{M}}{\partial \theta}+\frac{1}{\omega_k}\frac{\partial \mathbf{K}}{\partial \theta}\right)\phi_k \tag{123}$$

$$\frac{\partial \phi_k}{\partial \theta} = -\frac{1}{2}\phi_k^T \frac{\partial \mathbf{M}}{\partial \theta}\phi_k \phi_k + \sum_{i=1, i\neq k}^{N} \frac{1}{\left(\omega_k^2 - \omega_i^2\right)} \phi_i^T \left(-\omega_k^2 \frac{\partial \mathbf{M}}{\partial \theta} + \frac{\partial \mathbf{K}}{\partial \theta}\right)\phi_k \phi_i \tag{124}$$

In structural health monitoring applications, structural defects are typically assumed as local reductions in stiffness. For the sensitivity analysis, changes in local stiffness and local mass will be taken into account. The sensitivity analysis due to mass changes will serve useful in experimental cases were damage was simulated by means of local mass modifications.

For simple modifications, such as a local mass change, a change of linear spring stiffness between two DOFs, the actual mass or stiffness must not be known. In the case of an undamped system, and for the case of a local mass change in DOF r, the sensitivities of the k^{th} natural frequency, and k^{th} mode shape at DOF j are given respectively as

$$\frac{\partial \omega_k}{\partial m_r} = -\frac{\omega_k}{2}\phi_{rk}^2 \tag{125}$$

$$\frac{\partial \phi_{jk}}{\partial m_r} = -\frac{\phi_{jk}^2}{2}\phi_{jk} + \phi_{rk} \sum_{i=1, i\neq k}^{N} \frac{\omega_k^2}{\omega_i^2 - \omega_k^2}\phi_{rk}\phi_{ji} \tag{126}$$

For the case of a local stiffness change in DOF r, the sensitivities of the k^{th} natural frequency, and k^{th} mode shape between DOFs p and q are given respectively as

$$\frac{\partial \omega_k}{\partial k_{pq}} = \frac{\left(\phi_{pk} - \phi_{qk}\right)^2}{2\omega_k} \tag{127}$$

$$\frac{\partial \phi_{jk}}{\partial k_{pq}} = \left(\phi_{pk} - \phi_{qk}\right) \sum_{i=1, i\neq k}^{N_m} \frac{1}{\omega_k^2 - \omega_i^2}\left(\phi_{pi} - \phi_{qi}\right)\phi_{ji} \tag{128}$$

where N_m is the total number of modes of the system. In practice, only a limited number of modes are identified, but generally, the sensitivities can still be approximated using Eqs. (125)-(128).

7.2.2 Sensitivity-Based Modal Correlation

To improve damage localization results based on experimental modal parameters, we propose the following modal parameter sensitivity approach. Recognizing that each sensor location has a different sensitivity to structural changes at a specific location. We applied the derived sensitivity operators based on derivatives of known modal parameters to a modified mode shape correlation method. The proposed approach takes into account the fact that not all sensor locations will provide equal level of information when damage is localized to a particular area.

For a system with N_{DOF} measurement outputs, the k^{th} frequency-based and mode shape-based sensitivity matrices due to mass changes are given respectively as follows

$$\mathbf{S}_k^{(\omega)} = \left[\frac{\partial \omega_k}{\partial \theta_1}, ..., \frac{\partial \omega_k}{\partial \theta_r}, ..., \frac{\partial \omega_k}{\partial \theta_{N_{DOF}}} \right] \tag{129}$$

$$\mathbf{S}_k^{(\phi)} = \left[\frac{\partial \phi_k}{\partial \theta_1}, ..., \frac{\partial \phi_k}{\partial \theta_r}, ..., \frac{\partial \phi_k}{\partial \theta_{N_{DOF}}} \right] \tag{130}$$

where $\theta_r = \{m_r, k_{pq}\}$ indicates the localized modification at DOF r or between DOFs p and q, $\mathbf{S}_k^{(\phi)}$ is an $N_m \times N_{DOF}$ sensitivity matrix, and $\mathbf{S}_k^{(\omega)}$ is an $1 \times N_{DOF}$ sensitivity matrix.

By applying Eqs. (129)-(130) to all available or considered modes N_m, the overall sensitivity matrices for the eigenfrequencies and mode shapes are defined as follows

$$\mathbf{S}^{(\omega)} = \left[\mathbf{S}_1^{(\omega)}, \mathbf{S}_2^{(\omega)}, ..., \mathbf{S}_{N_m}^{(\omega)} \right] \tag{131}$$

$$\mathbf{S}^{(\phi)} = \left[\mathbf{S}_1^{(\phi)}, \mathbf{S}_2^{(\phi)}, ..., \mathbf{S}_{N_m}^{(\phi)} \right] \tag{132}$$

where $\mathbf{S}^{(\phi)}$ is an $N_m \times (N_m * N_{DOF})$ sensitivity matrix, and $\mathbf{S}^{(\omega)}$ is an $N_m \times N_{DOF}$ sensitivity matrix.

The objective in determining the sensitivity matrices is to improve the damage localization performance of the baseline damage localization methods. For this work, a sensitivity-analysis damage index (SDI) is developed using the mode shape sensitivity matrix and is defined as follows

$$SDI_j = \frac{\sum_{i=1}^{N_m} \mathbf{S}_i^{(\phi)} \left| \phi_{ji} - \phi_{ji}^* \right|}{2N_m} \tag{133}$$

A comparison of the input requirements for the proposed SDI and baseline damage localization techniques is given in Table 7.1.

Table 7.1. Input requirements for the damage identification methods. Input criteria - natural frequencies 'ω', operational mode shapes 'ϕ', operational mode shape curvature 'ϕ"', and frequency response '$H(\omega)$'.

	input criteria			
	ω	ϕ	ϕ"	$H(\omega)$
COMAC		X		X
MSC		X	X	X
SEDI		X	X	X
TFRAC				X
MAC		X		X
SDI	X	X		X

The latter mode shape- and frequency-based damage localization methods are based on the assumption that mode shapes and frequency response are correctly measured with minimal normal variability. In practice, measurement errors are bound to exist. System identification based on modal parameters is a powerful technique for building accurate parametric models of complex system under noisy data. In operational modal analysis, also known as ambient vibration testing, one of the main challenges is assessing the quality of the processed vibration test results when there is no previous reference for a dynamic properties of a structure. Reliability or

confidence in the extracted modal parameters from operational modal analysis may be questionable because of various uncertainties that impact different stages of the testing and analysis process. Numerous investigations have taken extracted modal properties and applied them to damage assessment problems. Vibration-based damage assessment, particularly in operational modal analysis, can be linked to high-levels of uncertainty in its implementation and interpretation.

Many researchers have discounted the value of conducting investigations into the behavior of the actual structural systems and its uncertainties. As a consequence, published research has claimed success for a multitude of isolated structural systems or components without facing a critical important and fundamental question of "how can the results obtained from a specific structure be generalized to provide information applicable to other structures?" As a consequence, the possibility of direct application of results from many experimental tests to real-world structural systems is rather limited.

7.2.3 Statistical Sampling

Discrimination of damage data, in terms of detection and localization, from healthy data is a question of evaluating the modal parameters distributions and/or boundaries. In order to obtain modal parameters distribution, the variance on the power spectrum estimates of the response signals must be evaluated. To improve damage localization results based on experimental modal parameters, we introduce the following statistical sampling approach. The particular statistical sampling approach is based on the work by Farrar et al. [49] which was applied to Alamosa Canyon Bridge damage assessment problem.

Using the assumption that the primary errors in the modal extraction process are random and uncorrelated with excitation and structural responses, and that the excitation input is from a single

source, the confidence interval $\sigma_\mu(\cdot)$ on the estimate mean of the auto and cross power spectra $\hat{\mathbf{G}}_{ij}$ magnitude is (according to Bendat and Piersol, 1980, [13])

$$\sigma_\mu\left(\left|\hat{\mathbf{G}}_{ij}(\omega)\right|\right) = \frac{\left|\hat{\mathbf{G}}_{ij}(\omega)\right|}{\left|\gamma_{ij}(\omega)\right|\sqrt{N_d}} \tag{134}$$

$$\hat{\gamma}_{ij}(\omega) = \frac{\left|\hat{\mathbf{G}}_{ij}(\omega)\right|^2}{\hat{\mathbf{G}}_{ii}(\omega)\hat{\mathbf{G}}_{jj}(\omega)} \tag{135}$$

where N_d is the number of the estimated auto- and cross-power spectra, $\hat{\gamma}_{ij}$ is the estimated coherence function.

For the problem at hand, it is important to note that biases in the signal are not taken into account. Bias errors generally arise from nonlinear and/or time-varying system parameters, propagation in time delays, correlated noise, among others. The statistical estimates of the spectral parameters are assumed to be free of biases. The work herein derives the statistical error analysis formulas for measurements of spectral density functions and associated modal parameter estimates. The derived statistical error estimates derived by Bendat et al. [13] and utilized by Farrar et al. [49] can be and have been used in multiple applications, which include the simulation of random environments for structural dynamics testing at multiple locations and directions, the determination of natural frequencies and modes of vibration of offshore platforms and bridges from accelerometer measurements of multiple recordings of ambient response data only [48]. As stated by Bendat, the key element that makes advanced applications, such as damage assessment, is the ability to distinguish statistical estimation errors (false-positives or false-negatives in damage diagnosis) from actual system changes, such as damage.

Typically, a Gaussian distribution is assumed, so that a percentage confidence level can be associated with the confidence interval $\sigma_\mu(\cdot)$. It should be noted that Eq. (134) are estimates of

the confidence intervals and not estimates of the standard deviation. The relationship between the estimate of the population standard deviation, $\sigma(\cdot)$, and the confidence interval on the mean estimate, $\sigma_\mu(\cdot)$, is given as

$$\sigma = \sigma_\mu \sqrt{N_d} \tag{136}$$

Now, the estimates of the standard deviation of the auto- and cross-power spectra are

$$\sigma\left(\left|\hat{\mathbf{G}}_{ij}(\omega)\right|\right) = \frac{\left|\hat{\mathbf{G}}_{ij}(\omega)\right|}{\left|\gamma_{ij}(\omega)\right|} \tag{137}$$

Alternatively, the most direct approach of deriving noise information on output-only data is to divide each response data sequence of N_t samples into P non-overlapping segments of D samples each, such that $P \times D < N_t$. Estimates of the average auto- and cross spectra estimates can be obtained from

$$\hat{\mathbf{G}}_{ij}(\omega) = \frac{1}{P}\sum_{r=0}^{P-1} \hat{\mathbf{G}}_{ij}^{(r)}(\omega) \tag{138}$$

where $\hat{\mathbf{G}}_{ij}$ is the average of P independent observations given that little or no overlap exists among all segments. Given that excitation is considered stationary, an estimate of the standard deviation of the cross power spectra is given by

$$\sigma\left(\left|\hat{\mathbf{G}}_{ij}(\omega)\right|\right) = \sqrt{\frac{1}{P-1}\sum_{r=0}^{P-1}\left|\hat{\mathbf{G}}_{ij}^{(r)}(\omega) - \hat{\mathbf{G}}_{ij}(\omega)\right|^2} \tag{139}$$

One drawback of using Eq. (139) to measure the standard deviation is overestimation of variance due to non-stationary excitation. Additionally, if only a limited number of time response samples are available, averaging reduces the spectral resolution and increases the possibility of introducing leakage errors into the estimates.

Given that the statistics of the spectral function errors are estimated, the next step is to propagate these errors through the modal parameter identification procedure. For this analysis, a statistical sampling technique will be applied to estimate the statistical measures of modal parameters. Two common methods to achieve this is by using Monte Carlo or bootstrap simulations. These two sampling techniques are discussed next.

The Monte Carlo method, which is a procedure where data is repeatedly simulated using an assumed statistical distribution of error on the data. The modal identification procedure is then applied to each of the simulated data sets, producing a set of identified modal parameters. After numerous simulations, the distribution of the modal parameters is assumed to be representative of the true distribution of the modal parameters. Figure 7.1 shows the overall process for applying the Monte Carlo method to estimate modal parameters statistics. The main drawback of Monte Carlo method is that it assumes the type of distribution of the variability of the test data.

An alternative to the Monte Carlo method is the bootstrap method, which randomly selects individual cross power spectra $\hat{\mathbf{G}}_{ij}$ measurements from the P non-overlapping segments to form the ensemble average. For each cross power spectra $\hat{\mathbf{G}}_{ij}$, the samples are selected at random and with replacement.

The bootstrap method is advantageous because it does not require an assumption of the form of the statistical distribution of the data. Once the randomly ensemble averages are formed, the operational modal analysis procedure is applied, which is repeated numerous times to form a histogram of the identified modal parameters. Using this histogram, statistics for the distribution of the modal parameters can be estimated.

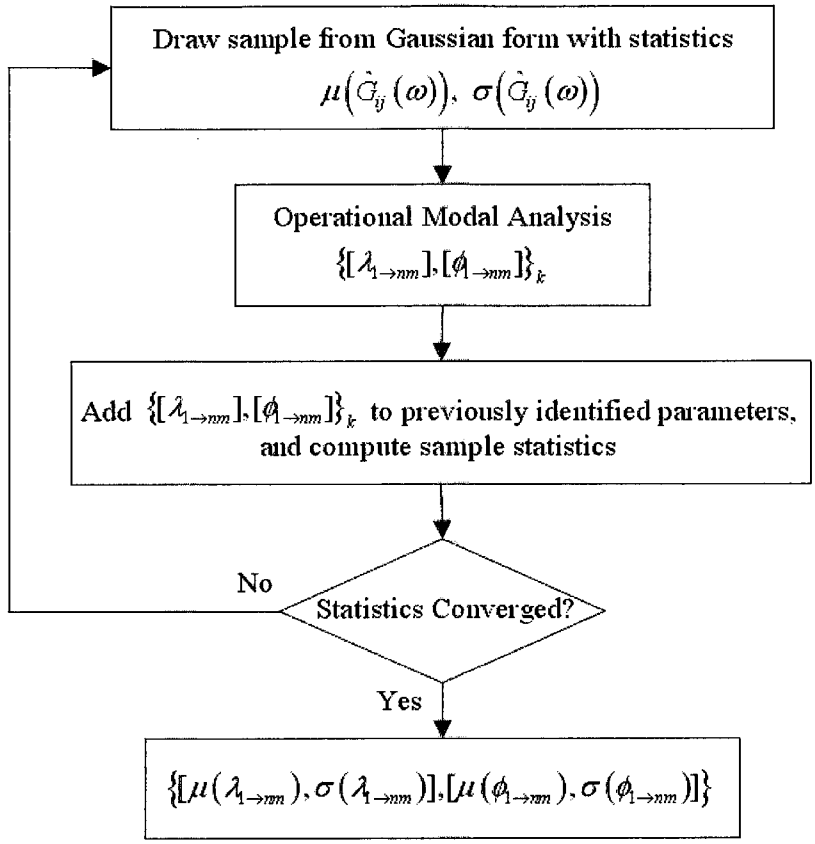

Figure 7.1. Monte Carlo procedure for estimating statistical measures of modal parameters.

Numerous other sampling techniques, such as Markov Chain Monte Carlo (MCMC), Gibbs sampling, and particle filter [75], have been proposed and used in the study of damage assessment with uncertainty. In this work, the Monte Carlo method will be utilized to quantify confidence levels of modal parameters and damage indicators. We chose to work with Monte Carlo simulation because of its simplicity and assumed Gaussian distribution, which can be easily described via well known statistical measures such as mean and variance.

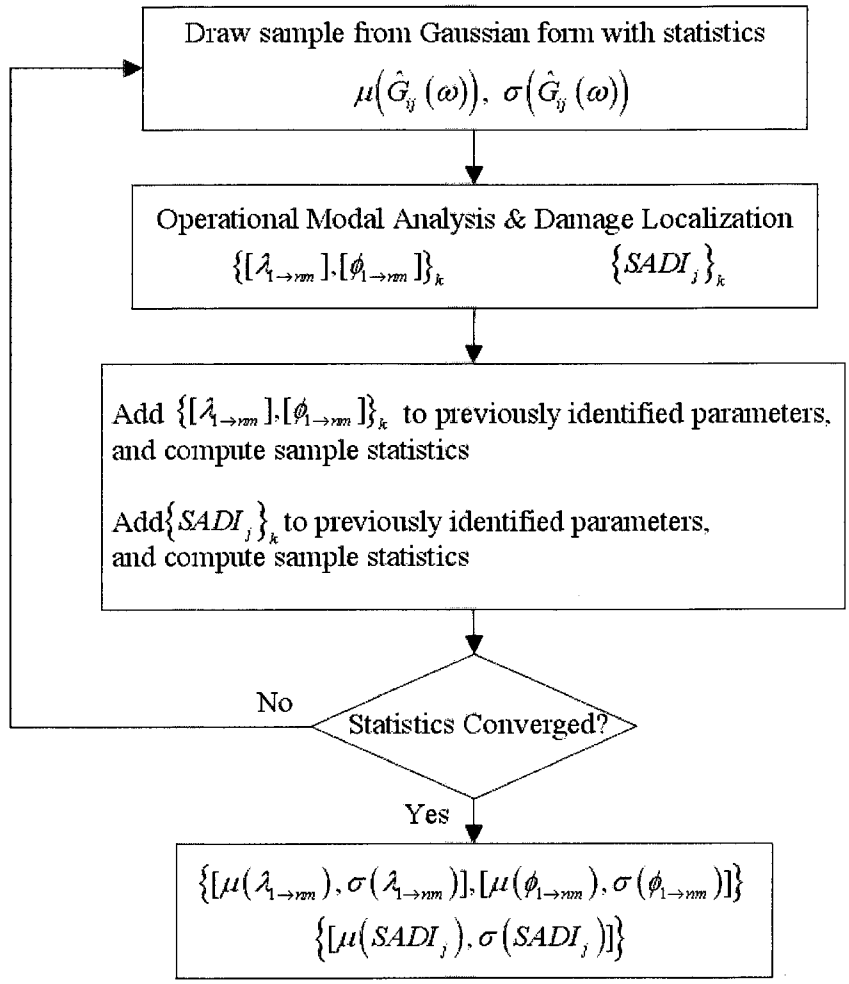

Figure 7.2. Monte Carlo method for estimating statistical measures of modal parameters, $\{\lambda,\phi\}$ (both undamaged and damaged states), and damage localization indicator, DI_{ij}, at each coordinate (i, j).

It is unavoidable that modal parameter estimation is always obtained with uncertainties. In practice the error in measured natural frequencies is negligible in comparison to the measurement error in the mode shapes. Taking into consideration that most of the damage localization techniques utilize some sort of mode shape correlation, it is important to quantify the uncertainty

associated with the damage localization metric obtained. Ideally, multiple measurements would be necessary to quantify the statistical measures of the obtained damage localization metric.

The extraction of operational mode shapes requires averaged auto and cross power spectral responses, and to extract multiple sets of operational mode shapes would be too exhaustive, and not always practical. The propagation of the mode shape and natural frequencies uncertainty levels to damage localization estimates will be studied via the previously described Monte Carlo method. Figure 7.2 shows the steps to implement the Monte Carlo procedure for estimating the statistical measures of the modal parameters and damage localization indicator.

7.3 Case Study I: Damage Localization for Plate Experiment

For a more quantitative comparison among the test cases, the damage localization indicators discussed in sections 7.1 and 7.2 were calculated and used for damage localization. The methods evaluated for damage localization are the coordinate modal assurance criterion (COMAC), strain energy damage index (SEDI), mode shape curvature (MSC), transmissibility frequency response assurance criterion (TFRAC), and the proposed sensitivity-analysis damage index (SDI) method. These techniques were chosen because of their similar input requirement, in other words frequencies and mode shapes, and their ability to identify damage without the use of a computational model of the structure. The damage localization techniques were applied to the 6 different plate damage scenarios previously described.

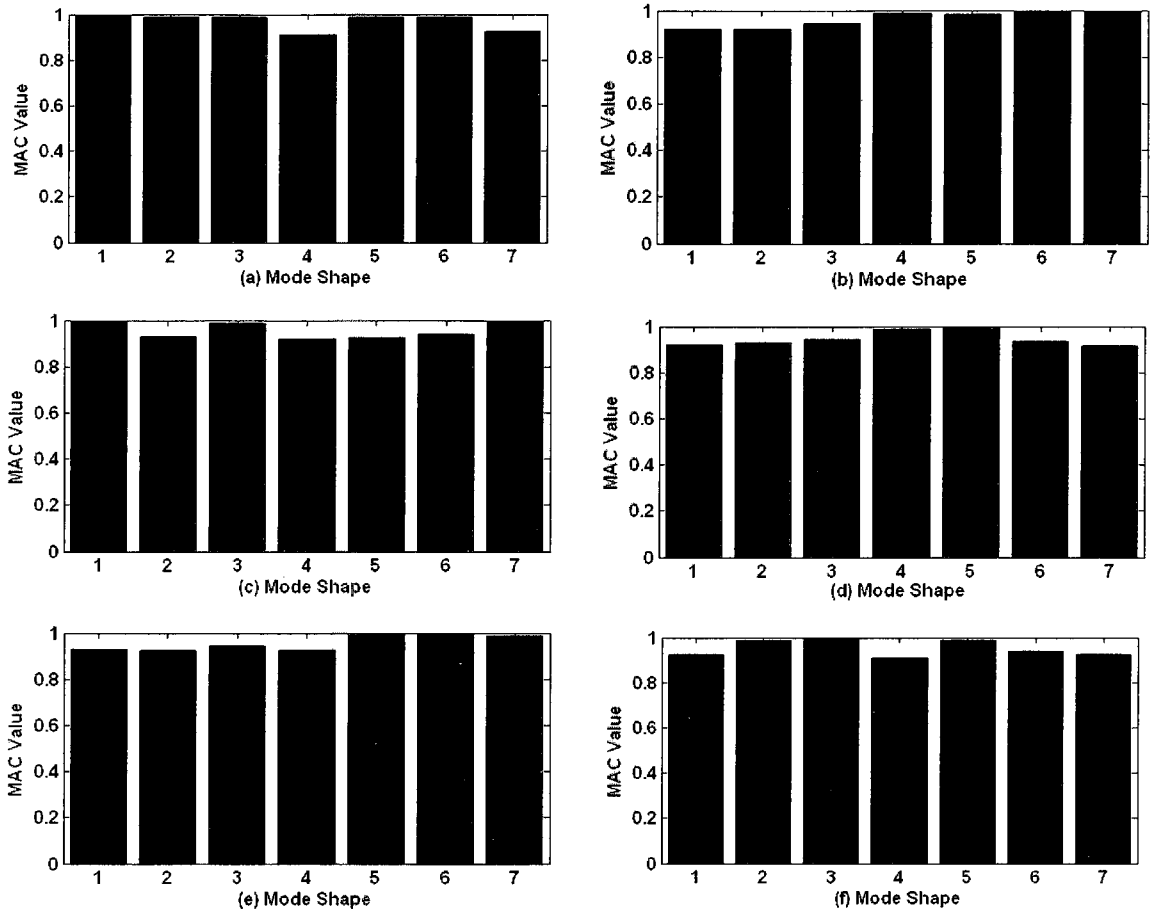

Figure 7.3. Diagonal MAC values between the mode shapes of the undamaged and damaged conditions for the plate experiment. MAC values for each damage condition 1-6 are shown in (a)-(f), respectively.

The differences between the undamaged and damaged conditions of the mode shapes are shown via the MAC values in Figure 7.3. Values close to 1 show high correlation, and values that deviate from 1 show lower correlation. According to the diagonal MAC values, the largest changes in mode shapes are not consistent throughout all damage conditions. Therefore, choosing modes that clearly and consistently indicate deviation from undamaged conditions cannot be made. Visual comparison of the MAC values of damage case 1 and case 6, Figure 7.3 (a) and (f) respectively, the MAC value for case 6 are overall a bit lower, which is due to the increasing mass modifications.

7.3.1 Damage Localization Results

The damage localization results are presented graphically. In the damage localization graphs, each node represents the location of an accelerometer. The damage indices for each DOF were plotted using finite element mesh, where a red color represents low correlation, and blue indicates high correlation. The true location of damage in these finite element models is indicated by a red circle.

For the first damage analysis series, the COMAC method was utilized for damage localization of the free-free boundary aluminum plate. With all 7 mode shapes taken into account, the COMAC method is not able to give a good approximation of the true location of the mass modification, see Figure 7.4. For the first three damage cases, where the mass modification is made on the top-left corner, the COMAC does provide approximate damage indications near the true damage location. For the first damage case, false-positive damage locations are given at the lower left-corner and at the right midsection of the plate. For the second and third damage cases, a substantial false-positive damage area is indicated in the lower-left midsection of the plate. For the damage cases 4-6, the damage is not localized at all, and substantial false-positive areas are given.

Next, the MSC damage localization method results are provided in Figure 7.5. This method used the curvature of the mode shapes as its basis for modal parameter correlation. Visual analysis shows that the results obtained using this particular method provided very imprecise indication of the true damage location. Multiple false-positives are seen through out the plate in all cases. For the third damage case, the lowest DOF correlation is indicated near the true damage location, which is a positive result. For cases 4 and 5, the lowest correlation is indicated just right of the true damage location. For case 6 where two mass modifications were utilized, the lowest level of DOF correlation are indicated near the true damage locations, but not very clearly.

For the SEDI damage identification method, its results shown in Figure 7.6 demonstrate also a poor performance in terms of correctly isolating the true damage location(s). For cases 1-3, the SEDI method provides approximate location of the damage at L1 near the top left-corner, but false-positives remain throughout the rest of the DOFs. For cases 4-6, the SEDI method completely fails to recognize any potential damage near the true damage location at the left midsection of the plate. For case 6 with the double mass modification.

The results of the TFRAC method are shown in Figure 7.7. In comparison to the MSC and SEDI results, the TFRAC provides 'cleaner' results with more localized damage indicators, which is very similar to the COMAC method results. For the smallest mass modification of case 1, the TFRAC method does not indicate any damage near the true damage location, and gives a major false-positive at the lower end of the plate. For cases 2 and 3, damage was localized at the top left corner of the plate. A symmetric damage location was also identified at the bottom left corner. Both cases also show a false-positive at the right top corner.

In contrast to the other baseline methods, for cases 4 and 5, the TFRAC provides a good location approximation for the mass modification at the left midsection. False-positive indications of lower strength (severity) are given at other locations, however overall the results are positive in comparison to the other methods. Case 6 also provides a good approximation of damage in the top-left corner. The midsection L2 mass modification is not well approximated. One observation is that most of the damage indication is localized to the left portion of the plate, which contains both mass modifications. The indication shown on the right midsection is again at the symmetric location of the true damage location.

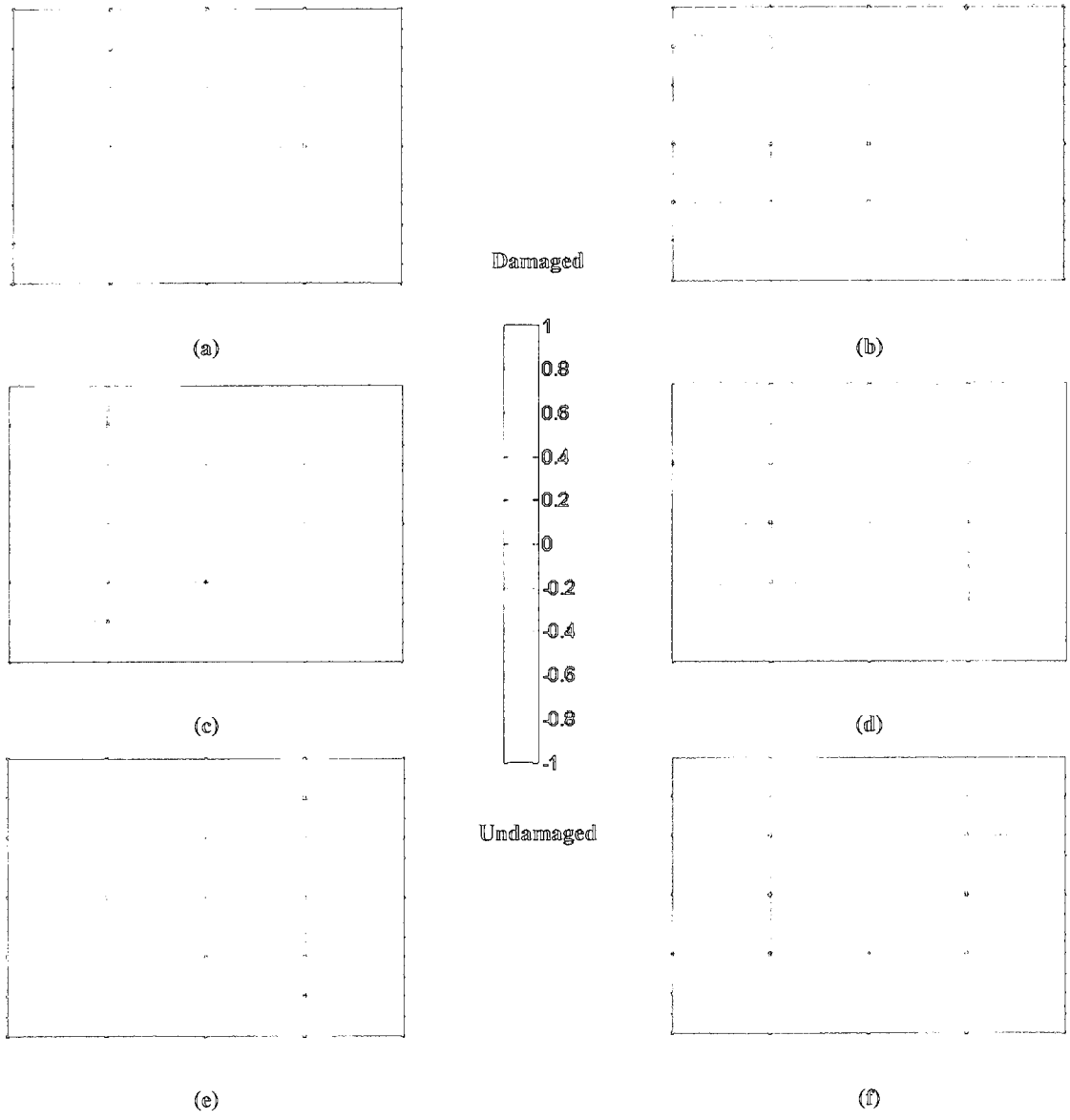

Figure 7.4. Normalized COMAC values on the basis of 7 mode shapes of the undamaged and damaged conditions. COMAC values for each damage condition 1-6 are shown in (a)-(f), respectively. True damage location indicated by red circle.

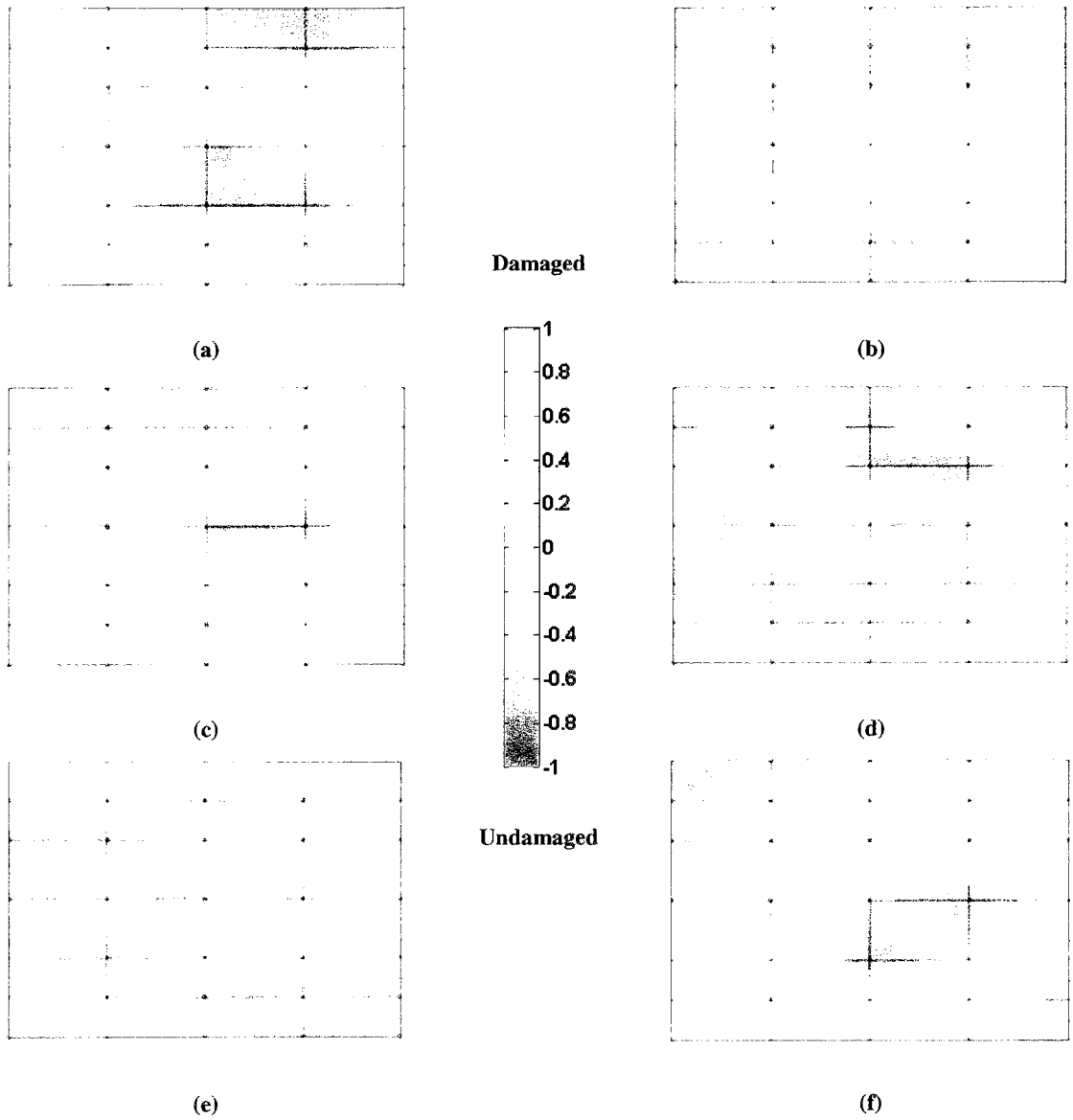

Figure 7.5. Normalized MSC values on the basis of 7 mode shapes of the undamaged and damaged conditions. MSC values for each damage condition 1-6 are shown in (a)-(f), respectively. True damage location indicated by red circle.

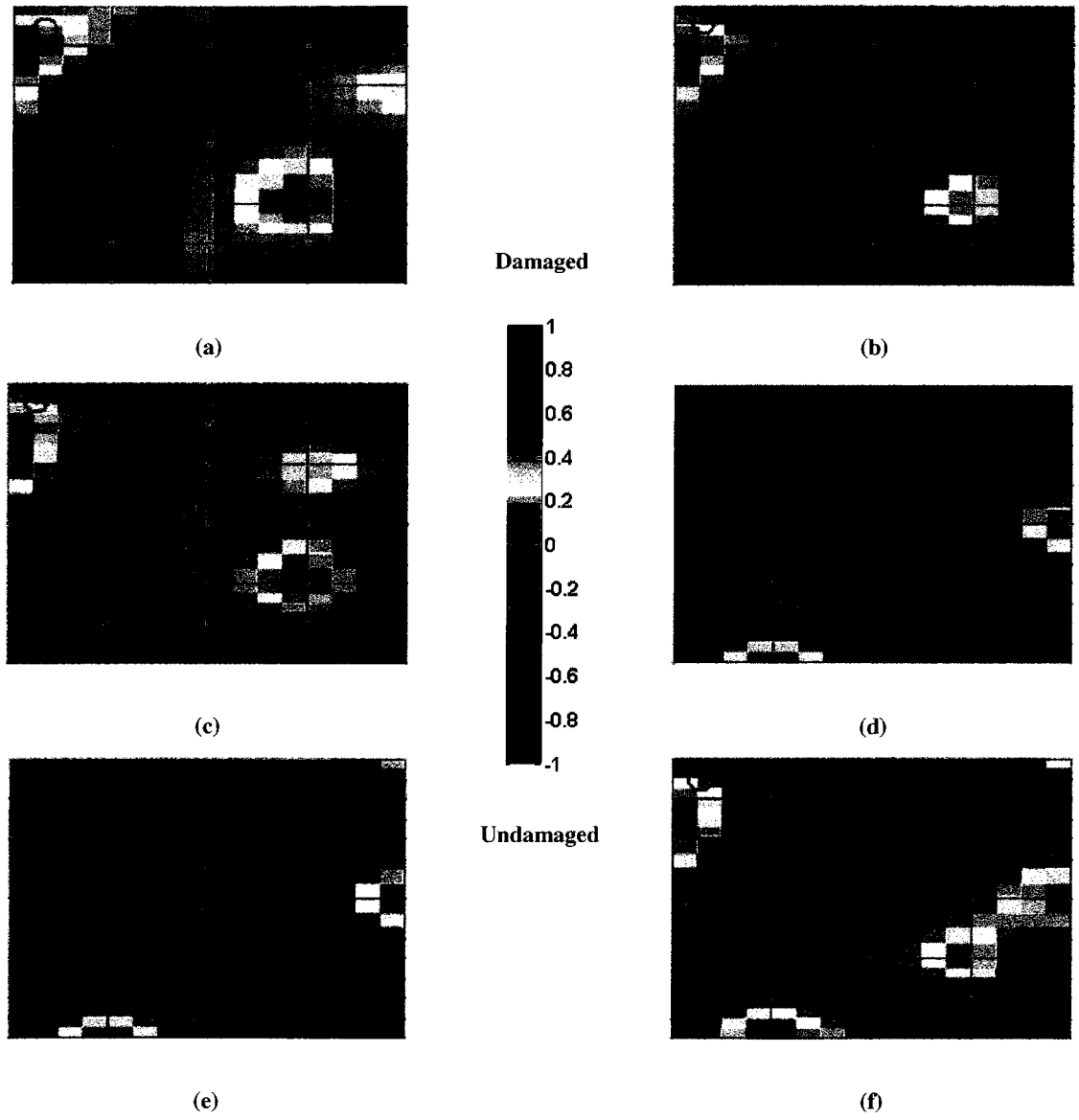

Figure 7.6. Normalized SEDI values on the basis of 7 mode shapes of the undamaged and damaged conditions. SEDI values for each damage condition 1-6 are shown in (a)-(f), respectively.

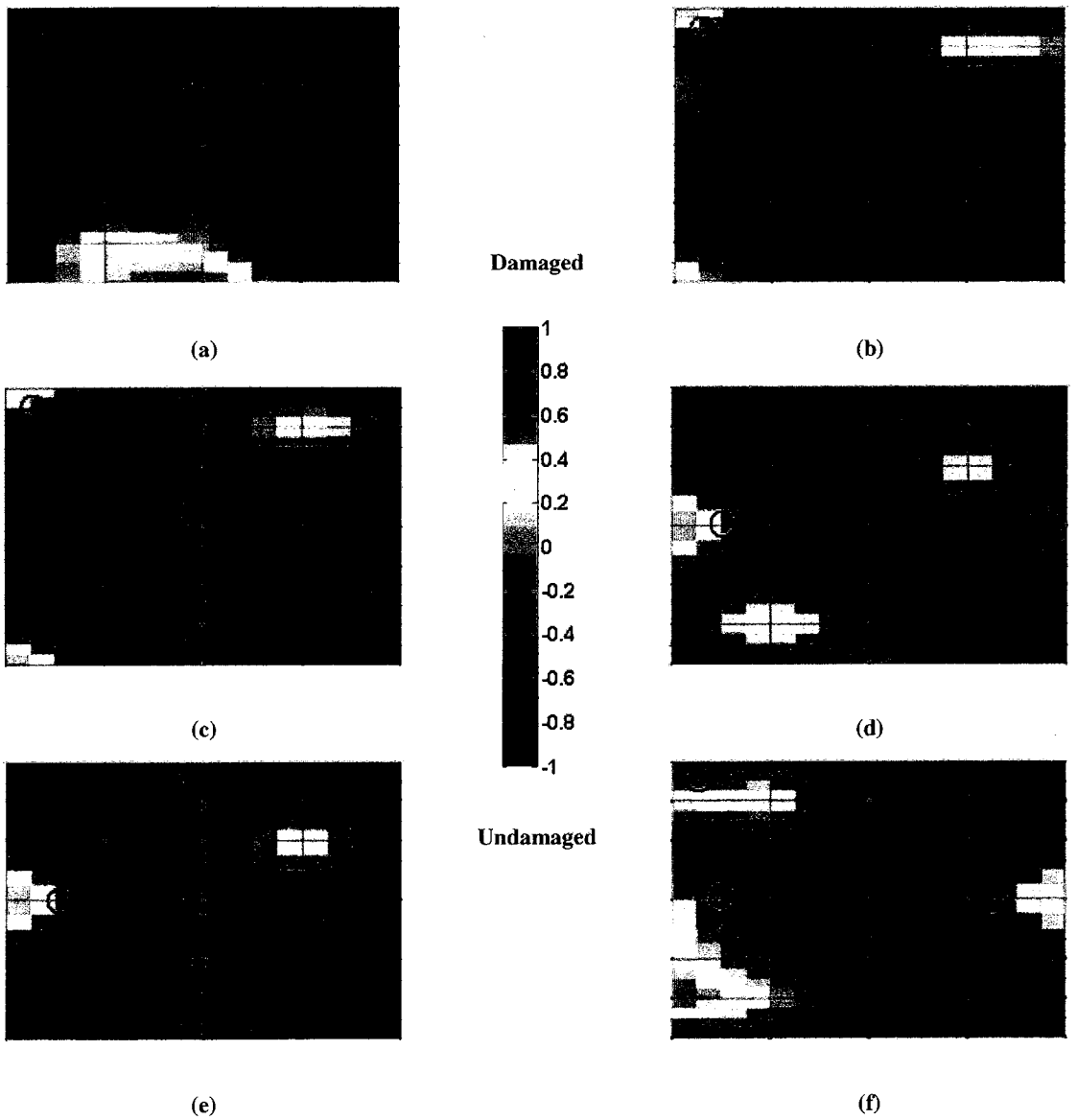

Figure 7.7. Normalized TFRAC values on the basis of 7 mode shapes of the undamaged and damaged conditions. TFRAC values for each damage condition 1-6 are shown in (a)-(f), respectively. True damage location indicated by red circle.

The TFRAC method, based on direct use of DOF transmissibility, seems to produce better results in comparison to the other baseline methods, which are based on mode shapes or mode shape curvature. The improved TFRAC results are primarily due to the increased noise content which exists in the approximated mode shapes, and also the derived mode shape curvatures. Because the TFRAC method used the direct transmissibility measurements to correlate the plate sensor measurements by each DOF, the noise content is limited to the signal processing process. Because the mode shapes extraction require additional data transformation steps, important information is lost and the relative noise content is increased due to the mode identification process. This increase in overall noise content explains the spread on damage indication observed in the MSC and SEDI results, Figure 7.5 and Figure 7.6 respectively. These two methods require additional steps to extract mode shape curvature, which further amplifies noise levels.

Hence, we come across a significant problem since the same feature extraction processes used to obtain damage indication and isolation, are magnifying the noise that exists in the analyzed data. Damage identification methods, such as the MSC and SEDI methods, make the assumption that modal parameter changes in all structures can be obtained via a general direct and almost blind application of mode shape derivatives and their numerical integration, which becomes a significant problem when noise is at the same or greater level of the damage being sought and identified. Therefore, these results demonstrate the increased need for domain specific knowledge about the structure under analysis.

One advantage of the proposed SDI damage assessment process is the capability of obtaining estimates on the confidence intervals of the identified mode shapes. As previously stated, the Monte Carlo sampling technique was utilized to obtain statistical measures. For this particular Monte Carlo study, convergence of the estimated statistical measures was obtained after approximately 70 runs.

Table 7.2 shows the 3σ statistical variance measures obtained for each mode shape at each measurement output. The 99.7% confidence bound $CB_{3\sigma}$ values for the i^{th} DOF and j^{th} mode shape are defined as

$$CB_{3\sigma} = \frac{3\sigma\left(\hat{\phi}_{ij}\right)}{\mu\left(\hat{\phi}_{ij}\right)} \times 100\% \tag{140}$$

The mode shape change due to damage is defined as

$$\Delta\phi_{ij} = \frac{\left|\phi_{ij}^{d} - \phi_{ij}^{u}\right|}{\phi_{ij}^{u}} \tag{141}$$

where the superscripts u and d refer to modes from the undamaged and damaged conditions, respectively.

Comparing the undamaged case and damaged case 3, Table 7.3 shows the absolute mean-to-mean change for each mode shape at each measurement output. Comparing the statistical variance error per mode shape in Table 7.2 and the average change in mode shape in Table 7.3 shows that the 3σ confidence intervals often exceed the changes resulting from damage. Only modes 1 and 3 show a bigger average error under the damage condition when compared to the undamaged 3σ average error. Although some of the mode shapes undergo significant $(>4\%)$ average change, none of the degrees of freedom undergo a consistent change greater than the 3σ over all modes.

Although the obtained statistical measures are only estimates, the results demonstrate the difficulty in obtaining damage indicators that exceed noise error. Basing our damage detection and localization analysis using just statistical measures would not be sufficient, and it would render significant false-diagnosis. In this particular case, based on the statistical measures, the diagnosis would be of a false-negative since the confidence intervals exceed the changes caused

by the mass modification. Therefore, with limited measurement data, the estimated statistical measures cannot be directly used to detect and localize damage. Using the mean mode shape parameter values extracted using the Monte Carlo method, we performed damage assessment based on the proposed SDI method.

The damage localization results of the proposed sensitivity-based SDI method are shown in Figure 7.8. Overall, the damage localization results obtained using the proposed method contain higher accuracy and reduced false-positives. For the smallest mass modification of case 1, the damage location was well approximated with the only drawback that a smaller severity area spread over the top half of the plate is also indicated. In contrast to the baseline methods, the proposed method provided improved results, especially for case 3 where the damage was well localized and false-positives were almost non-existent. For cases 4-5, the lowest correlation indications were given well in the vicinity of the true damage locations. For case 6, both damage locations were identified, but it did contain false-positives at the symmetric locations of the true damage locations.

Table 7.2. Undamaged case confidence bound at 3σ for identified mode shape parameters.

Measurement Output	Mode 1	Mode 2	Mode 3	Mode 8	Mode 9	Mode 10	Mode 13
1	2.39%	0.80%	12.41%	3.92%	3.36%	3.16%	5.13%
2	1.72%	2.99%	1.28%	4.29%	13.73%	4.60%	10.26%
3	0.70%	3.54%	1.95%	7.11%	3.36%	1.96%	15.12%
4	2.26%	2.17%	7.11%	5.32%	13.46%	4.80%	10.83%
5	2.84%	0.70%	4.94%	5.35%	3.73%	3.24%	5.91%
6	2.08%	1.99%	11.24%	2.65%	10.54%	3.65%	10.01%
7	1.43%	1.90%	3.26%	1.78%	7.26%	6.49%	5.23%
8	0.97%	2.18%	7.18%	2.04%	4.00%	2.27%	20.05%
9	1.77%	2.10%	1.57%	2.36%	7.19%	6.61%	5.49%
10	2.20%	1.43%	6.68%	2.27%	10.31%	3.80%	10.83%
11	1.78%	2.69%	2.04%	3.68%	14.05%	5.05%	5.52%
12	0.79%	0.75%	4.57%	5.91%	3.95%	4.38%	5.12%
13	0.92%	1.27%	4.20%	7.00%	3.88%	2.13%	15.52%
14	0.69%	1.10%	2.88%	2.26%	3.74%	4.72%	5.95%
15	1.65%	2.69%	9.05%	3.68%	14.25%	4.96%	5.99%
16	1.03%	3.61%	9.21%	7.03%	3.56%	1.87%	20.58%
17	0.92%	1.37%	10.64%	5.14%	3.94%	1.86%	20.94%
18	1.05%	1.34%	5.48%	6.73%	3.68%	2.31%	10.90%
19	1.15%	1.37%	3.52%	4.24%	3.91%	2.24%	20.92%
20	0.71%	3.33%	4.50%	7.60%	3.96%	1.54%	20.53%
21	1.39%	2.15%	2.48%	5.62%	13.44%	4.94%	5.72%
22	1.08%	1.21%	8.16%	4.09%	4.05%	4.39%	5.81%
23	0.91%	1.21%	11.09%	3.95%	3.41%	1.84%	10.74%
24	1.74%	1.00%	9.96%	2.31%	3.48%	6.27%	5.83%
25	2.16%	2.40%	9.15%	5.26%	13.45%	4.82%	5.06%
26	2.32%	2.17%	4.44%	1.90%	10.13%	3.64%	10.16%
27	1.54%	2.06%	2.36%	2.36%	7.04%	6.68%	5.77%
28	0.98%	2.88%	9.39%	2.36%	3.39%	2.24%	20.01%
29	1.39%	1.86%	3.95%	3.88%	7.11%	6.05%	5.91%
30	2.67%	1.41%	10.82%	1.77%	10.64%	3.25%	10.12%
31	2.69%	0.69%	6.18%	5.55%	4.21%	3.00%	5.67%
32	1.62%	2.69%	5.41%	2.31%	13.43%	5.25%	10.19%
33	0.81%	3.64%	6.40%	6.93%	3.96%	2.16%	15.29%
34	2.17%	2.55%	3.51%	4.09%	14.32%	4.37%	10.99%
35	2.92%	1.21%	4.56%	7.60%	3.58%	3.56%	5.96%
Average	**1.58%**	**1.95%**	**6.04%**	**4.30%**	**7.19%**	**3.83%**	**10.40%**

Table 7.3. Absolute mean-to-mean changes for identified mode shape parameters. Comparison of undamaged and damaged case 3 values.

Measurement Output	Mode 1	Mode 2	Mode 3	Mode 8	Mode 9	Mode 10	Mode 13
1	2.01%	0.56%	3.41%	1.49%	3.09%	1.37%	3.62%
2	1.10%	1.49%	6.56%	1.99%	0.12%	1.24%	7.27%
3	2.05%	1.96%	4.61%	3.39%	2.99%	0.81%	10.80%
4	2.74%	1.44%	8.43%	2.92%	3.41%	2.10%	6.69%
5	4.01%	1.75%	7.08%	2.73%	2.95%	1.37%	9.45%
6	3.12%	0.96%	4.45%	1.38%	6.09%	1.14%	6.76%
7	3.50%	0.98%	7.90%	0.98%	4.71%	2.25%	3.49%
8	0.53%	1.65%	5.56%	1.27%	2.83%	0.78%	13.42%
9	1.14%	1.18%	7.48%	0.85%	4.54%	1.63%	3.79%
10	1.81%	1.10%	5.50%	0.97%	6.13%	0.88%	7.20%
11	1.42%	1.66%	7.34%	2.29%	8.90%	1.43%	3.83%
12	2.50%	0.94%	5.60%	2.12%	2.45%	1.98%	10.40%
13	1.78%	0.89%	5.85%	2.72%	2.14%	1.13%	3.80%
14	0.96%	0.55%	6.48%	1.64%	2.27%	2.10%	3.74%
15	1.27%	1.38%	5.91%	1.79%	8.34%	1.49%	3.64%
16	0.97%	1.81%	7.70%	3.32%	3.00%	1.50%	7.10%
17	0.62%	0.53%	9.02%	2.23%	2.54%	0.71%	0.94%
18	0.95%	0.92%	7.50%	3.08%	3.02%	0.41%	7.59%
19	0.65%	0.54%	4.23%	2.00%	2.72%	1.05%	9.40%
20	0.79%	1.88%	6.91%	3.37%	2.53%	0.81%	1.40%
21	1.08%	1.48%	7.66%	3.09%	8.59%	1.66%	3.57%
22	3.45%	2.78%	3.86%	1.81%	2.11%	1.52%	3.66%
23	0.62%	0.85%	7.10%	2.26%	2.63%	1.21%	7.07%
24	1.33%	0.93%	4.80%	1.24%	2.88%	1.49%	3.49%
25	1.58%	1.65%	5.60%	2.08%	6.41%	1.30%	3.79%
26	1.85%	0.81%	6.16%	0.75%	7.11%	0.81%	7.59%
27	1.33%	1.36%	7.78%	1.29%	4.75%	2.09%	3.56%
28	0.67%	1.55%	5.76%	0.90%	2.23%	0.75%	13.89%
29	1.38%	1.41%	5.83%	1.44%	4.85%	2.45%	3.95%
30	2.05%	1.46%	3.54%	1.50%	6.88%	0.94%	6.75%
31	2.14%	0.79%	7.80%	2.55%	2.84%	1.11%	4.08%
32	1.22%	1.24%	6.41%	1.49%	0.71%	1.93%	7.55%
33	0.81%	1.80%	2.95%	3.66%	2.65%	0.37%	10.58%
34	1.25%	1.84%	4.50%	1.46%	8.46%	1.25%	7.05%
35	3.40%	0.73%	11.23%	3.11%	2.45%	1.13%	4.00%
Average	**1.66%**	**1.28%**	**6.24%**	**2.03%**	**4.01%**	**1.32%**	**6.14%**

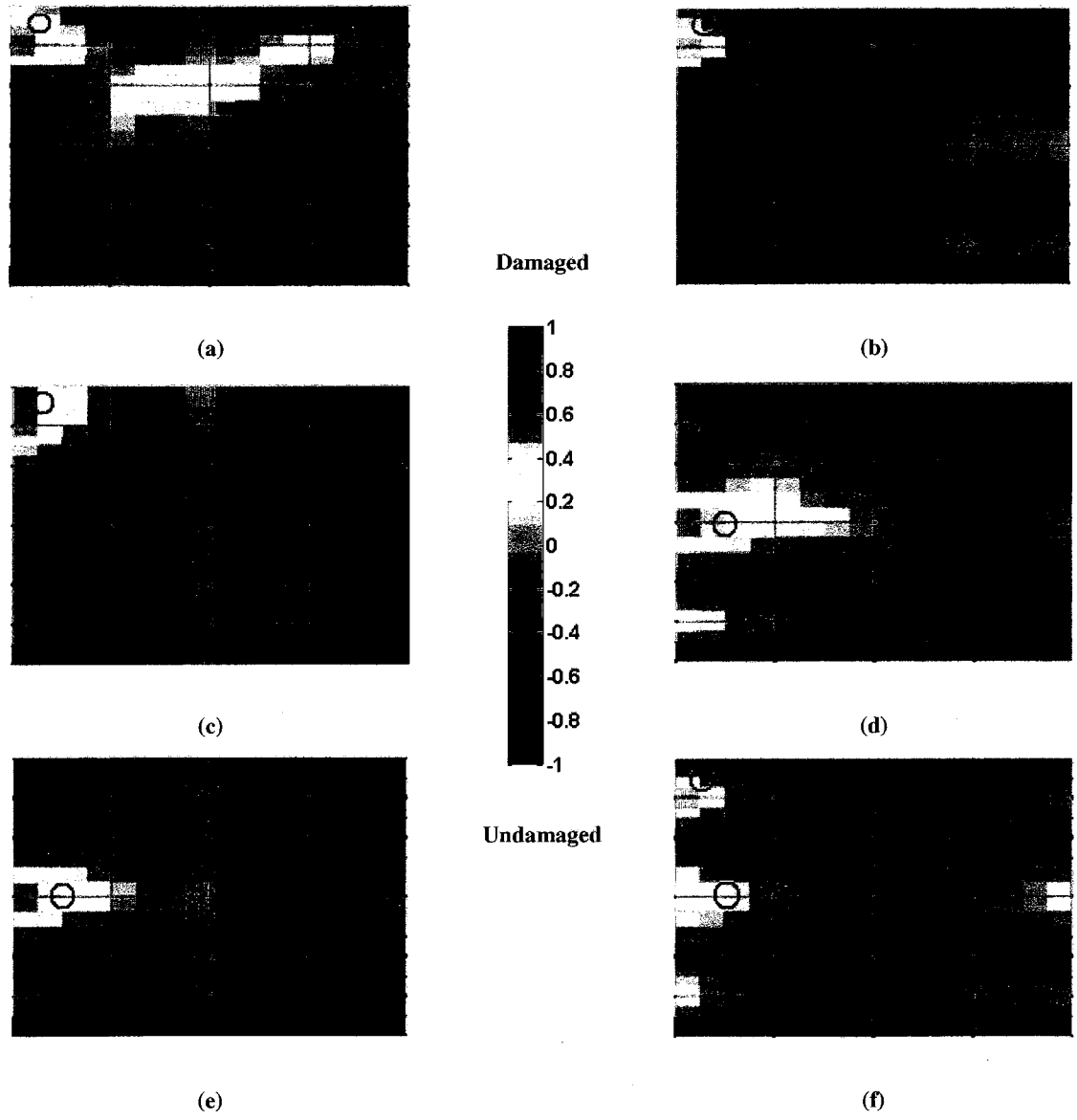

Figure 7.8. Normalized SDI values on the basis of 7 mode shapes of the undamaged and damaged conditions. SDI values for each damage condition 1-6 are shown in (a)-(f), respectively. True damage location indicated by red circle.

7.3.2 Discussion - Plate Damage Localization

After analyzing the damage localization results obtained using the baseline techniques, the following observations can be made:

(1) For some cases, especially those where the mass modification was on the top left corner, a maximum damage index was detected near the correct damage location, but all of the results showed distributed random patterns of false-positive damage indices. The presence of systematic or stochastic errors could account for this effect.

(2) Comparison of all the results shows the inefficacy in providing accurate damage localization results based on direct correlation of resonant frequencies and mode shapes. The exact damage location(s) could not be derived from the damage identification results.

(3) The more intricate techniques based on mode shape curvature, i.e. MSC and SEDI, instead of finding a single damage location, a distributed pattern of damage indices is obtained due to the additional manipulation of noisy modal parameters.

(4) Since the damage identification methods are based on identifying and interpreting changes in natural frequencies and mode shapes, damage localization problems can be partially attributed to the highly symmetrical experimental structure used. For example, in the COMAC results for cases 4-6, symmetric false-positive damage patterns are found.

Although the baseline damage localization techniques have been shown in other vibration applications to be effective, for this particular application, their damage identification performance was rather poor. It is opinion of the author that due to the presence of stochastic errors on the estimated modal parameters obtained using the proposed output-only modal analysis

approach, the baseline damage localization results were dismal. Thus, under higher levels of uncertainty, existing damage localization techniques are not reliable.

For the proposed SDI method, significant improvement in damage identification accuracy and consistency was made in all damage cases. By incorporating the domain-specific knowledge, such as sensitivity of modal parameters to structural changes, the performance was significantly improved in terms of damage localization accuracy and consistency. By recognizing that each sensor location has a different sensitivity to localized structural changes, the proposed SDI approach provided improved damage localization results. The presence of systematic or stochastic errors were taken into account by applying the Monte Carlo statistical sampling method, which minimized the false-positive damage locations. By obtaining multiple random samples from the same vibration dataset, converging estimates of the statistical measures of the modal parameters and damage localization indices were obtained. Although the average mode shape changes caused by the mass modifications were not consistently greater than the estimated 3σ standard deviation bounds, the estimated mean mode shape values used in the proposed modal-sensitivity damage assessment method were useful in providing improved damage localization results. For this experiment, it is important to note that the estimated statistical measures came from a single vibration dataset using the Monte Carlo technique. Therefore, the estimated confidence intervals of the extracted mode shapes are difficult to evaluate due to the limited experimental data. In order to obtain better estimates of the true statistical measures, many repeated experiments are needed, which can be rather expensive and not always possible.

A particular false-positive phenomena occurred for this particular structure. For both the baseline and the proposed damage assessment methods, symmetric false-positive damage indications were found in most of the test cases. The high symmetry nature of the free-free

boundary plate is the cause in the inability of the examined method to distinguish between true damage locations and symmetrically positioned healthy areas.

7.4 Case Study II: Damage Localization for I-40 Bridge

The full scale I-40 bridge tested by Farrar et al. [48] was adopted for a further validation of the proposed sensitivity-analysis damage index (SDI) method. The I-40 bridge vibration data has been extensively used as a benchmark to test damage detection methods. Briefly, in 1993, the I-40 bridge was programmed for demolition, and investigators from New Mexico State University and Los Alamos National Laboratory (LANL) carried out vibration tests introducing four incremental levels of damage by gradually cutting the web and the flange of the middle span of one plate girder.

Farrar and Jauregui [50] used the I-40 bridge data to check the performance of vibration-based damage localization approaches. More recently data recorded on the I-40 bridge has been used to study the performance of a non-modal damage localization index based on the so-called power mode shapes based on the statistical properties of the recorded signals [47]. Some valuable conclusions drawn from past studies on the I-40 bridge vibration data are: (1) standard modal properties, such as natural frequencies and mode shapes, are poor indicators of damage; (2) more sophisticated methods based on mode shape curvature, optimization or wavelet analysis showed improved capabilities to detect and locate damage; (3) mode shapes and derivatives usually have large statistical variability compared to natural frequencies; and (4) the smallest levels of damage of the I-40 bridge data were hard not well localized and even showed problems with damage detection.

7.4.1 Structure and Test Description

Forced vibration tests were carried out and the accelerations of 26 points, 13 on the middle height of the web of each plate girder, were measured. The bridge was excited by a hydraulic shaker. Using the output acceleration responses and the input force measurement, frequency response functions sampled at 0.03125 Hz and averaged in the frequency range 0-12.5Hz over 30 samples.

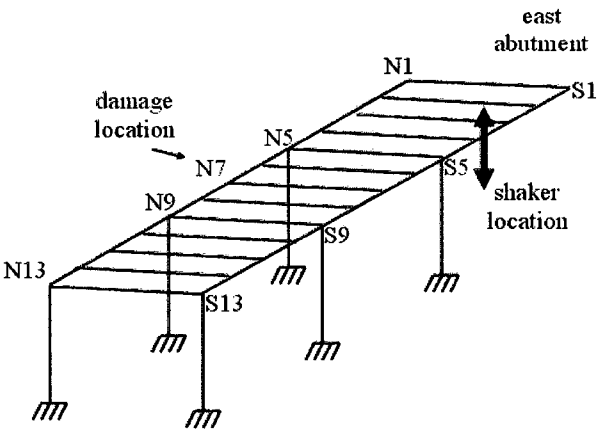

Figure 7.9. The I-40 bridge sensors network and induced damage location.

Farrar et al. [50] reported that for the first two levels of damage, the variation of temperature induced an increase of the fundamental frequency of the bridge that masked the reduction of stiffness induced by damage. Unlike what is expected when stiffness is reduced, the fundamental frequency value increased for the first two levels of damage. The third damage level gave nearly the same frequency values as those for the intact bridge. Only the last and most severe damage level, when half of the girder was cut out, gave obvious changes in the frequencies and could be used for damage identification. Therefore, the vibration data of the I-40 bridge can be used to check the performance of a damage assessment method with respect to varying environmental conditions. Six modes were identified from the I-40 bridge vibration data using experimental

modal analysis (EMA). Three flexural modes and three torsional modes were experimentally identified.

7.4.2 Changes in Modal Parameters

The experimental frequencies of the 6 identified modes during the undamaged state and progressive damage tests are given in Table 7.4. Because of the magnitude of the bridge natural frequency is proportional to its stiffness, as incremental damage is introduced to the bridge, one would expect the natural frequencies to drop off. The frequencies of the progressive damage vibration tests of the I-40 bridge show an increment in all 6 frequencies for the first two damage levels, which contradicts expected results. The last two levels of damage due have a decrease in frequency value. Farrar et al. [50] concluded that the ambient temperature of the bridge played a major role in the variation of the bridge's dynamic characteristics. The different damage vibration tests were carried over different parts of the day and thus were exposed to different ambient temperatures. Temperature variation can affect the asphalt elastic modulus, and can alter the boundary conditions of the structure as it expands and contracts due to its composite thermal expansion coefficient. The uncontrollable ambient conditions and induced damage affected the dynamic characteristics of the bridge to exhibit nonlinear frequency change as incremental levels of damage were incorporated.

The corresponding experimental mode shapes for the undamaged case are plotted in Figure 7.10. Since the damage was induced at the midsection of the bridge, modes 1, 2, 4 and 6 (in incremental order) would have a higher sensitivity to this damage since they show anti-nodes at this particular location. At the final level of damage, the resonant frequencies for the first two modes have dropped to values, 7.2% and 2.7% less, respectively, than those measured during the undamaged tests. As shown in Figure 7.10, modes 3 and 5 have a node at the midsection of the

bridge, and thus would have the least amount of sensitivity to structural changes at this particular location. At the final level of damage, modes 3 and 5 resonant frequencies' dropped by 0.2% and 0.5%, respectively, which correspond to the two smallest levels of change in resonant frequencies.

Table 7.4. Frequencies for I-40 bridge for all scenarios of the progressive damage tests.

Damage Case	Mode 1 - Hz $f(\Delta f\%)$	Mode 2 - Hz $f(\Delta f\%)$	Mode 3 - Hz $f(\Delta f\%)$	Mode 4 - Hz $f(\Delta f\%)$	Mode 5 - Hz $f(\Delta f\%)$	Mode 6 - Hz $f(\Delta f\%)$
None	2.48 (0.0)	2.96 (0.00)	3.50 (0.00)	4.08 (0.00)	4.17 (0.00)	4.63 (0.00)
Dam1	2.52 (+1.6)	3.00 (+1.3)	3.57 (+2.0)	4.12 (+0.1)	4.21 (+0.1)	4.69 (+1.3)
Dam2	2.52 (+1.6)	2.99 (+1.0)	3.52 (+0.5)	4.09 (+0.2)	4.19 (+0.5)	4.66 (+0.6)
Dam3	2.46 (-0.8)	2.95 (-0.3)	3.48 (-0.5)	4.04 (-0.1)	4.14 (-0.7)	4.58 (-1.1)
Dam4	2.30 (-7.2)	2.84 (-2.7)	3.49 (-0.2)	3.99 (-2.2)	4.15 (-0.5)	4.52 (-2.4)

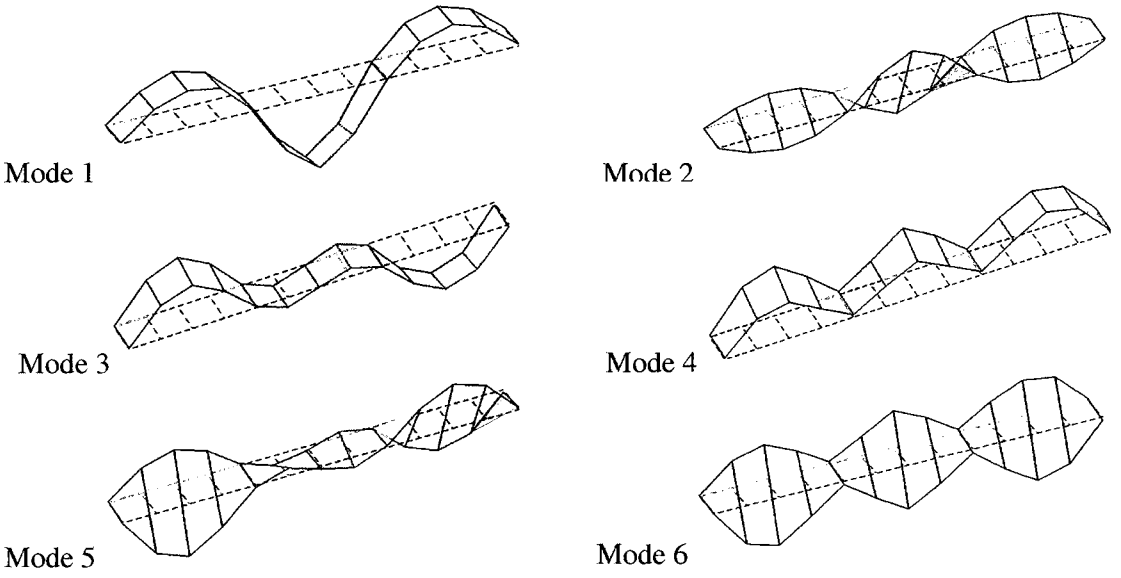

Figure 7.10. First six mode shapes identified from experimental modal analysis (EMA) of the undamaged I-40 bridge.

7.4.3 Statistical Analysis

The estimated statistical measures of the mode shapes obtained via Monte Carlo method are shown for modes 1, 3 and 6 in Figure 7.11 through Figure 7.16. Each figure shows a comparison of the undamaged and damaged mode shapes along with its corresponding 3σ confidence intervals. For this particular Monte Carlo study, convergence of the estimated statistical measures was obtained after approximately 100 runs. For location reference, the total number of measurement nodes is 26 with 13 on each side of the bridge. The true damage location is node 7, and its symmetric node is node 20. The obtained estimated statistical results are very similar to those reported in the literature which also used the benchmark I-40 bridge data.

Comparison of Figure 7.11 and Figure 7.12 shows the main difficulty in obtaining a clear damage indication and localization with the smallest damage case 1. For damage case 1 shown in Figure 7.11, the change in mode shape caused by the introduced damage is relatively small and does not cause a statistical significant change. The confidence intervals for both the undamaged and damaged case have significant overlap, which makes the damage identification rather difficult. In contrast, the first mode shape of damage case 4 shown in Figure 7.12 has a significant shift from the undamaged mode shape. The largest changes in mode shape parameter mean and variance are obtained at nodes 7 and 20, which correlates well with the true damage location. At both of these nodes, the confidence intervals are well separated. Thus, for damage case 4, there is a statistically significant change at these two components.

In a similar fashion, the third mode shape is plotted in Figure 7.13 and Figure 7.14 for damage cases 1 and 4, respectively. In contrast to the results of the first mode shape, the third mode shape results does not show any significant change due to damage at any damage level. Even after the fourth and most severe damage state is applied, there is very little change in the mode shape

components. Thus, mode shape 3 is very insensitive to the induced damage, which is a logical response since mode shape 3 has a modal node at the damage location as shown in Figure 7.10. Another observation is that the magnitude of the confidence intervals increases for mode shape 3 in comparison to mode shape 1. Figure 7.15 and Figure 7.16 show the sixth mode shape results for damage case 1 and damage case 4, respectively. Although a modal node is not existent at the true damage location for mode 6, the changes in mode shape due to the induced damage levels are not statistically significant.

The estimated statistical measures obtained would seem to support the notion that only the fourth and most severe damage case is the only one that demonstrates statistically significant changes in its modal parameters. Statistical analysis on raw modal parameters is currently the standard method for monitoring structures. For the I-40 bridge analysis, damage assessment based on the statistical measures would result on a false-negative for the first three damage cases in terms of damage detection and localization. Therefore, the improved measure of the statistical significance of the changes must be made with respect to the damage indicators previously described, and not with respect to the raw modal properties.

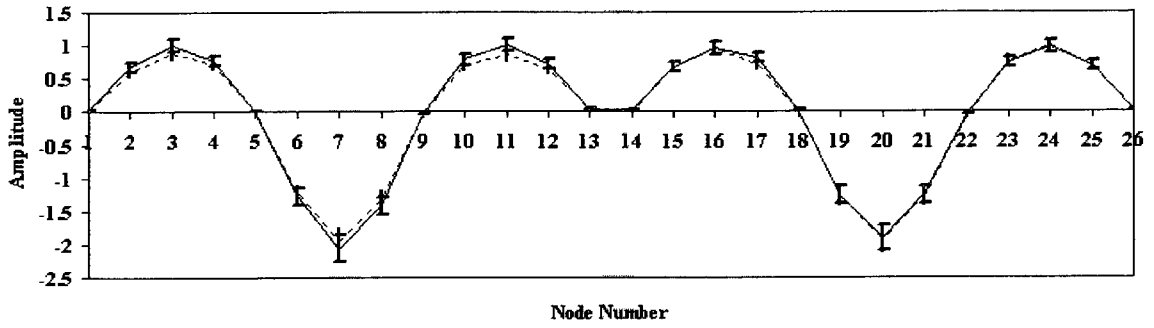

Figure 7.11. First mode shape for undamaged case (-) and damaged case 1 (--).

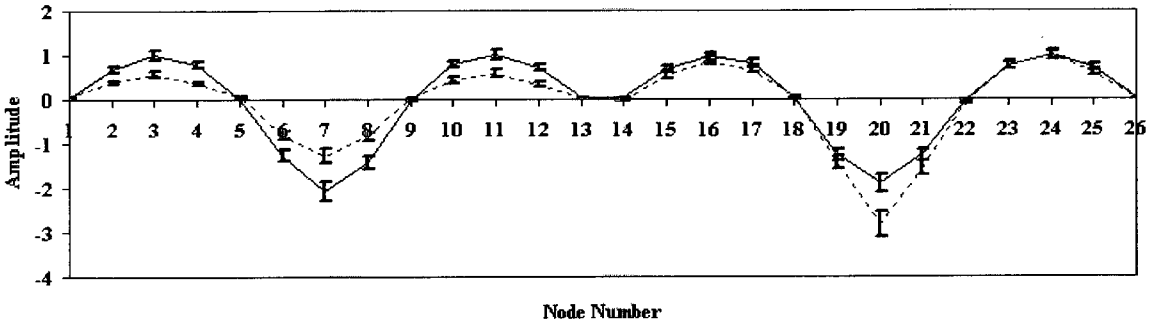

Figure 7.12. First mode shape for undamaged case (-) and damaged case 4 (--).

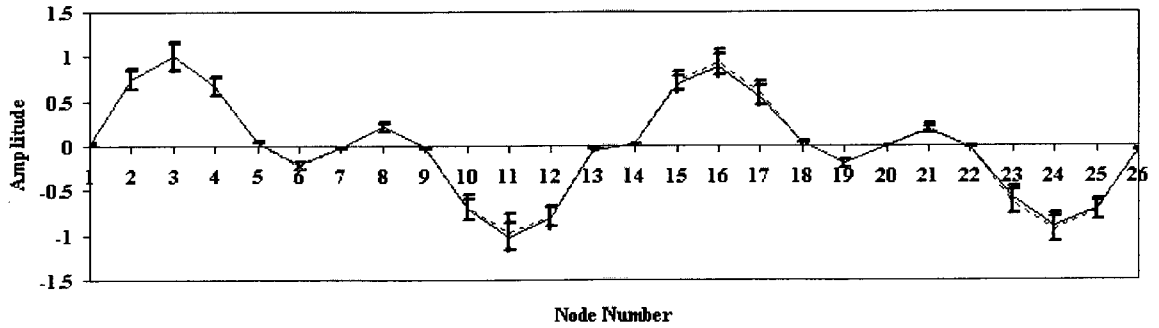

Figure 7.13. Third mode shape for undamaged case (-) and damaged case 1 (--).

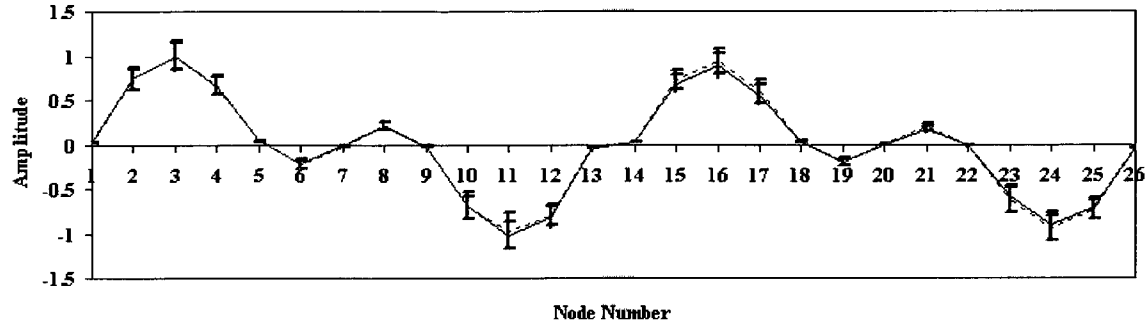

Figure 7.14. Third mode shape for undamaged case (-) and damaged case 4 (--).

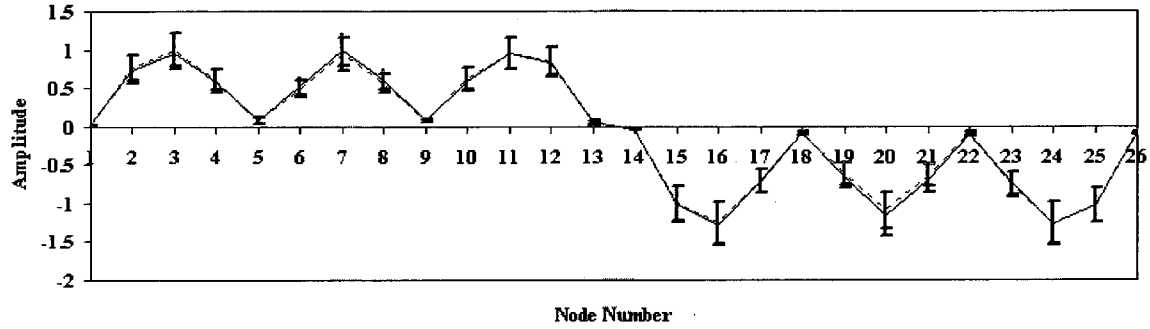

Figure 7.15. Sixth mode shape for undamaged case (-) and damaged case 1 (--).

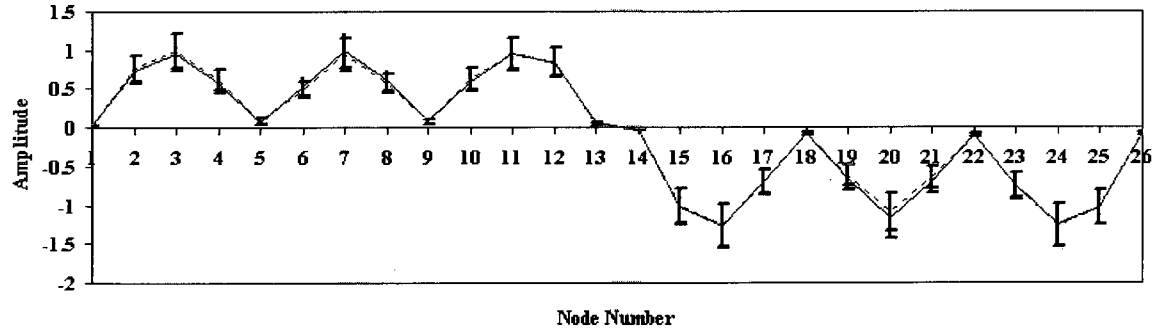

Figure 7.16. Sixth mode shape for undamaged case (-) and damaged case 4 (--).

7.4.4 Damage Localization Results

Modal assurance criterion (MAC) were also calculated for the I-40 bridge vibration to quantify the correlation between the undamaged and damaged mode shapes. As a guiding principle, multiple researchers use a value greater than 0.9 for correlated modes, and uncorrelated modes will yield a value less than 0.05. Figure 7.17 shows the diagonal MAC values that are calculated when mode shapes from the undamaged test and damaged tests are compared. The MAC values show no change in the mode shapes for the first three stages of damage. At the final damage level, significant drops in MAC values are observed, especially modes 1 and 2. Again, when the modes have a node near the damage location (modes 3 and 5), no significant reductions in MAC values are observed at any of the damage levels. It is worth noting that aside from damage, other factors cause less than perfect unity MAC values. MAC values of less than the expected value of unity (for highly correlated mode shapes) can be caused by nonlinearities, noise on the measured data, and incomplete or inappropriate choice of DOFs [44]. Because the damage vibration tests are carried in varying environmental conditions with limited number of sensors, the MAC criterion in then not very successful in detecting damage (structural modification or decrease in modal correlation).

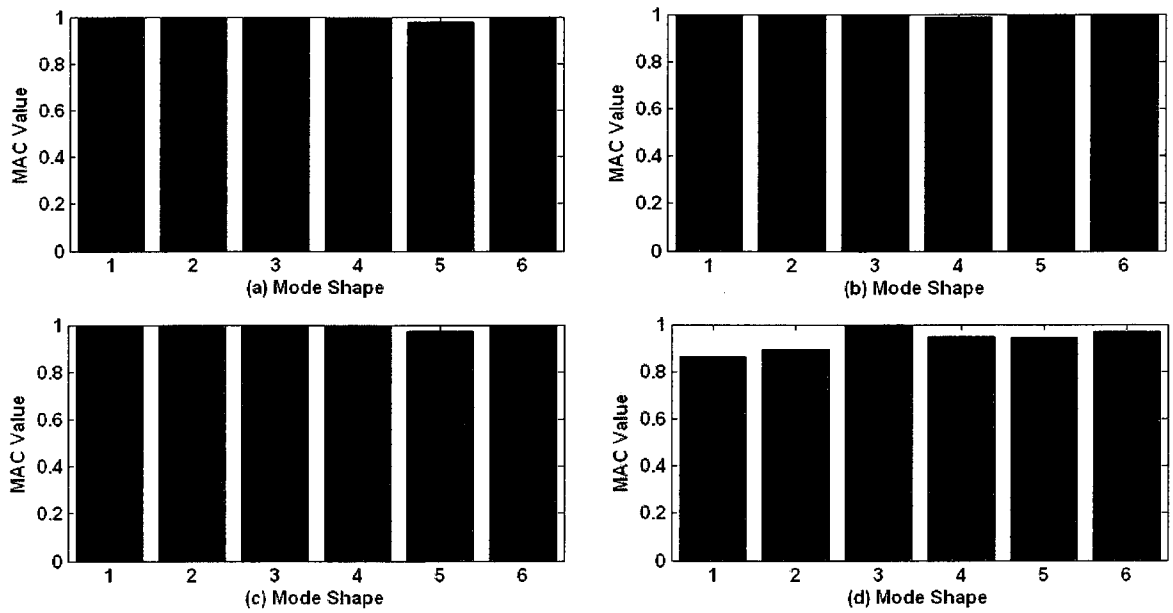

Figure 7.17. Diagonal MAC values between the mode shapes of the undamaged and damaged conditions for the plate experiment. MAC values for each damage condition 1-4 are shown in (a)-(d), respectively.

In this section, research will focus on the localization of the damage caused by the artificial cuts induced on the I-40 bridge. The damage localization methods that were applied to the I-40 bridge data are the coordinate modal assurance criterion (COMAC), frequency modal assurance criterion (FRAC), strain energy damage index (SEDI), and the proposed sensitivity-based damage index (SDI) with statistical sampling.

The FRAC, COMAC, and SEDI methods were chosen because each one belongs to a particular family of damage localization that is based on the correlation of frequency responses, mode shapes, and mode shape curvature, respectively. In the analysis, all damage localization results were normalized such that a value of -1 indicates well correlated DOF and a value of 1 indicates poor correlation for each DOF. All 6 experimental modes were used in the damage localization analysis. For graphical representation of the damage localization results, the damage indices for each DOF were plotted using bars finite elements. The true location of damage in these finite element models is at the right side of the midsection, with coordinates (2540,400).

For the first damage analysis series, the COMAC method was utilized for damage localization of the I-40 bridge vibration data. Figure 7.18 shows the results obtained using the COMAC method for all four damage levels. The damage levels 1 through 3, were not properly identified by the COMAC method. For the smallest damage level, the COMAC provides a false-location of damage at (4300,0). A partial damage indication is given at the midsection (2340,0) for the three lowest levels, but it's on the opposite side of the correct damage location. Only the largest damage level was approximately localized, again the highest level of damage is indicated on the opposite side of the true damage location. Taking into consideration that we have prior knowledge of true damage location, the COMAC damage localization results lack consistency and thus reliability.

For the next damage localization analysis, the SEDI method was utilized and its results are shown in Figure 7.19. For the smallest damage level, the highest indicator of damage is found at two locations, (3907, 400) and (2540,400). The true damage location shows the highest level of damage indication, but a secondary area shows the same level of indication. For the second level of damage, the highest indicator of damage is given at (3028,400), which is close to the true damage location. For the two lowest damage levels, damage indication or low correlation is seen through out the bridge or DOFs.

Because we have prior knowledge of the true damage location, we could falsely deduce that since the highest level of damage indication was found at the true damage location, then the damage localization method does work to a certain extent. Without prior knowledge of true damage location, damage localization results as those shown for the lowest damage levels can only be identified as random and unreliable damage indication. Significantly improved results were obtained for the third damage level, which clearly indicates damage at the midsection of the bridge. Again, some false-positive indication remains at other DOFs, but significantly reduced in

comparison to the two damage levels. The results obtained for the largest damage level are very accurate. The highest damage indicator is given at the true damage location without any false-damage indicators at any other DOF. The damage localization obtained for the largest level of damage is what is desired due to its minimal false-negative and false-positives.

Visual comparison of the damage localization results obtained from COMAC and SEDI methods shows a major difference in terms of false-positive localization. Although the COMAC failed to correctly localize the damage for the first three levels, the false-positive location indicators were minimal, mainly two or three bridge areas had indication of damage. In other words, good modal correlation was obtained in most DOFs. In contrast, the damage localization results using SEDI method shows poor modal correlation in most of the bridge areas or DOFs, with exception of the largest damage case. The SEDI method is based on the second derivative of the mode shapes. Given that noise corrupts the quality of experimental mode shapes, the noise content is propagated to the extracted damage localization indices based on mode shapes. The data manipulation to obtain the second derivatives of the mode shapes is intended to highlight the changes in mode shape curvature and thus locate the damage, but at the same time, this additional process also further propagates and magnifies the noise content. Thus, the lower correlation found at all DOFs in the SEDI method is mainly due to the additional manipulation performed on noisy mode shapes.

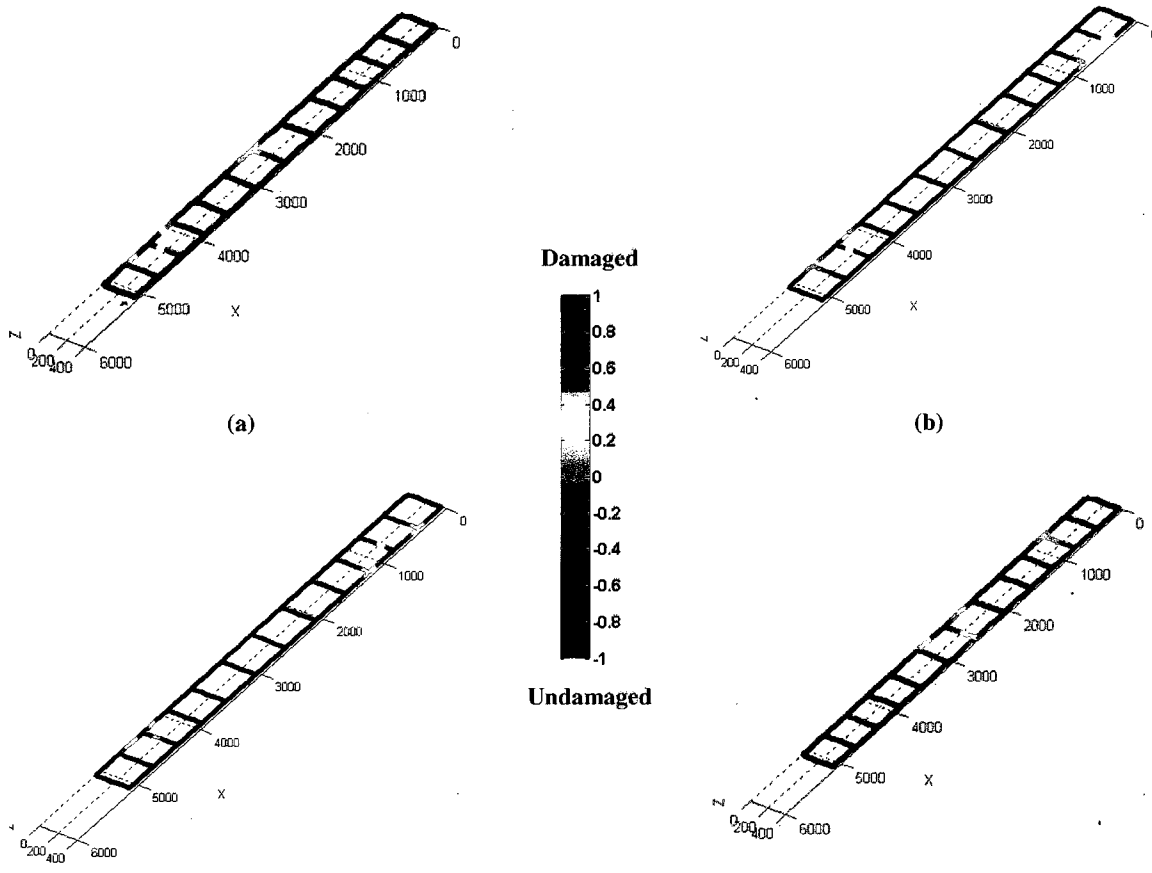

Figure 7.18. Normalized COMAC values on the basis of 6 mode shapes of the undamaged and damaged conditions. COMAC values for each damage condition 1-4 are shown in (a)-(d), respectively.

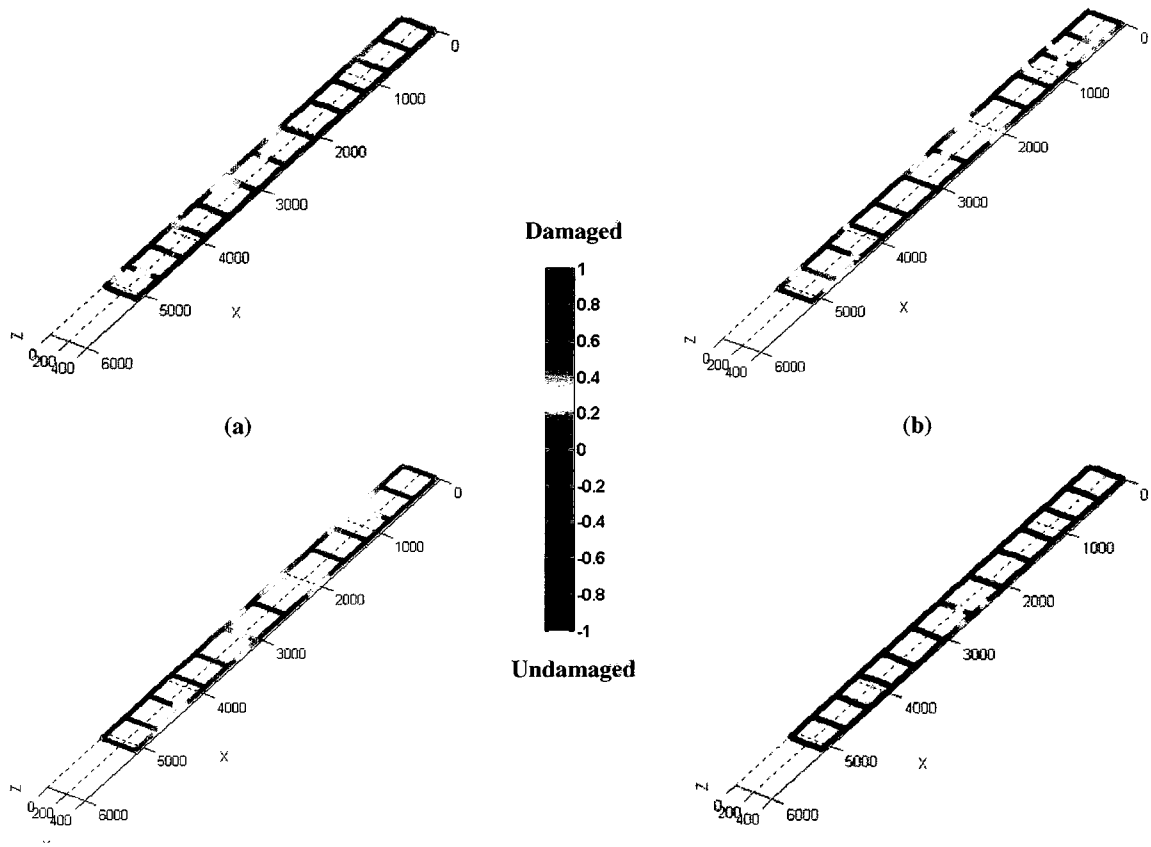

Figure 7.19. Normalized SEDI values on the basis of 6 mode shapes of the undamaged and damaged conditions. SEDI values for each damage condition 1-4 are shown in (a)-(d), respectively.

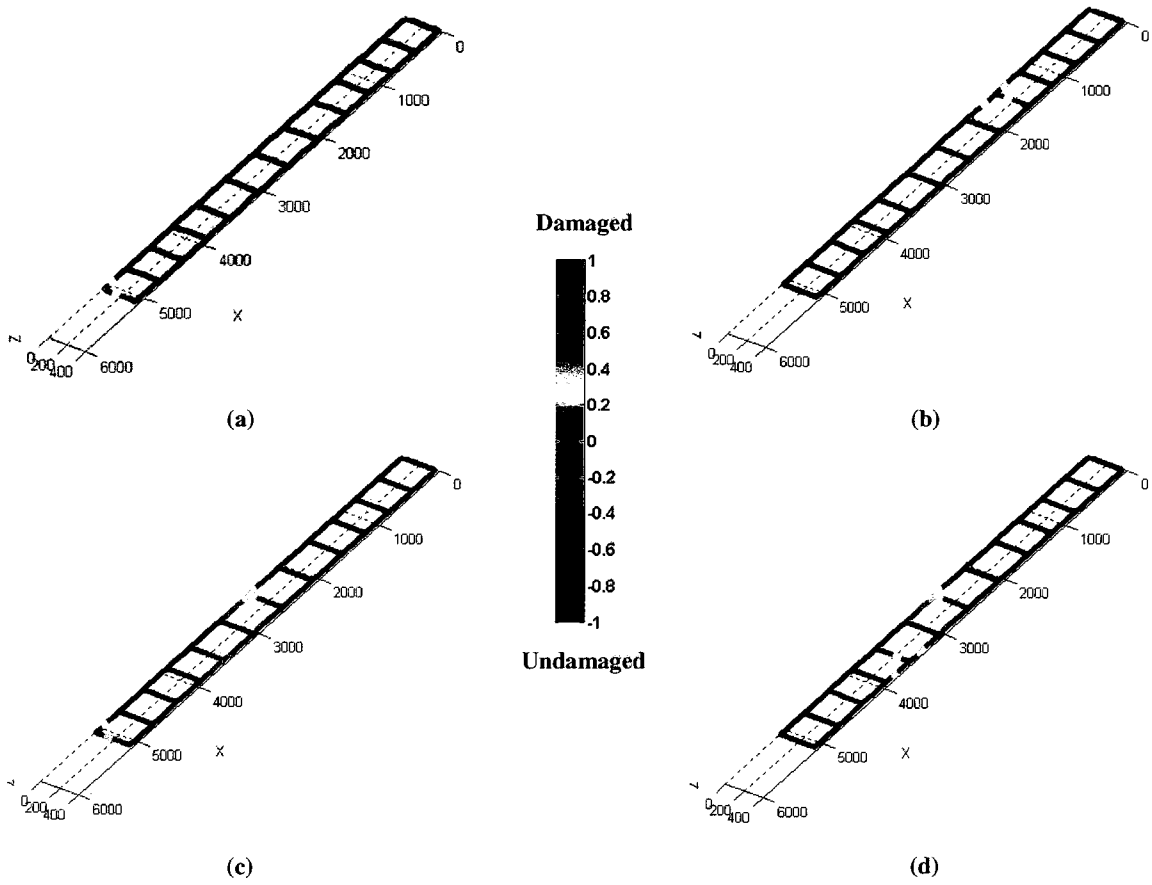

Figure 7.20. Normalized FRAC values on the basis of 6 mode shapes of the undamaged and damaged conditions. FRAC values for each damage condition 1-4 are shown in (a)-(d), respectively.

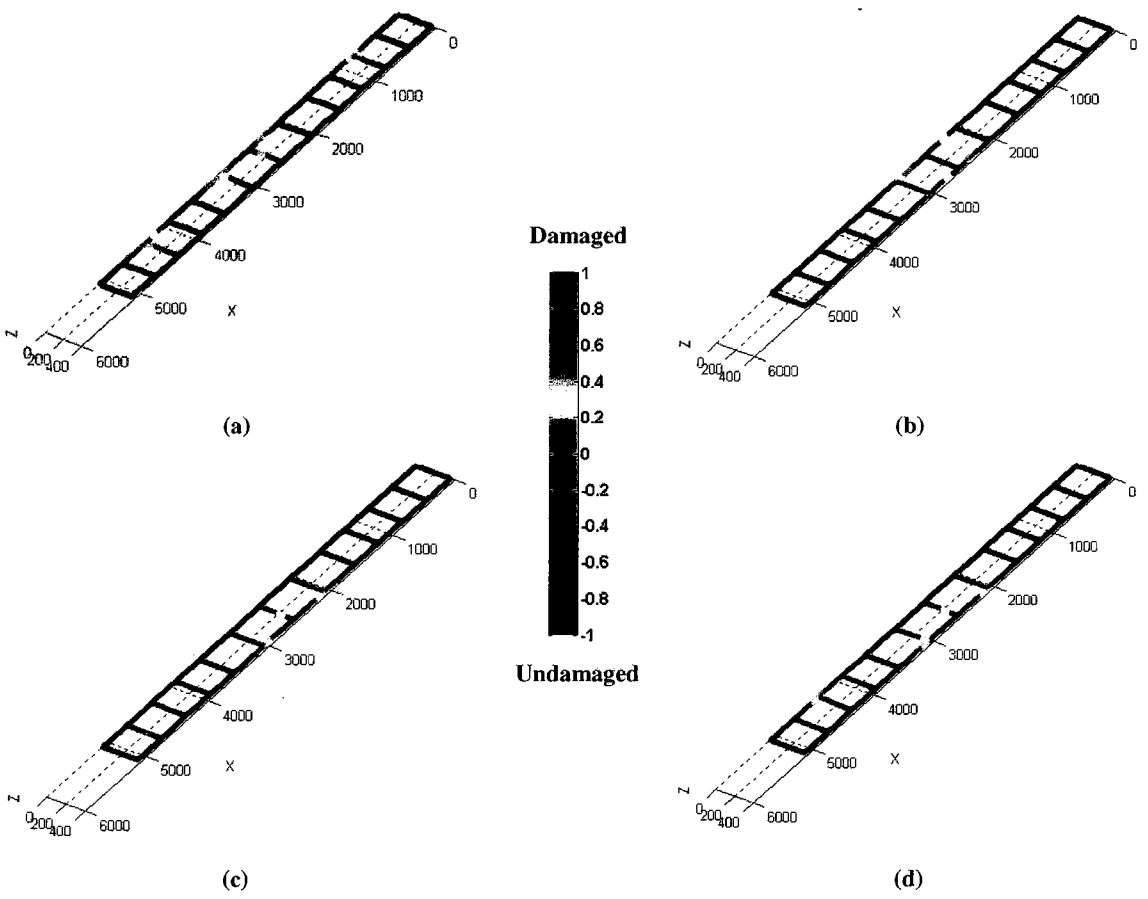

Figure 7.21. Normalized SDI values on the basis of 6 mode shapes of the undamaged and damaged conditions. SDI values for each damage condition 1-4 are shown in (a)-(d), respectively.

For the next damage localization analysis, the FRAC method was utilized. For this particular method, all four damage levels were incorrectly localized. Similar to the COMAC method, the damage indication was localized to a few discrete bridge areas. For the smallest damage case, the only damage indication (low DOF correlation) was given at the (5080,400) coordinate corresponding to the east abutment location. The second damage level was falsely located at the coordinate (1560,400). The third damage level located damage at two possible coordinates. The first location was again the east abutment location (5080,400), and the second location was (2540,400), which is close to the true damage location. Using the data from the largest damage level, damage was localized at two main sites. The first and highest indication was given at the coordinate (3500,0). The second site was again at the coordinate (2540,400).

Comparing the FRAC with the COMAC and SEDI results, this method obtained the poorest damage localization performance. All three methods had major difficulty obtaining clear and correct damage localization at the two first levels of damage. The COMAC method provided a good approximation of the damage location only for the largest damage level. Although with numerous false-positives, the SEDI method provided good localization for the third damage level. For all the different damage levels, the only clear and correct damage localization result was given by the SEDI method at the fourth damage level.

Finally, the proposed SDI method based on modal-parameter sensitivity analysis with Monte Carlo statistical method was applied to the damage identification experiment. The damage localization results obtained using the proposed SDI method are shown in Figure 7.21. By incorporating the sensitivity of each sensor location to stiffness modifications, the proposed SDI method improved the localization of the bridge damage. For the smallest damage level, the damage was approximately localized at the midsection coordinate (2540,0) with two false-positives at (4300,0) and (780,0). Comparing this result with those of the COMAC, FRAC and

SEDI approaches, the damage localization was significantly improved as the approximate damage location is now much closer to the true damage location. For the second damage level, the localization is improved since damage indication covers both sides of the midsection, which covers the true damage location (2540,400). The two most severe damage levels provided correct localization with minimal false-positives. Similar to some baseline damage localization techniques, the SDI damage results, especially at the two least severe damage levels, made no distinction between the correct damage location (2540,400) and its symmetric position (2540,0). This fact can be explained by the symmetric characteristics of the test structure combined with the fact natural frequencies and mode shapes were used.

7.5 Discussion

Damage localization study was presented using modal-based baseline techniques and a proposed modal sensitivity with statistical sampling approach. Analysis and comparison of these methods were conducted based on a laboratory aluminum plate vibration experiment and the I-40 bridge benchmark vibration data. In this study, the damage localization techniques assume that linearity applies prior and after damage occurs since they are based on modal analysis. For the aluminum plate experiment, modal parameters were extracted using a proposed output-only modal analysis techniques, which is useful when the number of sensor outputs is limited. Because damage was simulated by mass modifications, the proposed damage localization technique was based on modal parameter sensitivity due to mass changes. The I-40 bridge benchmark data is based on input-output modal analysis approach. For this case, damage was induced by incremental cuts to structural members, which is intended to reduce the overall structural stiffness. For this reason, the proposed damage localization technique was based on the modal parameter sensitivity due to stiffness changes.

The damage localization results obtained with the baseline modal-based methods are consistent with the results presented by Farrar and Jauregui [50]. Although the damage localization results obtained using the baseline methods were poor, the methods have been shown in numerous applications to be effective in detecting and localizing damage. To explain the low performing damage localization results obtained using the baseline methods, the following observations can be made:

(i) The I-40 bridge sensor network was of low density, i.e. large structure with small number of sensors. Ewins [44] reported that modal-based correlation methods are highly dependent to number of DOF measured in order to be effective. In addition, a limited number of mode shapes were utilized in this study. For modal-based correlation methods, the larger the number of resonant frequencies and mode shapes available, the better the correlation results will be. The quantity of available mode shapes is directly proportional to sensor network and highly dependent on excitation levels.

(ii) Examinations of the damage localization results are consistent with findings by other investigators, which verify that resonant frequencies and mode shapes are poor indicators of damage. The more sophisticated SEDI method showed improved abilities to locate damage, but only for the most severe damage cases. However, the generalization of the SEDI method assumes that mode shape second derivatives can be obtained with low noise levels.

(iii) With exception of the SEDI method, most modal-based correlation methods do not have a specific criterion for determining whether damage has occurred at a particular location. In other words, these methods only provide the location(s) with the lowest modal correlation, which can be ambiguous at times to determine whether these changes

indicate damage. Although not presented in this work, the SEDI method provides damage localization results with reduction in stiffness approximations, which can be useful for damage assessment.

(iv) The damage identification methods are linear, which implies that the structure can be modeled with linear dynamic models prior and after damage. The nature of the damage applied to the I-40 bridge is assumed to be linear damage models. The frequency changes shown in Table 7.4 demonstrate that as increasing levels of damage were induced, the fundamental resonant frequency changes in a nonlinear fashion. The latter result negates the linear relationship damage model assumed by using the baseline damage identification methods.

(v) Ambient variations influence significantly the measured and extracted modal parameters. The observed nonlinear relationship between damage level and resonant frequency was partially due to the varying ambient conditions under which the vibration tests were performed. Therefore, normalization techniques are required to take into account changes in ambient conditions or operations, such as temperature and mass loadings.

For the sensitivity-based method, significant improvement in damage identification accuracy and consistency was made for both the plate experiment and the I-40 bridge data. A few observations and conclusions can be made in regards to the proposed SDI approach with statistical sampling:

(a) By recognizing that each sensor location has a different sensitivity to structural changes at another structural location, the propose SDI approach provided improved damage localization accuracy and consistency. The propose modal correlation method takes into account that not all sensor locations will provide equal level of information when damage

is localized to a particular area. For example, a sensor located a node will not be able to provide significant information in regards to mode shape changes.

(b) The presence of systematic or stochastic errors were taken into account by applying the Monte Carlo statistical method, which minimized the false-positive damage locations. By obtaining multiple random samples from the same vibration dataset, converging estimates of the statistical measures of the modal parameters and damage localization indices were obtained. A particular disadvantage of the Monte Carlo method over other statistical sampling methods, such as bootstrap method, is that it relies on assumptions of Gaussian distribution in the excitation or response data.

(c) For highly symmetrical structures, such as the free-free boundary plate, the global character of the natural frequencies can cause an inability of the method to distinguish between damage locations and symmetrically positioned healthy areas. In both experiments, the damage localization approaches resulted in some false-positive locations, which were symmetric in location to the true damage location.

(d) Similar to COMAC and FRAC methods, the proposed SDI method does not have a specific criterion, in other words assessment, for determining whether damage has occurred at a particular location. The method only provide the location(s) with the lowest modal correlation, which can be ambiguous at times to determine whether these changes indicate damage. In order to provide damage assessment, such as percent reduction in stiffness or estimate of mass modification, a finite element model is required which can be utilized in parallel with experimental modal analysis. By performing finite element model updating, only then can quantifiable estimates of structural damage severity can be obtained.

Incorporation of domain knowledge, such as sensitivity of modal parameters to structural changes, can improve the performance in terms of damage localization accuracy. Because the methods analyzed are based on linear modal analysis, the type and size of detectable and localizable damage is limited to linear damage models. Vibration-based damage analysis is limited by multiple criteria, such as density and location of sensors, modal analysis techniques, and modeling errors. All these account to a lower range of damage, which is undetectable and thus must always be acknowledged. Now, it also contains an upper limit on the size of the damage assessment it can be applied to. Under sizeable damage or structural modifications, any structure will result in modified boundary conditions, continuity problems and non-linearities, which negate the main assumption of linearity required by modal analysis methods.

In terms of the vibration-based damage assessment methods presented in this thesis, damage detection and localization is achievable under uncertainty, but with certain limitations. Given the limits in the reliability of results from modal analysis, especially output-only modal analysis, the damage assessment performance becomes limited. For example, modal testing of complex structures often miss a critical modes due to modal coupling, limited measurement points, and/or high damping. Despite these shortcomings, vibration-based damage assessment methods are reliable as a health monitoring tool, especially when integrated with additional signal processing techniques and data-driven algorithms. Figure 7.22 exhibits the aforementioned damage assessment limitations in terms of confidence levels and damage level. As any other structural health monitoring tool, vibration-based damage assessment analysis is limited by the size and type of damage it can detect. The lower boundary, $\Delta\theta_{low}$, of reliable damage assessment is highly dependent on the size and sensitivity of the sensory system being utilized. Multiple studies have reduced $\Delta\theta_{low}$ by utilizing training data, which quantifies random noise and separates it from the data outlier caused by damage. The upper boundary, $\Delta\theta_{high}$, of reliable damage assessment is due

to the assumption limitations, such as linearity and non-modifiable boundary conditions, of the applied technique. The upper boundary $\Delta\theta_{high}$ has not been properly addressed in the literature even though it is of equal importance in understanding the applicability and reliability of the damage assessment method.

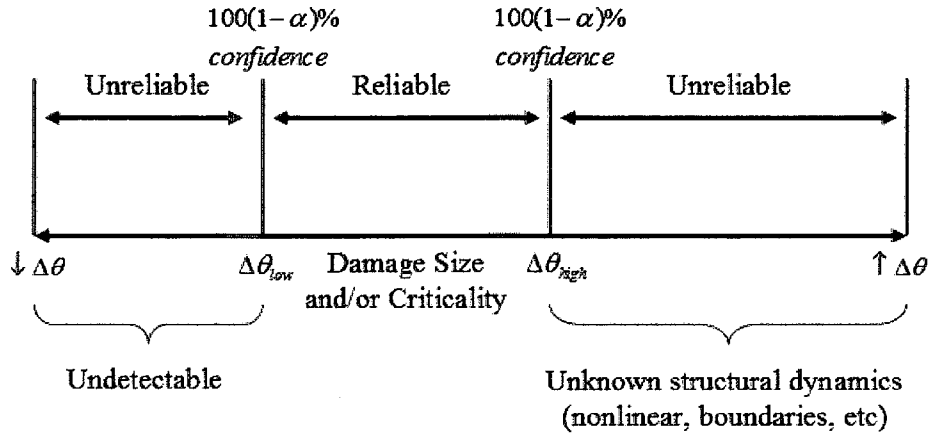

Figure 7.22. Capability and limitations of structural damage assessment.

7.6 Summary

For damage localization, we presented an improved approach based on the incorporation of modal-parameter sensitivity and statistical sampling. The proposed approach was validated using an in-house free-free boundary plate experiment, and using a real-life benchmark vibration data. In vibration-based damage assessment research, the modal parameters of a structure are identified, monitored and compared to a known baseline. Work presented in this thesis addresses one of the key issues of structural health monitoring, which is the management and quantification of uncertainty on the estimated modal parameters and damage indicators. Uncertainty management and quantification in structural damage assessment makes use of numerous variations of statistical methods, fuzzy-sets, and interval-based uncertainty analysis to

characterize the effect that parametric and non-parametric uncertainty has on physical experiment or numerical simulation. Uncertainty is not necessarily restricted to imperfect knowledge of the control parameters. Uncertainty may also take the form of stochastic equations of motion, environmental variability, measurement errors, changing boundary conditions, nonlinearities, to name only a few.

Chapter 8

Evidential Reasoning for Damage Assessment

Early attempts at building diagnostic systems contain the main drawback of lacking the means, and associate difficulties, in handling uncertain domain knowledge and imprecise non-specific evidence. The introduction of probability-based diagnostic reasoning methods, such as Bayesian networks, for knowledge representation and probabilistic inference represented an important stepping stone in the development of reliable diagnostic systems. However, even probability-based methods are limited as a formalism for managing uncertainty because of the assumption that relevant data is available for estimating and building probability functions, which adequately represent the situation at hand.

In the sequel, vibration-based damage localization is developed based on evidential reasoning for addressing epistemic uncertainty. This chapter presents a damage assessment method based on Dempster-Shafer evidence theory for two case studies: (i) aluminum plate problem; (ii) I-40 bridge benchmark problem. We first derive the evidential reasoning approach to determine the most probable damage event by comparing the relative damage basic belief assignments (BBA) of different damage events. The proposed evidential reasoning approach (i) explicitly considers both modeling and noise errors, (ii) has capability of dealing with imprecise information, and (iii) updates the damage evidential values whenever new data become available.

8.1 Introduction

One of the main problems of damage diagnostics is finding a way to handle uncertainty in data and information sources. Diagnostic decision-making is difficult to undertake given two possible

scenarios. First, the amount of relevant data and information, which is potentially conflictive, available to a decision maker in diagnostic systems far exceeds the human ability to review and comprehend them in a timely manner. Second, the lack of training data and information available for computational methods in diagnostic systems limits the capability of providing crisp decision-support for humans. Moreover, in numerous situations, diagnostic decisions usually have to be made under very stressful conditions which adversely affect humans and make them prone to error. All this leads to the need for the development of an automatic knowledge-based information fusion system that will support the decision process in a reliable, timely and consistent manner.

In the literature, a few studies have been found in modeling imprecise knowledge and to identify how automated reasoning can be applied in damage diagnostic decision-making [54,64,65,126,178]. Numerous approaches exist for reasoning about uncertain information and events, some of the approaches include probability measures, Dempster-Shafer (D-S) evidence theory, fuzzy sets, extensions to first order logic, Bayesian belief networks (BBNs), and others [136,172]. To date, most damage assessment under uncertainty studies have relied on precise probabilistic information.

In reality, information sources for structural damage assessment decisions are imprecise and incomplete to enable probabilistic analysis. The causes for information uncertainty can be lack of information, conflicting information (multiple indicators providing different results), indeterminate system states or condition, time-constraints (situations does not allow for increased collection and careful assessment of information), incapability of assessing or integrating different types of information, reduced order models, ambiguity, measurement errors, etc. Thus, in the present study, we will focus on the usage of evidential reasoning based on Dempster-Shafer evidence theory to obtain a rational damage assessment decision.

8.2 Evidential Reasoning in Structural Damage Assessment

In classification problems, complete or assumed statistical knowledge regarding the density functions of each class is required. Statistical pattern recognition along with the Bayesian decision rule has proved quite efficient in a wide range of applications, but suffers from severe shortcomings when data is limited [75,101]. When data is scarce, only poor estimated of the probability functions and expected losses, necessary for Bayes decision rule, can be obtained. While in situations where data is limited, it is sometimes reasonable to select the action with minimal estimated expected loss, it may sometimes be preferable to reject the pattern when the uncertainty is too high, in other words make no classification.

Furthermore, in the absence of training data belonging to certain classes or even the lack of knowledge regarding the exact number of classes, the Bayesian approach for classification may not be appropriate. Such situations arise typically in system diagnosis applications, because of the impossibility of gathering data corresponding to certain system states or because the number of states (damage configurations) is very high. To solve this problem, the "distance reject option" is utilized in statistical pattern recognition, which postpones the classification decision when the object is situated "far" from training samples. However, this approach requires determination of statistical distance thresholds, which cannot easily done without some underlying model or known and unknown states.

In order to address the latter classifications problems faced by statistical approaches, a pattern recognition approach based on Dempster-Shafer (D-S) evidence theory is presented for diagnostic decision making.

In damage assessment, to setup a frame of discernment, FoD, we need to define the objects around which the evidential reasoning process is to operate. Damage assessment diagnostic

objectives must be related to a corresponding FoD representing the diagnosis hypothesis. Different diagnostic hypothesis correspond to different levels on measurement accuracy and requirements. In damage detection, the main objective is to gain information about the existence of structural damage, and according to the D-S evidence theory, the FoD for this situation is defined as

$$\Theta_{jk} = \{H_o, \neg H_o\} \tag{142}$$

where H_o denotes the hypothesis for structure being damaged, and $\neg$ is its logical negation. To accommodate additional damage level conditions, the FoD can be expanded to

$$\begin{aligned} &\Theta_{jk} = \{H_0, H_1, ..., H_i, ..., H_{N_f}\} \\ &Ex: \{NoFault, Low, Medium, Severe, Failure\} \end{aligned} \tag{143}$$

where H_i and H_{N_f} indicate hypotheses for the i^{th} damage level and maximum damage-level N_f, respectively.

The power set composed with the latter propositions of Θ is given as

$$\Psi = \{\varnothing, H_0, H_1, ..., H_i, H_{N_f}, \Theta\} \tag{144}$$

which can be reduced to three possible hypothesis:

- $m(\varnothing) = 0$: mass of the empty set
- $m(H_i)$: belief mass to be in i^{th} damage level
- $m(\Theta)$: portion of total belief which remains unassigned, or assigned to the environment (unknown), after commitment of belief to various subsets of Θ.

Similar to the calculation of monotonic probability values, a key problem with evidential reasoning is the calculation of the basic belief assignment (BBA) obtained from the sources of information, such as sensors or extracted data features.

8.2.1 Basic Belief Assignment Calculation

In this section, we will present a method for obtaining basic belief assignments (BBAs) from the outputs of the damage localization process. Given these BBAs, we will then be able to perform diagnostic decision-making based on unsupervised classification, also known as clustering, of belief functions. Recently, a new concept of data clustering has been introduced, namely the credal partition or clustering developed in the framework of the evidence theory [32,33]. The concept of using belief functions as tools in the classification process generalized existing concepts based on crisp (black or white) and probabilistic data partitions by allowing an object (to be classified) to belong to several subsets of classes at once.

Let us consider a set of N_o objects, $O=\{o_1,o_2,...,o_{N_o}\}$ or measurement vectors, and a set of N_c possible classifications, $C=\{c_1,c_2,...,c_{N_c}\}$. Let us assume that we have only partial knowledge concerning each class membership of each object o_i, and that this knowledge is represented by a basic belief assignment (BBA) m_i on the set C. We recall that $m_i(\Theta)$ stands for complete ignorance of the class of object i, whereas $m_i(c_k)=1$ corresponds to full certainty (crisp classification) that object i belongs to class c_k, and all other situations correspond to partial knowledge of the class of o_i. The credal partition of O is defined as $M=(m_1,m_2,...,m_{N_o})$ which denotes the N_o number of BBAs related to the N_o.

In traditional clustering methods, objects are grouped in an exclusive way, so that if a certain object belongs to a cluster then it cannot be included in any other cluster. The defect in the underlying axiomatic model that each object be unequivocally grouped into single clusters is that it does not provide any apparent similarity to other objects in other clusters. One such manner to characterize an individual object's similarity to multiple clusters was introduced as fuzzy sets in 1965 by Zadeh [192]. The key idea behind fuzzy sets is to represent the similarity an object shares with each cluster with a function (termed the membership function) whose values (called memberships) are between zero and one. Fuzzy clustering allows each object to belong to two or more clusters with different degrees of membership. In this work, the fuzzy clustering based on Bezdek's fuzzy c-means approach [14] will be utilized to develop the evidential reasoning classification approach.

To obtain the credal clustering, an unsupervised classification technique based on k-means, see section 5.3, will be utilized to obtain the possible sets of classes for each object or measurement vector. Given a measurement matrix $\mathbf{X}=(x_{ij})$ of size $N_o \times p$, where p is the dimension of the feature space. Let each potential cluster (class) be represented by a center v_k. Let $\mathbf{V}$ denote a matrix of size $N_c \times p$ composed of the coordinates of the cluster centers such that V_{kq} is the q^{th} component of the cluster center v_k. Let $\mathbf{U}=(u_{ik})$ be the fuzzy cluster matrix of size $N_o \times N_c$. Fuzzy clustering looks for the matrices $\mathbf{U}$ and $\mathbf{V}$ by minimizing the following function

$$J_{fuzzy}(\mathbf{U},\mathbf{V}) = \sum_{i=1}^{N_o}\sum_{k=1}^{N_c} u_{ik}^{\beta} d_{ik}^2 \tag{145}$$

subject to the constraints

$$\sum_{k=1}^{N_c} u_{ik} = 1, \quad \forall i \in \{1,...,N_o\} \tag{146}$$

$$\sum_{k=1}^{N_o} u_{ik} > 0, \quad \forall k \in \{1,...,N_c\} \tag{147}$$

where each number $u_{ik} \in [0,1]$ is interpreted as a degree of membership of object i to cluster k, $\beta > 1$ is a weighing parameter that controls the fuzziness of the clustering, and d_{ik} denotes the similarity distance between x_i and the cluster center v_k. In our work, we used the Euclidean distance to obtain the similarity value as follows

$$d_{ik}^2 = |x_i - v_k|^2 \tag{148}$$

The objective function is minimized using an iterative algorithm, which optimizes the cluster centers and the membership degrees. The update formulas are obtained by introducing a Lagrange multiplier with respect to the constraint shown in Eq. (146) and setting the partial derivatives of the Lagrangian with respect to the parameters to zero. The fuzzy clustering algorithm starts from an initial guess for either the partitioning matrix or the cluster centers and iterates until convergence.

For evidential classification, the BBA m_i needs to be determined for each object o_i in such a way that $m_i(A_j)$ is low (high) when the distance d_{ij} between o_i and the focal set A_j is high (low), where A_j is any non-empty subset of Θ. Each subset A_j is associated to a center of mass $\hat{v}_j$ of the centers associated to the classes composing A_j. For generalization purposes, each focal set A_j may contain or consist of multiple classes c_k. For example, damaged level focal set can be defined by the following set of classes $\{Low, Medium, Severe\}$. The proposed method for obtaining BBAs for damage localization is based on the work of Masson and Denoeux [109] who developed the evidential clustering method (ECM).

The center of mass is computed as

$$\hat{v}_j = \frac{1}{c_j} \sum_{k=1}^{N_c} s_{kj} v_k \tag{149}$$

where $c_j = |A_j|$ denotes the cardinality (size) of A_j and s_{kj} is defined as

$$s_{kj} = \begin{cases} 1, & \text{if } c_k \in A_j \\ 0, & \text{otherwise} \end{cases} \tag{150}$$

To derive the evidence based partition $\mathbf{M} = (m_1, m_2, ..., m_{N_o})$ and the matrix $\mathbf{V}$ of size $N_c \times p$ containing the cluster centers, the following objective function is minimized

$$J_{D-S}(\mathbf{M}, \mathbf{V}) = \sum_{i=1}^{N_o} \sum_{\substack{j/A_j \neq 0 \\ A_j \subseteq \Theta}} \left(c_j^{\alpha} m_{ij}^{\beta} d_{ij}^2 \right) + \sum_{i=1}^{N_o} \delta^2 m_{i\varnothing}^{\beta} \tag{151}$$

subject to the following constraint

$$\sum_{\substack{j/A_j \subseteq \Theta \\ A_j \neq 0}} \left(m_{ij} + m_{i\varnothing} \right) = 1, \quad \forall i = 1, ..., N_o \tag{152}$$

where $m_{i\varnothing}$ denotes $m_i(\varnothing)$. The empty set $\varnothing$ is assimilated to a noise cluster considered to be at a fixed distance δ from each object, which is used to control the number of objects considered as outliers. The additional weighting coefficient α is introduced for penalizing the subsets in Θ of high cardinality.

To minimize Eq. (151), the following optimization scheme is used. First, consider matrix $\mathbf{V}$ to be fixed. To solve the constrained minimization problem with respect partition $\mathbf{M}$, we introduce N_o Lagrange multipliers λ_i as follows

$$\mathcal{L}(\mathbf{M}, \lambda_1, ..., \lambda_{N_o}) = J_{D-S}(\mathbf{M}, \mathbf{V}) - \sum_{i=1}^{N_o} \lambda_i \left(\sum_{\substack{j/A_j \subseteq \Theta \\ A_j \neq 0}} \left(m_{ij} + m_{i\varnothing} \right) - 1 \right) \tag{153}$$

By differentiating the Lagrangian with respect to the parameters $m_{ij}, m_{i\varnothing}$ and λ_i, and setting the derivatives to zero, we obtain

$$\frac{\partial \mathcal{L}}{\partial m_{ij}} = \beta c_j^{\alpha} m_{ij}^{\beta-1} d_{ij}^2 - \lambda_i = 0 \tag{154}$$

$$\frac{\partial \mathcal{L}}{\partial m_{i\varnothing}} = \beta \delta^2 m_{i\varnothing}^{\beta-1} - \lambda_i = 0 \tag{155}$$

$$\frac{\partial \mathcal{L}}{\partial \lambda_i} = \sum_{\substack{j/A_j \subseteq \Theta \\ A_j \neq 0}} \left(m_{ij} + m_{i\varnothing} - 1 \right) = 0 \tag{156}$$

Using Eqs. (154)-(156), we obtain the following solutions

$$m_{ij} = \left(\frac{\lambda_i}{\beta} \right)^{1/(\beta-1)} \left(\frac{1}{c_j^{\alpha} d_{ij}^2} \right)^{1/(\beta-1)} \tag{157}$$

$$m_{i\varnothing} = \left(\frac{\lambda_i}{\beta} \right)^{1/(\beta-1)} \left(\frac{1}{\delta^2} \right)^{1/(\beta-1)} \tag{158}$$

$$\left(\frac{\lambda_i}{\beta} \right)^{1/(\beta-1)} = \left(\sum_j \frac{1}{c_j^{\alpha/(\beta-1)} d_{ij}^{2/(\beta-1)}} + \frac{1}{\delta^{2/(\beta-1)}} \right)^{-1} \tag{159}$$

By introducing Eq. (159) into Eqs. (157) and (158), the necessary condition of optimality for $\mathbf{M}$ as

$$m_{ij} = \frac{c_j^{-\alpha/(\beta-1)} d_{ij}^{-2/(\beta-1)}}{\sum_{A_k \neq 0} \left(c_k^{-\alpha/(\beta-1)} d_{ij}^{-2/(\beta-1)} + \delta^{-2/(\beta-1)} \right)}, \quad \forall i = 1, \ldots, N_o, \quad \forall j / A_j \subseteq \Theta, \quad A_j \neq 0 \tag{160}$$

Let us now consider that $\mathbf{M}$ is fixed. The minimization of J_{D-S} is an unconstrained optimization problem. The partial derivatives with respect to the cluster centers are given by

$$\frac{\partial J_{D-S}}{\partial v_l} = \sum_{i=1}^{N_o} \sum_{A_j \neq 0} c_j^{\alpha} m_{ij}^{\beta} \frac{\partial d_{ij}^2}{\partial v_l} \tag{161}$$

$$\frac{\partial d_{ij}^2}{\partial v_l} = 2s_{lj}\left(x_i - \hat{v}_j\right)\left(-\frac{1}{c_j}\right) \tag{162}$$

From Eqs. (149), (161) and (162), we obtain

$$\frac{\partial J_{D-S}}{\partial v_l} = -2\sum_{i=1}^{N_o}\sum_{A_j \neq 0} c_j^{\alpha-1} m_{ij}^{\beta} s_{lj}\left(x_i - \frac{1}{c_j}\sum_k s_{kj} v_k\right), \quad \forall l = 1,\ldots,N_c \tag{163}$$

Setting to zero the partial derivatives with respect to centers gives the following N_c linear equations in v_k, which can be written as

$$\sum_i x_i \sum_{A_j \neq 0} c_j^{\alpha-1} m_{ij}^{\beta} s_{lj} = \sum_k v_k \sum_i \sum_{A_j \neq 0} c_j^{\alpha-2} m_{ij}^{\beta} s_{lj} s_{kj}, \quad \forall l = 1,\ldots,N_c \tag{164}$$

For a simplified notation, let $\mathbf{H}$, $\mathbf{U}$ and $\mathbf{B}$ be matrices of size $N_c \times N_c$, $N_c \times N_o$ and $N_c \times p$, respectively, such that

$$\mathbf{H}_{lk} = \sum_i \sum_{A_j \neq 0} c_j^{\alpha-2} m_{ij}^{\beta} s_{lj} s_{kj}, \quad \forall l,k = 1,\ldots,N_c \tag{165}$$

$$\mathbf{U}_{li} = \sum_i \sum_{A_j \neq 0} c_j^{\alpha-1} m_{ij}^{\beta} s_{lj}, \quad \forall i = 1,\ldots,N_o \tag{166}$$

$$\mathbf{B}_{lq} = \sum_{i=1}^{N_o} x_{iq} \sum_{A_j \neq 0} c_j^{\alpha-1} m_{ij}^{\beta} s_{lj} = \sum_{i=1}^{N_o} x_{iq} \sum_{c_l \in A_j \neq 0} c_j^{\alpha-1} m_{ij}^{\beta}, \quad \forall l = 1,\ldots,N_c, \quad \forall q = 1,\ldots,p \tag{167}$$

Using Eqs. (165) and (166), the N_c linear equations of Eq. (164) can be re-written as

$$\mathbf{HV} = \mathbf{B} \tag{168}$$

Eq. (168) can be solved for $\mathbf{V}$ using a standard linear system solver. The evidential classification technique starts with an initial guess for either the partition $\mathbf{M}$ or the cluster centers $\mathbf{V}$ and iterates until convergence. Figure 8.1 shows the process for obtaining the basic belief assignments (BBAs).

Due to the inexistent training data, in this research, we consider the magnitudes of the vibration-based damage indicators as evidence sources to obtain the BBAs. For each vibration-based damage indicator method, i.e. COMAC, MSC, SEDI, TFRAC and proposed SDI method, the normalized damage index value is $x_i \in [-1,1]$ at measurement point i. The next issues to be perform BBA information aggregation of partially conflictive evidence sources and how to perform diagnostic decision-making given the BBAs.

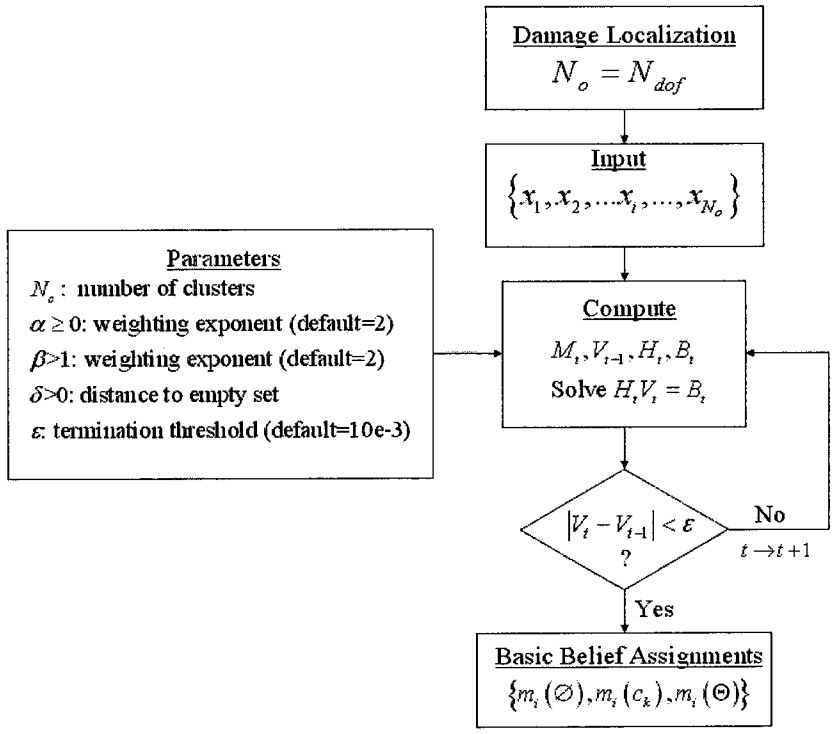

Figure 8.1. Process for obtaining basic belief assignments (BBAs).

8.2.2 Belief Aggregation

The next step would be to combine the belief masses of the individual damage indicator methods via the Dempster's rule. A classic problem with the Dempster's rule of combination in D-S theory is the counter intuitive result found when the evidences to be combined have a concentration of

belief in an element disjoint between them, and a common element with low degrees of belief assigned to it. Because Dempster's rule does not include any intrinsic mean of belief adaptation, proportionally to the amount of conflict, they can assign a majority of the belief to the element less believed but common to the evidences. To demonstrate this issue with the Dempster's rule, we will use the following example.

Example 1: Car does not start and two information sources are used for diagnostics. Source 1 states that 99% sure the problem is due to starter problem and 1% chance of being a battery problem. Source 2 assigns 99% certainty to problem being due to a blown fuse and 1% to battery. The BBA for this scenario is given by

$$m_1(\{starter\}) = 0.99 \quad m_1(\{battery\}) = 0.01$$
$$m_2(\{fuse\}) = 0.99 \quad m_2(\{battery\}) = 0.01$$

Direct application of Dempster's rule yields:

$$\Theta = \{starter, battery, fuse\}$$
$$m_1 \oplus m_2(\{starter\}) = 0$$
$$m_1 \oplus m_2(\{fuse\}) = 0$$
$$m_1 \oplus m_2(\{battery\}) = 1$$

The conclusion of this result is that the problem has a battery problem, when in fact none of the information sources think there is a very low chance of the problem being related to the battery. This limitation of Dempster's rule of combination with normalization leads to results that are contrary to what might be expected.

Furthermore, each individual information source has a different level of "credibility." When eliciting expert opinions for intelligent decision-making, it is well known that multiple evidence from multiple sources are not always combined with equal weights due to reliability of each information source. Various researchers [63,103,181] have proposed a weighted Dempster's rule

of combination handling sets of evidence from various sources with different priority. The main drawback to many of these methods is that the determination of such weights is not always clear and might simply state that they are obtained from expert user input.

Due to uncertainty that exists in obtaining vibration-based damage indicators, evidence conflict among different damage assessment techniques are very possible. To address the conflictive evidences and varying expert source reliability, we propose an extended D-S approach that not only corrects the counter intuitive effect shown in the latter example but also takes into account the reliability from each information source. The proposed method for weighted information sources under conflicting evidence is based on the work of Campos et al. [19] and Guo et al. [63].

For two evidences, the amount of conflict, Con, is given by

$$Con(m_1, m_2) = \log\left(\frac{1}{k}\right) = \log\left(\frac{1}{1 - \sum_{A \cap B = \varnothing} m_1(A) m_2(B)}\right) \tag{169}$$

If there is no conflict between m_1 and m_2, then $Con = 0$, but if there is nothing in common, i.e. full conflict, then $Con = \infty$. The combination of evidences with a high value of conflict can lead to counter intuitive results, as was shown in the car-start diagnosis example.

Given that we have two sources of information, each with a weighting coefficient w_i representing the relative reliability of the information source, the extended D-S combination rule for two bodies of evidence is given by

$$m_1' \oplus m_2'(C) = m_1'(A) \oplus m_2'(B) = \frac{k^{-1} \sum_{A \cap B = C} m_1^w(A) m_2^w(B)}{Con\left(m_1^w, m_2^w\right)} \tag{170}$$

where $m_i^w = w_i m_i$ and k is defined as

$$k = 1 - \sum_{A \cap B = \emptyset} m_1^w(A) m_2^w(B) \tag{171}$$

The division by the conflict between in Eq. (170) will result in a reduced value of $m(C)$ in comparison to Dempster's rule. This reduced belief becomes an additional belief assigned to the initial environment belief as follows

$$m_1 \oplus m_2(\Theta) = 1 + k^{-1} m_1^w(A) \oplus m_2^w(B) - \sum_{C \subset \Theta, C \neq \emptyset} m_1 \oplus m_2(C) \tag{172}$$

where $k^{-1} m_1^w(A) \oplus m_2^w(B)$ is equal to the weighted Dempster's rule. The proposed method adds to this belief a value proportional to the conflict between the evidences.

If more than two evidences are combined, the BBA assignments must first be assigned a proportional weight and combined using Dempster's rule, and then divide the result by the conflict among the BBAs, which is given as follows

$$Con\left(m_1^w, m_2^w, ..., m_n^w\right) = 1 + \log\left(\frac{1}{k_1 + k_2 + \cdots + k_{2^{n-1}-1}}\right) \tag{173}$$

where each k value is calculated from each possible pair of evidence combination.

Example 2: Applying the updated rule to the data from Example 1 with equal weights, we obtain the following

$$m_1 \oplus m_2(\{starter\}) = 0$$
$$m_1 \oplus m_2(\{fuse\}) = 0$$
$$m_1 \oplus m_2(\{battery\}) = 0.2$$
$$m_1 \oplus m_2(\{\Theta\}) = 0.8$$

where $k = 0.0001$ and $\log(k^{-1}) = 4$.

Comparing results of Example 2 with those of Example 1, it can be seen that the results are more reasonable and the uncertainty better represented, since 80% of the belief is assigned to the environment and not a particular hypothesis.

8.2.3 Belief Weight Calculation

The weighting parameter for the Dempster's rule combination is to be determined. The evaluation and application of weighting parameters is highly dependent on the specific engineering application and it training data in order to evaluate and compare the damage indicators techniques. To find the weighting parameters under limited experimental training data, repeated finite element analysis (FEA) simulations of the structure under varying noise content levels and excitation types can be utilized to obtained initial weighting parameters. By comparing the simulated damage localization performance of the available methods, weighted parameters can be obtained. One drawback to this simulation approach is that simulation cannot take into account all the different uncertainties and variations associated with the observed structure.

For this analysis, the evidence sources weights are obtained on the basis of the entropy measure. The term entropy refers to the Shannon entropy, which quantifies, in the sense of an expected value, the information contained in a message. In information theory, entropy is a measure of the uncertainty associated with a random variable. Let $X = \{x_1, ..., x_{N_{dof}}\}$ be the damage localization output vector for method i, the weighted coefficient is obtained as follows

$$w_i = \frac{1}{entropy(i)} = \frac{1}{-\sum_{j=1}^{N_{dof}} p(x_j)\log_2 p(x_j)} \tag{174}$$

The entropy measure has the following properties: (i) if $p(x_j) = 1$ and the rest is equal to 0, then $entropy(i) = 0$, which implies that there is not any uncertainty in the damage localization

vector and a decisive conclusion can be made; (ii) on the contrary, at the maximum level of uncertainty, then $p(x_j)=1/N_{dof}$ and *entropy(i)* reaches its maximum value. Therefore, the damage assessment method which contains the least variation (uncertainty) in its damage localization results, will be assigned the largest weighing coefficient, and vice-versa. The methodology for obtaining the weighing coefficients is based on the previously stated assumption that damage is localized and discrete.

8.2.4 Decision Analysis

Given that vibration-based damage localization indices have been obtained and the BBAs have been extracted using the evidential clustering method, then a measure of decision utility is required to evaluate if we have sufficient evidence for designating a particular structural locations as damaged, undamaged, or no decision can be reached. Let us assume we have a BBA m_j concerning the validity of hypothesis H_i, and we have to choose an action among a finite set of actions $\mathcal{A}$. A loss function $\lambda(a,\theta)$ for all $(a,y)\in \mathcal{A}\times\Theta$ denotes the loss occurred if one chooses action a and unknown damage variable θ.

The lower and upper expected loss associated with each possible action are given respectively by

$$R_{\min}(a\,|\,\theta)=\sum_{A\subseteq\Theta} m(A)\min_{\theta\in A}\lambda(a,\theta) \tag{175}$$

$$R_{\max}(a\,|\,\theta)=\sum_{A\subseteq\Theta} m(A)\max_{\theta\in A}\lambda(a,\theta) \tag{176}$$

When a decision must be made, beliefs can be transformed to a probability measure, which is commonly referred to as the pignistic (derived from Latin *pignus* = a bet) transformation [153], which is based on a two level mental models:

- The *credal level* where beliefs are entertained and represented by belief functions.
- The *pignistic level* where beliefs are used to make decisions and represented by probability functions called pignistic probabilities.

Beliefs held at the credal level induce a probability measure at the pignistic level denoted $BetP$. The transformation between beliefs and pignistic probabilities is achieved by the pignistic transformation as follows

$$BetP(A) = \sum_{B \subseteq \Theta} \frac{m(A)}{|A|}, \ \forall A \subseteq \Theta \tag{177}$$

where $|A|$ denotes the cardinality (number of elements of the set) of A. Using the pignistic probability for the expected risk becomes

$$R_{BetP}(a \mid \theta) = \sum_{A \subseteq \Theta} \lambda(a,\theta) BetP(\theta) = \sum_{A \subseteq \Theta} m(A) \frac{1}{|A|} \sum_{\theta \in A} \lambda(a,\theta) \tag{178}$$

which results in a different decision strategy.

In damage pattern classification of the j^{th} substructure, $\Theta_j = \{H_0, H_1, ..., H_i, ..., H_{nf}\}$ is the set of classes, where each H_i represents a damage state, and the elements of $\mathcal{A}$ are the actions a_i of assigning each substructure to each class H_i. With 0-to-1 losses, defined as $\lambda(a_i, \theta_j) = 1 - \delta_{i,j}$ for $i, j \in \{1, ..., nf\}$, it can be shown [153] that the minimization of the pignistic risk R_{BetP} leads to choosing the damage state hypothesis H_i with maximum pignistic probability, whereas the minimization of $R_{\min}$ leads to choosing the hypothesis with maximum plausibility.

In general, application of the principle of expected loss minimization leads to three distinct decision strategies [181]:

- minimization of the lower expected loss, yielding a decision rule $D_{\min}$ defined by

$$D_{\min}(\theta) = \min_{a \in \mathcal{A}} R_{\min}(a \mid \theta) \tag{179}$$

- minimization of the upper expected loss, yielding a decision rule $D_{\max}$ defined by

$$D_{\max}(\theta) = \min_{a \in \mathcal{A}} R_{\max}(a \mid \theta) \tag{180}$$

- minimization of the expected loss relative to $BetP$, yielding decision rule D_{bet} defined by

$$D_{BetP}(\theta) = \min_{a \in \mathcal{A}} R_{BetP}(a \mid \theta) \tag{181}$$

The different decision options leave the damage pattern recognition user with multiple alternatives. The upper expected loss and the pignistic expected loss minimization lead to a more conservative choice. The riskier approach would logically lead to considering the lower expected loss of each possible action. Which strategy should be chosen obviously depends on the situational context. For example, if a prompt diagnostic decision is not required, then a more conservative decision could be taken or no-decision could be made until further data is collected. In this work, we have chosen to use the pignistic expected loss to yield the diagnostic decision rule D_{bet}.

The D-S evidence theory offers a convenient framework for dealing with uncertainty in situations where the available information is limited. In many diagnostic applications, it is difficult or even impossible to build an exhaustive learning set for many reasons, such as some classes (damage events or anomalies) have very small prior probabilities, collecting samples from certain classes would be too dangerous or costly, the number of classes is very high, and an exhaustive list of all possible states of nature is not available. These problems in data collection for classification training arise especially in diagnosis of complex structural systems.

Damage detection and localization, which rely on the modal parameter estimation such as the one described in this study, might have the drawback that the damage locations and amount may

not be uniquely and adequately determined from the estimated modal data. Models with differently assumed damage locations and amount, i.e. output equivalent, can provide identical modal parameters. Since the modal testing measures dynamic responses at limited points and estimates only a few fundamental modes, the number of output equivalent models can increase. Therefore, multiple hypotheses should be examined to find the local maximum belief mass and potentially identify the correct damage event. The exhaustive search of all possible models (hypotheses) is infeasible, and the proposed evidential scheme may identify only some models, which locally maximize the *Bel* of existing damage.

In this study, the computational effort to find the most likely damage location increases with the number of potentially damaged substructures. Since the current damage assessment approach is developed for continuous monitoring of a structure, we intend to detect damage at its early stage. Therefore, for continuous monitoring, we can assume that damage is localized in small discrete number of regions.

8.3 Case Study: Damage Reasoning in Plate Experiment

The application considered in this work concerns the damage localization in an aluminum plate. The plate experiment of Chapter 6 and the damage assessment results of Chapter 7 are considered to demonstrate the proposed damage localization based on evidential reasoning. Modal parameters are used as the extracted features for performing damage assessment analysis. Damage was induced as localized mass modifications as shown in Figure 8.2. Due to noise content, the damage localization results obtained in Chapter 7 for each damage assessment method were imprecise and still require some final level of human reasoning and interpretation in order to accept or reject damage assessment results.

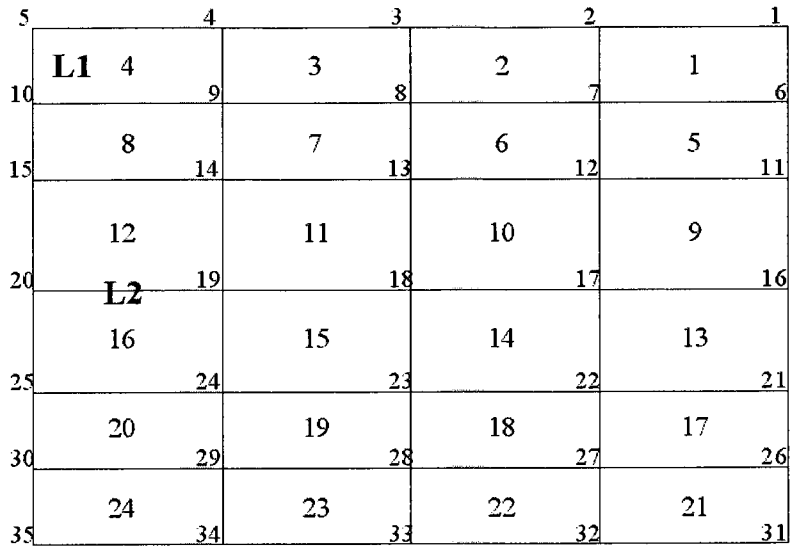

Figure 8.2. Finite element shells (1 through 24) and sensor locations (1 through 35) for aluminum plate. L1 and L2 correspond to the mass modifications locations.

Six damage (mass modifications) cases are studied, which are Cases 1-3: $\{L1:12g,27g,54g\}$, Cases 4-5: $\{L2:27g,54g\}$ and Case 6: $\{L1 \text{ and } L2:27g\}$. With the exception of Case 6, all cases of a single damage location. The damage indication results from the COMAC, MSC, TFRAC, SEDI and the proposed SDI method were obtained. For each damage indication method, the evidential clustering technique was applied to extract basic belief assignments (BBAs) for each node or sensor location. The proposed aggregation method is evaluated by combining the outputs from all the vibration-based damage localization methods. The belief functions based on evidential clustering were obtained at the node level (35 nodes) and the finite element shell level (24 shells). Although 35 nodes are reported, due to the finite element discretization of the plate structure, the damage localization results are also reported at the shell level. Aggregation of the BBA results for all five damage localization methods was also generated using the proposed modified Dempster's rule which utilized a weighting criterion based on the entropy measure.

The classification space was decomposed into three possible outcomes. The possible clusters for the evidential damage localization are $\{c_k : Damaged, Undamaged, No\ Decision\}$. The "No Decision" class is assigned to $m(\Theta)$, which is the portion of total belief which remains unassigned, or assigned to the environment (unknown), after commitment of belief to various subsets of Θ. The parameters of evidential clustering method are $\alpha = 1$, $\beta = 2$, $\delta^2 = 10$, and $\varepsilon = 1e-4$.

To provide crisp diagnostic decisions, the cluster with the highest BBA value is assigned to each shell. In other words, instead of providing numerical BBA values, the diagnostic results are provided as "Undamaged," "Damaged," or "No Decision." The "No Decision" diagnostic result is given when the unassigned BBA is the highest for the particular shell.

The reasoning behind the "No Decision" is as follows. Admission of imprecision in probabilities is needed to reflect the amount of information on which they are based. When limited data is available or classification is not clear, assessment of precise probabilities becomes impossible or impractical, and a damage state classification should then be avoided. In other words, for partial data, partial answers should be given. The D-S theory handles both the uncertainty and imprecision contained in data due to the belief and plausibility functions which can be seen as an interval enclosing imprecise probability. The D-S theory does not pretend to provide full answers to probabilistic data, but rather provides partial answers by estimating how much does the evidence supports the truth of a hypothesis, instead of estimating how close the hypothesis is to being true.

8.3.1 Data Analysis and Results

Given clear separation between undamaged and damaged clusters, the true damage locations would be signaled by a high damaged BBA and a low undamaged BBA. All the undamaged locations would have a high undamaged BBA and a low damaged BBA. Additionally, in clear damage localization, the BBA for the unassigned cluster should be minimal. The obtained BBAs at the node level are shown in Figure 8.3 through Figure 8.7 for damage case 3 only. Each figure reports the BBA for the empty set, the damaged cluster, the undamaged cluster, and the unassigned cluster. For damage case 3, the nodes showing a high damaged BBA should be nodes 4,5, 9 and 10 due to proximity to damage location.

Figure 8.3 shows the BBAs obtained using the damage localization results of the proposed SDI method. The only nodes indicating a high BBA are nodes 5 and 10, which is the correct indication. With the exception of node 3, all the other nodes have a high undamaged BBA. Node 3 has a high indication of unassigned BBA, which states that it is not clear that according to the evidence provided that this particular can be classified as damaged or undamaged.

Before analyzing the results of the MSC baseline damage localization, it is important to note that in section 7.4.4 the methods based on the mode shape derivatives, in other words SEDI and MSC approaches, provided localization results that were heavily affected by false-positives due to the uncertainty content. Now, Figure 8.4 and Figure 8.5 shows the BBAs obtained using the damage localization results of the MSC and SEDI method, respectively. In contrast to the results obtained using the SDI method, the BBA results of these two methods show significant variation in the BBA values. The results for the MSC method show a high damage BBA for the true damage nodes 5 and 10, but also at nodes 3, 7, 8, and 20-22, which are considered false-positives. Also, the number of nodes obtaining high undamaged BBAs is rather low compared to the SDI

results. Instead, an increasing number of nodes show a high unassigned BBA value. Similar results are observed for the SEDI method as shown in Figure 8.5.

Figure 8.6 and Figure 8.7 show the BBAs obtained for the COMAC and TFRAC methods, respectively. As expected, the results are more similar to the SDI results of Figure 8.3 since these methods are based on direct frequency measurements and mode shapes, which are smaller signal to noise ratio in comparison to the mode shape derivatives. For the COMAC method, Figure 8.6 shows a high damaged BBA at node 4 only. With exception of nodes 9, 10, 23-25, 29, and 31, which are unassigned, the rest of the nodes show a high undamaged BBA. For the TFRAC method, Figure 8.7 shows a high damage BBA for nodes 5, 7, and 35. Node 5 is a true positive, but nodes 7 and 35 are false positives. Node 6 has the unassigned BBA as its highest value. The rest of the nodes obtained a high undamaged BBA value.

In all the nodes with high damage (undamage) BBAs, the BBA for the undamaged (damaged) cluster is very small, which indicates that the similarity to this secondary cluster is minimal. In addition, the unclassified option becomes useful when a strong similarity does not exists between a particular cluster type and the node damage localization result.

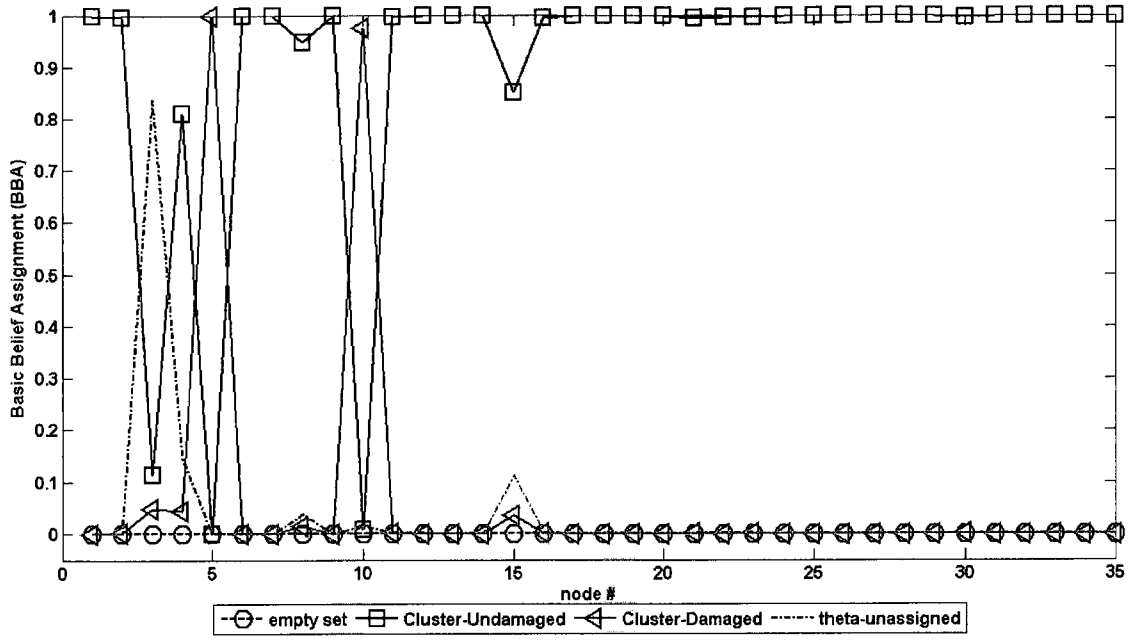

Figure 8.3. Basic belief assignment partition for damage case 3 using SDI damage localization results.

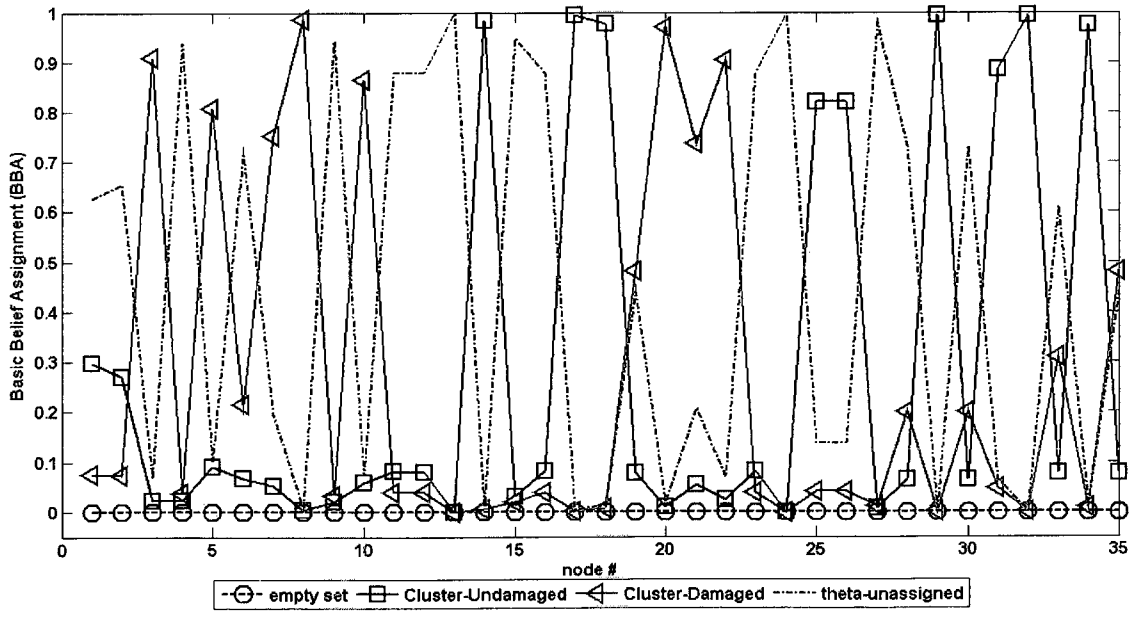

Figure 8.4. Basic belief assignment partition for damage case 3 using MSC damage localization results.

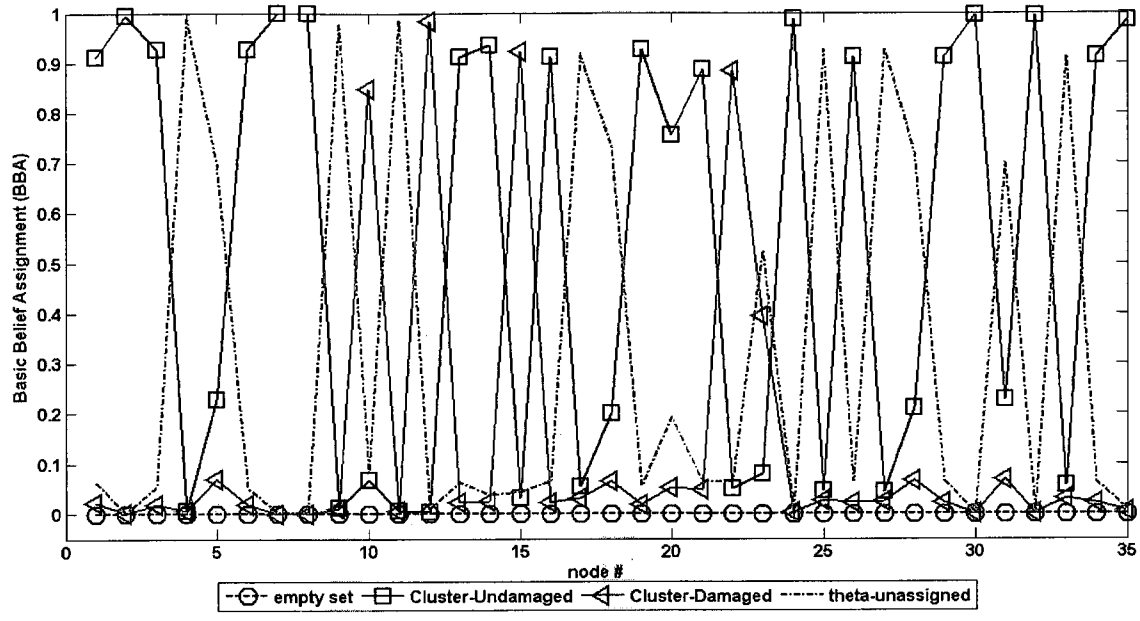

Figure 8.5. Basic belief assignment partition for damage case 3 using SEDI damage localization results.

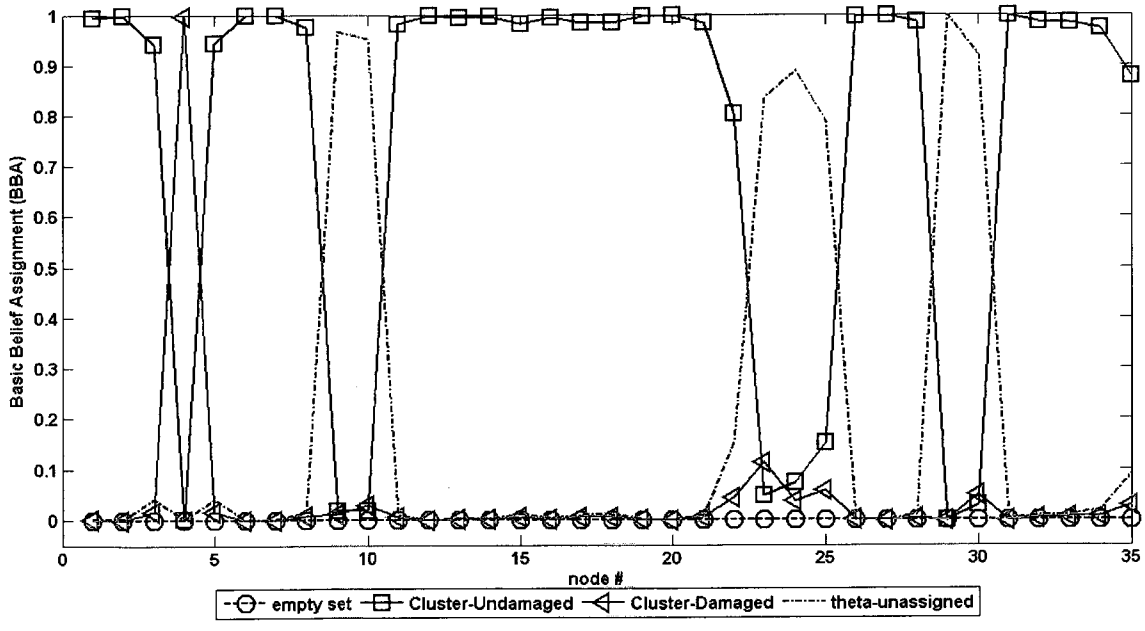

Figure 8.6. Basic belief assignment partition for damage case 3 using COMAC damage localization results.

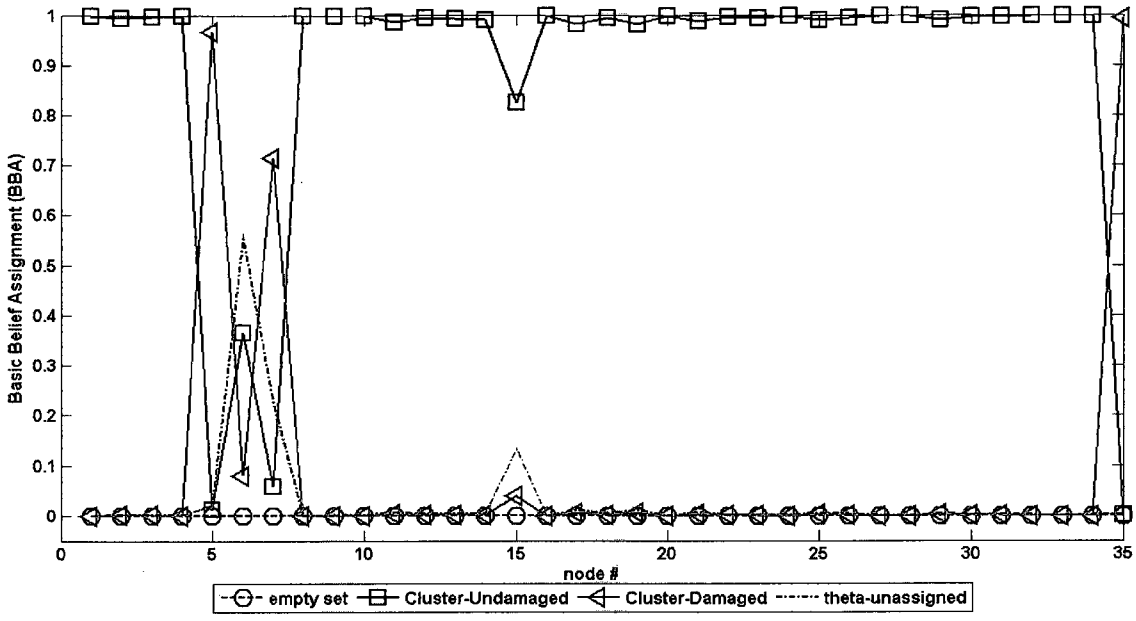

Figure 8.7. Basic belief assignment partition for damage case 3 using TFRAC damage localization results.

Next, the crisp diagnostic results are presented at the finite element shell level. Due to the discretization of the aluminum plate, the crisp diagnostic information can only be provided at the shell level, as shown in Figure 8.2. The evidential clustering approach was applied by combining for each shell its four corresponding damage localization node values. For quick visual inspection of the damage localization results, the cells are color coded, where a green color corresponds to a true-positive, a bluecolor corresponds to a true-negative, a red color corresponds to a false-positive, a magenta color corresponds to a false-negative, and a gray color corresponds to a no-decision result.

Table 8.1 shows the crisp diagnostic results for the proposed SDI method. Based on the SDI damage localization, correct localization was obtained for case 1, 3 and 5. In cases 2, 4 and 6, correct damage localization was not obtained, but it was also free of false-indication of damage since many of the shells did not produce a clear BBA value supporting either the damage or undamaged cluster, and resulted in a no-decision. Only case 1, the case with the smallest mass

modification, resulted in false-positives for shell numbers 6 and 11, which is expected since the small mass modification is hard to detect, yet alone correctly localized.

Next, Table 8.2 shows the crisp diagnostic results for the ensemble of the BBA results from all damage localization methods using the proposed modified Dempster's rule. The approach of combining multiple BBAs obtained from individual damage localization methods was aimed at obtaining a more robust damage localization robust results. For this particular case, the results demonstrate that using the ensemble method correct localization was achieved for all 6 cases including the case 1, which had the smallest mass modification. The only drawback was that relatively more false-damage indications were obtained in cases 2, 4, and 6.

Finally, Table 8.3 and Table 8.4 show the crisp diagnostic results for the SEDI and COMAC methods, respectively. The SEDI results show, as expected, a relatively high number of false-positives in all cases except cases 4 and 5, but also for these two cases, the true-positives were obtained. True-positive results were obtained for cases 2 and 3.

An interesting observation is that with exception of the SEDI method, all methods failed to recognize the secondary damage location at shell 4 in case 6. The COMAC results shown in Table 8.4 show something very interesting, this particular method did not achieve any true-positives, and did have multiple false-positives. Furthermore, in all cases, with the exception of two indications in the SEDI results, no false-negatives were obtained. One possible reason for such result is that the no-decision option in the evidential reasoning approach overcame the possible false-negatives.

The non-existent indications of false-negatives can also be due to the fact that indeed all damage localization methods are sensitive to the mass modifications, but they are also sensitive to noise content. Hence, the difficulty in diagnosing in damage location is increased due to the noise

content, and at not having a dominant similarity to damaged or undamaged cluster, the BBA of the particular shell results is not assigned to any of these two clusters, which results in the no-decision. The additional diagnostic decision tables for the TFRAC and MSC method are reported in Appendix B.

Table 8.1. Damage diagnostic decision for shell regions using proposed SDI method.

	True Positive	True Negative	False Positive	False Negative	NO DECISION	
Evidential Reasoning Damage Localization Results						
Shell #	**Case 1**	**Case 2**	**Case 3**	**Case 4**	**Case 5**	**Case 6**
1	NO DECISION	UNDAMAGED	UNDAMAGED	UNDAMAGED	UNDAMAGED	UNDAMAGED
2	UNDAMAGED	UNDAMAGED	NO DECISION	UNDAMAGED	UNDAMAGED	UNDAMAGED
3	NO DECISION	UNDAMAGED	NO DECISION	UNDAMAGED	UNDAMAGED	UNDAMAGED
4	DAMAGED	NO DECISION	DAMAGED	NO DECISION	NO DECISION	NO DECISION
5	NO DECISION	UNDAMAGED	UNDAMAGED	UNDAMAGED	UNDAMAGED	NO DECISION
6	DAMAGED	UNDAMAGED	UNDAMAGED	UNDAMAGED	UNDAMAGED	UNDAMAGED
7	NO DECISION	UNDAMAGED	UNDAMAGED	NO DECISION	UNDAMAGED	UNDAMAGED
8	NO DECISION	NO DECISION	NO DECISION	NO DECISION	NO DECISION	NO DECISION
9	NO DECISION	NO DECISION	UNDAMAGED	UNDAMAGED	UNDAMAGED	NO DECISION
10	NO DECISION	UNDAMAGED	UNDAMAGED	NO DECISION	NO DECISION	UNDAMAGED
11	DAMAGED	UNDAMAGED	UNDAMAGED	NO DECISION	NO DECISION	NO DECISION
12	NO DECISION	UNDAMAGED	UNDAMAGED	NO DECISION	NO DECISION	NO DECISION
13	UNDAMAGED	NO DECISION	UNDAMAGED	NO DECISION	NO DECISION	NO DECISION
14	UNDAMAGED	NO DECISION	UNDAMAGED	NO DECISION	NO DECISION	NO DECISION
15	NO DECISION	UNDAMAGED	UNDAMAGED	NO DECISION	NO DECISION	NO DECISION
16	NO DECISION	UNDAMAGED	UNDAMAGED	NO DECISION	DAMAGED	NO DECISION
17	UNDAMAGED	NO DECISION	UNDAMAGED	UNDAMAGED	NO DECISION	UNDAMAGED
18	UNDAMAGED	UNDAMAGED	UNDAMAGED	UNDAMAGED	NO DECISION	UNDAMAGED
19	UNDAMAGED	UNDAMAGED	UNDAMAGED	NO DECISION	UNDAMAGED	UNDAMAGED
20	UNDAMAGED	UNDAMAGED	UNDAMAGED	NO DECISION	NO DECISION	NO DECISION
21	UNDAMAGED	NO DECISION	UNDAMAGED	UNDAMAGED	UNDAMAGED	NO DECISION
22	UNDAMAGED	NO DECISION	UNDAMAGED	UNDAMAGED	UNDAMAGED	UNDAMAGED
23	NO DECISION	UNDAMAGED	UNDAMAGED	NO DECISION	UNDAMAGED	UNDAMAGED
24	UNDAMAGED	UNDAMAGED	UNDAMAGED	NO DECISION	NO DECISION	NO DECISION

Table 8.2. Damage diagnostic decision for shell regions using ensemble method.

	True Positive	True Negative	False Positive	False Negative	NO DECISION	
	Evidential Reasoning Damage Localization Results					
Shell #	**Case 1**	**Case 2**	**Case 3**	**Case 4**	**Case 5**	**Case 6**
1	UNDAMAGED	NO DECISION	UNDAMAGED	UNDAMAGED	UNDAMAGED	UNDAMAGED
2	UNDAMAGED	UNDAMAGED	UNDAMAGED	UNDAMAGED	UNDAMAGED	UNDAMAGED
3	NO DECISION	NO DECISION	NO DECISION	UNDAMAGED	UNDAMAGED	UNDAMAGED
4	DAMAGED	DAMAGED	DAMAGED	UNDAMAGED	UNDAMAGED	NO DECISION
5	UNDAMAGED	NO DECISION	UNDAMAGED	UNDAMAGED	NO DECISION	NO DECISION
6	NO DECISION	NO DECISION	UNDAMAGED	UNDAMAGED	UNDAMAGED	UNDAMAGED
7	NO DECISION	NO DECISION	NO DECISION	NO DECISION	NO DECISION	UNDAMAGED
8	NO DECISION	DAMAGED	NO DECISION	NO DECISION	NO DECISION	NO DECISION
9	NO DECISION	NO DECISION	UNDAMAGED	NO DECISION	NO DECISION	DAMAGED
10	NO DECISION	UNDAMAGED	UNDAMAGED	UNDAMAGED	NO DECISION	NO DECISION
11	NO DECISION	UNDAMAGED	UNDAMAGED	NO DECISION	NO DECISION	NO DECISION
12	UNDAMAGED	NO DECISION	UNDAMAGED	DAMAGED	DAMAGED	NO DECISION
13	NO DECISION	NO DECISION	NO DECISION	DAMAGED	NO DECISION	DAMAGED
14	NO DECISION	NO DECISION	NO DECISION	NO DECISION	UNDAMAGED	NO DECISION
15	UNDAMAGED	UNDAMAGED	UNDAMAGED	NO DECISION	NO DECISION	NO DECISION
16	UNDAMAGED	NO DECISION	UNDAMAGED	NO DECISION	DAMAGED	DAMAGED
17	UNDAMAGED	NO DECISION	NO DECISION	NO DECISION	NO DECISION	NO DECISION
18	UNDAMAGED	UNDAMAGED	NO DECISION	NO DECISION	UNDAMAGED	NO DECISION
19	UNDAMAGED	UNDAMAGED	NO DECISION	DAMAGED	UNDAMAGED	NO DECISION
20	UNDAMAGED	UNDAMAGED	UNDAMAGED	NO DECISION	UNDAMAGED	NO DECISION
21	UNDAMAGED	NO DECISION	UNDAMAGED	UNDAMAGED	NO DECISION	UNDAMAGED
22	NO DECISION	NO DECISION	UNDAMAGED	UNDAMAGED	NO DECISION	UNDAMAGED
23	NO DECISION	UNDAMAGED	UNDAMAGED	NO DECISION	UNDAMAGED	NO DECISION
24	UNDAMAGED	UNDAMAGED	NO DECISION	NO DECISION	UNDAMAGED	NO DECISION

Table 8.3. Damage diagnostic decision for shell regions using SEDI method.

	True Positive	True Negative	False Positive	False Negative	NO DECISION	
Evidential Reasoning Damage Localization Results						
Shell #	**Case 1**	**Case 2**	**Case 3**	**Case 4**	**Case 5**	**Case 6**
1	UNDAMAGED	UNDAMAGED	UNDAMAGED	UNDAMAGED	NO DECISION	NO DECISION
2	UNDAMAGED	UNDAMAGED	UNDAMAGED	UNDAMAGED	UNDAMAGED	NO DECISION
3	NO DECISION	NO DECISION	NO DECISION	UNDAMAGED	UNDAMAGED	NO DECISION
4	NO DECISION	DAMAGED	DAMAGED	UNDAMAGED	UNDAMAGED	DAMAGED
5	NO DECISION	NO DECISION	NO DECISION	UNDAMAGED	UNDAMAGED	NO DECISION
6	UNDAMAGED	UNDAMAGED	UNDAMAGED	UNDAMAGED	UNDAMAGED	UNDAMAGED
7	NO DECISION	NO DECISION	NO DECISION	UNDAMAGED	UNDAMAGED	UNDAMAGED
8	DAMAGED	DAMAGED	DAMAGED	NO DECISION	NO DECISION	DAMAGED
9	DAMAGED	NO DECISION	DAMAGED	NO DECISION	UNDAMAGED	NO DECISION
10	NO DECISION	NO DECISION	NO DECISION	UNDAMAGED	UNDAMAGED	NO DECISION
11	UNDAMAGED	UNDAMAGED	UNDAMAGED	UNDAMAGED	UNDAMAGED	UNDAMAGED
12	NO DECISION	NO DECISION	NO DECISION	NO DECISION	NO DECISION	NO DECISION
13	DAMAGED	NO DECISION	NO DECISION	NO DECISION	NO DECISION	DAMAGED
14	NO DECISION	NO DECISION	NO DECISION	NO DECISION	UNDAMAGED	NO DECISION
15	NO DECISION	UNDAMAGED	NO DECISION	UNDAMAGED	UNDAMAGED	UNDAMAGED
16	NO DECISION	NO DECISION	NO DECISION	UNDAMAGED	UNDAMAGED	NO DECISION
17	NO DECISION	NO DECISION	NO DECISION	UNDAMAGED	UNDAMAGED	NO DECISION
18	NO DECISION	DAMAGED	DAMAGED	UNDAMAGED	UNDAMAGED	DAMAGED
19	NO DECISION	NO DECISION	NO DECISION	NO DECISION	UNDAMAGED	NO DECISION
20	NO DECISION	NO DECISION	NO DECISION	UNDAMAGED	UNDAMAGED	NO DECISION
21	NO DECISION	NO DECISION	NO DECISION	UNDAMAGED	UNDAMAGED	NO DECISION
22	NO DECISION	NO DECISION	NO DECISION	UNDAMAGED	UNDAMAGED	NO DECISION
23	UNDAMAGED	NO DECISION	NO DECISION	NO DECISION	NO DECISION	DAMAGED
24	UNDAMAGED	NO DECISION	UNDAMAGED	NO DECISION	UNDAMAGED	NO DECISION

Table 8.4. Damage diagnostic decision for shell regions using COMAC method.

	True Positive	True Negative	False Positive	False Negative	NO DECISION	
Evidential Reasoning Damage Localization Results						
Shell #	**Case 1**	**Case 2**	**Case 3**	**Case 4**	**Case 5**	**Case 6**
1	UNDAMAGED	NO DECISION	UNDAMAGED	UNDAMAGED	NO DECISION	UNDAMAGED
2	NO DECISION	NO DECISION	UNDAMAGED	UNDAMAGED	NO DECISION	UNDAMAGED
3	DAMAGED	NO DECISION	NO DECISION	UNDAMAGED	UNDAMAGED	NO DECISION
4	NO DECISION	NO DECISION	NO DECISION	UNDAMAGED	UNDAMAGED	NO DECISION
5	UNDAMAGED	UNDAMAGED	UNDAMAGED	NO DECISION	DAMAGED	NO DECISION
6	UNDAMAGED	UNDAMAGED	UNDAMAGED	UNDAMAGED	NO DECISION	UNDAMAGED
7	NO DECISION	NO DECISION	NO DECISION	NO DECISION	NO DECISION	NO DECISION
8	NO DECISION	DAMAGED	NO DECISION	NO DECISION	NO DECISION	UNDAMAGED
9	NO DECISION	NO DECISION	UNDAMAGED	NO DECISION	DAMAGED	DAMAGED
10	UNDAMAGED	NO DECISION	UNDAMAGED	NO DECISION	NO DECISION	NO DECISION
11	UNDAMAGED	NO DECISION	UNDAMAGED	NO DECISION	NO DECISION	NO DECISION
12	UNDAMAGED	NO DECISION	UNDAMAGED	NO DECISION	NO DECISION	NO DECISION
13	NO DECISION	NO DECISION	UNDAMAGED	NO DECISION	NO DECISION	NO DECISION
14	NO DECISION	NO DECISION	NO DECISION	NO DECISION	NO DECISION	NO DECISION
15	UNDAMAGED	DAMAGED	NO DECISION	NO DECISION	NO DECISION	NO DECISION
16	UNDAMAGED	DAMAGED	NO DECISION	NO DECISION	NO DECISION	NO DECISION
17	UNDAMAGED	UNDAMAGED	UNDAMAGED	NO DECISION	DAMAGED	NO DECISION
18	UNDAMAGED	UNDAMAGED	NO DECISION	NO DECISION	NO DECISION	NO DECISION
19	UNDAMAGED	NO DECISION	NO DECISION	NO DECISION	NO DECISION	NO DECISION
20	NO DECISION	NO DECISION	NO DECISION	NO DECISION	NO DECISION	NO DECISION
21	UNDAMAGED	UNDAMAGED	UNDAMAGED	UNDAMAGED	NO DECISION	NO DECISION
22	UNDAMAGED	UNDAMAGED	UNDAMAGED	UNDAMAGED	NO DECISION	UNDAMAGED
23	NO DECISION	UNDAMAGED	NO DECISION	UNDAMAGED	UNDAMAGED	UNDAMAGED
24	NO DECISION	UNDAMAGED	NO DECISION	UNDAMAGED	UNDAMAGED	UNDAMAGED

To tabulate the accuracy of the damage localization results obtained using the proposed evidential reasoning method, the performance is evaluated using the following functions

$$\text{Damage Detection Rate (DDR)} = \frac{TP}{FN + TP} \tag{182}$$

$$\text{False Alarm Rate (FAR)} = \frac{FP}{TN + FP} \tag{183}$$

$$\text{Overall Accuracy (OA)} = \frac{TP + TN}{TP + TN + FP + FN} \tag{184}$$

$$\text{Overall Miss (OM)} = \frac{FP + FN}{TP + TN + FP + FN} \tag{185}$$

where TP, TN, FP and FN are true-positive, true-negative, false-positive, and false-negative, respectively. In addition, the portion of the possible $24 \text{ shells} \times 6 \text{ cases}$ diagnosis results with a "No-Decision" localization result are also reported.

Table 8.6 shows the obtained damage localization performance measures for all the damage localization approaches. Since only the SEDI method obtained false-negative results, the DDR values reported for each method are not of great value since they report a value of 1.00, even though perfect detection was not achieved. Comparing the FAR values, the worst diagnostic performance was obtained by the MSC method, which indicates a very high value of 0.83 for false alarm rate. The MSC overall accuracy stands only at 0.25. The best diagnostic performance was essentially the same for the proposed SDI method and the baseline TFRAC method. The SDI and TFRAC reported overall accuracy values of 0.98 and 0.97, respectively.

For the ensemble method, the weighted values based on the inverse entropy measures are reported in Table 8.5. For each case, the maximum and minimum weights are shown in bold-italics font. In all cases, the TFRAC method obtained the largest weighting values and the MSC method obtained the smallest weighting values. These weight results correlate well with the

visual analysis of the color variation in the damage localization results shown in section 7.3.1. Again the assumption behind the weighting mechanism is that damage is localized and discrete. Therefore, damage localization results demonstrating significant variance should receive the lowest weighting values. The ensemble method results obtained by using the modified weighted Dempster's rule also obtained a high overall accuracy value of 0.93. Although, the ensemble method did not obtain the best diagnostic performance, it does achieve the objective of increased robustness due to information conflict. The ensemble method consisted of the belief function aggregation of all the damage localization methods, including the poor performing MSC method. As presented and discussed in section 8.2.2, one of the advantages of the proposed belief function aggregation method is that it can deal with conflictive information sources. This advantage was demonstrated with the current damage localization results.

Table 8.5. Basic belief assignment weights used in modified Dempster's rule for aggregation.

	SDI	MSC	SEDI	COMAC	TFRAC
Case 1	0.319	***0.259***	0.299	0.328	***0.401***
Case 2	0.375	***0.248***	0.270	0.286	***0.413***
Case 3	0.439	***0.254***	0.291	0.257	***0.419***
Case 4	0.317	***0.233***	0.350	0.281	***0.401***
Case 5	0.342	***0.262***	0.337	0.280	***0.503***
Case 6	0.332	***0.273***	0.315	0.316	***0.336***

Table 8.6. Damage localization performance for the evidential reasoning approach.

	DDR	FAR	OA	OM	NO DECISION
SDI	1.00	0.02	0.98	0.02	0.41
Ensemble	1.00	0.07	0.93	0.07	0.49
MSC	1.00	0.83	0.25	0.75	0.51
SEDI	0.60	0.17	0.81	0.19	0.49
COMAC	0.00	0.13	0.87	0.13	0.58
TFRAC	1.00	0.04	0.97	0.03	0.40

Common to all damage localization methods was the high level of "No Decision" results. Out of the possible 144 (24 shells×6 cases) finite element locations, all methods reported in excess of 40% the "No Decision" diagnosis.

The high level of overall accuracy obtained by the damage localization methods, with the exception of the MSC approach, is mainly due to the fact that the number of false-positives (true-negatives) is relatively low (high). This high level of overall accuracy does have some potential drawback since the true damage location was not localized in all cases. The evidential reasoning analysis could be adjusted to take a more riskier decision-making approach in order to properly identify as "Damaged" additional true damage locations, but, excuse the redundancy, this comes at a risk, which would translate to additional false-positives being localized. This observation addresses one of the dilemmas in damage detection and localization, which is that an increase in true-positives is always accompanied by additional false-positives. In other words, the features that are sensitive to damage are also sensitive to noise.

8.4 Discussion

The damage diagnostic results obtained using the proposed evidential reasoning approach are much clearer and easier to interpret than the raw damage localization indication obtained by the vibration-based damage localization methods. The fusion results obtained via the weighted aggregation of the damage localization belief functions generates robust diagnostic results in comparison to the best individual damage localization method. The proposed aggregation of belief functions based on a modified weighted Dempster rule was shown to be capable of dealing with conflictive information sources. Hence, the modified Dempster's rule can deal with the problem of fusing multiple information sources of different importance or reliability by generating weights based on the inverse of the damage localization entropy values.

The experimental model-based, such as mode shapes, analytical (finite element method), and the data-driven (pattern recognition) approaches to damage assessment of continuous structures suffer from the fact that under real conditions no accurate mathematical or experimental model of the system can be obtained. Damage assessment methods cannot overcome this deficiency and the current structural health condition can only be known to a certain degree, and with significant effort. As it was previously observed in Chapter 7, the damage assessment results that has to be processed is commonly imprecise and incomplete. Imprecise because current state-of-the-art system identification methods are not at the level of providing precise location, size, type, and nature of structural changes, such as damage. Incomplete because current structural sensing capabilities do not provide information local to all structural members or points. For full structural sensing coverage, it is required that sensors themselves be part of the structure.

8.5 Summary

In this chapter, we have presented an evidential reasoning approach for structural damage assessment. The main contribution of this work is the additional decision-making capability achieved by introducing the Dempster-Shafer evidence theory, an AI approach, in order to deal with imprecise diagnostic information. The proposed evidential reasoning diagnostic decision-making approach has been demonstrated with the use of the imprecise vibration-based damage localization results obtained in Chapter 7.

One advantage of the Dempster-Shafer approach to damage classification is the fact that it can assign patterns or measurements to the frame of discernment (unassigned or no-decision cluster) and thus indicate to the analyst that there is insufficient evidence to make a classification of undamaged or damaged. Another advantage of the proposed evidential reasoning approach is that

it can be used to perform aggregation or fusion of possibly conflictive information sources. The overall diagnostic goal in structural health monitoring is to achieve a zero misclassification rate. The proposed evidential reasoning approach is a step closer towards this goal since the evidence-based diagnostic classifier will reject the data rather than produce an error.

Over the years, the evolution of data acquisition, signal processing, and data management and storage capabilities has enabled continuous advancements in the practice of condition monitoring and diagnosis. In the field of damage assessment for dynamic systems, rapid development is needed from the well established but limited efficiency traditional methods of vibration model correlation towards more powerful methods of decision-making under uncertainty.

One of the key aspects distinguishing current damage assessment methods from human intelligence in dealing with diagnosis of off-nominal events is the enhanced reasoning capability. Reasoning goes beyond basic diagnoses of observed condition indicators. Addressing and answering how does the human brain work in making decisions is beyond the current work, but at the very minimum, we can make observation of the human brain at making decision under uncertainty. The brain runs well in dealing with all kinds of uncertainty in sensation, perception, learning, reasoning, thinking, understanding and action.

The computer science research branch of artificial intelligence (AI) is concerned with the automation of intelligent behavior of machines. AI research aims at creating systems that not only think like humans, but more specifically, that think rationally with qualitative and quantitative information in an efficient and consistent manner. Thus, AI attempts to achieve human intelligence, but with the benefits of computer programs. A sub-research area of AI is decision-making under uncertainty, which is applicable to the work in damage assessment since diagnostic decision-making is a task that almost always involves uncertainty.

Chapter 9

Conclusion

In this dissertation, the research work formulated analytical and experimental vibration-based structural damage assessment methods in order to minimize the diagnosis errors caused by uncertainty. An overall intelligent diagnostic reasoning framework was developed to analyze and interpret structural health monitoring data. This research attempts to bridge the gap between laboratory-based and real-world implementation of vibration-based structural diagnostic approaches by directly addressing the issue of uncertainty.

This chapter will re-examine the questions and objectives posed in the introductory chapter, in the light of the research developments and findings. The main contributions will be presented and discussed. To conclude, future research directions and possibilities will be offered.

9.1 Summary and Discussions

The research was motivated by the need to improve the efficiency and accuracy of current vibration-based structural health monitoring (SHM) methods in order to meet the increasing demands in safety and challenges faced by the trend of a deteriorating infrastructure. As initially stated, SHM is defined as the use of in-situ, nondestructive sensing and analysis of structural characteristics for the purpose of detecting, localizing, estimating the severity of damage, and evaluating the consequences of identified damage on structure.

After a careful and extended review of current SHM techniques and methodologies, it is concluded that work to date on SHM has evolved significantly over the last decade, but multiple obstacles and deficiencies remain which prevent the transition from laboratory experiments to

practical and standard industry application. One of the major reasons for the slow progress of SHM research to industry practice is the existence of uncertainty at every step of the damage assessment process.

The main objective of this research was to improve the structural diagnostic performance under multiple uncertainty sources. The dissertation consisted of the following major research components. First, we developed a robust feature extraction method based on dimensional reduction methods to improved the performance of damage detection classification. Second, given the extracted damage sensitive features, a numerical study in automated damage assessment classification was performed. Third, through output-only modal analysis of the dynamic structure, modal parameters of the structure under analysis are identified. Next, damage localization was performed based on the comparison of identified modal parameters with the reference values determined for the structure in its pristine condition. The proposed vibration-based damage assessment studies were performed and validated via simulations using finite element models, laboratory experiments on plate structure, and benchmark vibration data from a real-world highway bridge.

9.2 Contributions

The motivating question behind this work is how information should be managed to support diagnostic decision-making under uncertainty. By addressing the uncertainty issue in structural diagnostics, the false-diagnosis in structural damage assessment is reduced. The main contributions of this dissertation are:

Uncertainty in SHM: a new vibration-based SHM methodology which directly accounts for uncertainty was developed. The developed systematic vibration-based SHM methodology recognizes and mitigates the associated damage assessment uncertainties. Damage detection and

localization is performed considering (i) uncertainties in the measurement noise and the analytical modeling; (ii) operational and environment variability; and (iii) the cases when only a small number of degrees of freedom are available for measurement and a few modes are estimated.

Uncertainty Management: The appropriate representation, analysis and management of context uncertainties were analyzed and studied. The multiple uncertainty management paradigms - probability, fuzzy-sets, and imprecise probabilities, such as the Dempster-Shafer (D-S) evidence theory, - were presented and assessed in terms of their advantages and disadvantages. The choice of uncertainty analysis method is not arbitrary. Thus, it was concluded that the choice of uncertainty analysis approach depends on the nature of the problem and the expertise of the user. Probability theory can handle aleatory uncertainty contained in data, but it cannot treat the imprecision. Fuzzy-sets theory can handle the vagueness type imprecision by replacing the additive axiom in probability theory with the weaker monotonicity axiom. In the case of insufficient information and no-conflicting evidence, the possibility theory is a suitable method to quantify uncertainty. D-S theory, and other similar imprecise probability approaches, are more appropriate where uncertainty cannot be assigned precise probability to a proposition, and conditioning effects are difficult or impossible to measure separately, and prior odds are not pertinent.

Damage Detection: an effective and robust damage detection technique was developed based on the ensemble of dimensional reduction techniques. Damage in structures needs to be detected at an early stage in order to reduce the cost of maintenance and possibility of an unsafe scenario, but the change of dynamic characteristics of structures is relatively insensitive to small scale damage. Increased robustness in the extraction of damage sensitive features was achieved by systematically incorporating pattern recognition techniques. Two case studies were conducted.

The aeroacoustic experimental studied impact damage detection in a sub-scale wing structure via acoustic measurements under varying excitation levels. The detection of structural cavities was achieved via dimensional reduction of multiple time measurements of frequency response datasets. The vibration experiment studied the detection of abrupt structural changes and their variation. The structural changes simulating damage were induced by localized mass modifications. By applying the proposed damage detection approach, clear indication of damage was obtained with zero false-positive or false-negative. From the results obtained, we may conclude that under test-to-test variability and with no clear visible changes of the frequency response, the proposed damage detection can serve as a means to effectively detect the presence of structural changes, which are characteristic of damage events. The idea of integrating decisions of several diverse feature extraction techniques into an ensemble, which improves upon the performance and robustness of the individual members, is novel. Comparison to damage detection results obtained via individual feature extraction methods demonstrated that proposed ensemble approach was more robust and reliable.

Modal Analysis: In order to perform model-based damage localization under limited sensor outputs, an output-only modal analysis technique was developed based on roving sensor approach. Given the experimental model obtained using output-only modal analysis approach, damage localization can then be performed on modal parameters correlation analysis of damaged and undamaged conditions. The proposed approach is quite useful when the number of required sensor outputs is much greater than the available measurement channels. The method was tested with an in-house aluminum plate experiment. Measurements were performed under 4xFree (FFFF) boundary conditions. The experimental results show that the proposed approach was able to extract well separated mode shapes.

Damage Localization: a damage localization approach was developed based on the modal parameter sensitivity to local structural changes, such as stiffness reduction and mass modifications, and integrated with a statistical sampling technique. The sensitivity-based damage index (SDI) is based upon the correlation interpretation of changes in modal parameters between an undamaged reference condition and a damaged one. The inclusion of modal-sensitivity into the damage correlation analysis improves the detection of the degree(s)-of-freedom which are affected the most by the structural changes. The proposed SDI method reduced false-negative damage diagnosis, but at the same time, it does not guarantee damage localization results free of false-positives. To minimize the event of false-positives (damage indication in damage-free areas), the Monte Carlo statistical sampling method was introduced into the damage localization process to obtain estimates of the modal parameter statistical measures. By applying the statistical sampling technique, the aleatory uncertainty due to measurement and estimate errors are minimized. The proposed damage assessment techniques were applied and thoroughly validated on a basis of in-house experiments on simple structures in laboratory conditions and real engineering structures.

Decision-Making Under Uncertainty: an evidential reasoning approach based on Dempster-Shafer evidence theory was developed for performing diagnostic classification under imprecise information. One advantage of the Dempster-Shafer approach to damage classification is the fact that it can assign patterns or measurements to the frame of discernment (unassigned or no-decision cluster) and thus indicate to the analyst that there is insufficient evidence to make a classification of undamaged or damaged. Another advantage of the proposed evidential reasoning approach is that it can be used to perform aggregation or fusion of possibly conflictive information sources.

9.3 Future Work

In order to make structural health monitoring a standard practice in industry, the issue of false-diagnosis needs to be addressed. Very important to the research area of damage diagnosis is the recognition and identification of the limitations of each particular approach in terms of performance and applicability. By understanding the limitations of the diagnostic system, the following two scenarios can be avoided: (1) unnecessary diagnostic system costs in order to achieve needless high-levels of accuracy performance; and (2) blind human dependence on diagnostic system due to belief that diagnostic system is always correct. Not all damage diagnosis problems require high accuracy performance. For example, damage localization in a civilian bridge is only desired at the sub-structure scale and not at the square millimeter scale. In addition, the understanding that no diagnostic system can reach 100% accuracy at all times and situations will enable acceptance and introduction of diagnostic systems into safety-critical applications, but with well developed processes for mitigating the possible false-diagnosis scenarios.

In damage assessment, all the context uncertainties cannot be well addressed by endless simulations and laboratory experiments. The application of the proposed methods, as well as those already available in the literature, must be incorporated and validated in additional real structures. First, validation must take place by incorporating developed techniques with appropriate equipment into existing dynamic structures. Second, the viability of damage diagnostics approaches can only be evaluated once new dynamic structures are designed and constructed with an embedded diagnostic system, which is evaluated during a complete life cycle of the dynamic structure. Development of such a validation and verification (V&V) environment will allow diagnostic sensitivities to be evaluated, inaccuracies to be quantified, and economic cost-benefit analysis to be determined, to name a few.

Finally, recent advances in sensory equipment, such as embedded sensors, smart materials, such as piezoelectric nanomaterials, information technologies, such wireless communication, and intelligent software, such as artificial intelligence, will have significant impact of the development of structural monitoring and diagnosis. The development of a cost-effective, large scale instrumentation based on these technologies must be carried out in parallel to make the continuous monitoring and diagnosis of dynamic structures a reality.

Appendix A

Additional Mode Shapes

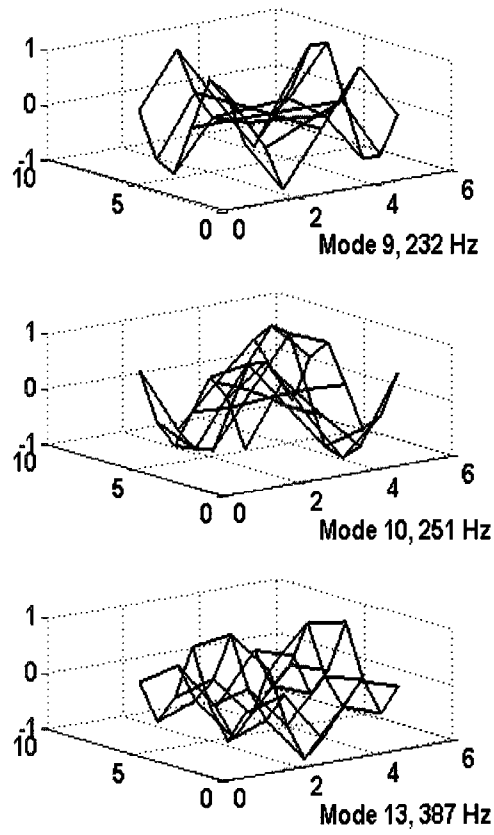

Figure A.1. Additional mode shapes identified in the presence of impact excitation for the plate experiment.

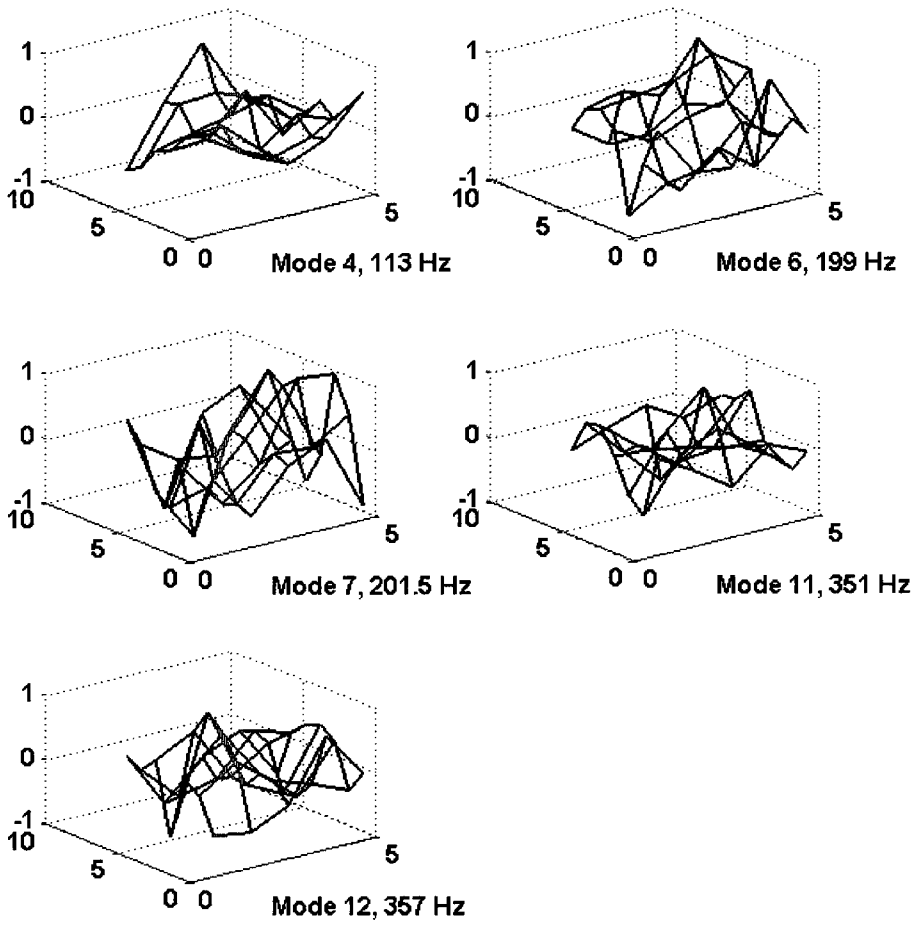

Figure A.2. Poor quality mode shapes not utilized in damage assessment process of the plate experiment.

Appendix B

Additional Evidential Reasoning Results

Table B.1. Damage diagnostic decision for shell regions using MSC method.

	TP	TN	FP	FN	NO DECISION	
	Evidential Reasoning Damage Localization Results					
Shell #	**Case 1**	**Case 2**	**Case 3**	**Case 4**	**Case 5**	**Case 6**
1	UNDAMAGED	NO DECISION	DAMAGED	DAMAGED	NO DECISION	UNDAMAGED
2	UNDAMAGED	DAMAGED	DAMAGED	NO DECISION	UNDAMAGED	NO DECISION
3	UNDAMAGED	DAMAGED	DAMAGED	DAMAGED	UNDAMAGED	NO DECISION
4	NO DECISION	DAMAGED	DAMAGED	NO DECISION	NO DECISION	DAMAGED
5	NO DECISION	DAMAGED	DAMAGED	NO DECISION	NO DECISION	NO DECISION
6	NO DECISION	DAMAGED	DAMAGED	NO DECISION	NO DECISION	NO DECISION
7	NO DECISION	DAMAGED	NO DECISION	DAMAGED	NO DECISION	NO DECISION
8	NO DECISION	DAMAGED	DAMAGED	NO DECISION	NO DECISION	NO DECISION
9	DAMAGED	NO DECISION	NO DECISION	NO DECISION	UNDAMAGED	DAMAGED
10	NO DECISION	NO DECISION	NO DECISION	NO DECISION	UNDAMAGED	DAMAGED
11	DAMAGED	DAMAGED	NO DECISION	DAMAGED	DAMAGED	DAMAGED
12	DAMAGED	DAMAGED	NO DECISION	NO DECISION	DAMAGED	NO DECISION
13	NO DECISION	NO DECISION	NO DECISION	DAMAGED	NO DECISION	NO DECISION
14	NO DECISION	UNDAMAGED	NO DECISION	NO DECISION	UNDAMAGED	UNDAMAGED
15	NO DECISION	NO DECISION	NO DECISION	DAMAGED	DAMAGED	NO DECISION
16	DAMAGED	DAMAGED	DAMAGED	DAMAGED	DAMAGED	DAMAGED
17	NO DECISION	NO DECISION	DAMAGED	DAMAGED	DAMAGED	DAMAGED
18	NO DECISION	NO DECISION	DAMAGED	DAMAGED	NO DECISION	NO DECISION
19	NO DECISION	NO DECISION	NO DECISION	DAMAGED	NO DECISION	NO DECISION
20	NO DECISION	NO DECISION	NO DECISION	DAMAGED	DAMAGED	NO DECISION
21	DAMAGED	NO DECISION	NO DECISION	DAMAGED	DAMAGED	DAMAGED
22	DAMAGED	DAMAGED	NO DECISION	DAMAGED	DAMAGED	DAMAGED
23	NO DECISION	NO DECISION	NO DECISION	DAMAGED	NO DECISION	DAMAGED
24	DAMAGED	DAMAGED	NO DECISION	NO DECISION	NO DECISION	NO DECISION

Table B.2. Damage diagnostic decision for shell regions using TFRAC method.

	TP	TN	FP	FN	NO DECISION	
	Evidential Reasoning Damage Localization Results					
Shell #	**Case 1**	**Case 2**	**Case 3**	**Case 4**	**Case 5**	**Case 6**
1	UNDAMAGED	UNDAMAGED	UNDAMAGED	UNDAMAGED	UNDAMAGED	UNDAMAGED
2	UNDAMAGED	UNDAMAGED	UNDAMAGED	UNDAMAGED	UNDAMAGED	UNDAMAGED
3	NO DECISION	UNDAMAGED	NO DECISION	UNDAMAGED	UNDAMAGED	UNDAMAGED
4	DAMAGED	DAMAGED	DAMAGED	UNDAMAGED	UNDAMAGED	NO DECISION
5	UNDAMAGED	UNDAMAGED	UNDAMAGED	UNDAMAGED	NO DECISION	NO DECISION
6	NO DECISION	UNDAMAGED	UNDAMAGED	UNDAMAGED	UNDAMAGED	UNDAMAGED
7	NO DECISION	UNDAMAGED	NO DECISION	NO DECISION	NO DECISION	UNDAMAGED
8	NO DECISION	NO DECISION	NO DECISION	NO DECISION	NO DECISION	NO DECISION
9	NO DECISION	NO DECISION	UNDAMAGED	UNDAMAGED	NO DECISION	DAMAGED
10	NO DECISION	UNDAMAGED	UNDAMAGED	UNDAMAGED	NO DECISION	NO DECISION
11	NO DECISION	UNDAMAGED	UNDAMAGED	NO DECISION	NO DECISION	NO DECISION
12	UNDAMAGED	NO DECISION	UNDAMAGED	DAMAGED	DAMAGED	NO DECISION
13	NO DECISION	NO DECISION	UNDAMAGED	NO DECISION	NO DECISION	DAMAGED
14	NO DECISION	NO DECISION	UNDAMAGED	UNDAMAGED	UNDAMAGED	NO DECISION
15	UNDAMAGED	UNDAMAGED	UNDAMAGED	NO DECISION	NO DECISION	NO DECISION
16	UNDAMAGED	NO DECISION	UNDAMAGED	NO DECISION	DAMAGED	DAMAGED
17	UNDAMAGED	NO DECISION	UNDAMAGED	NO DECISION	UNDAMAGED	NO DECISION
18	UNDAMAGED	UNDAMAGED	UNDAMAGED	NO DECISION	UNDAMAGED	NO DECISION
19	UNDAMAGED	UNDAMAGED	UNDAMAGED	DAMAGED	UNDAMAGED	NO DECISION
20	UNDAMAGED	UNDAMAGED	UNDAMAGED	NO DECISION	UNDAMAGED	NO DECISION
21	UNDAMAGED	NO DECISION	UNDAMAGED	UNDAMAGED	UNDAMAGED	UNDAMAGED
22	NO DECISION	NO DECISION	UNDAMAGED	UNDAMAGED	UNDAMAGED	UNDAMAGED
23	NO DECISION	UNDAMAGED	UNDAMAGED	NO DECISION	UNDAMAGED	NO DECISION
24	UNDAMAGED	UNDAMAGED	NO DECISION	NO DECISION	UNDAMAGED	NO DECISION

Bibliography

1. M. Abdelghani and M. I. Friswell, "Sensor validation for structural systems with multiplicative sensor faults," Mechanical Systems and Signal Processing, vol. 21, pp. 270-279, 2007.

2. D. E. Adams and M. Nataraju, "A nonlinear dynamical systems framework for structural diagnosis and prognosis," International Journal of Engineering Science, vol. 40, pp. 1919-1941, 2002.

3. S. Alampalli, "Effects of Testing, Analysis, Damage, and Environment on Modal Parameters," Mechanical Systems and Signal Processing, vol. 14, pp. 63-74, 2000.

4. R. Allemang and D. Brown, "A correlation coefficient for modal vector analysis," presented at the Proceedings of the 1st International Modal Analysis Conference (IMAC1), 1982.

5. E. Altunok, et al., "Possibilistic Approach for Damage Detection in Structural Health Monitoring," Journal of Structural Engineering, vol. 133, pp. 1247-1256, 2007.

6. H. Bae and R. Grandhi, "Uncertainty Quantification of Structural Response Using Evidence Theory," AIAA Journal, vol. 41, 2003.

7. H.-R. Bae, et al., "Epistemic uncertainty quantification techniques including evidence theory for large-scale structures," Computers & Structures, vol. 82, pp. 1101-1112, 2004.

8. N. Bakhary, et al., "Damage detection using artificial neural network with consideration of uncertainties," Engineering Structures, vol. 29, pp. 2806-2815, 2007.

9. E. Balmes, et al., "Merging Sensor Data from Multiple Temperature Scenarios for Vibration Monitoring of Civil Structures," Structural Health Monitoring, vol. 7, pp. 129-142, June 1, 2008.

10. Y. Bao, et al., "A Dempster-Shafer evidence theory-based approach for online structural health monitoring," in Health Monitoring of Structural and Biological Systems 2008, San Diego, California, USA, 2008, pp. 69351T-10.

11. O. Basir and X. Yuan, "Engine fault diagnosis based on multi-sensor information fusion using Dempster-Shafer evidence theory," Information Fusion, vol. 8, pp. 379-386, 2007.

12. J. L. Beck and K.-V. Yuen, "Model Selection Using Response Measurements: Bayesian Probabilistic Approach," Journal of Engineering Mechanics, vol. 130, pp. 192-203, 2004.

13. J. Bendat and A. Piersol, Engineering Applications of Correlation and Spectral Analysis: John Wiley, New York, 1980.

14. J. C. Bezdek, *et al.*, "FCM: The fuzzy c-means clustering algorithm," *Computers & Geosciences,* vol. 10, pp. 191-203, 1984.

15. I. Bloch, "Information combination operators for data fusion: a comparative review with classification," Systems, Man and Cybernetics, Part A, IEEE Transactions on, vol. 26, pp. 52-67, 1996.

16. P. P. Bonissone and P. C. Halverson, "Time-constrained reasoning under uncertainty," Real-Time Systems, vol. 2, pp. 25-45, 1990.

17. R. Brincker, et al., "Modal identification of output-only systems using frequency domain decomposition," Smart Materials and Structures, vol. 10, p. 441, 2001.

18. C. S. Byington, et al., "False Alarm Mitigation of Vibration Diagnostic Systems," in Aerospace Conference, 2008 IEEE, 2008, pp. 1-11.

19. F. Campos and F. M. C. d. Souza, "Extending Dempster-Shafer Theory to Overcome Counter Intuitive Results," presented at the IEEE Natural Language Processing and Knowledge Engineering (NLP-KE), Wuhan, China, 2005.

20. Y. Cao, "Bayesian Based Structural Health Management and Reliability Analysis Techniques Utilizing Support Vector Machine," Doctor of Philosophy, Mechanical Engineering, North Carolina State University, 2007.

21. E. P. Carden and P. Fanning, "Vibration Based Condition Monitoring: A Review," Structural Health Monitoring, vol. 3, pp. 355-377, December 1 2004.

22. P. Cawley and R. Adams, "The location of defects in structures from measurements of natural frequencies," Journal of Strain Analysis, vol. 14, pp. 49-57, 1979.

23. D. Cayrac, et al., "Handling uncertainty with possibility theory and fuzzy sets in a satellite fault diagnosis application," Fuzzy Systems, IEEE Transactions on, vol. 4, pp. 251-269, 1996.

24. M. Chandrashekhar and R. Ganguli, "Structural Damage Detection Using Modal Curvature and Fuzzy Logic," Structural Health Monitoring, vol. 8, pp. 267-282, July 1, 2009.

25. S. Chauhan, "Parameter Estimation and Signal Processing Techniques for Operational Modal Analysis," PhD Dissertation, Mechanical Engineering, University of Cincinnati, Cincinnati, OH USA, 2008.

26. J. Ching, et al., "Bayesian state and parameter estimation of uncertain dynamical systems," Probabilistic Engineering Mechanics, vol. 21, pp. 81-96, 2006.

27. P. Cornwell, et al., "Application of the Strain Energy Damage Detection Method to Plate-Like Structures," Journal of Sound and Vibration, vol. 224, pp. 359-374, 1999.

28. S. da Silva, et al., "Structural damage detection by fuzzy clustering," Mechanical Systems and Signal Processing, vol. 22, pp. 1636-1649, 2008.

29. Z. Dai, et al., "A Distributed Coordination Framework for Adaptive Sensor Uncertainty Handling," in Computational Science – ICCS, pp. 1171-1174, 2007.

30. S. Das, et al., "Classification of Damage Signatures in Composite Plates using One-Class SVMs," in IEEE Aerospace Conference., 2007.

31. G. De Sitter, et al., "Maximum likelihood identification of vibroacoustic modes using output-only measurements," presented at the Proceedings of the International Conference on Noise and Vibration Engineering (ISMA2002), 2002.

32. T. Denœux, "A k-Nearest Neighbor Classification Rule Based on Dempster-Shafer Theory," in Classic Works of the Dempster-Shafer Theory of Belief Functions. vol. 219, R. R. Yager and L. Liu, Eds., ed: Springer Berlin / Heidelberg, 2008, pp. 737-760.

33. T. Denoeux, "A neural network classifier based on Dempster-Shafer theory," Systems, Man and Cybernetics, Part A, IEEE Transactions on, vol. 30, pp. 131-150, 2000.

34. A. Deraemaeker, et al., "Vibration-based structural health monitoring using output-only measurements under changing environment," Mechanical Systems and Signal Processing, vol. 22, pp. 34-56, 2008.

35. M. DeSimio, et al., "Decision uncertainty in a structural health monitoring system," in Smart Structures and Materials 2005: Smart Structures and Integrated Systems, San Diego, CA, USA, 2005, pp. 530-541.

36. T. Dietterich, "Ensemble Methods in Machine Learning," in Multiple Classifier Systems, ed, 2000, pp. 1-15.

37. S. Doebling, et al., "Damage identification and health monitoring of structural and mechanical systems from changes in their vibrational characteristics: A literature review," Los Alamos National Laboratory, 1996.

38. S. W. Doebling and F. M. Hemez, "Overview of uncertainty assessment for structural health monitoring " in 3rd International Workshop on Structural Health Monitoring, Stanford University, 2001.

39. M. Döhler, et al., "Data Merging for Multi-Setup Operational Modal Analysis with Data-Driven SSI," presented at the 28th International Modal Analysis Conference (IMAC), Jacksonville, Florida, 2010.

40. R. Du, "Monitoring and Diagnosing Manufacturing Processes Using Fuzzy Set Theory," in Computational Intelligence in Manufacturing Handbook, J. W. e. al, Ed., ed: Boca Raton: CRC Press LLC, 2001.

41. S. Ebersbach, "Artificial Intelligence System for Integrated Wear Debris and Vibration Analysis in Machine Condition Monitoring," PhD Dissertation, School of Engineering, James Cook University, Queensland, Australia, 2007.

42. S. Ebersbach and Z. Peng, "Expert system development for vibration analysis in machine condition monitoring," Expert Systems with Applications, vol. 34, pp. 291-299, 2008.

43. B. I. Epureanu and S.-H. Yin, "Identification of damage in an aeroelastic system based on attractor deformations," Computers & Structures, vol. 82, pp. 2743-2751, 2004.

44. D. Ewins, Modal testing: theory and practice: Research Studies Press, 1995.

45. X. Fan and M. J. Zuo, "Fault diagnosis of machines based on D-S evidence theory. Part 1: D-S evidence theory and its improvement," Pattern Recognition Letters, vol. 27, pp. 366-376, 2006.

46. X. Fan and M. J. Zuo, "Fault diagnosis of machines based on D-S evidence theory. Part 2: Application of the improved D-S evidence theory in gearbox fault diagnosis," Pattern Recognition Letters, vol. 27, pp. 377-385, 2006.

47. S.-E. Fang and R. Perera, "Power mode shapes for early damage detection in linear structures," Journal of Sound and Vibration, vol. 324, pp. 40-56, 2009.

48. C. R. Farrar, et al., "Structural Health Monitoring Studies of the Alamosa Canyon and I-40 Bridges," Los Alamos National Lab. LA-13635-MS, 2000.

49. C. R. Farrar, et al., "Comparison study of modal parameter confidence intervals computed using the Monte Carlo and Bootstrap techniques," Los Alamos National Laboratory1998.

50. C. R. Farrar and D. A. Jauregui, "Comparative study of damage identification algorithms applied to a bridge: I. Experiment," Smart Materials and Structures, vol. 7, p. 704, 1998.

51. C. R. Farrar and N. A. J. Lieven, "Damage prognosis: the future of structural health monitoring," Philosophical Transactions of the Royal Society A: Mathematical, Physical and Engineering Sciences, vol. 365, pp. 623-632, 2007.

52. S. D. Fassois and J. S. Sakellariou, "Time-series methods for fault detection and identification in vibrating structures," Philosophical Transactions of the Royal Society A: Mathematical, Physical and Engineering Sciences, vol. 365, pp. 411-448, 2007.

53. R. Fox and M. Kapoor, "Rates of change of eigenvalues and eigenvectors," AIAA Journal, vol. 6, pp. 2426-2429, 1968.

54. P. M. Frank and B. Köppen-Seliger, "New developments using AI in fault diagnosis," Engineering Applications of Artificial Intelligence, vol. 10, pp. 3-14, 1997.

55. P. M. Frank and B. Köppen-Seliger, "Fuzzy logic and neural network applications to fault diagnosis," International Journal of Approximate Reasoning, vol. 16, pp. 67-88, 1997.

56. M. I. Friswell, "Damage identification using inverse methods," Philosophical Transactions of the Royal Society A: Mathematical, Physical and Engineering Sciences, vol. 365, pp. 393-410, 2007.

57. M. I. Friswell and D. J. Inman, "Sensor Validation for Smart Structures," Journal of Intelligent Material Systems and Structures, vol. 10, pp. 973-982, December 1, 1999.

58. N. Gang, et al., "A Comparison of Classifier Performance for Fault Diagnosis of Induction Motor using Multi-type Signals," Structural Health Monitoring, vol. 6, pp. 215-229, September 1, 2007.

59. D. F. Giraldo, et al., "Damage Detection Accommodating Varying Environmental Conditions," Structural Health Monitoring, vol. 5, pp. 155-172, June 1, 2006.

60. V. Giurgiutiu, et al., "Piezoelectric Wafer Embedded Active Sensors for Aging Aircraft Structural Health Monitoring," Structural Health Monitoring, vol. 1, pp. 41-61, July 1, 2002.

61. K. Goebel, "Management of uncertainty in sensor validation, sensor fusion, and diagnosis of mechanical systems using soft computing techniques," Ph. D., University of California at Berkeley, 1996.

62. H. Guo, et al., "Evaluating Sensor Reliability in Classification Problems Based on Evidence Theory," Systems, Man, and Cybernetics, Part B, IEEE Transactions on, vol. 36, pp. 970-981, 2006.

63. H. Guo and L. Zhang, "A weighted balance evidence theory for structural multiple damage localization," Computer Methods in Applied Mechanics and Engineering, vol. 195, pp. 6225-6238, 2006.

64. H. Y. Guo, "Structural damage detection using information fusion technique," Mechanical Systems and Signal Processing, vol. 20, pp. 1173-1188, 2006.

65. H. Y. Guo and Z. L. Li, "A two-stage method to identify structural damage sites and extents by using evidence theory and micro-search genetic algorithm," Mechanical Systems and Signal Processing, vol. 23, pp. 769-782, 2009.

66. R. F. Guratzsch and S. Mahadevan, "Sensor Placement for Aerospace Vehicle Health Monitoring Systems," in Earth & Space 2006, League City/Houston, Texas, USA, 2006.

67. D. L. Hall and J. Llinas, Handbook of Multisensor Data Fusion: CRC Press LLC, 2001.

68. M. A. F. Harrison, et al., "A comparison of time series analysis algorithms for detection of barely visible impact damage in UAV wings," in Nondestructive Evaluation and Health Monitoring of Aerospace Materials, Composites, and Civil Infrastructure V, San Diego, CA, USA, 2006, pp. 61760B-12.

69. F. v. d. Heijden, et al., Classification, Parameter Estimation and State Estimation: An Engineering Approach Using MATLAB: Wiley, 2004.

70. A. Heng, et al., "Rotating machinery prognostics: State of the art, challenges and opportunities," Mechanical Systems and Signal Processing, vol. 23, pp. 724-739, 2009.

71. W. Heylen, et al., Modal Analysis Theory and Testing: Katholieke Universiteit Leuven, Department of Mechanical Engineering, 1995.

72. J. Humar, et al., "Performance of Vibration-based Techniques for the Identification of Structural Damage," Structural Health Monitoring, vol. 5, pp. 215-241, September 1, 2006.

73. V. N. Huynh, et al., "Multiple-attribute decision making under uncertainty: the evidential reasoning approach revisited," Systems, Man and Cybernetics, Part A: Systems and Humans, IEEE Transactions on, vol. 36, pp. 804-822, 2006.

74. P. H. Ibarguengoytia, et al., "Real time intelligent sensor validation," Power Systems, IEEE Transactions on, vol. 16, pp. 770-775, 2001.

75. A. K. Jain, et al., "Statistical pattern recognition: a review," IEEE Transactions on Pattern Analysis and Machine Intelligence, vol. 22, pp. 4-37, 2000.

76. A. K. S. Jardine, et al., "A review on machinery diagnostics and prognostics implementing condition-based maintenance," Mechanical Systems and Signal Processing, vol. 20, pp. 1483-1510, 2006.

77. F. Jensen, *Bayesian Networks and Decision Graphs*. New York Springer-Verlag, 2001.

78. H. Kang, et al., "An application of fuzzy logic and Dempster-Shafer theory to failure detection and identification," in Decision and Control, 1991., Proceedings of the 30th IEEE Conference on, 1991, pp. 1555-1560 vol.2.

79. L. S. Katafygiotis and K.-V. Yuen, "Bayesian spectral density approach for modal updating using ambient data," Advances in Structural Engineering, vol. 30, pp. 1103-1123, 2001.

80. G. Kerschen, et al., "Sensor validation using principal component analysis," Smart Materials and Structures, vol. 14, pp. 36-42, 2005.

81. G. Kerschen, et al., "Bayesian Model Screening for the Identification of Nonlinear Mechanical Structures," Journal of Vibration and Acoustics, vol. 125, pp. 389-397, 2003.

82. G. Kerschen, et al., "Nonlinear normal modes, Part I: A useful framework for the structural dynamicist," Mechanical Systems and Signal Processing, vol. 23, pp. 170-194, 2009.

83. G. Kerschen, et al., "Past, present and future of nonlinear system identification in structural dynamics," Mechanical Systems and Signal Processing, vol. 20, pp. 505-592, 2006.

84. J. T. Kim and N. Stubbs, "Improved Damage Identification Method Based on Modal Information," Journal of Sound and Vibration, vol. 252, pp. 223-238, 2002.

85. J. M. Ko, et al., "Formulation of an uncertainty model relating modal parameters and environmental factors by using long-term monitoring data," in Smart Structures and Materials 2003: Smart Systems and Nondestructive Evaluation for Civil Infrastructures, San Diego, CA, USA, 2003, pp. 298-307.

86. K.-Y. Koo, et al., "Automated Impedance-based Structural Health Monitoring Incorporating Effective Frequency Shift for Compensating Temperature Effects," Journal of Intelligent Material Systems and Structures, vol. 20, pp. 367-377, September 3, 2009.

87. L. I. Kuncheva, Combining pattern classifiers: methods and algorithms: Wiley-Interscience, 2004.

88. Y. Lei, et al., "New clustering algorithm-based fault diagnosis using compensation distance evaluation technique," Mechanical Systems and Signal Processing, vol. 22, pp. 419-435, 2008.

89. J.-S. Lew, "Reduction of uncertainty effect on damage identification using feedback control," Journal of Sound and Vibration, vol. 318, pp. 903-910, 2008.

90. H. Li, et al., "Structural damage identification based on integration of information fusion and Shannon entropy," Mechanical Systems and Signal Processing, vol. 22, pp. 1427-1440, 2008.

91. L. Lieven and D. Ewins, "Spatial correlation of mode shapes, the co-ordinate modal assurance criterium," presented at the Proceedings of the 6th International Modal Analysis Conference (IMAC6), 1988.

92. M. P. Limongelli, "Frequency response function interpolation for damage detection under changing environment," Mechanical Systems and Signal Processing, vol. In Press, Corrected Proof, 2010.

93. X. Liu, et al., "Eigenspace updating for non-stationary process and its application to face recognition," *Pattern Recognition,* vol. 36, pp. 1945-1959, 2003.

94. I. Lopez, et al., "Application of Dimensional Reduction Techniques to Near-Field Aeroacoustic Damage Detection," presented at the International IEEE Prognostics and Health Management (PHM), Denver, CO, 2008.

95. I. Lopez, et al., "Scaled Acoustics Experiments and Vibration Prediction Based Structural Health Monitoring," presented at the ASME International Engineering Congress and Exposition, Boston, MA, USA, 2008.

96. I. Lopez and N. Sarigul-Klijn, "System Identification and Damage Assessment of Deteriorating Hysteretic Structures," in 49th AIAA/ASME/ASCE/AHS/ASC Structures, Structural Dynamics, and Materials Conference 2008.

97. I. Lopez and N. Sarigul-Klijn, "Impact Damage Assessment of Time-Varying Structures under Temperature Variations," in 4th European Structural Health Monitoring Workshop, Krokaw, Poland, 2008.

98. I. Lopez and N. Sarigul-Klijn, "Distance similarity matrix using ensemble of dimensional data reduction techniques: Vibration and aerocoustic case studies," Mechanical Systems and Signal Processing, vol. 23, pp. 2287-2300, 2009.

99. I. Lopez and N. Sarigul-Klijn, "Intelligent Aircraft Damage Assessment, Trajectory Planning, and Decision-Making under Uncertainty," presented at the 8th Mexican International Conference on Artificial Intelligence, Guanajuato, México, 2009.

100. I. Lopez and N. Sarigul-Klijn, "Situational Awareness and Decision-Making for Distressed Aircraft," presented at the Annual Conference of the Prognostics and Health Management Society, San Diego, CA USA, 2009.

101. I. Lopez and N. Sarigul-Klijn, "A review of uncertainty in flight vehicle structural damage monitoring, diagnosis and control: Challenges and opportunities," Progress in Aerospace Sciences, vol. In Press, Corrected Proof, 2010.

102. R. C. Luo, et al., "Multisensor fusion and integration: approaches, applications, and future research directions," Sensors Journal, IEEE, vol. 2, pp. 107-119, 2002.

103. W. Luo, "Imprecise Probability and Decision in Civil Engineering - Dempster-Shafer Theory and Application," PhD Dissertation, Civil Engineering, University of British Columbia, Vancouver, Canada, 1993.

104. L. v. d. Maaten, *et al.*, "Dimensionality Reduction: A Comparative Review," MICC, Maastricht University, Maastricht, The Netherlands, 2007.

105. N. Maia and J. Silva, Theoretical and Experimental Modal Analysis: John Wiley & Sons, 1997.

106. G. Manson, et al., "On the Long-Term Stability of Normal Condition for Damage Detection in a Composite Panel," Key Engineering Materials, vol. 204-205, 2001.

107. M. Markou and S. Singh, "Novelty detection: a review—part 1: statistical approaches," Signal Processing, vol. 83, pp. 2481 – 2497, 2003.

108. M. Markou and S. Singh, "Novelty detection: a review--part 2:: neural network based approaches," Signal Processing, vol. 83, pp. 2499-2521, 2003.

109. M.-H. Masson and T. Denoeux, "ECM: An evidential version of the fuzzy c-means algorithm," *Pattern Recognition,* vol. 41, pp. 1384-1397, 2008.

110. K. Matsuoka, "Noise injection into inputs in back-propagation learning," Systems, Man and Cybernetics, IEEE Transactions on, vol. 22, pp. 436-440, 1992.

111. N. Mehranbod, et al., "A method of sensor fault detection and identification," Journal of Process Control, vol. 15, pp. 321-339, 2005.

112. O. J. Mengshoel, et al., "Sensor Validation using Bayesian Networks," presented at the 9th International Symposium on Artificial Intelligence, Robotics, and Automation in Space, Los Angeles, CA, 2008.

113. A. Messina, *et al.*, "Structural Damage Detection by a Sensitivity and Statistical-Based Method," *Journal of Sound and Vibration,* vol. 216, pp. 791-808, 1998.

114. L. Mevel, et al., "Merging Sensor Data from Multiple Measurement Set-ups for Non-Stationary Susbspace-Based Modal Analysis," Journal of Sound and Vibration, vol. 249, pp. 719-741, 2002.

115. P. Mitra, et al., "Unsupervised feature selection using feature similarity," Pattern Analysis and Machine Intelligence, IEEE Transactions on, vol. 24, pp. 301-312, 2002.

116. B. Möller and M. Beer, "Engineering computation under uncertainty - Capabilities of non-traditional models," Computers & Structures, vol. 86, pp. 1024-1041, 2008.

117. Z. P. Mourelatos and J. Zhou, "Reliability Estimation and Design with Insufficient Data Based on Possibility Theory," presented at the AIAA/ISSMO Multidisciplinary Analysis and Optimization Conference, Albany, New York, 2004.

118. P. Moyo and J. M. W. Brownjohn, "Application of Box-Jenkins Models for Assessing the Effect of Unusual Events Recorded by Structural Health Monitoring Systems," Structural Health Monitoring, vol. 1, pp. 149-160, June 1, 2002.

119. M. M. Muto, "Application of Stochastic Simulation Methods to System Identification," Doctor of Philosophy, California Institute of Technology, 2006.

120. T. Nagayama, "Structural Health Monitoring Using Smart Sensors," Ph. D., Civil Engineering, University of Illinois at Urbana-Champaign, 2007.

121. S. Nandi and H. A. Toliyat, "Condition Monitoring and Fault Diagnosis of Electrical Machines - A Review," presented at the IEEE Industry Applications Conference, 1999.

122. S. A. Neild, et al., "A review of time-frequency methods for structural vibration analysis," Engineering Structures, vol. 25, pp. 713-728, 2003.

123. J. M. Nichols, et al., "Use of chaotic excitation and attractor property analysis in structural health monitoring," Physical Review E, vol. 67, p. 016209, 2003.

124. E. Nikolaidis, et al., "Comparison of Probability and Possibility for Design Against Catastrophic Failure Under Uncertainty," Journal of Mechanical Design, vol. 126, pp. 386-394, 2004.

125. G. Niu, et al., "A Comparison of Classifier Performance for Fault Diagnosis of Induction Motor using Multi-type Signals," Structural Health Monitoring, pp. 215-229, 2007.

126. H. Ogawa, et al., "An expert system for structure damage assessment," Pattern Recognition Letters, vol. 2, pp. 427-432, 1984.

127. R. A. Osegueda, et al., "Statistical and Dempster-Shafer techniques in testing structural integrity of aerospace structures," in Smart Nondestructive Evaluation and Health Monitoring of Structural and Biological Systems II, San Diego, CA, USA, 2003, pp. 140-151.

128. A. Pandey and M. Biswas, "Damage detection in structures using changes in flexibility," Journal of Sound and Vibration, vol. 169, pp. 3-17, 1994.

129. A. K. Pandey, et al., "Damage detection from changes in curvature mode shapes," Journal of Sound and Vibration, vol. 145, pp. 321-332, 1991.

130. C. R. Parikh, et al., "Application of Dempster-Shafer theory in condition monitoring applications: a case study," Pattern Recognition Letters, vol. 22, pp. 777-785, 2001.

131. R. Pascual, et al., "A Frequency Domain Correlation Technique for Model Correlation and Updating," presented at the Proceedings International Modal Analysis Conference, 1997.

132. R. J. Patton, et al., "Fault diagnosis in nonlinear dynamic systems via neural networks," in Control, 1994. Control '94. International Conference on, 1994, pp. 1346-1351 vol.2.

133. R. J. Patton, et al., "Artificial intelligence approaches to fault diagnosis," in Condition Monitoring: Machinery, External Structures and Health (Ref. No. 1999/034), IEE Colloquium on, 1999, pp. 5/1-518.

134. R. J. Patton, et al., "Soft computing approaches to fault diagnosis for dynamic systems: a survey," presented at the 4th IFAC Symposium on Fault Detection supervision and Safety, 2000.

135. P. M. Pawar and R. Ganguli, "Genetic fuzzy system for damage detection in beams and helicopter rotor blades," Computer Methods in Applied Mechanics and Engineering, vol. 192, pp. 2031-2057, 2003.

136. J. Pearl, Probabilistic Reasoning in Intelligent Systems: Networks of Plausible Inference, 2nd ed. San Francisco, CA: Morgan Kauffmann, 1988.

137. B. Peeters and G. De Roeck, "Stochastic System Identification for Operational Modal Analysis: A Review," Journal of Dynamic Systems, Measurement, and Control, vol. 123, pp. 659-667, 2001.

138. B. Peeters, et al., "Vibration-based damage detection in civil engineering: excitation sources and temperature effects," Smart Materials and Structures, vol. 10, pp. 518-527 2001.

139. S. G. Pierce, et al., "Uncertainty analysis of a neural network used for fatigue lifetime prediction," Mechanical Systems and Signal Processing, vol. 22, pp. 1395-1411, 2008.

140. S. G. Pierce, et al., "A novel information-gap technique to assess reliability of neural network-based damage detection," Journal of Sound and Vibration, vol. 293, pp. 96-111, 2006.

141. A. Raghavan and C. E. S. Cesnik, "Effects of Elevated Temperature on Guided-wave Structural Health Monitoring," Intelligent Material Systems and Structures, vol. 19, pp. 1383-1398, May 20 2008.

142. S. A. Ramu and V. T. Johnson, "Damage assessment of composite structures--A fuzzy logic integrated neural network approach," Computers & Structures, vol. 57, pp. 491-502, 1995.

143. L. Rogers, "Derivatives of eigenvalues and eigenvectors," AIAA Journal, vol. 8, pp. 943-944, 1970.

144. T. Ross, et al., "Quantifying total uncertainty using different mathematical theories in a validation assessment," presented at the ASCE Joint Specialty Conference on Probabilistic Mechanics and Structural Reliability, Albuquerque, NM, 2004.

145. O. S. Salawu, "Detection of structural damage through changes in frequency: a review," Engineering Structures, vol. 19, pp. 718-723, 1997.

146. N. Sarigul-Klijn, *et al.*, "Smart Monitoring of Structural Health In-Flight Environment," presented at the International Conference on Civil and Environmental Engineering (ICCEE), Higashi-Hiroshima, Japan, 2008.

147. M. H. Schoeller, et al., "Embedded Reasoning Supporting Aerospace IVHM," presented at the AIAA Infotech Conference and Exhibit, Rohnert Park, CA, 2007.

148. M. Schwabacher, "A Survey of Data-Driven Prognostics," presented at the AIAA Infotech@ Aerospace Conference, Arlington, VA, 2005.

149. G. Shafer, A Mathematical Theory of Evidence: Princeton Univ. Press, 1976.

150. D. Shepherd and A. Hollos, "Reasoning Systems for Diagnostics and Prognostics," in Aerospace Conference, 2008 IEEE, 2008, pp. 1-11.

151. Z. Y. Shi, et al., "Damage Localization by Directly Using Incomplete Mode Shapes," Journal of Engineering Mechanics, vol. 126, pp. 656-660, 2000.

152. C. Simon and P. Weber, "Imprecise reliability by evidential networks," Proceedings of the Institution of Mechanical Engineers, Part O: Journal of Risk and Reliability, vol. 223, pp. 119-131, 2009.

153. P. Smets, "Application of the transferable belief model to diagnostic problems," International Journal of Intelligent Systems, vol. 13, pp. 127-157, 1998.

154. A. Smyth and M. Wu, "Multi-rate Kalman filtering for the data fusion of displacement and acceleration response measurements in dynamic system monitoring," Mechanical Systems and Signal Processing, vol. 21, pp. 706-723, 2007.

155. H. Sohn, "Effects of environmental and operational variability on structural health monitoring," Philosophical Transactions of the Royal Society A: Mathematical, Physical and Engineering Sciences, vol. 365, pp. 539-560, 2007.

156. H. Sohn, et al., "Applying the LANL Statistical Pattern Recognition Paradigm for Structural Health Monitoring to Data from a Surface-Effect Fast Patrol Boat," ed, Los Alamos National Laboratory, LA-13761-MS, 2001.

157. H. Sohn, et al., "Structural Health Monitoring Using Statistical Pattern Recognition Techniques," Journal of Dynamic Systems, Measurement, and Control, vol. 123, pp. 706-711, 2001.

158. H. Sohn, et al., "Statistical Damage Classification Under Changing Environmental and Operational Conditions," Journal of Intelligent Material Systems and Structures, vol. 13, pp. 561-574, September 1, 2002.

159. P. Soundappan, et al., "Comparison of evidence theory and Bayesian theory for uncertainty modeling," Reliability Engineering & System Safety, vol. 85, pp. 295-311, 2004.

160. W. J. Staszewski, "Structural and Mechanical Damage Detection Using Wavelets," The Shock and Vibration Digest, vol. 30, pp. 457-472, November 1, 1998.

161. W. J. Staszewski, "Advanced data pre-processing for damage identification based on pattern recognition," International Journal of Systems Science, vol. 31, pp. 1381 - 1396, 2000.

162. W. J. Staszewski, "Intelligent signal processing for damage detection in composite materials," Composites Science and Technology, vol. 62, pp. 941-950, 2002.

163. W. J. Staszewski and A. N. Robertson, "Time–frequency and time–scale analyses for structural health monitoring," Philosophical Transactions of the Royal Society A: Mathematical, Physical and Engineering Sciences, vol. 365, pp. 449-477, 2007.

164. W. J. Staszewski and K. Worden, "Overview of optimal sensor location methods for damage detection," in Smart Structures and Materials 2001: Modeling, Signal Processing, and Control in Smart Structures, Newport Beach, CA, USA, 2001, pp. 179-187.

165. N. Stubbs, *et al.*, "Field verification of a nondestructive damage localization and severity estimation algorithm," presented at the 13th Int. Modal Analysis Conference, 1995.

166. M. M. R. Taha and J. L. Lucero, "A generic fuzzy metric for damage recognition in structural health monitoring systems," in Systems, Man and Cybernetics, 2005 IEEE International Conference on, 2005, pp. 1518-1523 Vol. 2.

167. M. M. R. Taha, et al., "Wavelet Transform for Structural Health Monitoring: A Compendium of Uses and Features," Structural Health Monitoring, vol. 5, pp. 267-295, September 1, 2006.

168. G. Vachtsevanos, et al., Intelligent Fault Diagnosis and Prognosis for Engineering Systems: John Wiley & Sons, 2006.

169. V. Venkatasubramanian, et al., "A review of process fault detection and diagnosis: Part II: Qualitative models and search strategies," Computers & Chemical Engineering, vol. 27, pp. 313-326, 2003.

170. V. Venkatasubramanian, et al., "A review of process fault detection and diagnosis: Part III: Process history based methods," Computers & Chemical Engineering, vol. 27, pp. 327-346, 2003.

171. V. Venkatasubramanian, et al., "A review of process fault detection and diagnosis: Part I: Quantitative model-based methods," Computers & Chemical Engineering, vol. 27, pp. 293-311, 2003.

172. P. Walley, Statistical Reasoning with Imprecise Probabilities: Chapman and Hall, 1991.

173. K. Wang, et al., "Crack-induced Changes in Divergence and Flutter of Cantilevered Composite Panels," Structural Health Monitoring, vol. 4, pp. 377-392, December 1, 2005.

174. T. Whittome and C. Dodds, "Monitoring offshore structures by vibration techniques," presented at the Proceedings of Design in Offshore Structures Conference, 1983.

175. K. Worden and J. M. Dulieu-Barton, "An Overview of Intelligent Fault Detection in Systems and Structures," Structural Health Monitoring, vol. 3, pp. 85-98, March 1, 2004.

176. K. Worden, et al., "A review of nonlinear dynamics applications to structural health monitoring," Structural Control and Health Monitoring, vol. In Press, p. n/a, 2007.

177. K. Worden and G. Manson, "The application of machine learning to structural health monitoring," Philosophical Transactions of the Royal Society A: Mathematical, Physical and Engineering Sciences, vol. 365, pp. 515-537, 2007.

178. K. Worden, et al., "An evidence-based approach to damage location on an aircraft structure," Mechanical Systems and Signal Processing, vol. 23, pp. 1792-1804, 2009.

179. X. Wu, et al., "Use of neural networks in detection of structural damage," Computers & Structures, vol. 42, pp. 649-659, 1992.

180. F. Xianfeng, et al., "A joint wavelet lifting and independent component analysis approach to fault detection of rolling element bearings," Smart Materials and Structures, vol. 16, p. 1973, 2007.

181. R. R. Yager, et al., Advances in the Dempster-Shafer theory of evidence: John Wiley & Sons, Inc., 1994

182. A. M. Yan, et al., "Structural damage diagnosis under varying environmental conditions--Part I: A linear analysis," Mechanical Systems and Signal Processing, vol. 19, pp. 847-864, 2005.

183. A. M. Yan, et al., "Structural damage diagnosis under varying environmental conditions--part II: local PCA for non-linear cases," Mechanical Systems and Signal Processing, vol. 19, pp. 865-880, 2005.

184. B.-S. Yang and K. J. Kim, "Application of Dempster-Shafer theory in fault diagnosis of induction motors using vibration and current signals," Mechanical Systems and Signal Processing, vol. 20, pp. 403-420, 2006.

185. J. N. Yang, et al., "Hilbert-Huang Based Approach for Structural Damage Detection," Journal of Engineering Mechanics, vol. 130, pp. 85-95, 2004.

186. J. N. Yang, et al., "An adaptive extended Kalman filter for structural damage identification," Structural Control and Health Monitoring, vol. 13, pp. 849-867, 2006.

187. Y.-M. Yang, et al., "Fault Diagnosis of Complex Systems Based on Multi-sensor and Multi-domain Knowledge Information Fusion," in Networking, Sensing and Control, 2008. ICNSC 2008. IEEE International Conference on, 2008, pp. 1065-1069.

188. J. Yen, "Generalizing the Dempster–Shafer Theory to Fuzzy Sets," in Classic Works of the Dempster-Shafer Theory of Belief Functions. vol. 219, R. R. Yager and L. Liu, Eds., ed: Springer Berlin / Heidelberg, 2008, pp. 529-554.

189. K.-V. Yuen, et al., "Two-Stage Structural Health Monitoring Approach for Phase I Benchmark Studies," Journal of Engineering Mechanics, vol. 130, pp. 16-33, 2004.

190. K.-V. Yuen, et al., "Unified Probabilistic Approach for Model Updating and Damage Detection," Journal of Applied Mechanics, vol. 73, pp. 555-564, 2006.

191. K.-V. Yuen and L. S. Katafygiotis, "Substructure Identification and Health Monitoring Using Noisy Response Measurements Only," Computer-Aided Civil and Infrastructure Engineering vol. 21, pp. 280-291, 2006.

192. L. A. Zadeh, "Fuzzy sets," Information and Control, vol. 8, pp. 338-353, 1965.

193. L. A. Zadeh, "Fuzzy sets as a basis for a theory of possibility," Fuzzy Sets and Systems, vol. 100, pp. 9-34, 1999.

194. C. Zang and M. Imregun, "Structural Damage Detection Using Artificial Neural Networks and Measured FRF Data Reduced Via Principal Component Projection," Journal of Sound and Vibration, vol. 242, pp. 813-827, 2001.

195. D. C. Zimmerman and M. Kaouk, "Structural Damage Detection Using a Minimum Rank Update Theory," Journal of Vibration and Acoustics, vol. 116, pp. 222-231, 1994.